Microwave treatment of oil contaminated drill cuttings produced on offshore oil platforms

Oluwatosin Ogunniran, MEng

Thesis submitted to the University of Nottingham for the degree of Doctor of Engineering

September 2016



ABSTRACT

This research project addresses the major processing challenges encountered in the current development of a microwave process, which can treat oil contaminated drill cuttings, from pilot scale to an industrial system. In addition, the dominant mechanism of oil removal during microwave heating of oil contaminated drill cuttings is established for the first time and the implication for the design of an industrial system discussed.

Currently, the prevalent practise is to transport oil contaminated drill cuttings produced from drilling activities offshore (United Kingdom Continental Shelf) to land for treatment and disposal. An offshore discharge limit of <1 wt% oil effectively sustains the ship to shore practise, as there are currently no established alternatives that are suitable for offshore operation.

A continuous microwave process that can reduce oil levels to <1 wt% has already been developed by researchers to pilot scale with a throughput of 0.5 t/h. This work investigates the two main processing issues encountered during the scaling up and optimisation of the process to an industrial system (4 t/h). They are: 1) thermal runaway and consequent damage to the microwave cavity, 2) effect of the material handling strategy on the efficiency of the microwave process.

It was found that the dielectric properties of the clay content of drill cuttings sustained heating rate at temperatures above 100 ^{o}C in drill cuttings. This ensured that the temperature increased from the normal operating temperature of the industrial system (100 ^{o}C) to 400 ^{o}C. The low thermal conductivity of the drill cuttings material is also thought to contribute to the temperature increase from 100 ^{o}C to 400 ^{o}C during processing.

At 400 ^{o}C, there is an exponential rise in dielectric constant and loss factor of the drill cuttings material shown to be initiated by the dehydroxylation of the chemically bound water in the clay mineral content. Consequently the temperature of the drill cuttings material increases from 400 ^{o}C to ≥1400 ^{o}C, vitrifying the material and causing thermally induced damages to the microwave cavity. The oil components were found to be transparent to microwaves from ambient temperature to their end point, therefore the exponential rise in dielectric properties at 400 ^{o}C cannot be attributed to the oil content but to the solid phase. Interestingly, the barite and halite mineral components of the drill cuttings material was shown to absorb more microwaves at ≥700 ^{o}C than the clay minerals, suggesting that although thermal runaway is not initiated in the barite and halite components, they ensure vitrification temperatures can be reached. These findings were used to optimise the industrial microwave continuous system by: 1) ensuring no build-up of drill cuttings in the microwave cavity, 2) designing the cavity and process safety systems to ensure temperatures within the cavity does not reach 400 ^{o}C.

A twin screw conveyor, which shears the drill cuttings during transport, is the chosen material handling technique within the industrial microwave system. This work demonstrates that the bulk density of drill cuttings can be reduced significantly when sheared. At low microwave power densities, it was found that oil removal from low bulk density materials can be up to 25% less efficient than oil removal from high bulk density materials. However, oil removal efficiency remained the same for both high and low bulk density materials at high power densities.

In the past steam stripping, steam distillation and physical entrainment have been identified by researchers as competing mechanism of oil removal from drill cuttings

during microwave heating. This work shows that oil removal increases when the steam velocity within the material's pore increases. It was also shown that high pore steam velocities corresponds to high microwave power densities. Higher oil removals observed at high power densities is as a result of higher pore steam velocities. A mass transfer correlation showing that pore steam velocity has a significant effect on the mass transfer coefficient of oil was developed. The relationship between the pore steam velocity and the mass transfer coefficient shows that steam stripping is the dominant mechanism of oil removal, and accounts for up to 80% oil removal.

ACKNOWLEDGEMENTS

I would like to extend a deep sense of appreciation to my supervisors: Professor Colin Snape and Dr John Robinson for their guidance in completing this work. Special thanks goes to Dr John Robinson for his invaluable advice, support and patience. I am most grateful.

I would like to thank all the members of the microwave processing group that supported me through the course of completing this work. Recognition goes to Dr Angelique Sklavounou for helping with impedance matching, electric field simulations and dielectric properties, and to Mr Joe Meehan for his general assistance.

I would like to thank National Oilwell Varco (Brandt) for the opportunity to work with them on this very exciting project. I enjoyed working in a dynamic team led by George Burnett who provided invaluable insight into the engineering aspect of waste management in oil and gas drilling.

My family and friends have been incredibly supportive over the course of this project, without which I would never have made this milestone. I am immensely grateful for their love and support.

DEDICATION

To my dearest mother, Omoladun Omolola Ogunniran.

Table of Contents

Chapter 1 Introduction 1

Chapter 2 Literature Review – Background Information on Oil Contaminated Drill Cuttings 6

2.1 Drilling Fluids 8

2.1.1 Water Based Drilling Fluids 8

2.1.2 Non-aqueous Based Drilling Fluids 9

2.1.2.1 Oil Based Drilling Fluid 10

2.1.2.2 Synthetic Based Drilling Fluid 11

2.2 Environmental Impact of drill cuttings 13

2.3 Offshore Treatment and Disposal of Drill Cuttings 15

2.3.1 Cuttings Re-injection 15

2.3.2 Thermal desorption 15

2.4 Onshore Treatment and Disposal of Drill Cuttings 16

2.4.1 Treatment methods 16

2.4.1.1 Bio-remediation 16

2.4.1.2 Solidification and Stabilization 17

2.4.1.3 Solvent Extraction 17

2.4.1.4 Thermal Treatment 18

Chapter 3 Microwave Heating Review 21

3.1 Theory of Microwave Heating 23

3.1.2 Material Interaction with Microwaves 24

3.1.2.1 Dipolar polarisation 26

3.1.2.2 Ionic Conduction 27

3.1.2.3 Interfacial Polarisation 28

3.1.3 Dielectric Properties 28

3.1.3.1 Variation of dielectric properties with water content 30

3.1.3.2 Variation of dielectric properties with frequency 32

3.1.3.3 Variation of dielectric properties with temperature 34

3.1.3.4 Variation of dielectric properties with density 35

3.1.4 Dielectric properties of soil 37

3.2 Microwave Heating Systems 38

3.2.1 Microwave Generators 38

3.2.2 Waveguides 40

3.2.3 Microwave Applicators 42
3.2.3.1 Multi-mode applicators 42
3.2.3.2 Single mode applicators 44
3.2.3.3 Travelling wave applicators 46
3.2.4 Power density and Penetration depth 47
3.2.5 Thermal runaway and Arcing 49
3.3 Applications of Microwave Heating 50
3.3.1 Application of microwave heating to hydrocarbon removal from granular solids 51
3.3.1.1 Application of Microwave Heating to Oil Contaminated Drill Cuttings 52
3.3.1.2 Conventional and Microwave Stripping of Contaminated Solids 54
3.4 Current Processing Issues in the Industrial System 57
Chapter 4 Experimental Methods and Analytical Techniques 61
4.1 Microwave Heating Experiments – System A 61
4.2 Microwave Heating Experiments – System B 68
4.3 Microwave Heating Experiments – System C 70
4.4 Dielectric Property Measurement 72
4.5 Thermo – Gravimetric Analysis (TGA) 74
4.6 Density and Porosity Measurements 75
4.7 Shearing Methodology 76
4.8 Scanning Electron Microscopy 77
4.9 X-ray Diffraction Analysis (XRD) 79
4.10 Particle Size Analysis – Laser Diffraction Particle Size Analyser 81
4.11 Oil Content Measurement 82
4.12 Water Content Measurement 85
Chapter 5 Thermal Runaway – Dielectric Properties of Key Microwave Absorbing Components in Drill Cuttings 87
5.1 Dielectric properties of contaminated drill cuttings from 20^{o}C to 150^{o}C 88
5.2 Dielectric properties of contaminated drill cuttings from 20^{o}C to 850^{o}C 92
5.2.1 Dielectric and heat transfer properties of contaminated drill cuttings between 100 ^{o}C and 400 ^{o}C 98
5.2.1.1 Dielectric and heat transfer properties of sandstone based drill cuttings 101

5.2.2 Dielectric properties of contaminated drill cuttings between 400 ºC and 850 ºC....104
5.3 High temperature dielectric properties of the main solid components in drill cuttings....108
5.3.1 Calcite....110
5.3.2 Quartz....111
5.3.3 Anhydrite and Barite....112
5.3.4 Halite and Clay Minerals....114
5.4 Dielectric properties of vitrified drill cuttings....118
5.5 Conclusion....121
Chapter 6 Effect of shear on energy requirement for the remediation of oil contaminated drill cuttings....122
6.1 Introduction....122
6.2 Sample Characterisation....123
6.3 Changes to physical properties of drill cuttings from shearing....123
6.3.1 Why rheology is unsuitable for shear characterisation in this work....128
6.3.2 Clay content contribution to bulk density change in drill cuttings....129
6.4 Microwave treatment of sheared and unsheared shale based drill cuttings....135
6.4.1 Microwave treatment of drill cuttings sheared to 1.4 g/cm^3....136
6.4.2 Microwave Treatment of drill cuttings sheared to 1.7 g/cm^3 and 1.83 g/cm^3....145
6.4.3 Microwave treatment of sheared and unsheared drill cuttings at 3kW microwave power....150
6.4.4 Microwave treatment of sheared and unsheared drill cuttings at 5 kW input power....153
6.5 Microwave treatment of sheared and unsheared sandstone based drill cuttings....156
6.6 Conclusion....160
Chapter 7 Establishing the dominant mechanism of oil removal during the microwave heating of oil contaminated drill cuttings....161
7.1 Introduction....161
7.2 Oil removal mechanisms from drill cuttings....162
7.2.1 Theoretical energy requirement for the oil removal mechanisms....162
7.2.1 Physical Entrainment....167

7.2.2 Direct vaporisation 170
7.2.3 Steam distillation and steam stripping 171
7.3 Effect of microwave power and heating time on oil and water removal ... 173
7.3.1 Microwave treatment of drill cuttings in system A 173
7.3.2 Microwave Treatment of drill cuttings in system B 175
7.3.3 Microwave treatment of drill cuttings in system C 179
7.4 Steam Velocity: Assessment of steam stripping mechanism 180
7.4.1 Effect of microwave power and porosity on steam velocity 183
7.4.2 Mass transfer coefficient 186
7.4.3 Estimating the mass transfer coefficient empirically 189
7.4.4 Mass transfer model 191
7.4.4 Comparison of mass transfer model with previous work in conventional gas stripping 196
7.5 Conclusion 199
Chapter 8 Conclusions and Future Work 200
8.1 Thermal runaway 200
8.2 Effect of material transport on the energy efficiency of the microwave process 202
8.3 Mechanism of oil removal 203
8.4 Future Work 205
Chapter 9 References 207
Appendices 218

List of Figures

Figure 2.1: Schematic of a drilling rig, well and mud circulating system. 6
Figure 2.2: Typical composition of water based drilling fluid.....9
Figure 2.3: Typical composition of non-aqueous based drilling fluid 10
Figure 2.4: Schematic showing an indirect thermal desorption unit.....19
Figure 3.1: The electromagnetic spectrum 23
Figure 3.2: Categories of materials based on their microwave absorption characteristics 25
Figure 3.3: Schematic showing interaction between dielectric materials and microwaves.....26
Figure 3.4: Structure of water showing the charge distribution 26
Figure 3.5: Variation of dielectric properties of soil with moisture content at 10^{o}C and 4 GHz. K* is the complex permittivity, K' is the dielectric constant, K" is the dielectric loss factor.....31
Figure 3.6: Variation of the dielectric constant and loss factor of water with frequency at 20^{o}C 33
Figure 3.7: The variation of the dielectric constant of yellow corn with bulk density. Measurements at 24^{o}C and 20MHz. 36
Figure 3.8: Schematic of a typical domestic microwave oven.....38
Figure 3.9: Schematic of a magnetron.....39
Figure 3.10: Schematic of a hollow rectangular waveguide. b is the direction of microwave propagation 40
Figure 3.11: Propagation of microwaves in waveguides at TE and TM modes ...41
Figure 3.12: Damping and frequency shift of mode patterns in a multimode applicator due to the effect of loading a dielectric material 43
Figure 3.13: Electric field distribution in typical multimode oven at 2.45GHz....44
Figure 3.14: Schematic of a travelling wave applicator. Choke prevents microwave leakage; PTFE supports is microwave transparent. 46
Figure 3.15: Schematic showing the make-up of oil contaminated drill cuttings .53
Figure 3.16: The current processing concept in the microwave treatment of oil contaminated drill cuttings 57
Figure 3.17: A section of the twin screw conveyor in the industrial system (120 mm diameter) 58
Figure 3.18: Damage to ceramic cavity due to thermal runaway.....58
Figure 3.19: Drawing of the fibre glass belt conveyor system.....59
Figure 3.20: Drawing of the continuous microwave extrude system.....60
Figure 4.1: Picture of the microwave treatment system A 61
Figure 4.2: Schematic of microwave treatment system A.....62
Figure 4.3: Reflected and absorbed power in system A at 1kW input power.....65
Figure 4.4: Process flow diagram for the dual piston rig – system B 68
Figure 4.5: Schematic of the processing concept for microwave remediation of drill cuttings - System C.....70
Figure 4.6: Drawing of the rotary wheel applicator 70

Figure 4.7: Schematic of the cylindrical resonant cavity measurement system....73
Figure 4.8: Diagrammatic representation of the shearing equipment 76
Figure 4.9: Schematic showing the principle of operation in a scanning electron microscope.....78
Figure 4.10: Diagram showing how X-ray interacts with samples in a diffractometer (Bragg's law).....80
Figure 4.11: Soxhlet extraction equipment 82
Figure 4.12: Dean and Stark apparatus 86
Figure 5.1: The variation of dielectric properties of shale based contaminated drill cuttings (13.8 wt% water, 11 wt% oil) with temperature 912 MHz 88
Figure 5.2: The relationship between dielectric loss factor and temperature of shale based drill cuttings (13.8 wt% water, 11 wt% oil), and sandstone based drill cuttings (9 wt% water, 8 wt% oil).....90
Figure 5.3: XRD showing the major mineral components in shale based drill cuttings; M-montmorillonite (clay); MC-muscovite (clay); K-kaolinite (clay); Q-quartz; A-anhydrite (gypsum), B-barite; C-calcite; H-halite 91
Figure 5.4: Data showing the variation of the dielectric constant and loss factor of shale based contaminated drill cuttings (13.8 wt%, 11 wt% oil) with temperature at 912MHz.....93
Figure 5.5: Dielectric constant and loss factor of oil at 912MHz as a function of temperature.....94
Figure 5.6: Dielectric properties of oil contaminated shale based drill cuttings (13.8 wt% water, 11 wt% oil) and oil free shale based drill cuttings at 912MHz as a function of temperature 95
Figure 5.7: Schematic of drill cuttings showing thermal properties 100
Figure 5.8: Dielectric properties of shale based drill cuttings (13.8 wt% water, 11 wt% oil) and sandstone based drill cuttings (9 wt% water, 8 wt% oil) at 912MHz as a function of temperature 102
Figure 5.9: Dried shale based drill cuttings (colour – brown).....105
Figure 5.10: Residue produced from the microwave vitrification of shale based drill cuttings showing a dark grey/black colour distinct from the brown colour before microwave vitrification 106
Figure 5.11: Vitrified drill cuttings showing a yellowish brown colour after oxidation in air to 850^{o}C 107
Figure 5.12: Thermogravimetric analysis of shale based drill cuttings; A=loss of moisture; B=loss of hydration and interlayer water; C=loss of chemically bound water from clay minerals (dehydroxylation); D=dehydroxylation and loss of carbon dioxide from calcite. 35mg sample, 5 ^{o}C/min heating rate 109
Figure 5.13: Dielectric properties of calcite at 912MHz as a function of temperature. Reagent grade calcite used with 97% purity. 111
Figure 5.14: Dielectric properties of quartz as a function of temperature at 2.45GHz. Results represent one set of experiments.....112
Figure 5.15: Dielectric properties of Anhydrite (99% purity) and Barite (97% purity) at 912MHz as a function of temperature 113

Figure 5.16: Dielectric properties of halite (97% pure) at 912MHz as a function of temperature 114
Figure 5.17: Dielectric constant of clays (Kaolinite, montmorillonite and muscovite) at 912MHz as a function of temperature 115
Figure 5.18: Dielectric loss factor of clays (kaolinite, montmorillonite and muscovite) at 912MHz as a function of temperature 116
Figure 5.19: Loss tangent of the key solid microwave absorbing components of drill cuttings as a function of temperature. 117
Figure 5.20: The dielectric properties of vitrified drill cuttings as a function of temperature 118
Figure 5.21: Loss tangent of drill cuttings and vitrified residue at 912MHz as a function of temperature 120
Figure 6.1: (a) Unsheared (as received) oil contaminated drill cuttings (b) sheared oil contaminated drill cuttings 124
Figure 6.2: Bulk density of drill cuttings at varying times during shearing at 210 rpm and 275 rpm 125
Figure 6.3: XRD showing the major mineral components of shale 1 and shale 2; M-Montmorillonite, MC-muscovite; K-kaolinite; Q-quartz; A-anhydrite; B-barite; C-calcite; H-halite 129
Figure 6.4: XRD showing the major mineral components in sandstone; M-montmorillonite; MC-muscovite; K-kaolinite, Q-quartz; A-anhydrite; B-barite; C-calcite; H-halite 130
Figure 6.5: Conceptual representation of the water/oil/mineral phases in shale based drill cuttings 133
Figure 6.6: Conceptual representation of water/oil/mineral phases in sandstone 133
Figure 6.7: Energy input over time during microwave treatment of oil contaminated drill cuttings (shale 1) 136
Figure 6.8: Oil removal from unsheared and sheared (210 rpm for 3 minutes) oil contaminated drill cuttings (Shale 1) plotted against specific energy input. 1 kW microwave power 137
Figure 6.9: Dielectric constant of sheared and unsheared oil contaminated drill cuttings (Shale 1) at 912MHz 138
Figure 6.10: Dielectric loss factor of sheared and unsheared oil contaminated drill cuttings (Shale 1) st 912MHz 138
Figure 6.11: Water removal from sheared and unsheared shale based oil contaminated drill cuttings (shale 1). 1 kW microwave power 142
Figure 6.12: Unsheared oil contaminated drill cuttings (Shale 1 at 1.87 g/cm^3) (a) before microwave heating, (b) after microwave heating 143
Figure 6.13: Sheared oil contaminated drill cuttings (shale 1 at 1.4 g/cm^3) (a) before microwave heating, (b) after microwave heating 143
Figure 6.14: Water removal from unsheared and sheared oil contaminated drill cuttings (shale 1) plotted against specific energy input. 1 kW microwave power 146

Figure 6.15: Oil removal from unsheared and sheared oil contaminated drill cuttings (shale 1) plotted against specific energy input. 1kW microwave power 147
Figure 6.16: Water removal from sheared (210 rpm for 3 min) and unsheared oil contaminated drill cuttings (Shale 1A) plotted against specific energy input. 3Kw microwave power 150
Figure 6.17: Oil removal from sheared (sheared at 210 rpm for 3min) and unsheared oil contaminated drill cuttings (Shale 1A) plotted against specific energy input. 3 kW input microwave power 151
Figure 6.18: Water removal from sheared (210 rpm for 3 min) and unsheared oil contaminated drill cuttings plotted against specific energy input. 5 kW microwave power input.....154
Figure 6.19: Oil removal from sheared (210 rpm for 3min) and unsheared oil contaminated drill cuttings plotted against specific energy input. 5 kW microwave power.....155
Figure 6.20: Water removal from sheared (210rpm 3min) and unsheared oil contaminated drill cuttings (Sandstone) plotted against specific energy input. 1 kW microwave power 156
Figure 6.21: Sandstone based oil contaminated drill cuttings (a) Unsheared at 1.55 g/cm^3, (b) Sheared at 210 rpm for 3 minutes to 1.5 g/cm^3.....157
Figure 6.22: Oil removal from sheared (210 rpm for 3 min) and unsheared oil contaminated drill cuttings (Sandstone) plotted against specific energy input. 1 kW microwave power 158
Figure 7.1: Schematic showing water and oil in the pores of (a) shale based drill cuttings at 1.9 g/cm^3 (b) shale based drill cuttings sheared to 1.5 g/cm^3.....169
Figure 7.2: Oil removal plotted against heating times for treatment in system A (70 g sample mass).....174
Figure 7.3: Water removal plotted against heating times in system A (70 g sample mass).....175
Figure 7.4: Water removal plotted against heating times during microwave treatment of drill cuttings in System B.....177
Figure 7.5: Oil removal plotted against heating times during the microwave treatment of drill cuttings in system B 177
Figure 7.6: Oil removal plotted against energy input, showing that oil removal increases at high power densities and equivalent energy input.....178
Figure 7.7: Evaporation rate of water from oil contaminated drill cuttings as a function of time (Power = 1 kW, Sample = shale 1, System A) 181
Figure 7.8: The relationship between pore steam velocity and microwave power during microwave treatment of drill cuttings at 80 kWh/t in systems A and B ..184
Figure 7.9: The effect of steam velocity on mass transfer coefficient during microwave heating of oil contaminated drill cuttings (System A).....191
Figure 7.10: The effect of steam velocity on mass transfer coefficient during microwave treatment of oil contaminated drill cuttings (System A and B).....192

Figure 7.11: The effect of steam velocity on mass transfer coefficient during the microwave treatment of oil contaminated drill cuttings (System A, B and C) ...193

List of Tables

Table 2-1: Typical components in drilling fluids and their functions 12
Table 3-1: Variation of the dielectric properties of water with temperature at 3GHz 34
Table 4-1: Sample mass after microwave treatment at 1kW and 3kW, and 40 kJ 66
Table 5-1: SEM-EDX analysis showing the elemental composition of shale based drill cuttings 97
Table 5-2: Parameters used for the estimation of the heating rate in shale based drill cuttings 98
Table 5-3: Mineral composition in shale based drill cuttings 103
Table 5-4: Mineral composition of sandstone based drill cuttings 103
Table 5-5: SEM-EDX analysis showing the elemental composition in drill cuttings and vitrified drill cuttings 108
Table 6-1: Properties of drill cuttings. The water and oil contents and density of oil contaminated drill cuttings as received 123
Table 6-2: Composition of the solid phase in the drill cuttings sample in this work 128
Table 6-3: Particle size distribution of shale and sandstone based drill cuttings 132
Table 6-4: Oil and water contents of oil contaminated drill cuttings used in microwave heating at 5 kW 153
Table 7-1: Parameter assumptions in calculating the theoretical energy requirement of oil removal mechanisms 163
Table 7-2: Temperature of drill cuttings components during microwave heating 164
Table 7-3: Applicable terms from equation 7.1 required to estimate the energy requirement for individual oil removal mechanisms…. 164
Table 7-4: Theoretical microwave energy requirement to reduce oil content to 1 wt% in contaminated drill cuttings (14 wt% water, and 11 wt% oil) 166
Table 7-5: Oil and water content, and bulk density of oil contaminated drill cuttings treated in system A (70 g sample mass) 173
Table 7-6: Oil and water content, and bulk density of oil contaminated drill cuttings in system B (sample mass = 6.5 kg) 175
Table 7-7: Incident and reflected powers during the microwave heating treatment of drill cuttings in system B 176
Table 7-8: Oil and water content and bulk density of oil contaminated drill cuttings treated in system C 179
Table 7-9: Data from microwave heating tests in system C including the final oil and water content of samples after treatment 179
Table 7-10: The relationship between microwave power, porosity and steam velocity during microwave heating of oil contaminated drill cuttings (shale 1, system A, 80 kWh/t energy input) 185
Table 7-11: Parameters and physical constants used in calculating Schmidt number and Reynolds number 188

Table 7-12: Comparison of mass transfer models from microwave and conventional gas stripping of fixed beds.....196
Table 7-13: Peclet and Reynolds number, and mean particle size from mass transfer correlations in literature and this work.....197

Nomenclature

bbl - barrel

g – gram

kg – kilogram

kg/h – kilogram per hour

kWh/t – kilowatt hour per tonne

kJ – kilojoule

K – Kelvin

t – tonne

t/h – tonne per hour

wt% (w/w) - weight percent

Chapter 1 Introduction

The current world oil consumption is 92 million bbl/day and is estimated to increase to 112 million bbl/day by 2035 (BP, 2015; BP, 2016). Consequently, exploration and production of oil and gas is increasingly being carried out in challenging deep offshore wells and other remote locations in order to meet future demand.

Drill cuttings are generated from drilling activities in the exploration and production of oil and gas. They consist mainly of rock fragments from the reservoir being explored and drilling fluids (Ball et al., 2012). Drilling fluids or 'muds' are used to maintain well-bore stability, lubricate the drill bit, provide hydraulic power and transport drill cuttings back to the surface on drilling rigs (Mahmood et al., 2012; Okpokwasili & Nnubia, 1995; Davies et al., 1984). Oil contamination of drill cuttings arise from using oil-based drilling fluids, which are preferred by operators in deep offshore wells. Two other main types of drilling fluids are water-based drilling fluid, considered to be the most environmentally friendly, and synthetic-based drilling fluid. Nevertheless, challenging drilling conditions such as horizontal drilling, and high temperatures and pressures associated with challenging drilling regimes mean that operators use oil-based drilling fluid is these conditions for better safety and cost-effective performance.

Disposal of drill cuttings generated on an offshore drilling rig is an operational necessity due to space and storage limitations. In the past, drill cuttings were discharged into the sea bed adjacent to the drilling rig. However, oily drill cuttings were found to have potential for long term environmental impact on the marine environment, especially high levels of toxicity to the benthic fauna in the vicinity of the pile of disposed drill cuttings (Jorissen et al., 2009; Gray et al., 1990; Gerrard

et al., 1999; Daan & Mulder, 1996; Breuer et al., 2004). Therefore, regulations were introduced to limit the oil content of drill cuttings discharged offshore. In the United Kingdom Continental Shelf (UKCS), the oil content in drill cuttings must be reduced to <1 wt% before disposal (OSPAR, 2000). In contrast, oil levels must be <5 wt% before discharge in the Gulf of Mexico (Shang et al., 2006). Oil contaminated drill cuttings can contain 5-15 wt% oil (IOGP, 2016; Robinson et al., 2009a). This means that treatment is essential for drilling operators in the UKCS before disposal due to the OSPAR 2000/3 decision.

There are currently no offshore technologies capable of treating the volume of oil contaminated drill cuttings produced offshore, meaning that large quantities (81% of oily drill cuttings from UKCS in 2014) of contaminated drill cuttings are transported to shore (Oil & Gas UK, 2015). After treatment onshore, disposal usually involves landfilling. However, there are stringent restrictions on the landfill of toxic wastes (Council Directive, 1999), which includes oil contaminated drill cuttings. There are a few onshore treatment options including thermal desorption (Ball et al., 2012), bio-remediation (Turner, 2001), and solvent extraction (Childs et al., 2005)

The ship to shore practice is expensive and poses considerable logistical implications. The offloading of heavy drill cuttings storage containers in harsh weather environments, such as in the North Sea weather, generates serious health and safety concerns. Harsh weather conditions may hamper drilling operations if the storage capacity on the drilling rig is reached, which will significantly increase drilling costs. The drawbacks of the ship to shore practice mean that an offshore treatment process is highly desirable by drilling operators.

Re-injecting oil contaminated drill cuttings into dedicated wells is a widely used offshore disposal technique, however, only small volumes of contaminated drill cuttings (8% of oily cuttings produced in the UKCS in 2014) are currently disposed using this technique (Gilmour, 2007; IOGP, 2016; Oil & Gas UK, 2015). Other offshore treatment methods include using centrifugal dryers, and thermal desorption (IOGP, 2016). The efficiency of the dryers is limited to 3-6.9 wt% oil after treatment which still prohibits offshore disposal in the UKCS. In addition, the thermal desorption equipment consumes significant amounts of energy (700 kWh/t). The poor thermal conductivity properties of drill cuttings means that large residence times are needed for processing which requires large equipment. Therefore, conventional processing equipment are unsuitable for installation on an offshore drilling rig because of the significant deck space impact.

Microwave treatment has been identified as a viable alternative offshore technology to the current treatment options which can be retrofitted on a drilling rig, and has been proven to remediate oil levels to below the 1wt% environmental threshold (Robinson et al., 2009a). Microwave heating is advantageous because only microwave absorbers, in this case water, are selectively heated in the drill cuttings material. This provides significant energy savings, and eliminates poor heat transfer often associated with surface heating in conventional processes. The processing time using microwaves can be as low as 1% of the conventional thermal processing time (Meredith, 1998). Moreover, the oil recovered from microwave treatment retains its original quality and can be recycled for drilling fluid formulation (Shang et al., 2006).

Previous studies on the microwave treatment of drill cuttings have shown that high microwave powers improve oil removal (Shang et al., 2006). High microwave

power reduces processing times, and as a result, increases the throughput of a continuous microwave process. Researchers have developed a pilot scale continuous microwave process that can treat up to 0.5 t/h of drill cuttings (Robinson et al., 2009a; Robinson et al., 2010; Pereira, 2012). This process is currently being scaled up from a pilot scale to a 4 t/h industrial microwave system.

This work addresses the processing issues encountered during the scale up to the industrial microwave system. The processing issues investigated are;

- Exponential rise in temperature in the microwave reactor (cavity) observed during the continuous microwave treatment of drill cuttings. Volumetric breakdown or arcing was suspected as the most probable cause of the exponential temperature rise in cavity in the past. However, in this work it is thought that the exponential rise in temperature occurs due to thermal runaway in the mineral phase. As a result, the dielectric properties, which is the ability to absorb microwave power, of the oil and mineral phases are investigated to ascertain the contribution of each component to the thermal runaway hypothesis.
- Twin screw conveyors are used to transport the drill cuttings material in the industrial microwave system. The twin screw conveyor is a high shear transport system which changes the consistency of some drill cuttings materials. It is thought that the change in consistency may fundamentally affect the interaction of the material with microwaves. Therefore, the effect of using this material handling strategy on the energy efficiency of the microwave process is investigated.

Finally, steam distillation, physical entrainment and steam stripping have been suggested in the past as competing mechanisms of oil removal from drill cuttings during microwave heating. However, there is no consensus or conclusive evidence establishing a dominant mechanism(s) of oil removal to date. In this work, the hypothesis is that steam stripping is the dominant oil removal mechanism, with the efficiency of oil removal related to the steam velocity in the pores of the drill cuttings material.

Chapter 2 Literature Review – Background Information on Oil Contaminated Drill Cuttings

Drill cuttings are rock fragments generated from drilling wells during the exploration and production of oil and gas. The mineralogy of the rock fragments can vary depending on the geographical location, nonetheless, shale-based, sandstone-based, and chalk-based are the most common in the United Kingdom Continental Shelf (UKCS). Drilling fluids, also known as muds, transport rock fragments produced from the grinding rotational motion of the drill bit to the surface. Figure 2.1 is a schematic showing a drilling rig and mud system.

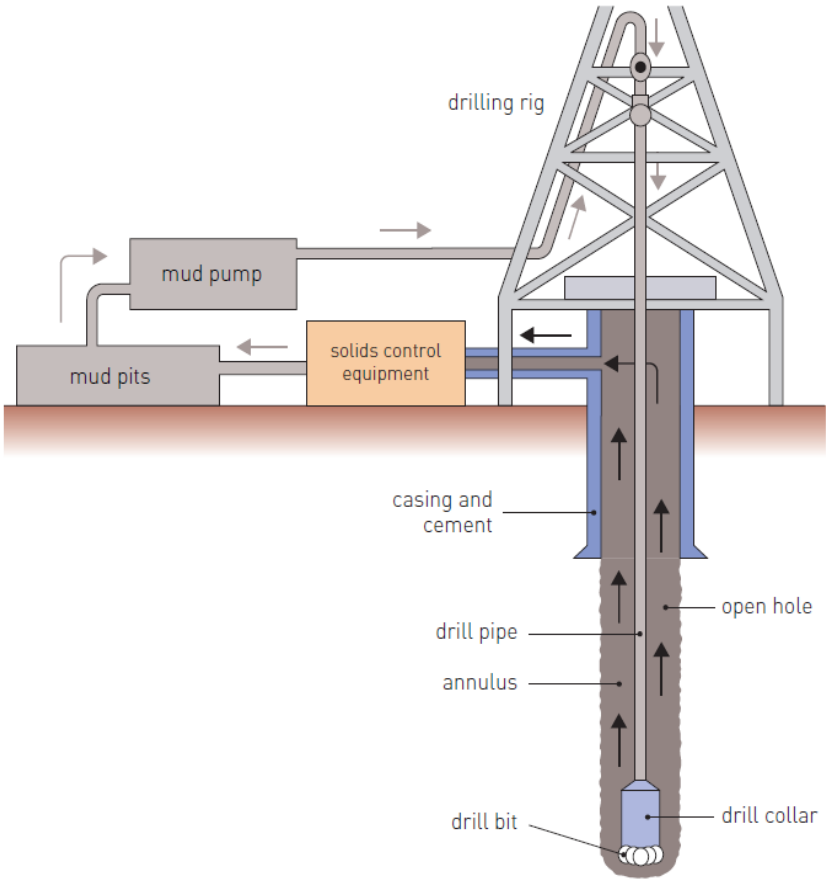


Figure 2.1: Schematic of a drilling rig, well and mud circulating system (IOGP, 2016).

Drilling fluid is pumped down the drill pipe to remove rock fragments which will otherwise clog the well. It carries the rock fragments through the annulus (space between wall of the well and drill pipe) to the surface where the separation of the drilling fluid from the drill cuttings takes place. The 'solid control equipment' in Figure 2.1 is the primary separation unit and consists of vibrating screens (also known as shale shakers). The mixture of drill cuttings and drilling fluid is passed over the shale shakers where the liquid component is separated, recycled into the mud pits and re-used for formulating new drilling fluids. The separated solid is drill cuttings, but is usually coated with the components of drilling fluids, especially the base fluid, due to the inherent limitations of the primary separation units. As much as 100 litres of drilling mud per metre of well drilled is lost as a result of the limitations. The separated drill cuttings, along with the retained drilling fluid components, constitute drilling waste for which operators require appropriate treatment and disposal strategy.

In addition to transporting drill cuttings back to the surface, drilling fluids serve many functions which include (Okpokwasili and Nnubia, 1995; Bernier et al., 2003):

- Cooling and lubricating the drill bit
- Protecting and stabilising the bore hole
- Control of subsurface pressure
- Transmission of hydraulic power to the drill bit
- Bottom hole cleaning and cooling
- Buoyancy support for the drill pipe
- Suspension of drill cuttings

2.1 Drilling Fluids

The composition of drilling fluid varies widely and can contain a plethora of additives and chemicals. However, there are two major types of drilling fluids classified according to their base fluids. They are non-aqueous drilling fluid and water based drilling fluids (IOGP, 2016; Ball et al., 2012).

2.1.1 Water Based Drilling Fluids

Water based drilling fluids (WBDF) are formulated using seawater or freshwater as the continuous phase. Drilling operators usually consider WBDFs first when drilling, partly because of the relative low costs when compared to other drilling fluids, but also due to the fact that it is considered the most environmentally friendly. The use of WBDF dominates shallow wells and the upper sections of deep wells, with only minimal use in the bottom sections of deep wells or in horizontal wells (HSE, 2000). Horizontal and deep wells are usually characterised by instability and high temperature and pressure. But base water lacks the lubricity and thermal stability needed in these conditions which makes WBDFs unsuitable. In addition, the technical performance of WBDFs may be affected from the interaction between swelling clays in shale based formations and the water base, leading to borehole instability. For these reasons, non-aqueous based drilling fluids are preferred when drilling horizontal and deep wells. Figure 2.2 shows the typical major components in water based drilling fluids. Barite, for example, is used as a weighting agent to control formation pressure.

Efforts have been put into improving the performance of water based drilling fluids over the years to make them viable alternatives to the less environmentally friendly non-aqueous based drilling fluid (HSE, 2000). Even though less toxic in the aquatic

environment, water based drilling fluids still pose a health hazard to rig workers (Searl and Galea, 2011).

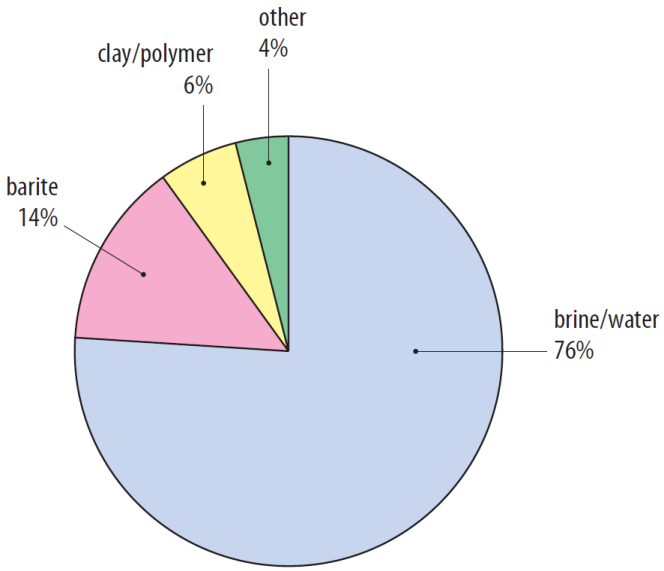


Figure 2.2: Typical composition of water based drilling fluid (IOGP, 2009)

2.1.2 Non-aqueous Based Drilling Fluids

Non-aqueous based drilling fluid (NADF) is an emulsion with organic liquids as the continuous phase. Figure 2.3 shows the typical composition of non-aqueous based drilling fluid. NADFs are more suited to high temperature and pressure deep wells because of their thermal stability at high temperatures in excess of 260 ^{o}C (Growcock and Patel, 2011; Mahmood et al., 2012). Furthermore, NADFs give increased borehole stability, low formation damage, high penetration rates and high lubricity when compared with water based drilling fluids (Zhong et al., 2011; Van Oort, 2003; HSE 2000). NADFs are the more economic option in the bottom sections of deep wells due to their superior technical performance. This suggests that NADFs will still be the predominantly used drilling fluid in offshore drilling in the UKCS, since the current and future UK drilling activities will be in offshore

deep sea reserves (Oil and Gas Authority, 2016; Oil & Gas UK, 2016).The main types of NADFs are oil based drilling fluids and synthetic based drilling fluid, which are discussed in the next section.

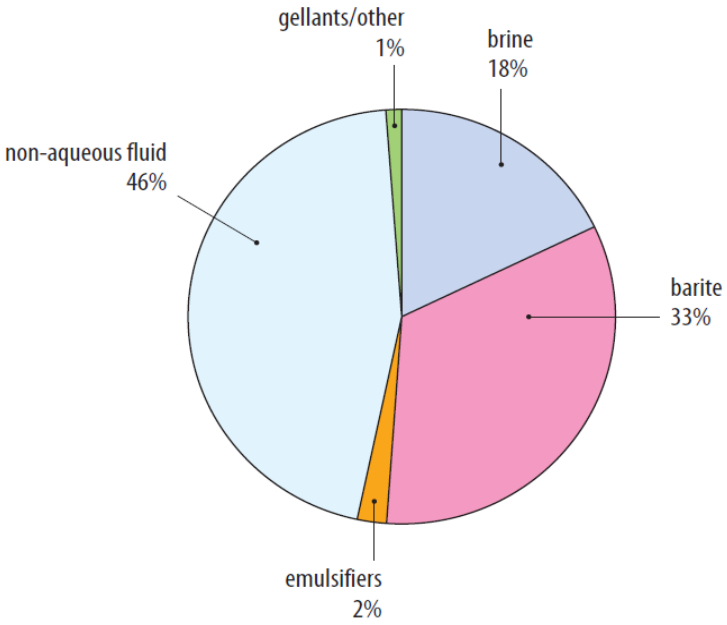


Figure 2.3: Typical composition of non-aqueous based drilling fluid (IOGP, 2009)

2.1.2.1 Oil Based Drilling Fluid

The oil base fluid is derived from crude oil through separation processes such as distillation and fractionation. The base fluid include diesel, mineral oil and hydro-treated mineral oil. Diesel based drilling fluids were extensively used offshore UK in the 1970's, but where phased out and banned in the mid 1980's due to their high aromatic content (5 – 35 wt%), and high toxicity levels to workers (HSE, 2000; IOGP, 2009). There has been a transition to base fluids with lower aromatic contents since then. For example, minerals oils, which are also produced from crude oil and are now commonly used, have 0.5-5 wt% aromatic content.

2.1.2.2 Synthetic Based Drilling Fluid

Synthetic base fluids are produced either from chemical reactions involving purified chemical feedstocks or from highly refined mineral oil in such a way that the base fluid has little or no connection with the original crude oil (HSE, 2000). Synthetic base oils are the latest type of base fluids due to increasingly strict regulations on the disposal of drill cuttings with toxic base fluids. Typically, the aromatic content of synthetic base oils is <0.5 wt%, and <0.001 wt% polycyclic aromatic content ((IOGP, 2009). Common components of synthetic oils include linear paraffins (LPs), linear alpha olefins (LAOs), Ethers, Esters, Internal olefins (IOs) and Acetals.

Chemical additives, such as potassium chloride and lignite, also have specific functions in drilling fluids just as important as the major components. Table 2-1 shows the function of the typical components and additives in drilling fluids (Neff, 2005; Growcock and Patel, 2011; IOGP, 2009; HSE, 2000; Ball et al., 2012).

Table 2-1: Typical components in drilling fluids and their functions

Component/Additive	Function
Base fluids	Transport drill cuttings back to the surface, cool the drill bit, provide lubricity, ensure thermal stability
Barite, calcium carbonate	Weighting agent – Provides hydrostatic head to ensure the pressure in the well is slightly higher than formation pressure
Bentonite (Clay), organic polymers, starch, gum	Rheology control – promotes thixotropy, and maintains the suspension of drill cuttings even when drilling stops
Calcium chloride, potassium chloride, Silicates, amines, glycols	Inhibition – promote shale formation stability by preventing reactive clays from swelling
Calcium hydroxide, sodium hydroxide, biocides, iron oxide	Corrosion control – maintains an alkaline pH to prevent corrosion damage to the drill pipe
Polyalkoxylated superamides, calcium soaps	Emulsifiers – ensures stability of the water in oil emulsion in non-aqueous based drilling fluids
Imidazoline derivatives	Oil wetting agent – ensures dispersed solids in drilling fluids are oil wet
Lignite, polymers, gilsonite	Fluid loss control – prevents base fluid loss when drilling through permeable and porous formations, maintains well bore pressure, reduces formation damage

2.2 Environmental Impact of drill cuttings

After the primary separation of drill cuttings from drilling fluids, some components of the drilling fluid are retained on the drill cuttings (Ball et al., 2012). Oil films form on the surface and within the pore structure of drill cuttings. This occurs due to the inherent limitations in the primary separation process. As a result, operators must meet environmental regulations regarding the impact of the additives and base fluid retained on the drill cuttings before disposal.

When water based drilling fluid is used, the resulting drill cuttings are generally regarded as environmentally friendly. However, some restrictions still apply, in for example, cadmium and mercury content in the barite used in formulating drilling fluid. Cadmium should be <3 mg/kg (dry basis), while mercury should be <1 mg/kg (dry basis) before disposing drill cuttings offshore (IOGP, 2016). The water content in drill cuttings varies significantly between geographical location and depth of the well, and can reach up to 30 wt%.

Drill cuttings can vary in particle size from <2 microns to the size of a gravel, with particle size distribution dependent upon the formation being drilled. Part of the limitations of the primary separation units on a drilling rig is the ineffective separation of smaller drill cuttings particles from the contents of the drilling fluid (Sadiq et al., 2003). Particularly problematic for operators is the retention of non-aqueous base fluid on drill cuttings, with a typical concentration of 5-15 wt% (Sadiq et al., 2003; IOGP, 2016). This can be problematic because of the environmental legislation preventing the offshore disposal of contaminated drill cuttings. In recent years the non-aqueous base fluid is either mineral or synthetic oil, as diesel has been phased out.

Several workers investigated the potential impact of the base oil on the marine environment, and found them to have low biodegradability, encourage anoxic conditions, and are highly toxic to the benthic community (Gerrard et al., 1999; Davies et al., 1984; Jorissen et al., 2009; Melton et al., 2000). Furthermore, high levels of hydrocarbon concentration that altered the diversity of benthic communities were found up to 5km away from drilling rigs (Gerrard et al., 1999; Neff, 2005; Gray et al., 1990). These findings led to discouraging offshore discharge and restricting the oil content of drill cuttings disposed offshore. In the European Union, starting from the year 2000, offshore discharge could only be carried out if the total oil levels are <1 wt% (OSPAR, 2000). In contrast the discharge limit is <5-6.9 wt% in the Gulf of Mexico (IOGP, 2016).

Operators in the UKCS regard the <1 wt% discharge limit as technically infeasible for existing technologies to treat the volume of oily drill cuttings generated. As a result, the majority of the oily drill cuttings are transported to shore for treatment and disposal.

Oil contaminated drill cuttings are stored in 6-10 tonne containers on the rig before offloading to a ship for transport to shore. A major drawback is space limitation on an offshore drilling rig, meaning that drilling activities may be stopped once the storage capacity is reached. This occurs frequently in harsh weather conditions, particularly in the UKCS, which means that offloading is restricted in this weather condition, and drilling can only continue before the deck storage capacity is exhausted. Moreover, the offloading of heavy storage containers from the drilling rig poses significant safety risks to workers. Given these unfavourable conditions, an offshore treatment technology is highly desired by operators.

2.3 Offshore Treatment and Disposal of Drill Cuttings

Treatment refers to the secondary treatment, after undergoing primary separation on the drilling rig. The two treatment methods used by operators to manage oil contaminated drill cuttings are cuttings re-injection and thermal desorption.

2.3.1 Cuttings Re-injection

Cuttings reinjection is a disposal method where drill cuttings are slurrified to reduce the particle size and produce a mixture that can be pumped into the subsurface (IOGP, 2016; Derrick, 2001; Gilmour, 2007). Re-injection is attractive because it ensures zero discharge into the sea bed, and eliminates the logistics associated with the ship to shore practice. It can be a particularly cost effective solution for drilling rigs isolated from alternative drill cuttings disposal infrastructure (Oil & Gas UK, 2016). A disadvantage of this technique is the use of dedicated injection wells which when blocked can shut down drilling operations. Also, there is a limit on the volume of drill cuttings that can be disposed via cuttings re-injection because only suitable dedicated wells and formations can receive, hold the drill cuttings slurry in place, and prevent leakages.

2.3.2 Thermal desorption

There has been concerted effort to use offshore treatment technologies in recent years, which is a consequence of the <1 wt% offshore discharge. One of such technologies is the thermomechanical cuttings cleaner. It operates by using mechanical rotating arms to generate heat from friction. Temperatures of 240 ^{o}C – 300 ^{o}C are generated in the desorption chamber, which volatilizes the oil and water content (IOGP, 2016). A study claimed that <1 wt% oil can be achieved using this

method (IOGP, 2016), however, it has a large deck space impact. Heat transfer limitations in the units mean long residence times, and hence the need for large-scale equipment. This is a major disadvantage, as this has confined installation to only a few drilling rigs with the space capacity. Another disadvantage is the noise pollution associated with the grinding action of the rotating arms. The limitations of the thermo-mechanical system provided the motivation for NOV Brandt to pursue a microwave heating technology as an alternative.

2.4 Onshore Treatment and Disposal of Drill Cuttings

Oil contaminated drill cuttings are categorised as hazardous waste as a result of their organic phase and drilling fluid additives. Onshore treatment techniques ensure that the oil content in drill cuttings meet the disposal requirements for hazardous wastes (Council Directive, 1999), which are increasingly prohibitive due to high costs required for industrial scale wastes. Drill cuttings are commonly disposed onshore by landfilling after the hydrocarbon component has been removed.

2.4.1 Treatment methods

There are a number of onshore treatment technologies that remove contaminants from drill cuttings or reduce contaminant mobility to prevent leaching after landfilling. They include bioremediation, solidification/stabilisation, solvent extraction and thermal desorption.

2.4.1.1 Bio-remediation

Bio-remediation is the natural decomposition of the toxic content of drill cuttings using organisms (fungi, bacteria) or their enzymes. Careful manipulation of the waste composition and the bio-remediation environment is needed for optimal

treatment (Ball et al., 2012). Studies have shown that treatment is slow and can take weeks to complete. For example, Rojas-Avelizapa, et al. (2007) showed that 180 days was required to remove 94% of hydrocarbon from contaminated soils, and Turner (2001) reported that 4 weeks was needed to remove 96% of oil from drill cuttings. This technique is attractive because it is not as energy intensive as other treatment options, however, it is slow and therefore unable to keep pace with the volume of drill cuttings currently generated. Another drawback to the bioremediation process is the significant land area required for disposal after treatment.

2.4.1.2 Solidification and Stabilization

Solidification and stabilization are a combined set of techniques used for physical and chemical immobilization of the oil contaminant in drill cuttings. This involves encapsulating the oil content within the matrix of the material and converting them into their least mobile or toxic form (Ball et al., 2012). The technique changes the physical and chemical structure of the drill cuttings material in order to isolate the oil contaminant within the matrix. Materials such as lime and fly ash are used to stabilize and solidify the drill cuttings material, after which they can be made into bricks, concrete or road bed materials. A major concern of using this technique is the possibility of contaminants leaching out in the long term. Also, the addition of materials in the encapsulation process tend to add to the volume of wastes overall.

2.4.1.3 Solvent Extraction

Solvent extraction is an ex situ process that exploits the miscibility of the contaminant oil of drill cuttings with solvents. Drill cuttings are washed in a liquid solvent usually at a temperature near the boiling point of the solvent. Oil dissolves in the solvent during the extraction process, and the oil-solvent mixture is separated

through a distillation or stripping processes. Solvents such as methanol, acetone and dichloromethane have been investigated in the past for the extraction of contaminants from contaminated soil and drill cuttings (Saim et al., 1997; Turner, 2001), with high oil removals reported. A drawback to this technique is that it uses large quantities of solvent which may cause further environmental problems. Furthermore, long residence times are needed which means that large equipment is required.

Other workers studied the effect of using supercritical fluid (carbon dioxide, propane) as the solvent when removing hydrocarbons from soil and drill cuttings, and discovered high levels of oil removal at lower residence times than liquid solvent extraction (Eldridge, 1996; Saim et al., 1997). Residence times of 6–10 hours for solvent extraction (Turner, 2001), and 0.5-3 hours for supercritical solvent extraction (Eldridge, 1996) have been reported. Microwave assisted solvent extraction on the other hand requires significantly lower treatment times (Sporring et al., 2005).

2.4.1.4 Thermal Treatment

Onshore thermal treatment technologies use heat to remove or destroy contaminants at high temperatures. Examples are pyrolysis, gasification, stripping, desorption and incineration (Ball et al., 2012). This technique is particularly suitable for materials with a high hydrocarbon content, such as drill cuttings. Incineration and thermal desorption are widely adopted for the treatment of drill cuttings in the UK (IOGP, 2016). An incinerator oxidizes waste at 820 ^{o}C-1600 ^{o}C, and as a result, destroys the contaminant and often, the structure of the material. Incineration of drill cuttings is generally not necessary except in sensitive environments where other disposal options are unavailable. The volume of solid

waste after incineration is greatly reduced, which is an advantage over thermal desorption. Nevertheless, thermal desorption enables recovery of the base fluid after treatment, which is crucial in drill cuttings management as the recovered base fluid can be recycled for use in formulating new drilling fluids. This is a major reason why many operators in the UK prefer thermal desorption units.

Thermal desorption vaporises the oil and water content of drill cuttings in a non-oxidising process at 250-600 ^{o}C (Ball et al., 2012). Heat is either supplied indirectly through hot fluids or direct electrical heating. Figure 2.4 schematic of a typical indirect thermal desorption unit.

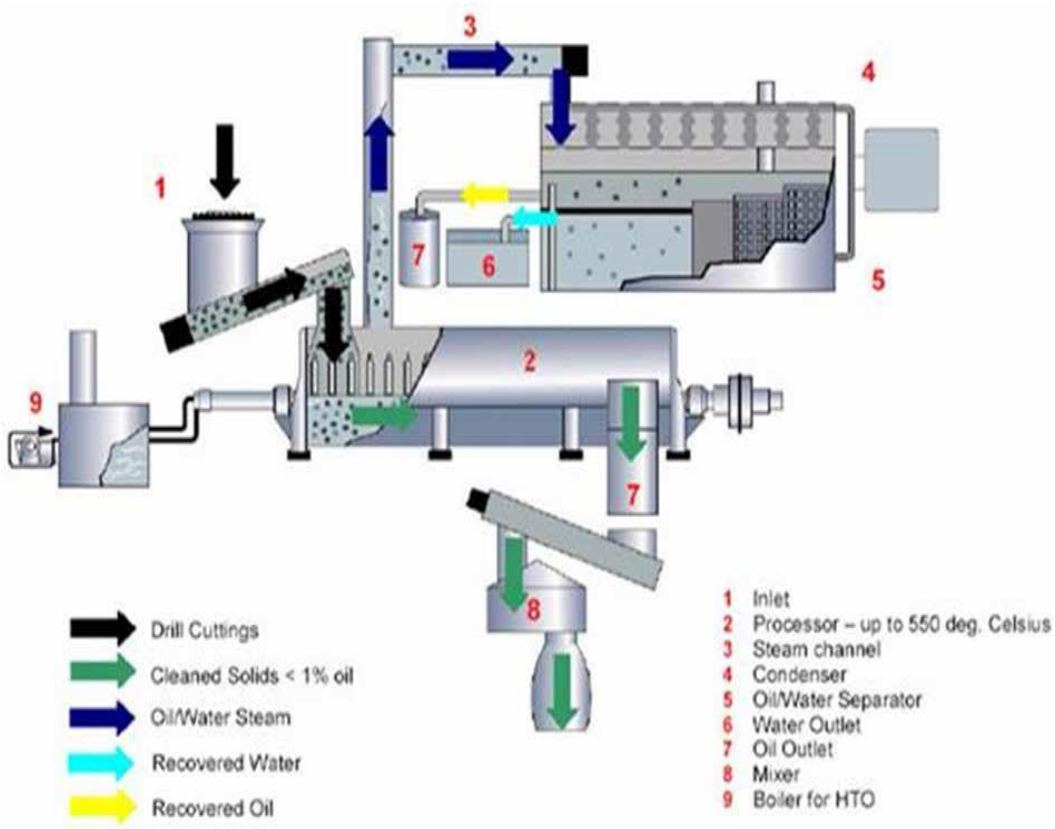


Figure 2.4: Schematic showing an indirect thermal desorption unit (IOGP, 2016)

Usually, an electrically heated rotating rotor is used to transport drill cuttings through the desorption unit to improve heat transfer to drill cuttings due to the poor heat transfer properties of drill cuttings.

Onshore thermal desorption plants are characterised by long processing times and large footprints which make them unsuitable for installation and use offshore. In contrast, a microwave process will provide fast heating times, high throughput, and can be retrofitted on existing drilling rigs. As the world population and world economy grow over the next two decades, energy consumption will increase by 34% on current levels (BP, 2016). This will be reflected in a 22% increase in daily oil consumption worldwide by 2035 (BP, 2016), which poses a significant challenge to oil and gas operators, as they need to increase the level of oil production while complying with environmental regulations like the OSPAR 2000/3 decision. A continuous microwave process installed offshore provides an opportunity for operators to replace the huge running costs associated with the ship to shore practise whilst enabling compliance with environmental legislation on offshore discharge of drill cuttings.

Chapter 3 Microwave Heating Review

Heating is a ubiquitous process in manufacturing and chemical industries, however, it still remains a difficult process to control and optimise. In conventional heating, energy is transferred to materials via conduction, radiation and convection. The rate of heat transfer from a surface is related to the specific heat capacity, thermal conductivity, and density properties of the surface heated. The combination of the three physical properties is regarded as the thermal diffusivity (Meredith, 1998). Thermal diffusivity determines the rate of temperature rise from the surface being heated, and it depends on the distance from the surface, and the heating time. A major disadvantage of conventional surface heating is that the rate of heat transfer to enclosed materials is dependent on the thermal gradient from the surface of the material. Once the maximum surface temperature is reached, internal temperature distribution is limited by the thermal diffusivity to the enclosed materials (Meredith, 1998). A common method of optimisation in conventional heating is to increase the area of the surface being heated. This only extends the heating times as the thermal diffusivity of the surface (now with a larger area) is still a limiting factor.

The thermal diffusivity limitations mean that surface heating is characterised by non-uniform temperature distribution in thick materials, with the surface and edges considerably hotter than the materials on the inside (Meredith, 1998). These limitations can render surface heating slow, imprecise and difficult to control (Meredith, 1998).

Microwave heating exploits the interaction of molecules with electromagnetic waves by delivering energy directly into material. In a heterogeneous, multiphase

system, only certain materials can absorb microwaves. This is referred to as selective heating. Moreover, volumetric heating occurs when all the elements in a volume of workload are heated individually at the same rate (Meredith, 1998). Clearly, this gives microwave heating some advantages over conventional surface heating as each component in a workload is heated electromagnetically, and is not limited by the rate of heat transfer from a working surface.

Other advantages of microwave heating include;

- Heating times during microwave heating can be reduced to less than 1% of the time required using conventional heating (Jones et al., 2002; Metaxas and Meredith, 2008)
- Volumetric heating leads to compact size equipment with reduced space impact (Metaxas amd Meredith, 2008; Thostenson and Chou, 1999; Kim et al., 2012)
- A microwave process is easy to control when compared with conventional processes (Jones et al., 2002).

3.1 Theory of Microwave Heating

Microwaves are electromagnetic waves which lie within the 300MHz – 300GHz frequency range in the electromagnetic spectrum (Figure 3.1), with corresponding wavelength is 1 mm–1 m. Frequency and wavelength of the microwaves are related by;

$$c = \lambda f \quad [3.1]$$

where λ is the wavelength in metres (m), c is the speed of light in free space (3 x 10^8 m/s), and f is the frequency in Hertz (Hz).

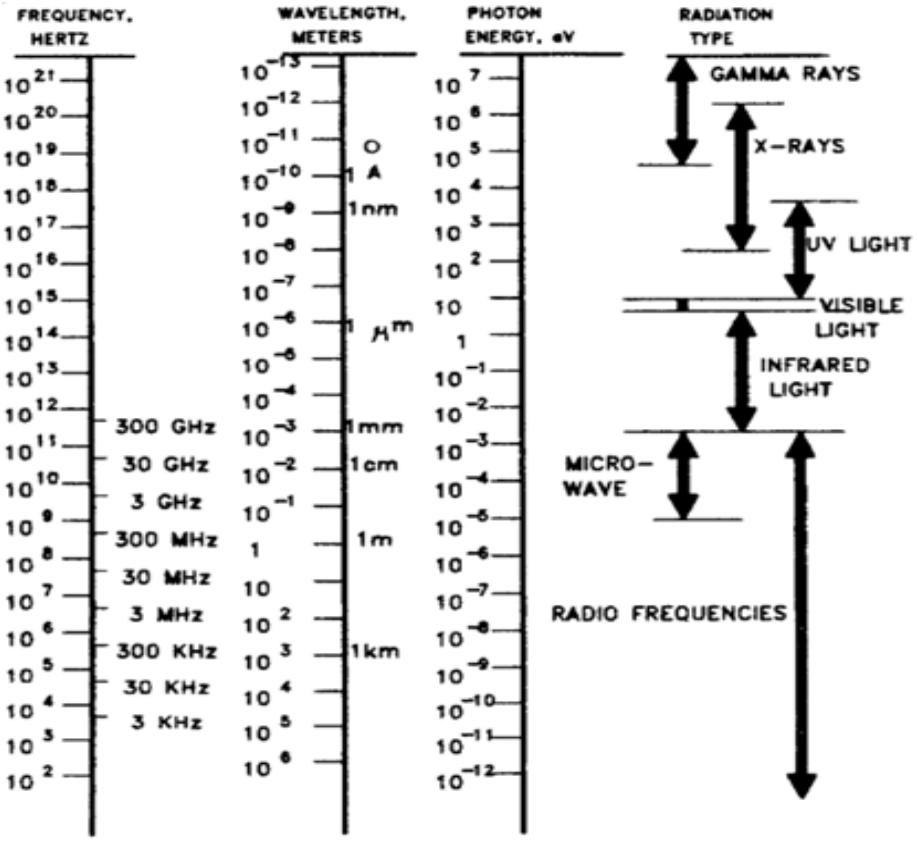


Figure 3.1: The electromagnetic spectrum (Metaxas and Meredith, 2008; Kim et al., 2012).

Microwave technology was predominantly focused in the area of navigation and communication for the military. But by the 1970's, the technology had developed in leaps and bounds to a point where the domestic use of microwave ovens was widespread. The frequency of microwaves used in industrial processing are chosen to minimise interference with communication services. In the United Kingdom, 896 MHz and 2.45 GHz are the frequencies used for microwave heating, which correspond to wavelengths of 33.4 cm and 12.2 cm. This can vary in other countries, for example, 912 MHz is the microwave heating frequency used in North and South America. These frequencies are designated as the industrial, scientific, and medical (ISM) frequencies, and are constantly reviewed by the relevant international communications bodies (Meredith 1998).

3.1.2 Material Interaction with Microwaves

The interaction of materials with the electric field component of microwaves lead to the dissipation of heat in some materials. Materials that absorb microwaves and convert it to heating are referred to as dielectrics (Jones et al., 2002; Daniel, 1967). Nonetheless, some materials do not absorb microwaves, or heat under the influence of microwaves. Figure 3.2 shows that materials are characterised into conductors, insulators and absorbers based on the nature of their interaction with microwaves.

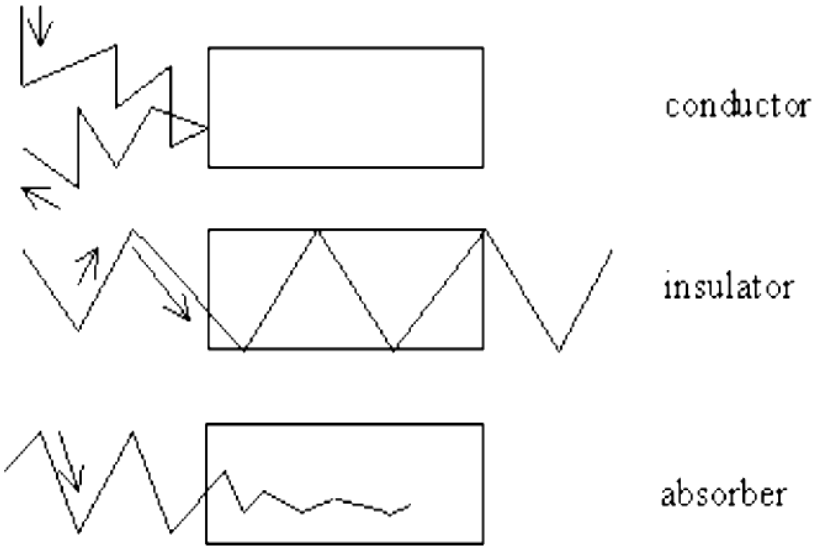


Figure 3.2: Categories of materials based on their microwave absorption characteristics (Jones et al., 2002).

Conductors, such as metals, reflect microwaves without absorption. Insulators are transparent to microwaves, of which quartz and teflon are good examples (Meredith 1998). Dielectric materials absorb and heat under microwaves due to the ability of the electric field component of microwaves to polarise charges in the material, and the inability of the polarisation to follow extremely rapid reversals of the electric field (Metaxas & Meredith 2008). Figure 3.3 shows an illustration of the polarisation that occurs within a dielectric material.

The mechanism of interaction with microwaves depends on the materials' geometry, mass and electron distribution. Two main mechanisms where microwave power is dissipated as heat energy in materials are dipolar polarisation and conduction mechanisms (Meredith 1998, Metaxas & Meredith 2008). Maxwell-Wagner polarisation can also occur but is not thought to be of great importance in industrial microwave heating.

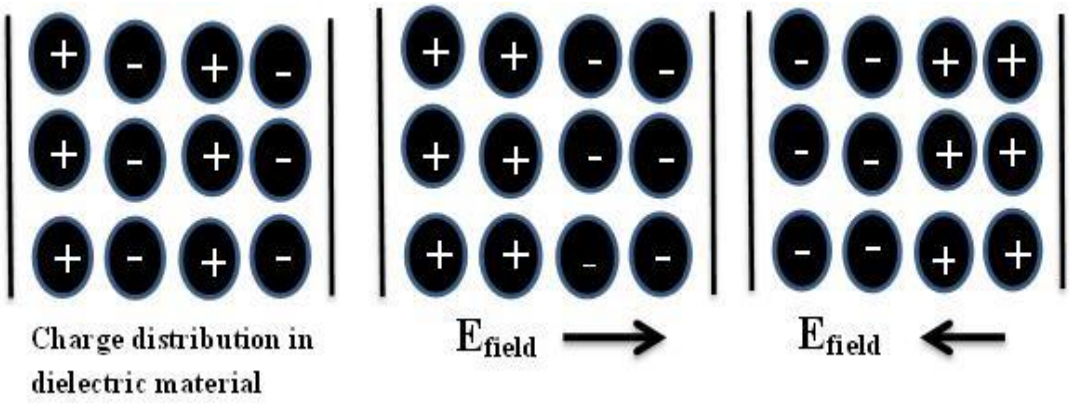


Figure 3.3: Schematic showing interaction between dielectric materials and microwaves.

3.1.2.1 Dipolar polarisation

This mechanism is very important because it is the most significant in industrial microwave heating at ≥1 GHz (Meredith, 1998). Dipolar polarisation or orientational polarisation occurs in materials with permanent or induced dipoles in their structure. The covalent bond in water molecule is an example of a permanent dipole. Figure 3.4 show that it has a non-linear structure and an angle of (θ)104.474^{o} in the HOH bond (Hasted, 1973).

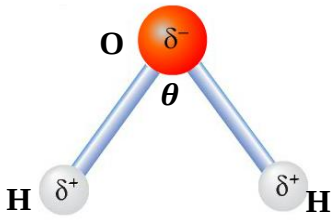


Figure 3.4: Structure of water showing the charge distribution (DoITPoMS, 2016).

Permanent dipole arises from the unique shape of the water molecule (atoms at a finite distance apart), and the differences in electronegativity of the constituent atoms. When an external alternating electric field is applied across the water molecule, it attempts to respond by rotating in the direction of the applied electric

field. The water molecule realigns constantly in order to keep up with the alternating electric field. Thus energy is dissipated in the dielectric due to frictional losses between the rotating molecules. There is a lag between the frequency of the applied electric field and the frequency of molecular rotation, which is referred to as relaxation time (Daniel, 1967). If the molecule is able to keep pace with the frequency of the applied electric field, then, there is no relaxation, and hence no heat losses. Gases realign rapidly, but, this is more difficult in liquids because of the close proximity of other molecules. This is why dielectric relaxation causes heating in liquids with dipoles. Molecular rotations are usually restricted in solids, as a result, dipolar polarisation generally do not contribute to storing or converting microwave power to heat in solids (Gabriel et al., 1998).

Electric fields can induce polarisation by distortion of the electron distribution in the molecule. This is more common in non-polar molecules with atoms of similar electronegativity. The induced dipole allows the molecule to respond to an electric field stimulus like a polar molecule. However, polar molecules, such as water, are able to respond quicker to an electric field stimuli when compared with non-polar molecules with induced dipoles.

3.1.2.2 Ionic Conduction

When microwaves are applied to dielectric materials with mobile charge carriers (ions, electrons), there is translational motion of these carriers within the material (Gabriel et al., 1998). Polarisation of these charges arise from the extreme reversals of the applied electric field. The movement of the charges under the electric field stimulus is akin to current flow, with heat being generated from resistance to the flow of charges in the dielectric material. This mechanism can become more dominant than dipolar polarisation in solutions containing large amounts of ionic

salts (Stuerga, 2006). The dependence of conduction on temperature and frequency is discussed later.

3.1.2.3 Interfacial Polarisation

Interfacial polarization or Maxwell-Wagner is a complex mechanism that occurs as a result of charge build-up in interfaces between components in heterogeneous, multiphase system (Metaxas and Meredith, 2008). Interfacial polarisation has been identified as the reason for enhancement in microwave absorption observed in a heterogeneous mixture of immiscible solvents (polar and non-polar) (Stuerga, 2006). The enhanced microwave absorption was thought to be as a result of the interfacial interaction between the macroscopic bubbles of the two liquids. It is important to note that this mechanism will not occur in a homogeneous system, in for example, pure water or sodium chloride. Interfacial polarisation mechanism occurs simultaneously along with dipolar and conduction mechanisms in multiphase systems but are thought to be insignificant, in terms of their contribution to heating in industrial microwave processing.

3.1.3 Dielectric Properties

There are two components to the definition of dielectric properties; firstly, it indicates the ability to be polarised under the stimulus of an alternating electric field (illustrated in Figure 3.3). This is referred to as dielectric constant, and is represented as (ε') (Metaxas and Meredith, 2008; Nelson, 1994). Polarisation here refers to the ability to store microwave energy. This is similar to the ability of a capacitor to reduce the electric field across it when under the influence of an alternating current. Secondly; it indicates the ability of the material to convert the stored microwave energy into heating. This is defined as the dielectric loss factor, represented as $(\varepsilon^{"})$.

The dielectric loss factor $(\varepsilon^{"})$ and dielectric constant (ε') are related by the complex dielectric constant or complex permittivity (ε^{*}) as follows;

$$\varepsilon^{*} = \varepsilon' - j\varepsilon^{"} \quad [3.2]$$

Where the dielectric constant is the real part, and the loss factor is the imaginary part of equation 3.2.

The dielectric constant (ε') is actually the ratio of the absolute dielectric constant (ϵ) of a material to that of free space (ε_o) as shown in the following equation;

$$\varepsilon' = \frac{\varepsilon}{\varepsilon^{o}} \quad [3.3]$$

Conductivity (σ) is related to the dielectric loss factor as shown in equation 3.4;

$$\varepsilon^{"} = \frac{\sigma}{\varepsilon_o f} \quad [3.4]$$

where f is the microwave frequency.

Consider two materials with different dielectric constant values, the velocity of microwave propagation (v_m) in the material with the lower dielectric constant will be faster. Meaning that attenuation of the waves will occur at a greater distance from the surface in the material with lower dielectric constant. The relationship between velocity of microwave propagation in a material and its dielectric constant is shown in equation 3.5;

$$v_m = \frac{1}{\sqrt{\mu\varepsilon}} \quad [3.5] \quad \text{(Nelson, 2010)}$$

where μ is the magnetic permeability, and ε is the dielectric constant.

The loss tangent ($\tan\delta$), or dissipation factor, is a parameter that is helpful in determining the heating rate in dielectric materials. If two materials have similar dielectric constant values, but vary to some extent in dielectric loss factor, the loss tangent can be used to determine which of the materials will heat faster under microwaves.

The loss tangent is defined as;

$$\text{loss tangent } (\delta) = \frac{\varepsilon^{"}}{\varepsilon'} \qquad [3.6] \text{ (Gabriel et al., 1998)}$$

It is important to note that while loss tangent is a useful parameter in assessing the heating rate of materials, other physical properties such as the heat capacity and density may be required in order to determine reliable heating rates.

Dielectric properties are affected by several factors including water content, density, temperature, and frequency of the incident wave.

3.1.3.1 Variation of dielectric properties with water content

The amount of water in a material exerts a dominant influence on the dielectric properties of the material. This is because water is an efficient microwave absorber. For example, at 3 GHz, water has a dielectric constant of 77.7 and a loss factor of 13 at 20^{o}C (Hasted, 1973; Nelson and Trabelsi, 2012). On the other hand, the dielectric constant of dry sand is 2.55, with a loss factor value of 0.016 at 25^{o}C at the same frequency (Metaxas and Meredith, 2008). The permittivity (ε) of water-saturated sand sample may be estimated from equation 3.7;

$$(\varepsilon)^{\frac{1}{2}} = v_1(\epsilon_1)^{\frac{1}{2}} + v_2(\varepsilon_2)^{1/2} \qquad [3.7] \text{ (Nelson, 1994)}$$

Where v_1 and v_2 are the volumetric composition of the components, and $\varepsilon_1$and ε_2 represent the permittivity of the components. It is clear from equation 3.7, based on the high dielectric constant and loss factor of water, that the amount of water present in the sand-water mixture will have a dominant effect on the dielectric properties of such mixture.

Increasing water content leads to higher dielectric properties (Hallikainen et al., 1985; Robinson et al., 2002). This is shown in the data in Figure 3.5.

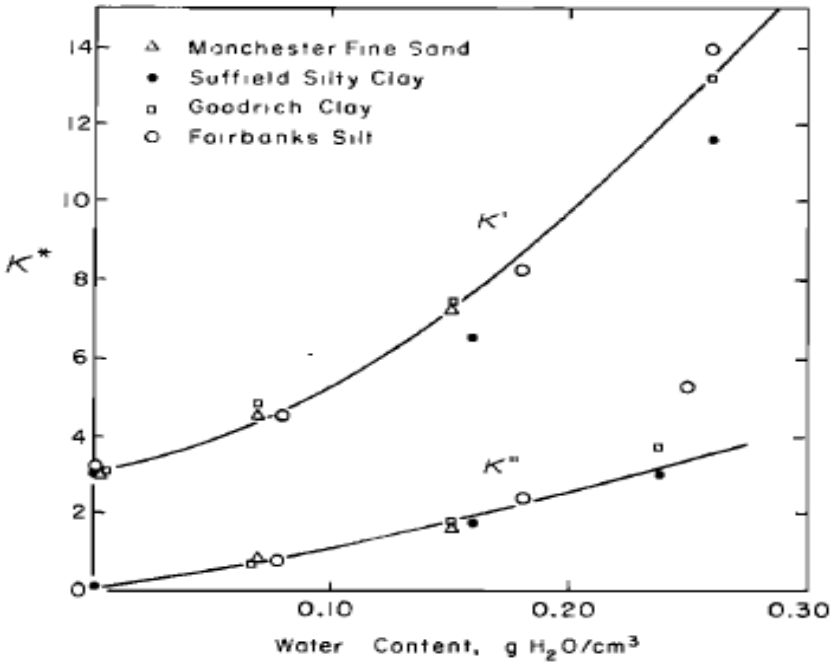


Figure 3.5: Variation of dielectric properties of soil with moisture content at 10°C and 4 GHz. K* is the complex permittivity, K' is the dielectric constant, K" is the dielectric loss factor (Hoekstra and Doyle, 1971).

3.1.3.2 Variation of dielectric properties with frequency

The frequency dependence of the dielectric properties of materials have been studied extensively (Nelson, 1994; Nelson and Trabelsi, 2012; Gabriel et al., 1998; Stuerga, 2006; Metaxas and Meredith, 2008). The frequency of the incident wave determines how the dielectric material is able to respond to the electric field stimulus. In other words, frequency determines the relaxation time of the dielectric material. Recall that relaxation time is the time taken for the dielectric material to align in the direction of the applied electric field. The relaxation time and frequency of electromagnetic wave is related to the dielectric properties of a material in equations 3.8 and 3.9 as follows;

$$\varepsilon' = \varepsilon_\infty + \frac{\varepsilon_s - \varepsilon_\infty}{1+\omega^2\tau^2} \quad [3.8]$$

$$\varepsilon'' = \frac{(\varepsilon_s - \varepsilon_\infty)\omega\tau}{1+\omega^2\tau^2} \quad [3.9]$$

where τ is the relaxation time, $\varepsilon_s$and ε_∞ are the values of complex permittivity at extremely low frequencies or a 'static system' ($\ll \tau^{-1}$) and high frequencies ($\gg \tau^{-1}$), ω is the angular frequency.

At extreme microwave frequencies (too high or too low), dielectric materials, especially polar liquids, may not heat under microwaves. At low frequencies the electric field component of microwave alternates very slowly which means that the period of change of the electric field is much longer than the relaxation time. The polarization of the irradiated molecule can keep pace with the alternating electric field, hence frictional losses are minimised, and little or no heating would occur. The period of change of the electric field at extremely high frequencies is a lot quicker than the relaxation time. The relaxation polarization cannot keep pace with

the period of change of the alternating electric field, therefore there is no tangible heat dissipation. The optimum permittivity ε^* and maximum dielectric loss factor value for a polar substance is at frequency(f), where $\varepsilon_s < \varepsilon^* < \varepsilon_\infty$.

Industrial high frequency heating takes place in the frequency range of $10^7 < f < 3 \times 10^9$ Hz, where the mechanism of converting microwave power to heat is dominated by dipolar polarisation (Meredith, 1998; Gabriel et al., 1998). This means that materials containing water will respond well and heat under microwaves, as illustrated in the variation of dielectric properties of water with frequency in Figure 3.6. Conduction and Maxwell-Wagner loss mechanisms occur to a lesser extent in the industrial microwave frequency range, with conduction being the dominant loss mechanism at frequencies $< 10^7$Hz (Meredith, 1998).

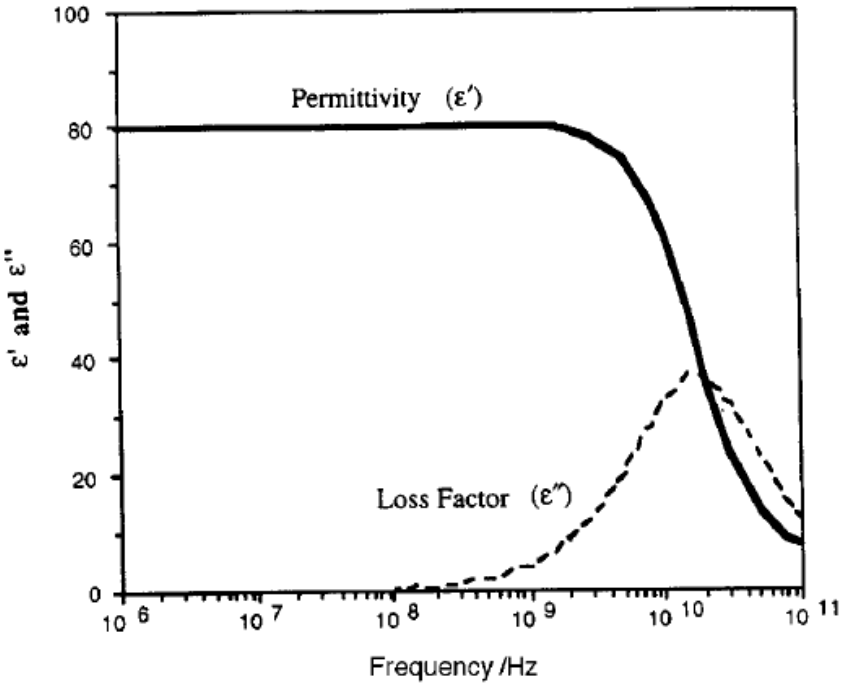


Figure 3.6: Variation of the dielectric constant and loss factor of water with frequency at 20°C (Gabriel et al., 1998).

3.1.3.3 Variation of dielectric properties with temperature

In materials consisting of polar molecules, there is a significant variation of dielectric properties with temperature. In liquid water at 20ºC, for example, there is random thermal motion of molecules in the settled state. Under the influence of an electric field, the molecules rotate and align in the direction of the field, however, the thermal motion of the molecules will still have an influence. In this case not all molecules will be perfectly aligned with the electric field, and the permittivity is in fact a reflection of the average orientation of the molecules. As temperature increases from 20 ºC, the thermal motion of the molecules increases, hence the relaxation time decreases (Nelson, 1994; Hall et al., 1999). This leads to increased deviation from an ideal alignment of the polar molecules with the electric field, and as a result, dipolar polarisation is not fully exploited and dielectric constant decreases. Table 3-1 (Hasted, 1973) shows that the dielectric loss factor and dielectric constant of liquid water decreases with increasing temperature.

Table 3-1: Variation of the dielectric properties of water with temperature at 3GHz.

Temperature (ºC)	**Dielectric constant (ε')**	**Dielectric loss factor (ε'')**
0	80.2	24
10	79.4	17.5
20	77.7	13
30	75.3	9.9
40	72.6	7.55
50	69.7	5.95
60	66.4	4.6

Relaxation times in solids have also been found to decrease as temperature increases, which results in an increase in dielectric constant (Bottcher and Bordewijk, 1978; Nelson, 1994). This does not apply to the dielectric loss factor. It may increase or decrease depending on thermal effects on the structure of the solids. Predicting this is complicated, therefore, empirical data is the most reliable way of determining the effect of temperature on the dielectric loss factor at high temperatures.

Some workers have developed models to estimate the effect of temperature of dielectric materials. For example, the effect of temperature on the relative permittivity of bulk water over temperature can be estimated from equation 3.10 (Wraith and Or, 1999). Others have developed models linking the dielectric constant and loss factor of materials with temperature (Sheng et al., 2013). The models are useful in predicting the dielectric properties but often have limitations.

$\varepsilon'(\mathrm{T}) = 78.54\ [1\text{-}4.579 \times 10^{-3}(\mathrm{T}\text{-}25) + 1.19 \times 10^{-5}\ (\mathrm{T}\text{-}25)^2 - 2.8 \times 10^{-8}\ (\mathrm{T}\text{-}25)^3]$ [3.10] (where $\varepsilon'$the static dielectric constant of water, and T is in degree celsius)

3.1.3.4 Variation of dielectric properties with density

The mechanism through which dielectric materials dissipate microwave power as heating depends on the close interaction of the components in a material. Gases, for example air at standard temperature and pressure, are known to have low dielectric properties. This can be related to the fact that air has relatively low density. The density of dielectric materials has an effect on their dielectric properties (Nelson, 1994). The effect of density on the dielectric constant of yellow corn was investigated by Nelson and Trabelsi (2012) and shown in Figure 3.7. Clearly,

increasing density leads to increasing dielectric properties. The relationship with density is very useful in determining the dielectric properties of granular samples such as soil and crop grains.

Sacilik, et al. (2007) also noted that the dielectric loss factor of safflower seeds increased with increasing bulk density. This can be attributed to the low air volume composition at high bulk densities, since air is a poor dielectric ($\varepsilon' = 1, \varepsilon'' = 0$).

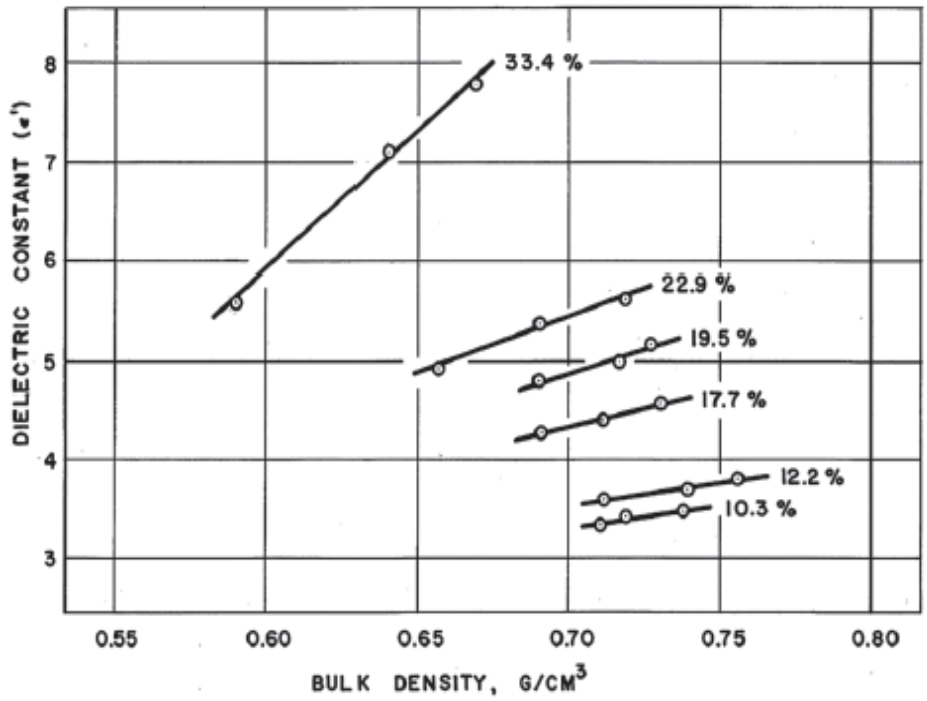


Figure 3.7: The variation of the dielectric constant of yellow corn with bulk density. Measurements at 24ºC and 20MHz (Nelson and Trabelsi, 2012).

3.1.4 Dielectric properties of soil

Soil components include kaolinite, montmorillonite, quartz, calcite, muscovite and iron oxides (Robinson, 2004; Grim, 1968), which are similar to the components in drill cuttings (Pereira, 2012). The similarity between the mineral compositions of soil and drill cuttings makes it useful to understand the dielectric properties of soil. It provides an understanding of how drill cutting will interact with microwaves during microwave processing. Several workers have researched the dielectric properties of unsaturated soil (Hallikainen et al., 1985; Dobson et al., 1985; Hoekstra and Doyle, 1971; Saarenketo, 1998; Robinson, 2004). The dielectric properties of the mineral components of soil is generally low. For example, the dielectric constant and loss factor of dry sand is 2.55 and 0.016, and 2.280 and 0.026 for calcite at 25^0C (Erle et al., 2000; Metaxas and Meredith, 2008). This indicates that dry drill cuttings may not heat under microwaves.

The dielectric properties of soil generally increases with increasing moisture content. It was found that the state of the water content in soils affects the dielectric properties (Saarenketo, 1998). Water is either free, physically bound or chemically bound in a porous media like soil or drill cuttings. The loss mechanisms of physically bound water, i.e water either adsorbed to the mineral surface or whose free movement is restricted in the soil pores, occurs at a lower microwave frequency and higher temperature when compared to free water (Metaxas and Meredith, 2008). Thus, if two soil samples with similar mineralogy and the same water content were tested for their dielectric properties, the sample with the greater amount of free water will absorb more microwaves, so far temperature and frequency are unchanged.

It has been shown that a greater amount of water in soil generally increases the dielectric constant and loss factor (Saarenketo 1998), which indicates that higher water content in drill cuttings is beneficial for microwave heating.

3.2 Microwave Heating Systems

The basic components of a kitchen microwave are similar to what obtains in an industrial microwave system. From Figure 3.8, the components of a microwave system includes the magnetron (microwave generator), waveguides (or transmission lines), and an applicator (cavity) where the interaction of materials with microwaves occurs.

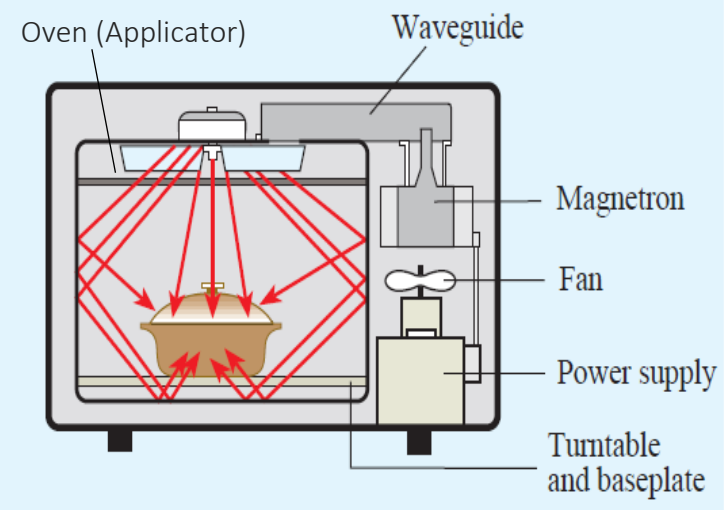


Figure 3.8: Schematic of a typical domestic microwave oven (Vollmer, 2004).

3.2.1 Microwave Generators

Types of microwave generators available in the market currently are magnetrons, travelling wave tubes (TWTs) and klystrons, with magnetrons being the most common (Thostenson and Chou, 1999; Vollmer, 2004; Chandrasekaran et al., 2012). These generators are vacuum tubes that produce microwaves from charge

acceleration. Figure 3.9 is a schematic of magnetron, which shows a cylindrical cathode some distance from a hollow circular anode. The anode has a number of cavities designed to resonate at a specified frequency, this is because magnetrons can only operate at a single frequency

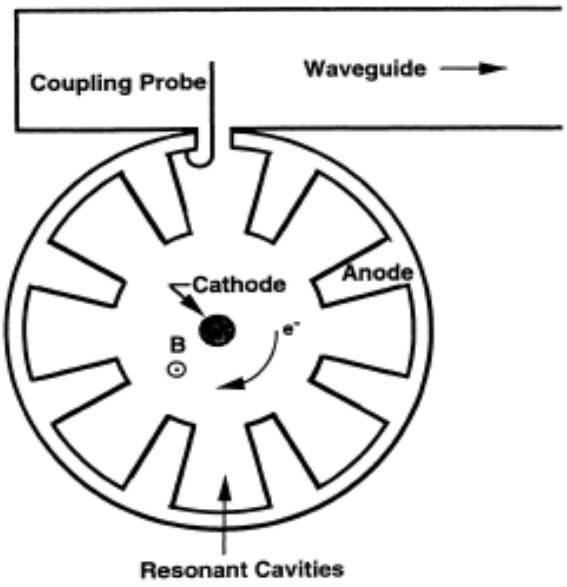


Figure 3.9: Schematic of a magnetron (Thostenson and Chou, 1999).

Several Kilovolts are applied between the electrodes, and a magnetic field is applied parallel to the axis of rotation such that magnetic and electric fields are perpendicular to each other. This causes electrons to be removed from the cathode and accelerated towards the anode. The electrons produced are forced to pass through the resonant cavities due to the effect of the magnetic field. The cavities set up oscillations in the electron cloud as the electrons pass through them (Thostenson and Chou, 1999). The microwave energy produced is coupled from a resonant cavity and transmitted through the waveguide.

3.2.2 Waveguides

Waveguides, an example of transmission lines, act as a conduit for electromagnetic waves from the generator to the workload. They are made of metals and come in different sizes. In this work, hollow rectangular waveguides are used, and their dimensions depend on the frequency of the microwaves propagating through it (Metaxas and Meredith, 2008). Consider the rectangular waveguide in Figure 3.10, the width of the waveguide (**a**) is related to the wavelength of the microwaves in;

$$a = n\frac{\lambda}{2} \qquad [3.11]$$

where λ is the wavelength, and n is the number of half wavelengths. The minimum value of n is 1, meaning that microwaves will not propagate if **a** is less than half wavelength.

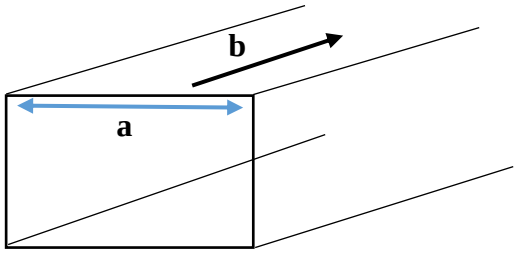


Figure 3.10: Schematic of a hollow rectangular waveguide. b is the direction of microwave propagation

The minimum width of the waveguide (**a)** at 896 MHz is 16.7 cm, and 6.1 cm at 2.45GHz.

Waveguides are made of metals because they reflect microwaves, and consequently, electric fields reduce to zero on their surface (Metaxas and Meredith, 2008). In theory, microwaves can be propagated through the waveguides without any loss in power. In practice, negligible power may be lost through microwave penetration in a small layer of the metal. This is measured by skin depth (δ_s)which

shows the depth at which the electric field is attenuated by 1/e from the surface, and defined in equation 3.12 (Metaxas and Meredith, 2008) as;

$$\delta_s = \sqrt{\frac{2}{\sigma\omega\mu_o}} \qquad [3.12]$$

where σ is the conductivity of the material, ω is the angular frequency, and μ_o is the permeability of free space. To put this into perspective, the skin depth for metals is approximately 10^{-6}m, meaning that power loss in metal waveguides is negligible.

There are two possible modes of microwave propagation in a rectangular waveguide: transverse electric mode (TE), and transverse magnetic mode (TM). The electric field intensity is zero in the direction of propagation for the TE mode, while the magnetic field intensity is zero in the direction of propagation for the TM mode. Figure 3.11 shows typical TM and TE mode propagation in waveguides.

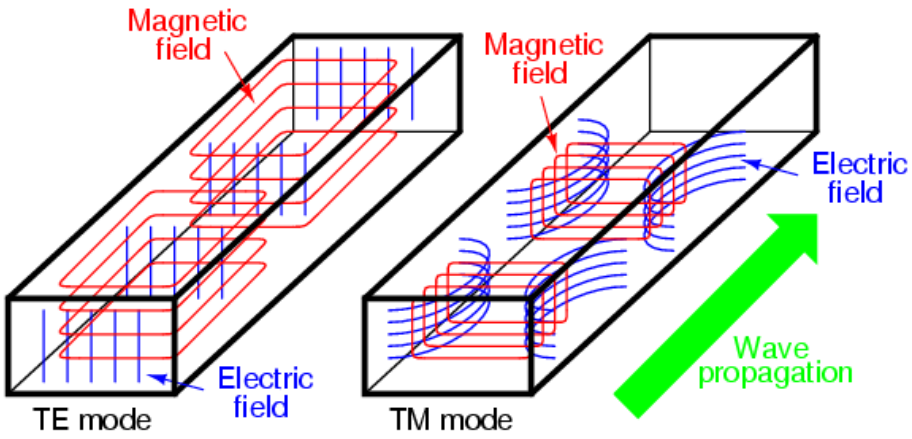


Figure 3.11: Propagation of microwaves in waveguides at TE and TM modes (All About Circuits, 2016).

3.2.3 Microwave Applicators

A microwave applicators (cavity) is a chamber within the microwave system where the dielectric material interacts with microwaves. Types of microwave applicators include travelling wave applicators, multimode applicators, and single mode applicators (Metaxas and Meredith, 2008). The factors that separate the applicator types are the applicator volume, electric field intensity, and power density distribution. These factors allow applicators to be selected based on their suitability for a process.

3.2.3.1 Multi-mode applicators

The field pattern distribution in an applicator is referred to as the mode. For example TE_{20} refers to two half wavelengths of the electric field as standing waves in the applicator. This means that '2 electric field patterns' will be supported in the applicator. Applicators that support several modes are referred to as multi-mode. TE_{10} represents the distribution of only one mode in the applicator, which is supported in a single mode applicator. Multi-mode applicators, such as the domestic kitchen microwave, are very popular. They are closed metal boxes whose dimensions are several wavelengths long in at least two dimensions. As a result, multi-mode applicators are usually larger than one wavelength of microwaves, with a substantial volume (Thostenson and Chou, 1999).

The design of applicators has to take the field distribution and damping when dielectric materials are introduced into consideration. Figure 3.12 shows sharp resonance modes in an empty multimode applicator at f_1 and f_2, and the damping and shift in resonance frequency when a dielectric workload was added. This is a common phenomenon with all types of applicators, which may lead to inefficient energy absorption in the workload if not considered. Nonetheless, impedance

matching is employed to ensure that the system energy loss that may occur from the shift in resonant frequency is minimised.

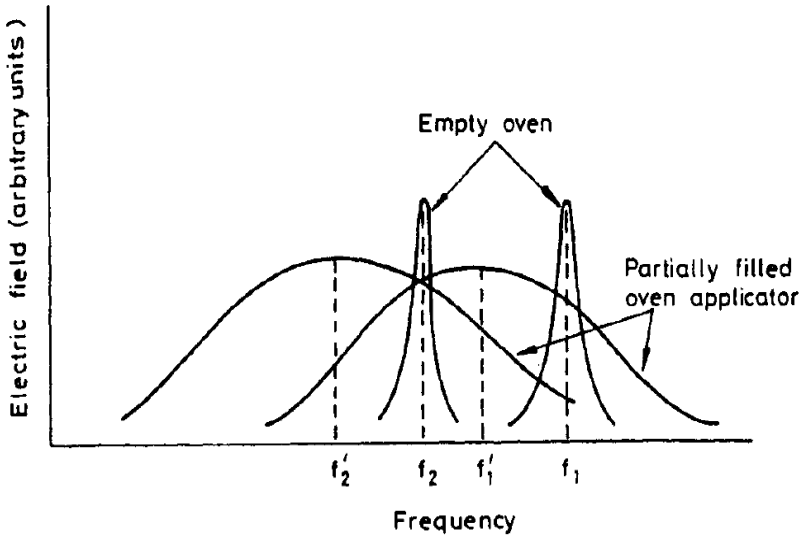


Figure 3.12: Damping and frequency shift of mode patterns in a multimode applicator due to the effect of loading a dielectric material (Metaxas and Meredith, 2008).

In practise, impedance matching is carried out by comparing the forward and reflected power between the generator and the sample load in the system. The ideal sample location within the applicator results in minimum energy loss within the system (Metaxas and Meredith, 2008).

The multi-mode applicator has the simplest design amongst all the types of applicator. It is versatile, and a wide variety of dielectric samples can be processed in it. A major disadvantage is non-uniform heating due to the multiple mode patterns, and consequently, several hot spots within the applicator (Dubey et al., 2016; Bradshaw et al., 1997; Mehdizadeh, 2015). This leads to varying temperature distribution within the treated material. Figure 3.13 shows a typical electric field

distribution in a multi-mode applicator. The temperature in a dielectric material positioned at the antinodes (highest electric field intensity) will be high in contrast to the low temperatures at the nodes, where little or no heating takes place.

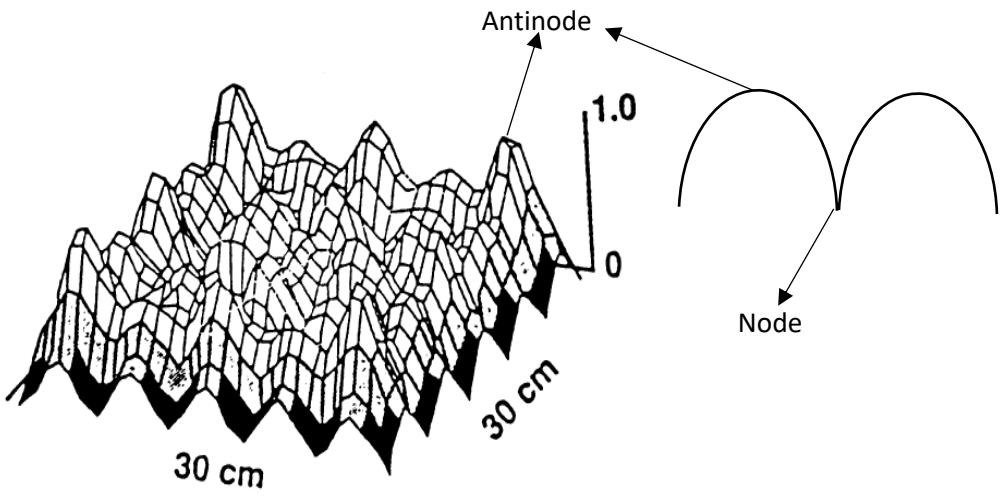


Figure 3.13: Electric field distribution in typical multimode oven at 2.45GHz (adapted from Thostenson and Chou, 1999).

Many methods are employed to achieve uniform heating in a multi-mode applicator. For example, the kitchen microwave uses a turntable to rotate samples in order to achieve uniformity in heating. The travelling wave and single mode applicator are used in several applications as an alternative to improve uniformity in heating and power density distribution. Power density is discussed in detail in section 3.2.4.

3.2.3.2 Single mode applicators

Singe mode applicators are also referred to as resonant applicators as they support only one resonant mode. This means that operating a single mode applicator at varying frequencies, although possible in multi-mode applicators, is infeasible (Thostenson and Chou, 1999; Metaxas and Meredith, 2008). Single mode applicators are designed to approximately the size of one wavelength, at the

resonant frequency of the system, invariably leading to a small sized, compact applicator (Thostenson and Chou, 1999).

A single mode applicator will establish a greater electric field intensity for the same power input than multi-mode and travelling wave applicators, meaning that single mode applicators can be successfully used to treat materials with low loss factors. The electric field distribution in a single mode applicator are predictable by solving the relevant Maxwell equations. This is an advantage, as the location of low electric field and the high electric field ('only hot spot') within the structure can be predicted (Metaxas and Meredith, 2008). Researchers have been able to focus the microwave electric fields in a single mode applicators in order to utilise the high electric field strength. Thostenson and Chou (1999) mentioned the joining of ceramics by concentrating microwave energy in the surfaces to be joined and not heating the bulk material, Robinson, et al. (2015) induced high heating rates in biomass samples when placed in the area of high electric field intensity in a single mode applicator.

Another advantage is that high power densities of the order of 10^7 kW/m^3 can be reached in single mode applicators, which can be considerably higher than the power densities obtainable in other types of applicators (Metaxas and Meredith, 2008). A disadvantage is the non-uniformity of heating patterns that may occur. This occurs because of uneven field distribution; the materials in the high electric field intensity zone are well-treated, while materials near the walls of the applicator receive insufficient microwave energy. Small sample sizes located in the high electric field zone is a technique that has been used to overcome this, but that invariably limits the sample size.

3.2.3.3 Travelling wave applicators

Travelling wave applicators are often used in continuous microwave processing with a conveyor system. Their efficiency depends on the dielectric properties (dielectric constant and loss tangent) of the samples. Figure 3.14 shows a schematic of a travelling wave applicator.

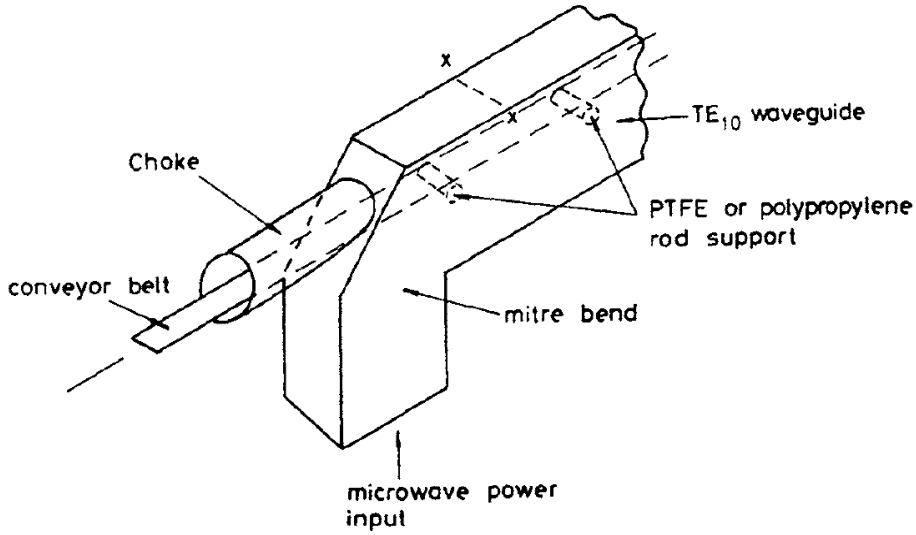


Figure 3.14: Schematic of a travelling wave applicator (Metaxas and Meredith, 2008). Choke prevents microwave leakage; PTFE support is microwave transparent.

Generally, the electric field strength and field distribution is not as defined as in a single mode applicator. However, high electric fields similar to that of a single mode cavity can be produced by fitting an aperture plate at the generator end, and making other adjustments as detailed in (Metaxas and Meredith, 2008). This means that low loss factor materials can be processed in a travelling wave applicators. There are several applications of travelling wave applicators in literature (Metaxas and Meredith, 2008), including the continuous processing of oil contaminated drill cuttings (Robinson et al., 2009a; Robinson et al., 2010)

3.2.4 Power density and Penetration depth

Power density is a measure of amount of energy that can be dissipated in a volume of dielectric material. It is a reflection of the dielectric properties of the treated material and the design of the applicator. Power density can be estimated from;

$$P_d = 2\pi f \varepsilon_o \varepsilon^{"} |E|^2 \quad [3.13]$$

where P_d is the power density (kW/m^3), and E is the electric field strength (kV/m). Clearly, the electric field intensity has the greatest effect on the power density in equation 3.13 because doubling the electric field intensity will result in a fourfold increase in power density. The power density is also affected by the frequency of the microwaves and the loss factor of the workload. A higher loss factor ($\varepsilon^{"}$) will lead to greater power density.

The power density can be used to estimate the heating rate during processing, as follows in equation 3.14 (Metaxas and Meredith, 2008);

$$\frac{\Delta T}{\Delta t} = \frac{P_d}{\rho c_p} \quad [3.14]$$

where ΔT is the change in temperature in the material heated (K), Δt is the duration of microwave heating (s), ρ is the material density (kg/m^3) and C_p is the specific heat capacity of the material (kJ/kgK). The full derivation of equation 3.14 is in appendix 4.

The amount of power dissipated in a sample, and temperature distribution within the sample is affected by the ability of microwaves to penetrate the material. This phenomenon is the penetration depth, and is defined as the distance from the surface of the material at which the incident microwave power reduces to 1/e (37%) of its value at the surface. It follows then that the absorbed power at the penetration depth

is approximately 63%. Penetration depth (D_p) is affected by the dielectric properties of the treated material, with equation 3.15 (Risman, 1991) showing the relationship between penetration depth and dielectric properties.

$$D_p = \frac{\lambda}{2\pi(2\varepsilon')^{1/2}} \left[(1 + (\tan\delta)^2)^{1/2} - 1\right]^{-1/2} \qquad [3.15]$$

where λ is the free-space wavelength (12.2cm at 2.45GHz, and 33.4cm at 896MHz). Equation 3.15 is suitable for dielectrics with loss tangents greater than 1. For low loss dielectrics with loss tangent $\ll 1$, equation 3.16 (Robinson et al., 2012; Risman, 1991) gives the appropriate penetration depth correlation.

$$D_p = \frac{\lambda\sqrt{\varepsilon'}}{2\pi\varepsilon''} \qquad [3.16]$$

When treating materials with a high loss factor (ε''), penetration depth is lower, and vice versa for materials with low loss factor. For high loss materials where the penetration depth is small, there is non-uniformity in the heating and temperature distribution in the workload, especially workloads with appreciable depth. For example during microwave drying of a workload with high water content (highly absorptive of microwaves), the bulk of the power will be dissipated in the water phase near the surface of the material. Nonetheless, the penetration depth improves over treatment time as water evaporates.

A loss factor value of $0.01 < \varepsilon'' < 5$ is recommended in industrial microwave heating to avoid non-uniformity in heating that may be brought about by low penetration depth (Metaxas and Meredith, 2008).

3.2.5 Thermal runaway and Arcing

The uncontrolled rise in temperature in a material during microwave heating is thermal runaway (Meredith, 1998). As temperature increases during treatment, the dielectric properties increase, which causes the temperature to increase exponentially, leading to increased microwave absorption, and a further increase in dielectric properties. Often, the loss factor and dielectric constant only begin to increase uncontrollably with temperature when the 'initiation temperature' is reached. Therefore, the microwave system has to be designed to avoid such initiation temperatures by either removing the samples from the applicator or interrupting the microwave power supply (Metaxas and Meredith, 2008).

Usually only a section or component of a workload shows a rise in dielectric properties with temperature. This leads to uneven heating because power is preferentially dissipated in the high loss factor component (Metaxas and Meredith, 2008). Thermal runaway reduces product quality, causes damage to the material being treated, and can lead to heat related mechanical damage in equipment.

Arcing or voltage breakdown occurs when the electric field outside a workload breaks down the resistance to electron flow in the workload. A dielectric workload reduces the electric field across it just like a capacitor, however, the electric field can reach levels high enough to ionise the gas phase within the workload. This is because the gas phase represents the path of least electrical resistance. Arcing is a serious processing issue, causing considerable power to be dissipated to any material in the vicinity and burn damage.

3.3 Applications of Microwave Heating

Microwave heating has been reported to offer significant benefits over conventional processing in areas such as energy efficiency and shorter processing times when drying wood (Vongpradubchai and Rattanadecho, 2009). In the pyrolysis of biomass, microwaves offer better liquid product quality than in conventional heating (Robinson et al., 2015). Microwave heating have been employed in waste treatment and found to be more energy efficient than a conventional process with a realistic means of energy recovery from waste (Lam and Chase, 2012). It has been demonstrated that microwave treatment can reduce treatment times by 90% in ceramics processing, producing quality materials at much lower bulk temperatures than in conventional heating (Agrawal, 1998). In chemical reactions, microwaves ensure short reaction times and an expanded reaction range (Lidström et al., 2001; Larhed and Hallberg, 2001).

It has been shown that microwave heating can be used to produce coke from the devolatilisation of coal (Lester et al., 2006), and can be used to reduce the sulphur content in coal as part of fuel pre-treatment for power plants (Binner et al., 2014). In mineral processing, microwaves have been used to induce thermo-mechanical stresses in the treated material thereby reducing grinding energy (Jones et al., 2002), and increasing the recovery of valuable minerals (Kingman et al., 2000). Also, Folorunso, et al. (2012) demonstrated the feasibility of a continuous microwave process used for the exfoliation of vermiculite.

3.3.1 Application of microwave heating to hydrocarbon removal from granular solids

Microwave heating has been demonstrated to extract oil from oil sands with a high yield, and is capable of upgrading the oil quality (Mutyala et al., 2010). The aqueous phase within the oil sand matrix is heated selectively and volumetrically, with the mineral phase transparent to microwaves. Robinson, et al. (2014) showed that high temperatures of 250 ^{o}C needed to remove bitumen can be achieved during the microwave heating of clay laden low grade oil sands. They found this is possible because the chemically bound water in the clay component are able to heat under microwaves at temperatures >100 ^{o}C when all the free water content has been removed. 2-5 barrels of water per barrel of oil is produced during conventional processing of oil sands which contain toxic chemicals that pose serious environmental challenge (Schindler, 2010). In contrast, microwave processing provides a dry processing route, thereby providing an environmentally friendly alternative.

Microwave heating has been shown to significantly reduce the time required to remove hydrocarbons from contaminated soils when compared with conventional processing due to the rapid selective and volumetric heating of the water content (Kawala and Atamanczuk, 1998; Robinson et al., 2012). Microwave treatment can remove contaminants in soil at lower bulk temperatures than conventional heating, thereby preserving the soil structure and biological activity (Kawala and Atamanczuk, 1998). It is thought that the oil contaminant is removed via physical entrainment, steam distillation or direct vaporisation under moderate processing conditions (Robinson et al., 2009b; Acierno et al., 2003; Falciglia et al., 2013). Other phases within the soil material, such as the carbon rich organic content, have

been heated under microwaves to raise the temperature of the soil matrix to the boiling point of the heavy hydrocarbon contaminants (Robinson et al., 2009b). Dawei, et al. (2009) have shown that microwave absorbing additives can be used to enhance oil removal from contaminated soil. Additives, such as carbon, are high loss materials. Therefore, the use of additives means that contaminated soil with low moisture content can be treated using microwaves. Abramovitch, et al. (1999) have also demonstrated the feasibility of using additives in heavy hydrocarbon removal from soil, moreover, they demonstrated that this can be applied to in situ remediation of contaminated soils. Buttress, et al. (2016) have demonstrated the feasibility of a continuous microwave process (150 kg/h) that can treat contaminated soils, and is suitable for up to 75% contaminant removal.

3.3.1.1 Application of Microwave Heating to Oil Contaminated Drill Cuttings

Microwave treatment has been proven on a laboratory scale to be able reduce the oil content in oil contaminated drill cuttings to less than the 1wt% environmental discharge limit (Shang et al., 2005; Shang et al., 2006). Drill cuttings are treated at a lower bulk temperature (100 ^{o}C) than in conventional thermal desorption units (up to 600 ^{o}C). The water content is selectively heated by microwaves as the mineral and oil phase are microwave transparent. Oil is located mainly on the surface of the pores, while water resides in the pores (Robinson et al., 2008). Figure 3.15 is a schematic showing the matrix make-up of oil contaminated drill cuttings.

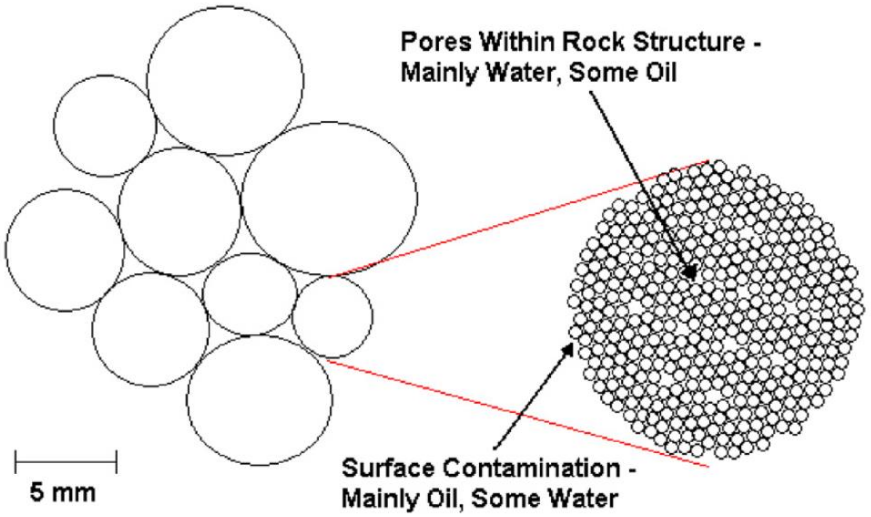


Figure 3.15: Schematic showing the make-up of oil contaminated drill cuttings (Robinson et al., 2008)

Physical entrainment has been identified as an oil removal mechanism, where the water within the pores is heated and converted to steam, and as steam escapes, oil is physically entrained (Robinson et al., 2008; Robinson et al., 2009a). Other oil removal mechanisms suggested are steam distillation and steam stripping (Robinson et al., 2009a). It is thought that oil is removed via indirect heating during steam distillation and stripping.

It has been shown that applicators (cavities) that can induce high electric field strengths lead to greater oil removal, with greater oil removal observed at higher power densities (Shang et al., 2006). It has been proven that that oil removal levels increased with increasing moisture content (Shang et al., 2006), although increasing the moisture content will cause the energy consumption to increase. The quality of the oil removed during microwave treatment has similar qualities to the original oil, meaning that oil from microwave treatment can be re-used in formulating drilling fluids (Shang et al., 2006).

Robinson, et al. (2008) demonstrated that pyrolysis temperatures of approximately 300 ^{o}C can be achieved during the treatment of drill cuttings. They suggested that such high temperatures are reached due to the bound water content of the mineral phase absorbing microwaves at >100 ^{o}C.

It has been reported that microwave assisted gas stripping can enhance oil removals from a fixed bed of drill cuttings (Robinson et al., 2008). The continuous microwave processing of drill cuttings have been investigated, and found to be able to reduce oil levels to less than the 1 wt% environmental discharge limit (Robinson et al., 2009a; Robinson et al., 2010). This continuous process is capable of treating materials up to 500 kg/h. Major design considerations in the scale up to a continuous process include material handling, sample geometry, dielectric properties of feedstock, power density and a cavity geometry that will ensure a high electric field intensity in the feedstock (Robinson et al., 2010).

3.3.1.2 Conventional and Microwave Stripping of Contaminated Solids

During the thermal liberation of hydrocarbons from a multicomponent media such as oil contaminated drill cuttings, hydrocarbon contaminated soils, and oil sands, remediation is often carried out by treatment in a fixed bed. Electrical heating and air stripping have been explored for in situ remediation of contaminated soil (Buettner and Daily, 1995). It was found that increasing the temperature increases desorption of contaminants from the fixed bed. Raising the temperature of the bed increases desorption due to an increase in the vapour pressure of the hydrocarbons relative to the partial pressure within the contacting gas (Missen et al., 1999). It has been shown that volatilisation of contaminants from a fixed bed of soil is feasible at low temperatures (less than 25 ^{o}C) when stripped with air (Yoon et al., 2002;

Wilkins et al., 1995; Gierke and Mckenzie, 1992; Kearl et al., 1991). It was found that oil removal increased at higher stripping gas flow rates.

It has been demonstrated that in situ stream stripping can significantly reduce oil levels in contaminated soil (Arthur and Lord, 1998). The bulk temperature of the soil was approximately 100 ^{o}C during steam stripping, which is thought to be the reason steam stripping is beneficial for oil removal. Robinson, et al. (2008) reported that steam stripping of a fixed bed of drill cuttings removed 55% of oil compared with 18% removal when nitrogen was used, with both stripping gases at 120^{o}C. Steam stripping is thought to support more oil removal due to steam distillation. J. Robinson, et al. (2008) also showed that microwave assisted nitrogen stripping increased oil removal to 95% after 2 minutes of treatment, whereas oil removal only increased to 80% from 55% during microwave assisted steam stripping in the same treatment time. This was attributed to a reduction in the penetration depth as a result of steam condensation on the surface and in the pores of the material. The difference between normal microwave treatment of contaminated drill cuttings and microwave assisted stripping is that the latter uses an external source of stripping gas to enhance the mass transfer of oil.

Previous workers have studied the rate of mass transfer of hydrocarbons from soils to a gas stripping medium and derived empirical models relating mass transfer coefficient with the velocity of the stripping medium (Wilkins et al., 1995; Van der Ham and Brouwers, 1998; Yoon et al., 2002). They studied the effect of introducing gas from an external source into a partially saturated contaminated soil media. Wilkins et al., (1995) noticed that the residual water content and water distribution affected the mechanism of hydrocarbon mass transfer into the stripping gas, which could either be governed by diffusive or convective transport. In this scenario,

hydrocarbon droplets may become trapped between aqueous phases in small pores, restricting movement into the gas phase. This phenomenon is known as channelling, where the stripping medium bypasses the trapped organic phase, and is a common disadvantage of gas stripping in conventional fixed bed systems. Yoon, et al. (2002) corroborated the findings of Wilkins, et al. (1995) by showing that hydrocarbon mass transfer can become diffusion rate-limited, even at high gas velocities.

A number of studies have speculated that entrainment, steam stripping or steam distillation are possible mechanisms that explain empirical hydrocarbon removal results, but none have offered conclusive evidence to date. One of the objectives of this work is to establish the extent to which steam-stripping occurs during microwave heating of a fixed bed of oil contaminated drill cuttings.

3.4 Current Processing Issues in the Industrial System

The current processing concept is shown in Figure 3.16. The material is transported via high shear twin screw conveyors to the applicator.

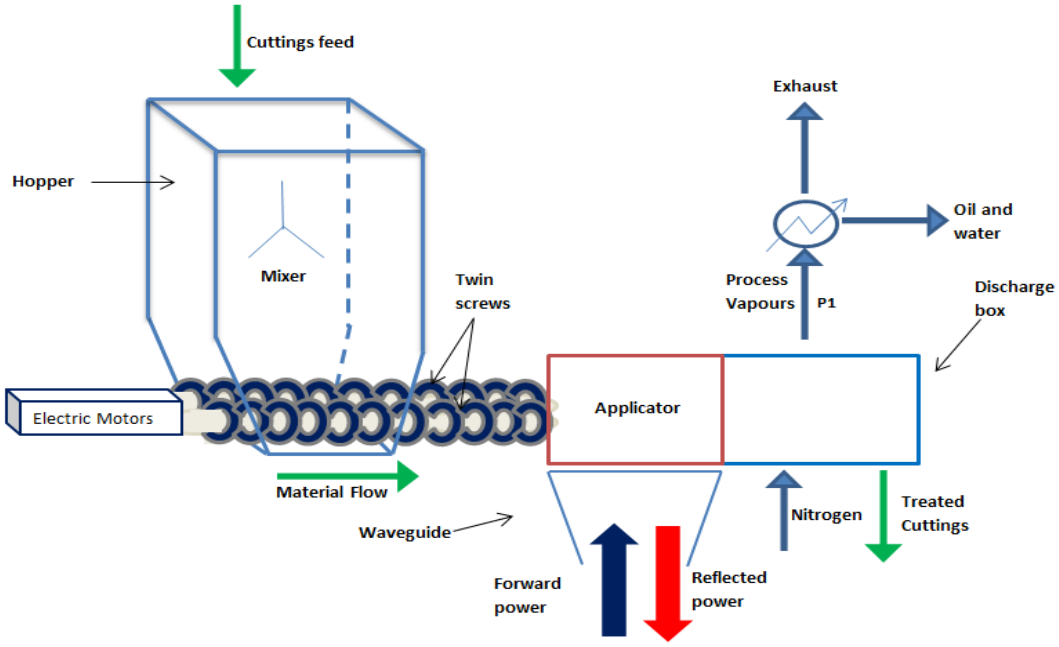


Figure 3.16: The current processing concept in the microwave treatment of oil contaminated drill cuttings.

The first processing issue is the implication of using a high shear twin screw conveyor (Figure 3.17) on oil removal efficiency in the applicator. Physical inspection of the material reveals a change in consistency after it has passed through the screw conveyors. Therefore this work investigates the effect of shearing on oil removal efficiency of the microwave system.



Figure 3.17: A section of the twin screw conveyor in the industrial system (120 mm diameter).

The second processing issue is thermal runaway, which has been observed as irreparable burn damage to the ceramic insert in the cavity (applicator), as shown in Figure 3.18. This is as a result of the accumulation of drill cuttings in the cavity over time. When this happens the system is shut down until a new set of ceramic cavities can be designed and fabricated.



Figure 3.18: Damage to ceramic cavity due to thermal runaway.

In the past, a continuous feed system using fibre glass as the conveyor belt was used to prevent accumulation in the cavity (Figure 3.19). However, this system was unsuccessful because the belt had to be constantly replaced due to the damage from arcing.

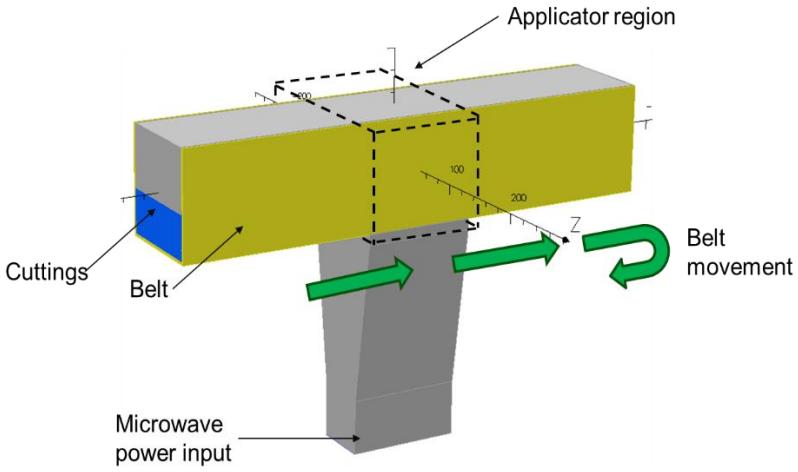


Figure 3.19: Drawing of the fibre glass belt conveyor system

A continuous microwave system (Figure 3.20) using twin screw conveyors was investigated after the fibre glass conveyor system. Although arcing was reduced, the wet drill cuttings would stick to the walls of the ceramic insert and accumulate in the cavity. Thermal runaway then ensued causing great damage to the ceramic insert. Consequently the process shuts down and new cavities are required.

To prevent recurring system shutdown and expensive redesign of new cavities (which costs approximately £15,000), a rotary wheel system conveyor system was designed. This system ensures there is no accumulation of drill cuttings in the cavity. A description of the system is given in section 4.3.

Despite the wheel system, investigations were carried out in this work to understand the temperature that thermal runaway is initiated, and the main microwave

absorbing components in drill cuttings responsible. This will enable a robust system design, where the thermal runaway temperature can be avoided.

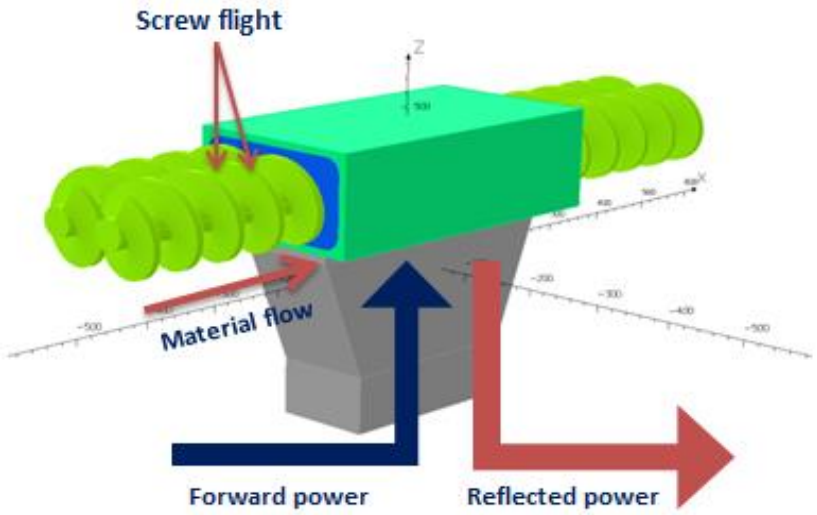


Figure 3.20: Drawing of a continuous microwave system with screws passing through the cavity.

Chapter 4 Experimental Methods and Analytical Techniques

4.1 Microwave Heating Experiments – System A

The microwave system consists of a 6 kW rated microwave generator operating at 2.45 GHz, waveguides for microwave energy transport to the applicator, a three stub automatic tuner for power analysis and impedance matching. The picture of the system is shown below (Figure 4.1)

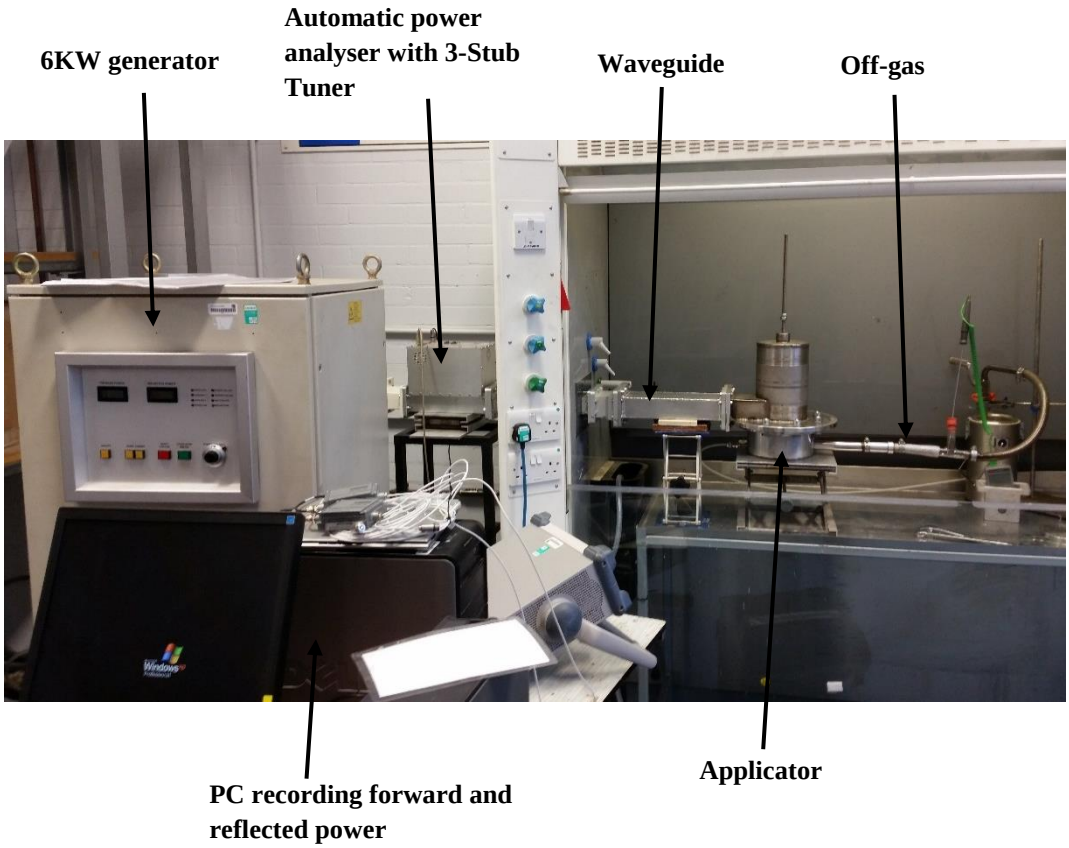


Figure 4.1: Picture of the microwave treatment system A

The waveguide is a TE_{10} waveguide with a height of 55 mm, and 110 mm width (internal dimensions). Microwave power is transmitted to a TM_{01n} applicator. There is a coupling aperture at the entry point of the TM_{010} applicator (Figure 4.2) which enables microwave power to be coupled into the applicator ensuring there is interaction between the electric field and the samples in the applicator (Metaxas and Meredith, 2008). The applicator is made of mild steel, and can withstand temperatures in excess of 1000 ^{o}C.

The applicator resonates in a single mode, and was specifically designed to able to support high electric field intensities and power densities of the order of 10^5 kW/m^3.

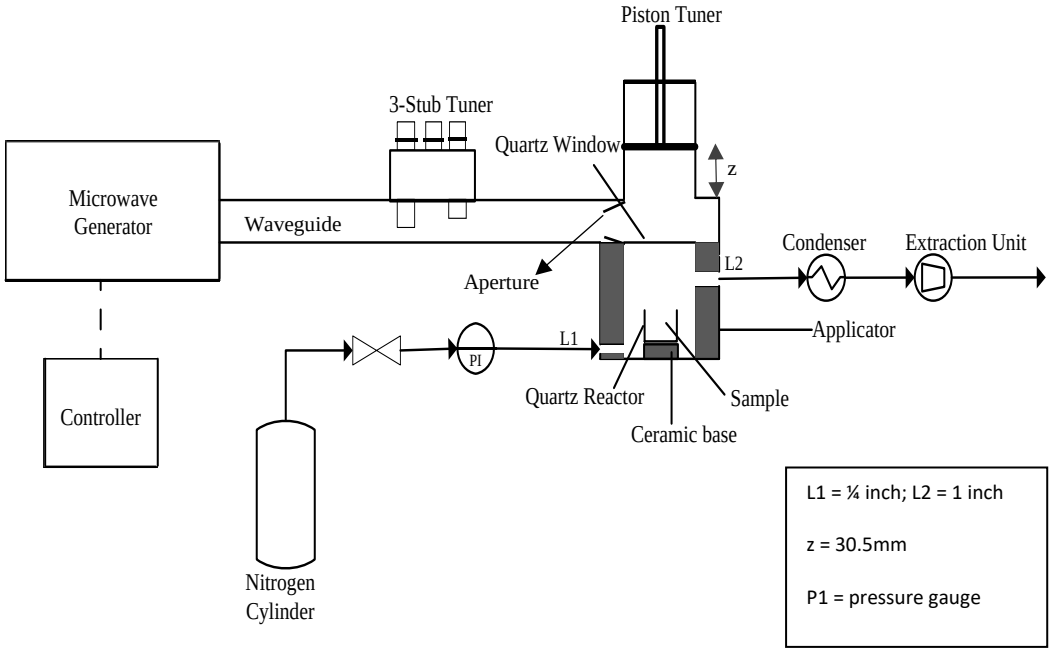


Figure 4.2: Schematic of microwave treatment system A

The internal diameter of the applicator is 110 mm, which is less than one free space wavelength of microwaves at 2.45 GHz (122 mm). This is to allow only one mode to be generated in the cylindrical cavity radially. The height of the applicator (from the ceramic base to the quartz window) is 78 mm.

The resonant frequency of the applicator is affected by the dielectric properties of the samples. Therefore for each sample, impedance matching was carried out to minimise reflected power, and hence energy loss. There are two types of tuners in microwave system A; 1) the sliding short circuit (piston tuner) which is part of the applicator, 2) the 3-stub tuner. The tuners ensure that the resonant frequency does not drift during treatment because the resonant frequency may drift due to temperature change in the samples or voltage variations from the generator.

Before the treatment of each drill cuttings sample, impedance matching was carried out. This was done first, by setting up the system for treatment with samples positioned in the applicator. Low power (<1 mW) microwave signal is transmitted into the applicator from a vector network analyser. The signals were transmitted at the operating frequency of the microwave generator. This test is also sometimes referred to as cold testing, indicating that the power in the signal is insufficient to cause the sample to heat. The positions of the 3-stubs and the piston tuner (Figure 4.2) corresponding to minimum reflected power are recorded and used during the microwave treatment of each sample. The optimum height of the piston tuner (z) was determined to be 30.5 mm for all the samples treated, although the 3-stub positions changed from one sample to another, mainly due to different water contents.

The quartz reactor and window (Figure 4.2) are essentially microwave transparent (Metaxas and Meredith, 2008). The quartz window acts as a barrier between the treatment zone and the waveguide and top of the applicator. The ceramic base has a height of 10 mm, and is used to position the sample in the area of highest electric field intensity. The ceramic base is also microwave transparent.

Experiments were carried out by placing 70 g of drill cuttings sample in the applicator as shown in Figure 4.2. The reactor has a diameter of 76.7 mm, and a height of 43 mm. The average sample height in the quartz reactor ranged from 10 to 12 mm. A mass of 70 g was consistently used for all the samples treated in this system. Samples were treated at microwave powers of 1-5 kW for 5-62 s to give energy input ranges from 20-55 kJ depending on the duration of the treatment.

Nitrogen (5 L/min) was introduced to the applicator through the inlet port (L1 = ¼ inch) at 1 bar. Nitrogen was used to purge the system and maintain an oxygen free atmosphere. This is important to prevent combustion because the oil content are flammable at high temperatures, or minimise the risk of combustion if arcing occurs during processing. Nitrogen is also used as a sweep gas to aid the removal of process gas from within the applicator. Generated vapours exit through L2 (1 inch), and is trapped in the condenser (dry ice and acetone), while incondensable gases were sent to the extraction unit. The samples were tested for oil and water content before and after microwave heating to determine the extent of oil and water removals.

Reflected and incident power was recorded using the automatic power analyser (Figure 4.1) and Homsoft4002 software. The reflected power was less than 5% microwave power due to the high water content of the samples treated (Figure 4.3). Therefore, the incident power is generally reported in this work for system A. The energy input is calculated from the integration of absorbed power over treatment time.

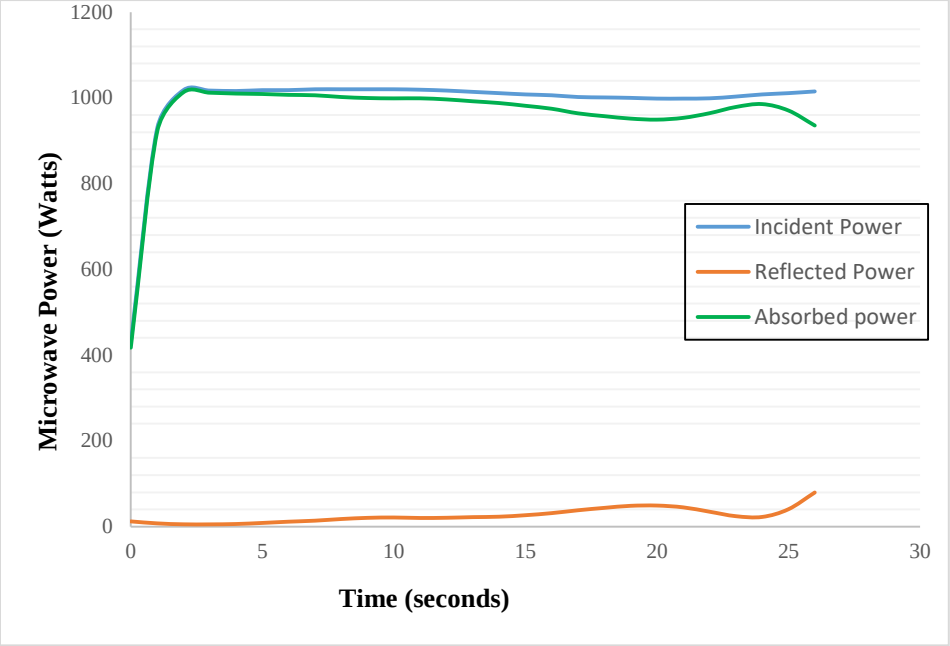


Figure 4.3: Reflected and absorbed power in system A at 1kW input power.

The energy input is reported as the specific energy input. For example, if 25 kJ energy input was absorbed by 70 g sample, the specific energy input (kWh/t) is calculated as follows;

$$\frac{25\ \text{kJ}}{70\ \text{g}} \times \frac{10^6\ \text{g}}{1\ \text{tonne}} \times \frac{1\ \text{kwh}}{3600\ \text{kJ}} = 99.2\ \text{kWh/t}$$

Time, and as a result energy input, was used as the control parameter. The time required for the sample to absorb a specified amount of energy reduced with increasing power. For example, it took approximately 22-23 s for 20 kJ energy input at 1 kW, while 7-8 s was needed for the same energy input at 3 kW.

The process of treating contaminated drill cuttings in system A was observed to be a repeatable process, as similar liquid mass loss was recorded for the same energy input, irrespective of the power input. By analysing the mean and standard error of the sample masses after microwave treatment, there is strong evidence that this is

the case. For example, Table 4-1 shows that at 40 kJ input energy, and input powers of 1 kW and 3 kW, there is negligible variation in the sample mass after treatment. The data in Table 4-1 shows 8 experimental runs each at 1 kW and 3 kW with a sample mass of 70 g (initial water content of 14 wt%, initial oil content of 11 wt%).

Table 4-1: Sample mass after microwave treatment at 1kW and 3kW, and 40 kJ

	Sample mass after treatment (g), 1 kW	**Sample mass after treatment (g), 3 kW**
	58.65	59.11
	58.57	58.89
	58.39	58.89
	58.61	57.92
	58.29	58.55
	58.68	57.86
	58.84	58.21
	58.35	58.45
Mean	58.55	58.49
Standard Error	0.07	0.16

The standard errors in Table 4-1 show that variability is low for sample masses after treatment at the same energy input at constant input power.

To demonstrate that the variability between the mass of the samples after microwave treatment at different powers, and a constant energy input, is also minimal, a simple t-test was carried out. Using data from Table 4-1, an alternate hypothesis (H_1) was developed based on the condition that the difference between the means of the sample mass after treatment is less than 0.5 g.

Therefore; $H_1 : -0.5 < \mu_{1kW} - \mu_{3kW} < 0.5$

where μ_{1kW} is mean of the sample mass after microwave treatment at 1 kW, μ_{3kW} is mean of the sample mass after microwave treatment at 3 kW.

The first null hypothesis (H_{o1}) against the alternate hypothesis is as follows;

$$H_{01}: \mu_{1kW} - \mu_{3kW} \geq 0.5$$

The *P* – value is between 0.025 and 0.01 meaning that this hypothesis (H_{o1}) can be rejected.

The second null hypothesis (H_{o2}) against the alternate hypothesis is as follows;

$$H_{02}: \mu_{1kW} - \mu_{3kW} \leq 0.5$$

The *P* – value is between 0.01 and 0.005 meaning that this hypothesis (H_{o2}) can also be confidently rejected. Hence, there is strong evidence that the alternate hypothesis holds.

4.2 Microwave Heating Experiments – System B

This system is a semi-batch process for the treatment of oil contaminated drill cuttings. The system was designed to provide alternative material handling strategy and ensure that treated materials do not accumulate in the applicator (cavity). The process flow diagram of the system is shown in Figure 4.4.

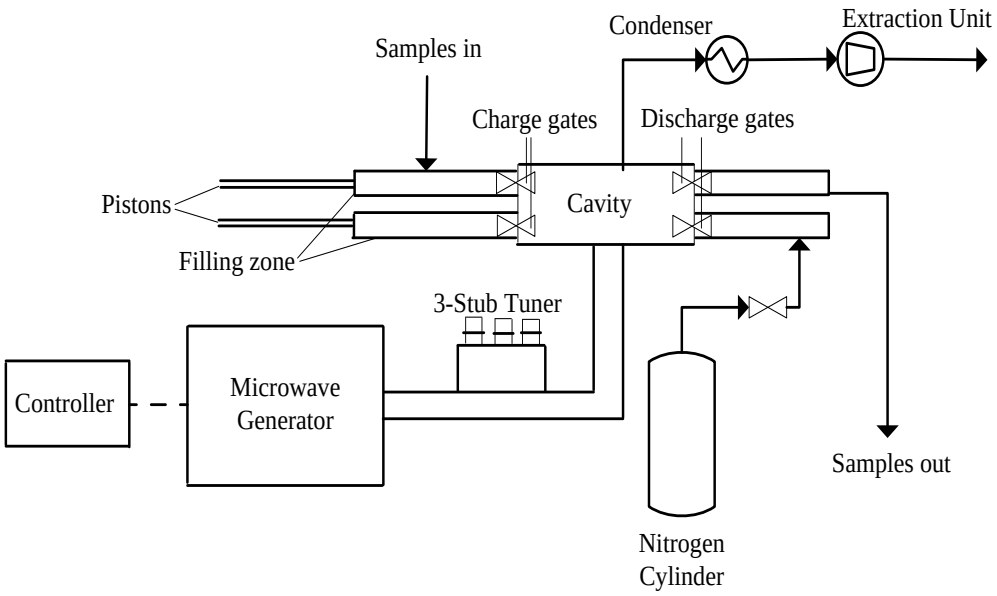


Figure 4.4: Process flow diagram for the dual piston rig – system B

The idea behind the design was for the piston to move through the cavity during treatment, while discharging treated material. Nonetheless, this work investigated the time required to reduce the oil levels in drill cuttings to less than 1 wt% in the system, using the cavity as a fixed bed.

Drill cuttings were placed in the filling zone whilst keeping the charge gates closed to prevent the samples running into the cavity. The charge gates are opened and the pneumatic pistons are used to charge the cavity with the drill cuttings material. The

cavity is a metal casing with ceramic inserts (dieelctric constant = 3.1, loss factor = 0 at 25 ^{o}C), which is microwave transparent. The cavity consists of two bores each with a length of 400 mm and a radius of 50 mm. At a sample bulk density 1.95 kg/m^{3}, each bore has a capacity of 6.5 kg. In this work, only one bore of the cavity was filled with drill cuttings. The samples were sourced from North Sea drilling operations.

A 100 kW microwave generator operating at 896 MHz was used as the power source, and was connected to the cavity with waveguide (248 mm width, and 124 mm heigh internal dimensions). Impedance matching was carried out to minimise reflected power and energy loss. Experiments were carried out at 50 – 100 kW for 19-53 s. Reflected and incident power were recorded using an automatic power analyser and Homsoft4002 software. The absorbed power is reported in the results section (Chapter 7) of this work, which ranged from 40-91 kW.

Nitrogen is used as a purge gas to prevent potential combustion of the oil content during microwave heating. Oil and water vapours are condensed and non-condensable gases are sent to the extraction unit. After treatment the discharge gates are fully opened for the pistons to empty the cavity of the treated materials. The oil and water contents of drill cuttings before and after microwave heating are measured to determine the efficiency of oil removal.

4.3 Microwave Heating Experiments – System C

This is the latest processing concept in the microwave treatment of oil contaminated drill cuttings. Drill cuttings are transported via high shear twin screw conveyors to the applicator (Figure 4.5). The applicator is a rotary wheel system shown in Figure 4.6.

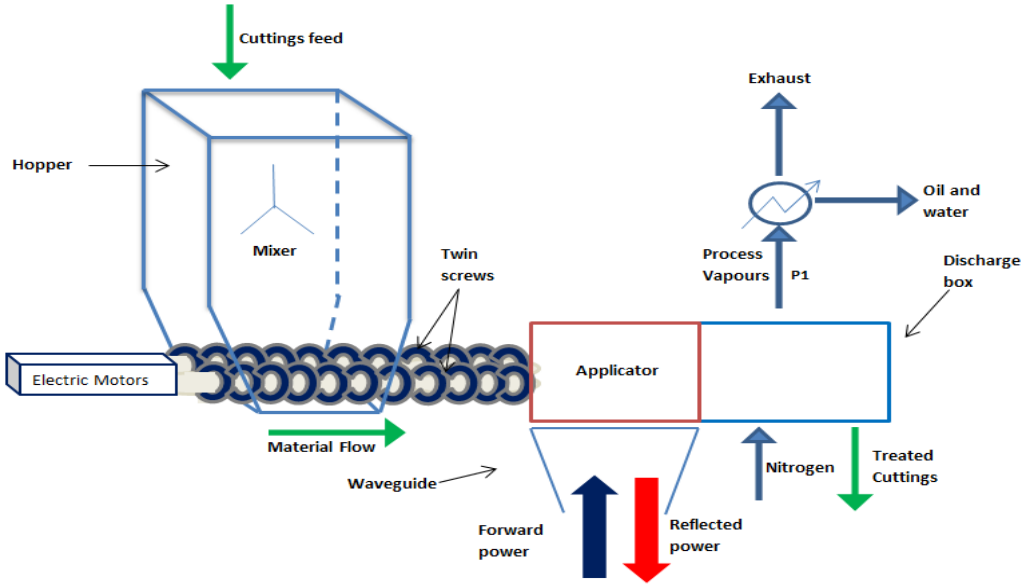


Figure 4.5: Schematic of the processing concept for microwave remediation of drill cuttings - System C

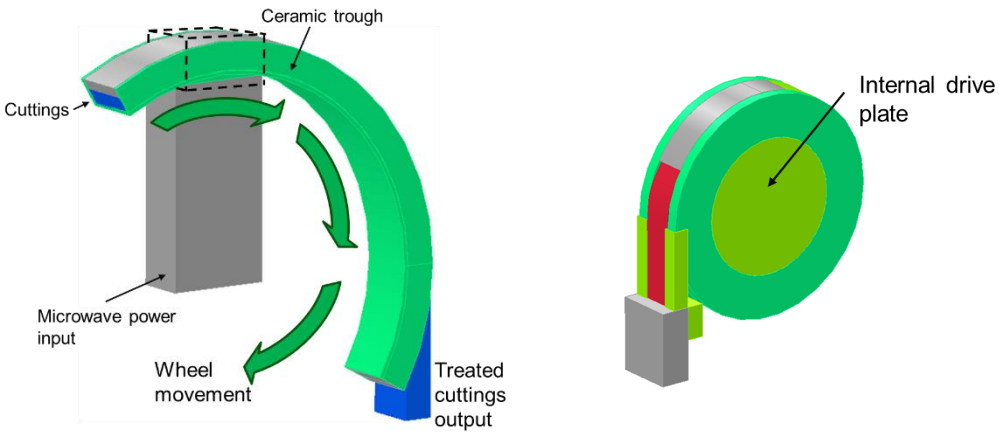


Figure 4.6: Drawing of the rotary wheel applicator

This system allows for a controlled residence time of drill cuttings in the applicator, thereby eliminating the problem of material accumulation over time. Moreover, it was found that the system is more robust than the fibre glass conveyor belt system, due to the fact that arcing is mitigated.

The applicator is designed into a Ferris wheel-like configuration. The wheel is driven by a shaft attached to an internal metal drive plate. The trough of the wheel is made from a microwave transparent ceramic. The interaction between drill cuttings and microwaves occur in the applicator in an area of 185 mm width, and 250 mm length. The height of the drill cuttings bed flowing into the applicator is controlled and monitored continuously by a level indicator. The flow rate of drill cuttings is determined by the wheel speed.

A 100 kW microwave generator operating at 896 MHz was used as the power source. The generator is connected to the applicator via waveguide of 248 mm width, and 124 mm height. Experiments were carried out at 35-45 kW, and a flow rate of 0.31-0.42 t/h.

Nitrogen is used as a purge gas to prevent potential combustion of the oil content during microwave heating, and as a sweep gas to aid the removal process gases fom within the applicator. Oil and water vapours are separated from the offgas in a scrubber, while non-condensable gases are sent to the extraction unit. The oil and water contents of drill cuttings before and after microwave heating are measured to determine the efficiency of oil removal.

4.4 Dielectric Property Measurement

The dielectric properties of samples were measured using the cavity perturbation technique. The concept of the cavity perturbation technique is that placing a small dielectric sample in a resonant cavity will cause a decrease in the quality factor and a shift in the resonance frequency (Sheen, 2005; Meredith, 1998; Lester et al., 2006) The quality factor (Q) is defined in equation 4.1;

$$Q = \frac{\varepsilon'}{\varepsilon''} \qquad [4.1]$$

The dielectric dielectric constant (ε') and dielectric loss factor (ε'') can then be calculated from the change in quality factor and frequency shift observed as a result of inserting the dielectric sample in the cavity. Equations 4.2 and 4.3 (Lester et al., 2006; Folorunso et al., 2012) are developed from the perturbation theory and show how the dielectric properties are calculated.

$$\varepsilon'' = J_1^2 (X_{l,m}) \left(\frac{1}{Q_1} - \frac{1}{Q_2} \right) \frac{V_c}{V_s} \qquad [4.2]$$

$$\varepsilon' = 1 + 2J_1^2 \left(X_{l,m} \right) \frac{f_o - f_1}{f_o} \frac{V_c}{V_s} \qquad [4.3]$$

Where J_1 is the first order Bessel function, $X_{l,m}$ is a function of the geometry of cavity, Q_1 is the quality factor of the empty cavity, Q_2 is the quality factor of the cavity with the dieelctric material, V_c is the cavity volume (m^3), V_s is the sample volume (m^3), f_o is the resonant frequecny of the empty cavity (Hz), and f_1 is the resonant frequency of the cavity when dielectric material is inserted (Hz).

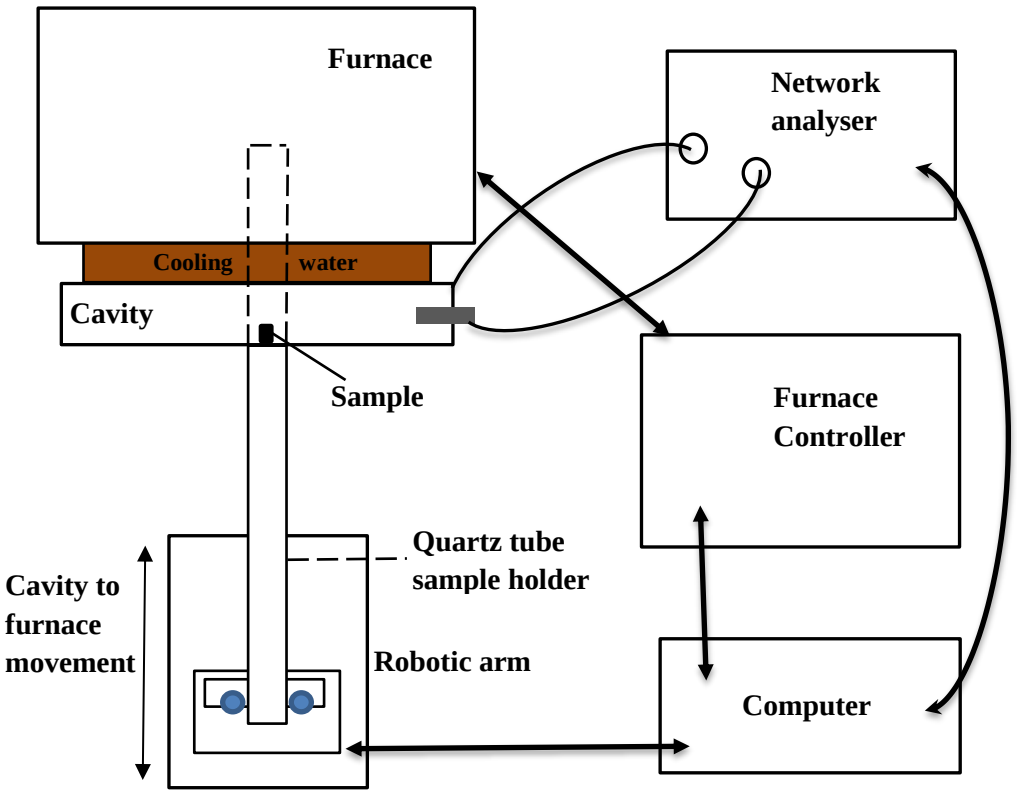


Figure 4.7: Schematic of the cylindrical resonant cavity measurement system.

The samples measured were placed into a quartz tube (4 mm internal diameter), with the height and mass measured. This is important because, for example, a change in height or mass during high temperature measurements will lead to volume change, which affects the V_s term in equations 4.2 and 4.3. The robotic arm moves the sample holder (Figure 4.7) between the cavity and the furnace.

The cavity is located under a furnace, which is a conventional electrically heated furnace. The cavity is maintained at $\leq 20\ ^{o}C$ by a cooling water system. During high temperature experiments, samples are heated in the furnace, and transferred to the cavity by the robotic arm for measurement. The duration of the samples in the cavity is only for a few seconds to prevent temperature rise in the cavity.

The resonant cylindrical cavity, shown in Figure 4.7, is where the measurement occurs. The cavity has a height of 55 mm, and a width of 550 mm. It resonates in

the TM_{0n0} mode at 912 MHz and 2.45 GHz. A Hewlett Packard 8753C vector network analyser was used to transmit microwave frequency signals to the cavity. The network analyser measures the change in resonant frequency and quality factor at 912 MHz and 2.45 GHz, which is recorded in a computer connected to the experimental system.

For the dry drill cuttings samples and mineral components tested, the sample height in the quartz tube ranged from 18 mm to 20 mm. Sample mass was dependent on the density of the samples. Sample height of wet drill cuttings varied from 6 mm to 8 mm. The base of quartz tube was tapped 15 times for all the samples to ensure uniform measurements. The dieelctric properties were measured from 20 ^{o}C to 850 ^{o}C.

4.5 Thermo – Gravimetric Analysis (TGA)

TGA was used to monitor the change in mass of dry drill cuttings, which occurs from decomposition reactions, as a function of temperature.

The instrument used for this analysis is the SDT Q600 TGA-DSC (TA instruments). The oil and water content of the sample were removed by Soxhlet extraction and Dean & Stark analysis (sections 4.11 and 4.12). The samples were then dried in an oven for 24 hr at 105 ^{o}C. The moisture content of wet granular materials, such as soil, can be removed at 105 ^{o}C (Reeb and Milota, 1999).

The thermal analysis was carried out by heating 35 mg of samples in nitrogen at 5 ^{o}C/min. Some workers have used similar heating rates during the thermal analysis of soil minerals (Grim, 1968; Stucki et al., 1963). The sample was then heated isothermally at 105 ^{o}C for 5 minutes, and at 5 ^{o}C/min to 1000 ^{o}C.

4.6 Density and Porosity Measurements

Bulk density was determined by filling a measuring cylinder with wet drill cuttings to the 500 ml mark. The base of the cylinder was tapped 10 times for a uniform bulk density measurement for all samples. The bulk density was then calculated using the sample mass.

Porosity was calculated using equation 4.4;

$$1 - \frac{\rho_b}{\rho_s} \quad [4.4]$$

where ρ_b is bulk density and ρ_s is the skeletal density.

Skeletal (true) density is defined as the ratio of discrete pieces in a solid material to the sum of the volumes of the solid material in the pieces and closed pores within the pieces (ASTM D3766).

The instrument used to measure skeletal density is the Accupyc 1330 Gas Pycnometer (Micrometrics). Helium is used as the purge gas in the analysis.

7 g of dry drill cuttings samples are filled to approximately ¾ of a 10cm^3 sample chamber in the instrument. The instrument uses the ideal gas law, gas displacement techniques, and the difference between the gas pressure in the sample chamber and a reference empty chamber to calculate the true volume of the sample. The skeletal density is then calculated from the ratio of the sample mass to the true volume.

4.7 Shearing Methodology

A mixer was used to simulate the shearing effect of the twin screw conveyors in the industrial microwave system. The experimental set up is shown in Figure 4.8.

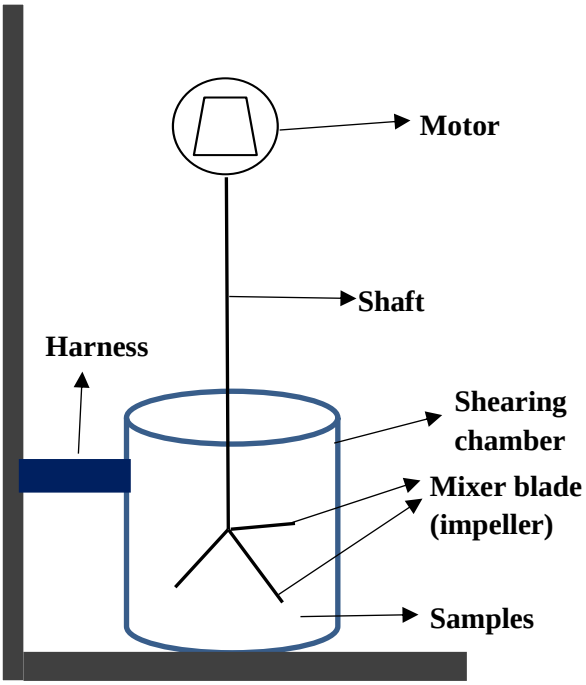


Figure 4.8: Diagrammatic representation of the shearing equipment

The mixer blade is 15 cm in diameter. The shearing chamber is made of stainless steel, and has a height of 25 cm, with a diameter of 21 cm. The harness minimises the vibration of the shearing chamber during experiments.

The minimum mixer speed is 210 rpm. Initial studies were carried out which determined that there were no changes to the material bulk density at shearing times less than 1 minute at 210 rpm. At 275 rpm, which is the next available mixer speed due to the specification of the mixer's manufacturer, it was found that the rate of bulk density change was faster than observed at 210 rpm. Nevertheless, 210 rpm was chosen as the mixer shaft speed to use in this study. This is partly because the

experimental set-up works better at a lower shaft speed. During the initial studies, it was also found that the density of the material remained constant after 3 minutes of shear at 210 rpm.

For the experiments reported in chapter 6 of this work, 3 kg of oil contaminated drill cuttings are placed in the shearing chamber. To shear the material, the mixer speed was set to 210 rpm for 1-3 minutes. The bulk density before and after shearing was measured and recorded to characterise the level of shear in the material.

4.8 Scanning Electron Microscopy

Scanning electron microscopes are used for sample imaging, and for obtaining information on the morphology, topography and composition. They operate by focussing electron beams on the surface of a sample. The beams are only able to penetrate into a few nanometres from the sample surface because of their short wavelength (Reimer, 1998).

The electron beam interact with the sample atoms, leading to a range of effects (Reimer, 1998): 1) Elastic interactions i.e. no energy is transferred from the electron beam to the sample, as a result, the beams are transmitted through the sample with no energy loss, 2) Inelastic interactions, where energy is transferred to the sample leading to a number of signals being emitted from the sample. The signals include X-rays, auger electrons, backscattered electrons and secondary electrons (see Figure 4.9).

Most of the energy from the beam is used to excite the electrons in the sample atomic lattice. However, the signal emitted depends on the energy of the electron

beam (kV), and the corresponding penetration depth into the sample. The higher the beam energy, the greater the depth of penetration. For example, secondary electrons are emitted close to the sample surface, while X-rays are emitted when high energy electron beam removes an inner shell (K-shell) electron, causing energy (X-ray) release when a higher energy electron fills the vacated shell.

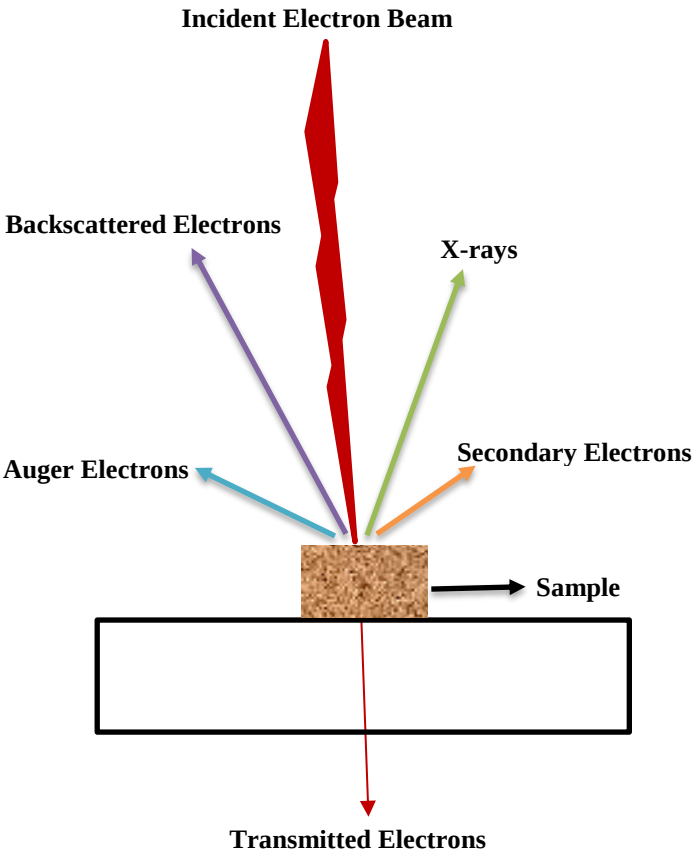


Figure 4.9: Schematic showing the principle of operation in a scanning electron microscope.

The samples were analysed for their elemental composition using a FEI 650 Quanta ESEM (Environmental SEM). Similar technique have been used in the elemental analysis of contaminated soil (Robinson, et al. 2009b). The oil and water content of the samples were removed, after which they are dried in an oven at 105 ^{o}C for 24 hrs. The dried samples are riffled down and sieved to <212 µm, after which they

were analysed in the ESEM instrument. The use of ESEM allows the sample to be analysed without carbon coating. An electric gun emits high energy electron beams (20 kV) to the surface of the sample under low vacuum to avoid charging the sample. The equipment uses Energy Dispersive X-ray Spectroscopy (EDX) by means of an Oxford Instruments X-Max silicon drift detector to analyse the X-rays emitted from the sample. The X-rays are completely unique to the element interacting with the incident electron beam, as they indicate the energy difference between two shells in the element. EDX allows the qualitative and qualitative elemental composition to be measured.

4.9 X-ray Diffraction Analysis (XRD)

The mineral composition of the drill cuttings samples in this work were identified using X-ray powder diffraction analysis. This technique works on the basis of X-ray diffraction according to the space between atoms in a crystal lattice. There are several atoms in a crystal lattice, each having unique and random orientations. X-rays of known incident angle (θ) is scanned on a sample, and the angle of X-ray diffraction from the sample is recorded. The angle of diffraction is unique to the atomic spacing in a crystal lattice, which means that each mineral can then be identified (Cullity, 1956).

A Bruker D8 Advance X-ray Diffractometer is the instrument used in this analysis. The instrument consists of an X-ray tube that produces monochromatic waves and can be rotated to produce incidents rays at 0-90 degrees. The samples are prepared by drying, riffling and sieving down to <212 μm. An electronic detector is located

opposite the sample in the instrument which detects diffracted X-rays from the sample.

Diffraction only occurs when the wavelength of the incident X-rays is of the same magnitude as the distance between the atomic planes (Cullity, 1956). The wavelength is given by Bragg's law in equation 4.8;

$$n\lambda = 2d \sin\theta \qquad [4.8]$$

where λ is the wavelength of X-rays, n is an integer number of wavelengths, and d is the spacing between atomic planes.

By varying the angle of incident of X-rays, the d spacing in each mineral in the sample can be determined. The unique characteristic of each mineral in a sample is shown by plotting the angular positions (2θ) and the intensity of the resultant diffraction peak. Figure 4.10 is a schematic of how samples interact with X-rays during analysis. Identification of each mineral component is achieved by comparing the diffraction pattern of an unknown sample with a database.

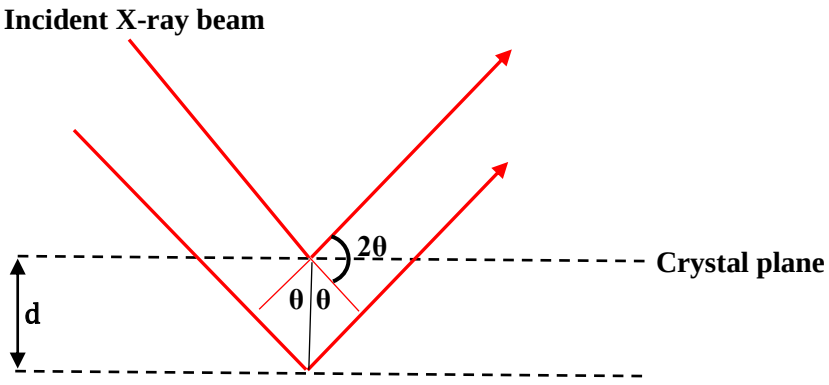


Figure 4.10: Diagram showing how X-ray interacts with samples in a diffractometer (Bragg's law).

4.10 Particle Size Analysis – Laser Diffraction Particle Size Analyser

The particle size analysis of the samples were carried out in a Beckman Particle Size Analyser LS200. This instrument uses laser diffraction to determine particle size distributions by measuring the variation in light intensity scattered when a laser beam passes through a dispersed particulate sample. The instrument is capable of measuring particle sizes from 0.4 – 2000 µm.

The instrument operates on a principle that a particle passing through a laser beam will diffract light at an angle inversely proportional to its size. Furthermore, the intensity of the diffracted beam at any angle corresponds to the number of particles with a specific cross-sectional area in the path of the beam (Ferro & Mirabile 2009).

The samples were prepared for analysis by removing the oil (Soxhlet Extraction – section 4.11) and water content (Dean and Stark – section 12), and drying in an oven at 105 ^{o}C for 24 hours. The Samples were then milled and sieved to <212 µm. The samples were dispersed in a calgon solution for 24 hours to prevent agglomeration. This is important because agglomerates will give inaccurate particle size results. The calgon solution is made from 35 g hexametaphosphate, 7 g bicarbonate power and 1 litre of water. 0.25-0.5 g of the sample was dispersed in 10 ml calgon solution. The samples are then introduced into the instrument which uses the Mie theory (Ferro and Mirabile, 2009) to estimate the particle size distribution in the samples.

4.11 Oil Content Measurement

The oil content of the drill cuttings samples were determined using Soxhlet extraction. It is a common leaching technique in solid-liquid extraction, and is a standard method of measuring oil content in contaminated soils and solids (Yeung et al., 1994; Martin and Raymond, 1985). A Soxhlet equipment consists of a thimble (sample holder), distillation flask, the extractor body, condenser, and heating mantle (Figure 4.11).

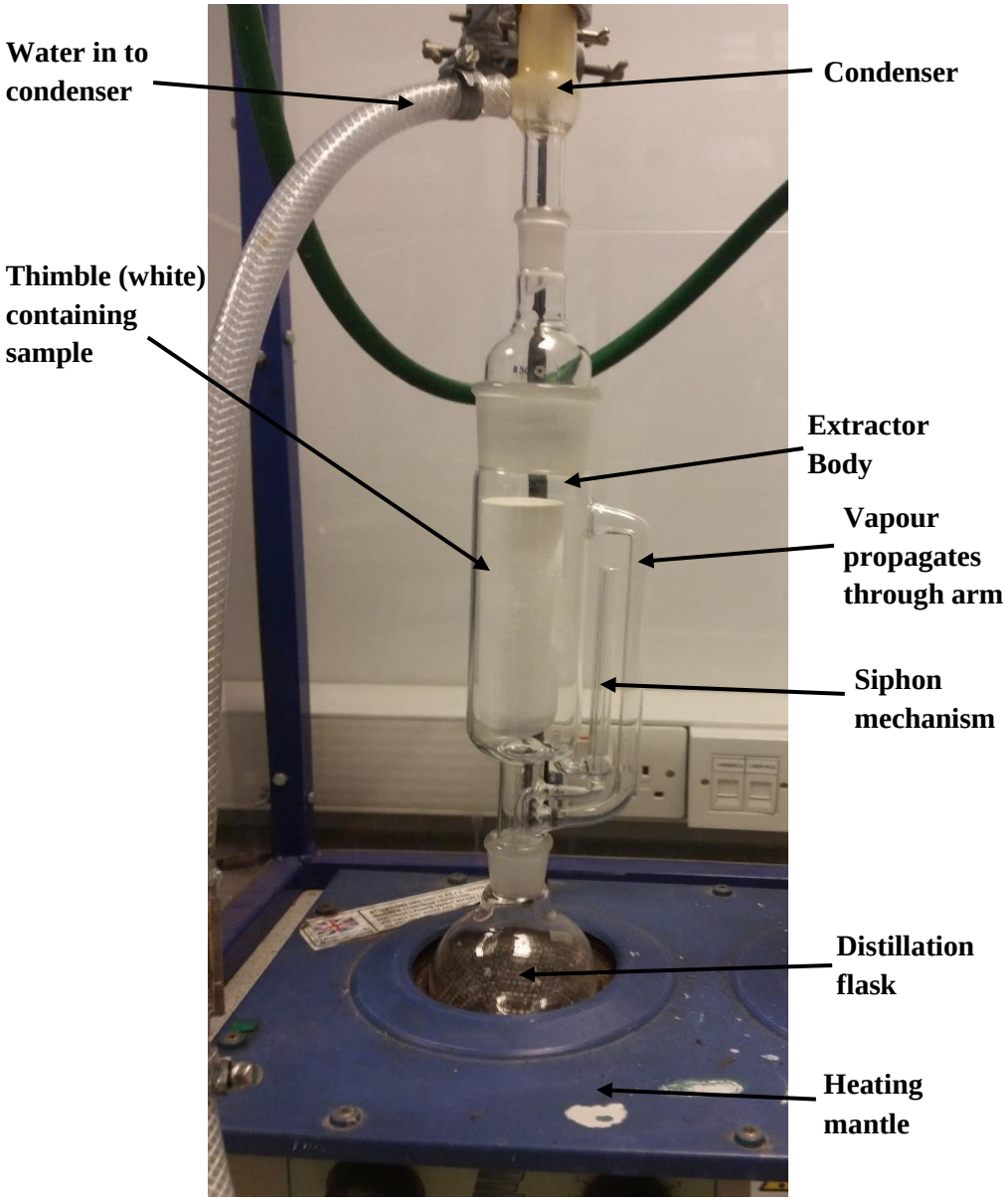


Figure 4.11: Soxhlet extraction equipment.

30 g of the sample was placed in a pre-weighed thimble holder. The thimble was then placed in the extractor body. The distillation flask was filled with 100-150 ml of dichloromethane. Dichloromethane is used because it has been proven to be more efficient at oil extraction from contaminated drill cuttings than other solvents such as acetone, hexane, and toluene (Turner, 2001). Furthermore, other researchers have used dichloromethane in the extraction of an organic content from contaminated solid media (Martin and Raymond, 1985; Yeung et al., 1994). The distillation flask is connected to the extractor, which is then connected to the condenser (Figure 4.11).

The whole assemble was placed on a heating mantle and heated to 40 ^{o}C (boiling point of dichloromethane). The solvent vapour propagates through an arm of the extractor body, after which it is cooled in the condenser. The condensed dichloromethane fills the extractor body where the thimble containing the sample is located. The extraction is driven by the oil concentration difference between the condensing solvent liquid and the drill cuttings.

When the solvent reaches an overflow level in the extractor body, it is siphoned back into the distillation flask. This carries the extracted oil into the bulk liquid allowing fresh solvent to condense in the extractor body. The cycle is repeated until extraction is complete, which was found to be 6-8 hours in this work.

After the extraction the oil-solvent mixture was concentrated by removing dichloromethane. This was carried out by heating the mixture to 40^{o}C in a water bath under low vacuum. The concentrate was transferred to 10 ml vials, which were then allowed to evaporate in air at room temperature for 24 hours.

The mass of oil extracted was estimated by taking the difference between the mass of the vial when empty and with oil after 24 hours of drying in air. The oil content can be calculated from equation 4.9 as follows;

$$x_o = \frac{m_o}{m_s} \text{ x } 100 \qquad [4.9]$$

where x_o is the calculated mass fraction percentage of oil (%), m_o is the mass of oil extracted and m_s is the sample mass before treatment. The accuracy of this method was determined to be ±0.5 wt%.

4.12 Water Content Measurement

The water content of the samples are measured using a technique proposed by Dean and Stark (ASTM D-95). This is a reflux distillation method based on the miscibility and density of a solvent and water.

30 g of drill cuttings samples are placed in a distillation flask. 100 cm^3 of toluene is added to the sample, with the sample completely submerged in the solvent. Toluene is used because it is miscible with the oil content but immiscible with the water content. The distillation flask is then connected to a distilling tube and a condenser. The base of the assembly (distillation flask) is heated in an electric heating mantle as shown in Figure 4.12. The temperature of the distillation flask is approximately 110^oC, which is the boiling point of toluene.

As the experiment progressed, water separates out of the toluene-water mixture in the graduated receiver. This is possible because of gravity separation as water is denser (1 g/cm^3) than toluene (0.87 g/cm^3). The duration of each run was 4-6 hours. The volume of water collected in the graduated receiver is recorded.

The water content of the sample can be estimated as follows;

Since the density of water is 1 g/cm^3, if the volume of water collected was 3 cm^3, then the mass of water will be 3 g.

Equation 4.10 shows the calculation method for the percentage water content.

$$x_w = \frac{m_w}{m_s} \text{ x } 100 \quad [4.10]$$

where x_w is the percentage water content, m_w is the mass of water collected and m_s is the sample mass. The accuracy of the method in measuring the water content of drill cuttings was determined to be ±0.2 wt%.

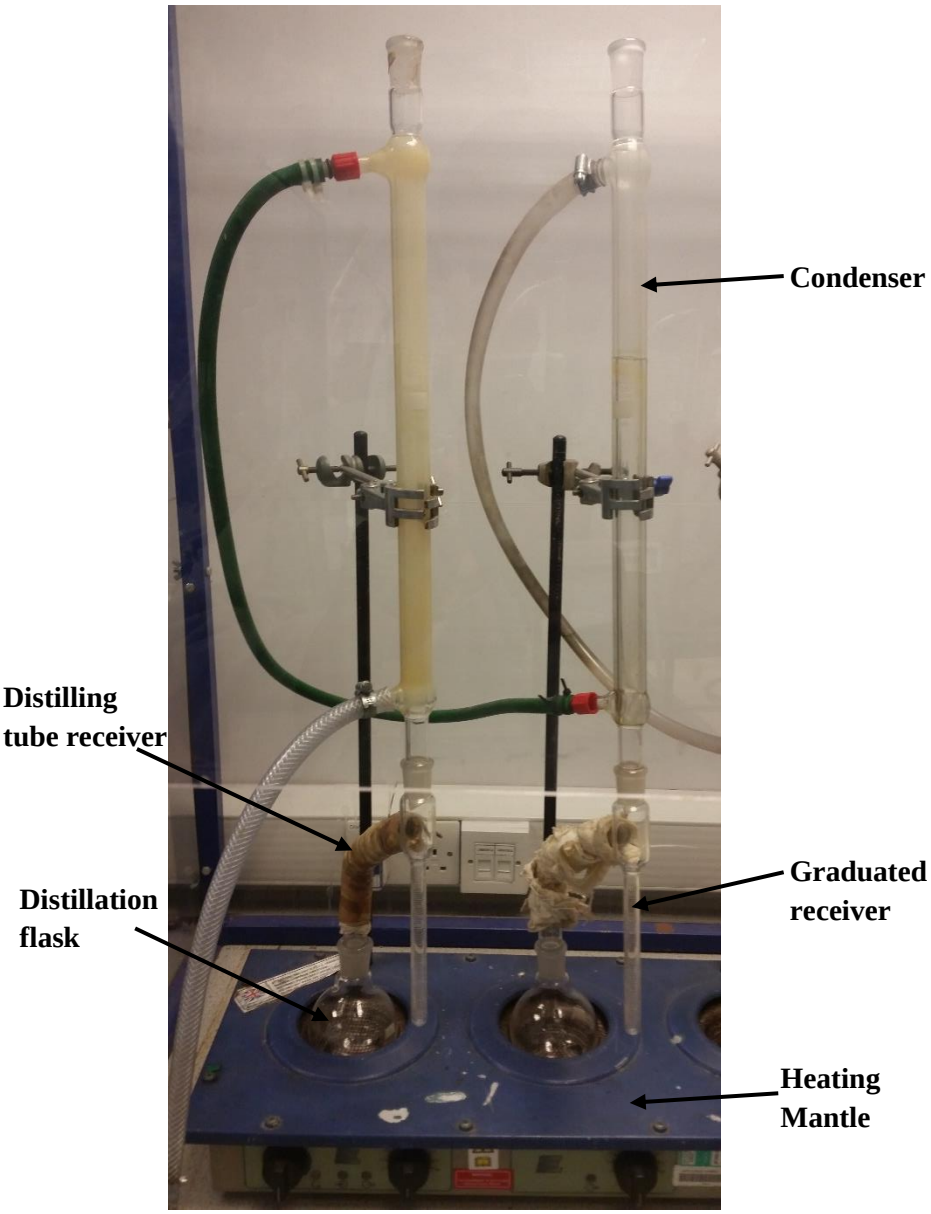


Figure 4.12: Dean and Stark apparatus.

Chapter 5 Thermal Runaway – Dielectric Properties of Key Microwave Absorbing Components in Drill Cuttings

There are two main reasons why understanding the variation of dielectric properties with temperature is crucial in this work. Firstly, dielectric data are an essential input in the optimum design of cavities for all microwave processing systems. This chapter details the dynamic changes observed in the dielectric properties of contaminated drill cuttings with increasing temperature, taking into account the dielectric properties of the key microwave absorbing components.

Secondly, thermal runaway is a serious processing challenge in the microwave processing of drill cuttings. This has been discussed earlier in chapter 3, and is attributed to the accumulation of drill cuttings in the microwave cavity over time. Some drill cuttings samples show significant increase in dielectric properties after the water content, the main microwave absorbing phase, has been removed. As a result, high temperatures and mechanical damage to the cavity have been observed in areas of drill cuttings accumulation. This chapter discusses the dielectric data of the main solid components in drill cuttings in order to evaluate the potential contribution of each component to thermal runaway.

5.1 Dielectric properties of contaminated drill cuttings from 20°C to 150°C

The results presented in Figure 5.1 shows the variation of dielectric constant and loss factor of contaminated drill cuttings with temperature. The dielectric properties were measured using the cavity perturbation technique as detailed in section 4.4. The results highlight the range in dielectric properties of the material in the cavity during microwave treatment. The dielectric data shown throughout this chapter is an average of 3 – 5 independent measurements, and the standard deviation is represented by the error bars.

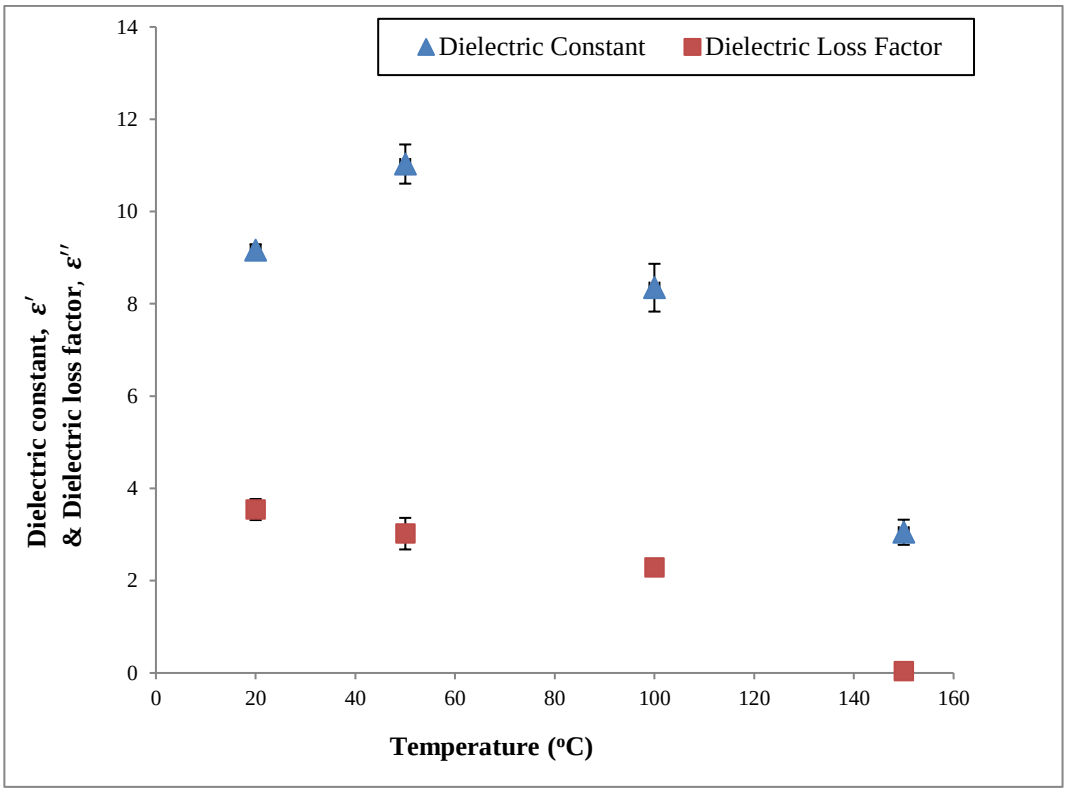


Figure 5.1: The variation of dielectric properties of shale based contaminated drill cuttings (13.8 wt% water, 11 wt% oil) with temperature 912 MHz. Uncertainty in dielectric constant is 0.32-0.77, and 0.12-0.52 in dielectric loss factor.

At 20 °C, water is the main microwave absorbing phase, therefore microwaves will be converted to heating mainly by orientation polarisation. As temperature

increases from 20 ^{o}C to 100 ^{o}C, the material loses the majority of the free water. As a result, the dielectric loss factor decreases, which indicates that the ability of the material to convert microwave energy into heat diminishes as temperature rises. At 100 ^{o}C, which is approximately the normal bulk operating temperature of the continuous microwave treatment system (system C – section 4.3), the dielectric loss factor is 2.29 (Figure 5.1). This can be attributed to the presence of some free water, and physically bound water in the capillaries, and interlayer of the minerals which require higher temperatures to desorb. Bound water will still be present in the pores of the material at 100 ^{o}C because they do not fully exert their vapour pressure. This means that a slightly higher temperature may be required to fully dehydrate the material of the bound water content. Also, it is possible that the presence of ions from dissolved minerals ensure the loss factor is 2.29 at 100 ^{o}C, since the presence of ions generally tend to increase the dielectric properties of materials (Metaxas and Meredith, 2008). Therefore, the explanation for the loss factor value of 2.29 at 100 ^{o}C partly resides in the presence of bound water and ions in the material.

The data in Figure 5.1 shows that the shale based contaminated drill cuttings used in this study has a loss factor of 2.29 at 100 ^{o}C, which indicates it will retain the ability to heat appreciably at the normal bulk operating temperature (100 ^{o}C) of the continuous microwave system. On the other hand, it is most likely that a drill cuttings sample with a significantly smaller proportion of physically bound water (e.g. sandstone based drill cuttings), will lose most its water content at a faster rate at 100 ^{o}C and display a lower loss factor. To assess this, the dielectric properties test of a shale based drill cuttings sample and a sandstone based drill cuttings were carried out. Figure 5.2 shows the variation of the dielectric loss factor of shale based drill cuttings and sandstone based drill cuttings with temperature.

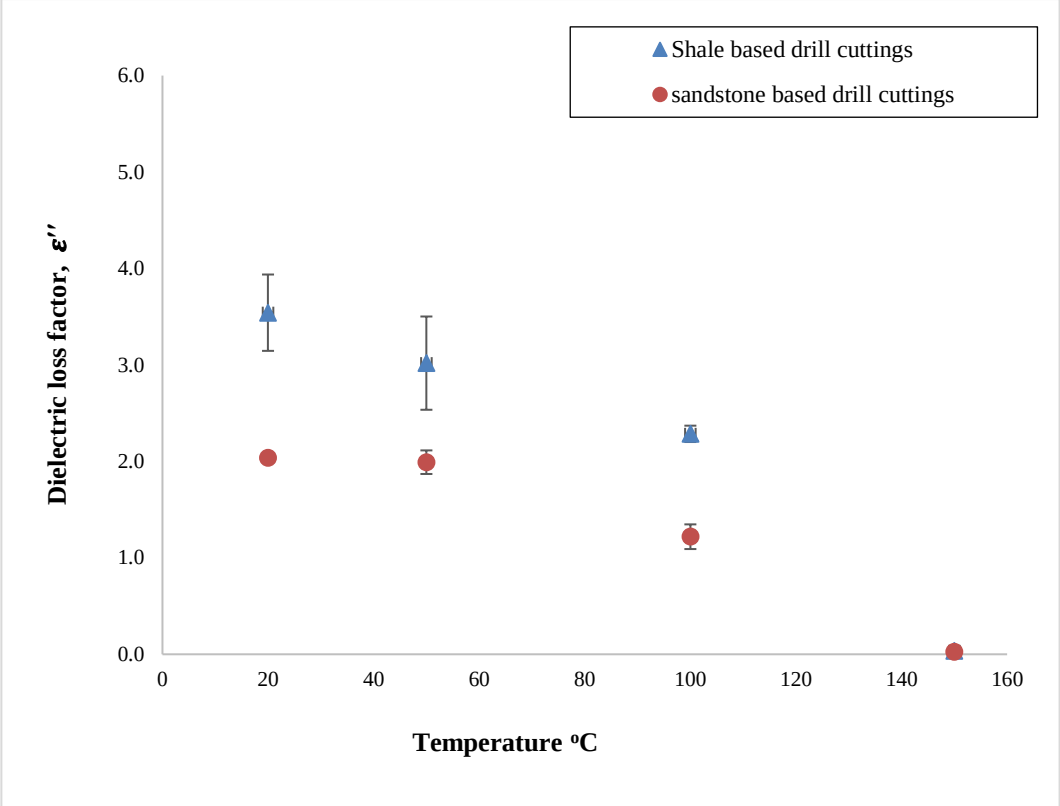


Figure 5.2: The relationship between dielectric loss factor and temperature of shale based drill cuttings (13.8 wt% water, 11 wt% oil), and sandstone based drill cuttings (9 wt% water, 8 wt% oil). Uncertainty in measurement for both samples is 0.01-0.48.

The loss factor values of shale based drill cuttings are clearly greater than that of the sandstone based cuttings at temperatures less than 100 ^{o}C, mainly due to the fact that shale based drill cuttings contains a higher water content (13.8wt%), than sandstone based drill cuttings (9wt%). At 100 ^{o}C, the loss factor of shale based drill cuttings is 2.29, while that of sandstone based drill cuttings is 1.22. This implies that shale based drill cuttings are able to retain a relatively higher quantity of bound water at 100 ^{o}C.

The loss factor decreased from 2.29 at 100 ^{o}C to 0.04 at 150 ^{o}C (Figure 5.1). It is thought that the loss factor decreased to 0.04, and not significantly less than 0.01 (which will classify the material as microwave transparent), because of the presence

of interlayer and hydration water in the material at 150 ^{o}C. While dehydration of some of the interlayer and hydration water would have occurred at 150 ^{o}C, more energy, and higher temperatures, are required to completely desorb these water molecules from the material's solid mineral components. Figure 5.3 shows the major solid mineral components in the shale based drill cuttings sample, which include gypsum, calcite and clay minerals. Studies have shown that the water of hydration in calcite and gypsum may not be completely released until 220 ^{o}C (Strydom et al., 1995; Lindholm et al., 2009; Schmidt et al., 2014), likewise the interlayer and hydration water of clay minerals may not fully desorb until 400 ^{o}C (Mikhail and Guindy, 2007; Xie et al., 2001)

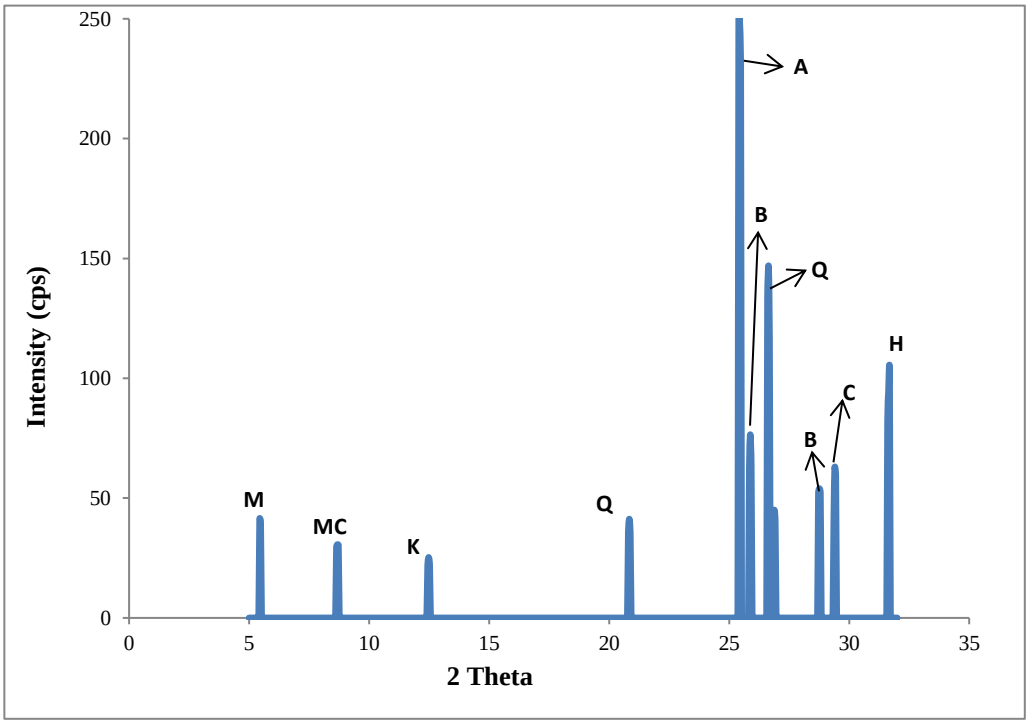


Figure 5.3: XRD showing the major mineral components in shale based drill cuttings; M-montmorillonite (clay); MC-muscovite (clay); K-kaolinite (clay); Q-quartz; A-anhydrite (gypsum), B-barite; C-calcite; H-halite.

Despite the low loss factor value of 0.04 at 150 ^{o}C (Figure 5.1), it is important to note that the material will still heat using microwaves, as materials with loss factors ≥0.01 will heat appreciably under microwave (Metaxas and Meredith, 2008). The heating rate in a material during microwave processing can be estimated using equation 5.1. The full derivation of equation 5.1 is in appendix 4.

$$\frac{\Delta T}{\Delta t}(\text{heating rate}) = \frac{2\pi f \varepsilon_o \varepsilon'' |E|^2}{\rho C_p} \quad [5.1]$$

From equation 5.1, a loss factor of 0.04 at 150 ^{o}C indicates that the material will still heat using microwaves although at a slower rate than at 100 ^{o}C.

According to Figure 5.1, the dielectric constant of contaminated drill cuttings generally decreases as temperature increases from ambient to 150 ^{o}C. This is mainly because of the loss of water from the material's matrix with temperature. There is a slight increase in dielectric constant between 20 ^{o}C and 50 ^{o}C which could be as a result of the decrease in physical binding of water in the pores within the material (Meredith, 1998).

5.2 Dielectric properties of contaminated drill cuttings from 20^{o}C to 850^{o}C

Presented in Figure 5.4 is the high temperature dielectric behaviour of contaminated drill cuttings from 20 ^{o}C to 850 ^{o}C. The dielectric constant and loss factor diminishes rapidly from 20 ^{o}C to 150^{o}C mainly due to the loss of moisture. During microwave treatment, oil is also removed from the material from 20 ^{o}C to 150 ^{o}C, the proportion of which depends on heating rate in the material. Oil is a low loss material and therefore transparent to microwave heating.

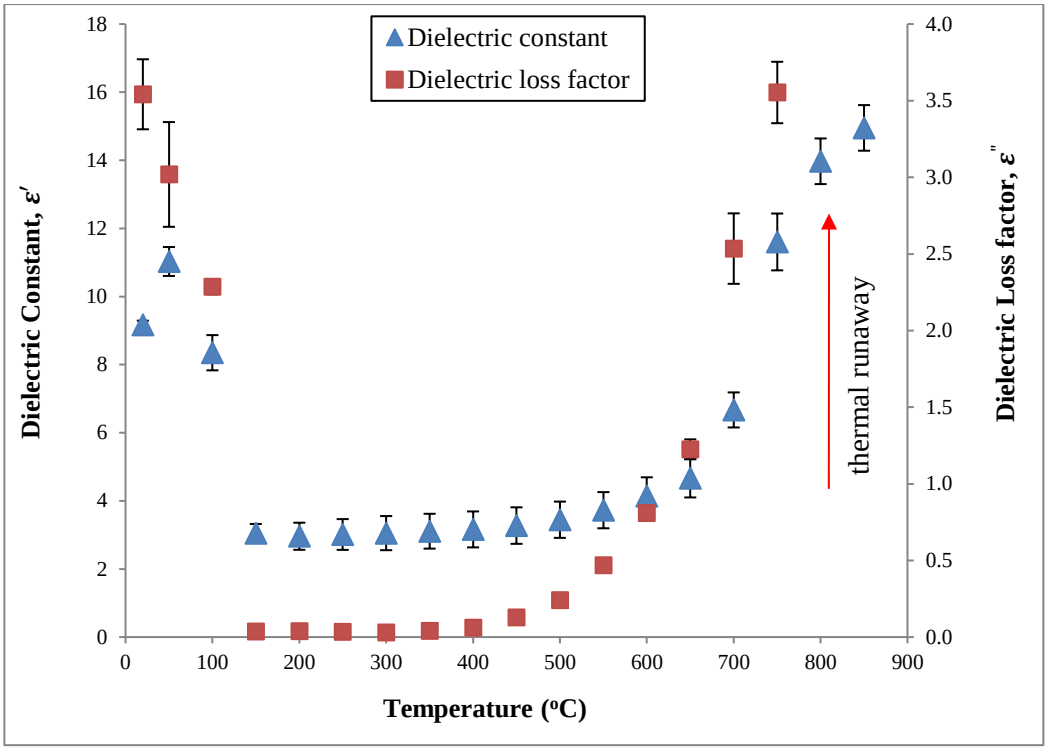


Figure 5.4: Data showing the variation of the dielectric constant and loss factor of shale based contaminated drill cuttings (13.8 wt%, 11 wt% oil) with temperature at 912MHz. Uncertainty in dielectric constant data is 0.22-1.45, and 0.01-0.48 for dielectric loss factor.

Figure 5.5 shows that the dielectric constant and loss factor of oil does not vary significantly with temperature. The dielectric property measurements for oil excluded the 200 – 250 °C range because of the volume change in the sample in this temperature range, as the end point of oil is 250 °C.

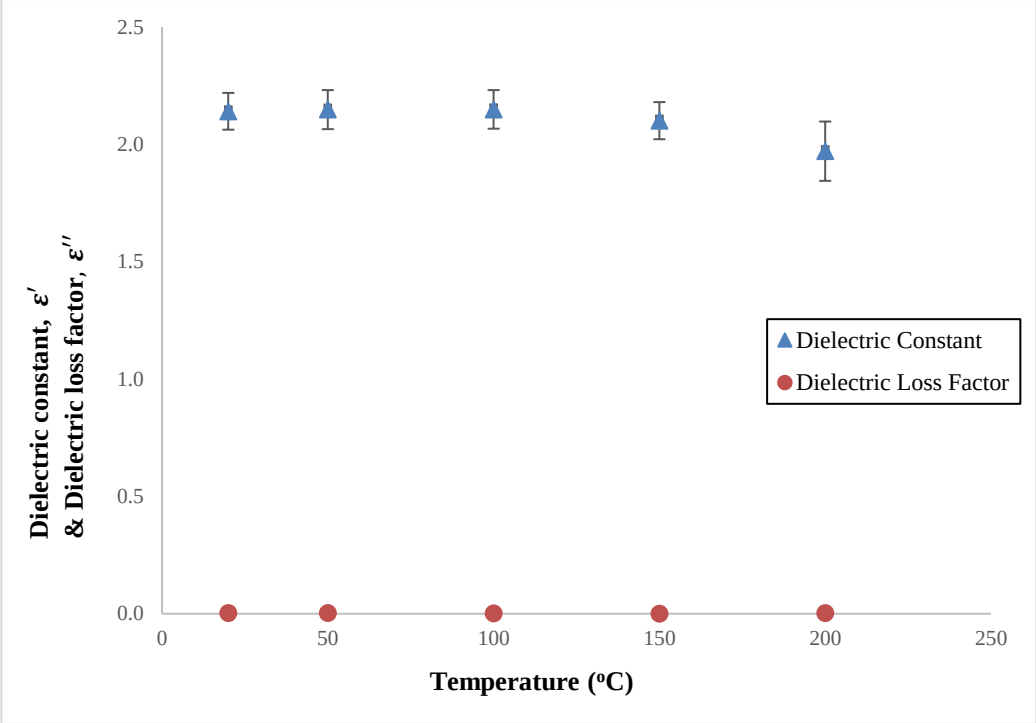


Figure 5.5: Dielectric constant and loss factor of oil at 912MHz as a function of temperature. Uncertainty in the dielectric constant data is 0.02-0.13, and 0.002 for loss factor.

The dielectric loss factor of oil is 0.003 at 20 °C, which reduces slightly to 0.002 at 100 °C. This confirms that the oil phase will be essentially transparent to microwaves. This is in agreement with previous work which demonstrated that aliphatics, the main component in the oil phase of contaminated drill cuttings, are transparent to microwaves because they are non-polar (Stuerga, 2008). The dielectric constant did not display significant changes between 20 °C and 200 °C.

The oil phase is expected to be fully desorbed from the drill cuttings matrix at 250 °C. However, it is possible that a small fraction may be deposited in the drill cuttings material as a carbon rich solid residue during thermal treatment or microwave heating. Carbon or carbon rich materials have been shown to be highly responsive to microwaves, especially at high temperatures (Lester et al., 2006; Atwater and Wheeler, 2003). To ensure that the exponential increase in the

dielectric properties of drill cuttings at 400 ºC and above (Figure 5.4) is not a result of carbon residue from oil during microwave heating, oil was removed from a sample of shale based drill cuttings through Soxhlet extraction using dichloromethane (section 4.11). The sample was dried in an oven for 24 hours at 105 ºC, and its dielectric properties measured. Figure 5.6 shows the dielectric properties of the oil-free shale based drill cuttings as a function of temperature. SEM-EDX analysis was carried out on the dried sample to determine the elemental composition.

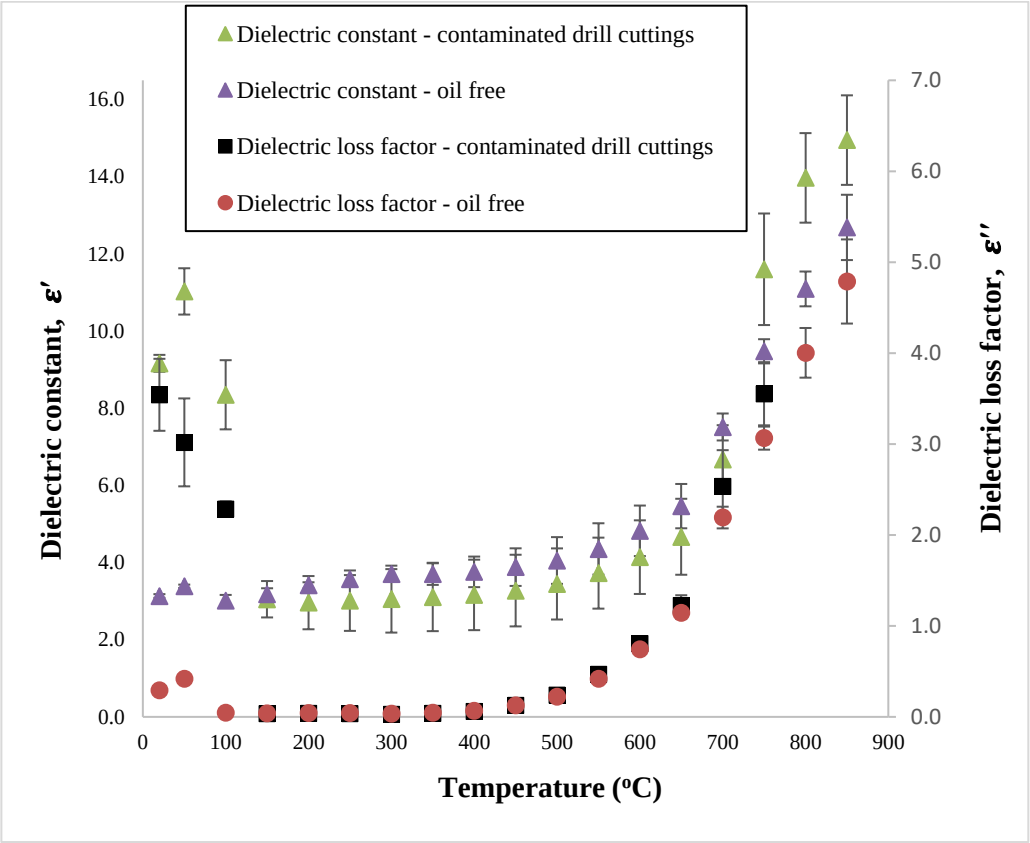


Figure 5.6: Dielectric properties of oil contaminated shale based drill cuttings (13.8 wt% water, 11 wt% oil) and oil free shale based drill cuttings at 912MHz as a function of temperature. Uncertainty in the dielectric constant data is 0.04-1.45, and 0.001-0.48 for loss factor.

According to Figure 5.6 the dielectric constant and loss factor of the oil-free sample are 3.13 and 0.29 respectively at 20 ºC, which increases to 3.39 and 0.42 at 50 ºC.

The loss factor of the oil-free sample decreases to 0.04 at 100 ^{o}C – 400 ^{o}C, which is comparable with the loss factor at 150 ^{o}C – 400 ^{o}C in the contaminated material, coinciding with the removal of all free water and a significant proportion of physically bound water. The value of 0.04 is most likely as a result of interlayer and hydration water still present in the sample at this point.

If one compares the dielectric properties of oil-free drill cuttings with the oil contaminated sample between 100^{o}C and 400^{o}C (Figure 5.6), and the dielectric properties of oil (Figure 5.5), one can conclude that the oil phase does not significantly affect the dielectric behaviour of drill cuttings between 100 ^{o}C and 400 ^{o}C. Interestingly, the dielectric properties of the oil-free sample show an exponential increase above 400^{o}C, similar to the dielectric behaviour of the contaminated drill cuttings sample (Figure 5.6). This means that the oil phase does not affect the dielectric properties of contaminated drill cuttings at temperatures greater than 400^{o}C. Table 5-1 and Figure 5.3 indicate that the oil-free sample contains no carbon, meaning that the increase in dielectric properties at 400^{o}C cannot be attributed to carbon, a carbon based mineral or the oil phase of drill cuttings.

Table 5-1: SEM-EDX analysis showing the elemental composition of shale based drill cuttings

Element	**Dry (oil-free) shale based drill cuttings**
	Weight (%)
Carbon	0
Oxygen	41.89
Sodium	2.24
Magnesium	3.27
Aluminium	6.44
Silicon	12.71
Sulphur	7.25
Chlorine	2.71
Potassium	2.24
Calcium	15.05
Barium	2
Iron	3.41

Data is the average of 3 runs

5.2.1 Dielectric and heat transfer properties of contaminated drill cuttings between 100 ºC and 400 ºC

According to Figure 5.4 the loss factor of shale based drill cuttings is 0.04 between 150 ºC and 400 ºC which suggests that the material will still absorb microwaves in this temperature range, although not to the same extent as at ≤ 100 ºC. Dielectric loss factor directly influences the heating rate as illustrated in equation 5.1. From equation 5.1, the heating rate between 150 ºC and 400 ºC will be significantly lower than at 100 ºC. For example, if we consider the microwave treatment of 70 g of shale based drill cuttings in system A at 1 kW, Table 5-2 shows the value of the parameters in equation 5.1 used to estimate the heating rate at 100 ºC and 150 ºC.

Table 5-2: Parameters used for the estimation of the heating rate in shale based drill cuttings.

Parameters	Values
Frequency, f	2.45×10^{9} GHz
Permittivity of free space, ε_o	8.854×10^{-12} F/m
Sample mass	0.007 kg*
Sample volume	3.33×10^{-5} m^3*
Specific heat capacity, c_p	1.59 kJ/kgK[a]
Dielectric loss factor, ε”	2.29[b], 0.04[c]
Electric field intensity, E	10971 v/m[b,d], 16227 v/m[c,d]

a – specific heat capacity is from (Shang et al., 2012), and is assumed constant from 100 ºC to 150 ºC,
b – value at 100 ºC, c – value at 150 ºC,
d – average electric field intensity estimated from simulations (appendix 5),
* - used in estimating the density (ρ)

From equation 5.1, the average heating rate is 11 ^{o}C/s at 100 ^{o}C, 28 times higher than 0.4 ^{o}C/s at 150 – 400 ^{o}C. Therefore, if the material is allowed to accumulate for long periods of time in the cavity, the heating rate (0.4 ^{o}C/s) suggests that the material will eventually attain temperatures of 400 ^{o}C, which may lead to thermal runaway (Figure 5.4).

There are two main possible reasons why the bulk temperature of drill cuttings increases from 150 – 400 ^{o}C during microwave heating. Firstly, localised temperatures increases from 150 ^{o}C to 400 ^{o}C (or to the equivalent thermal runaway 'initiation temperature' of a microwave system) due to low thermal conductivity of the material. Drill cuttings are granular materials similar to soil in composition, therefore the thermal conductivity will be akin to that of soil. The thermal conductivity of dry soils have been estimated to be < 0.5 W/mK (Yun and Santamarina, 2008; Chen, 2008), and that of dry clay estimated at 0.06 – 0.19 W/mK (Dong et al., 2015). The low thermal conductivity implies that temperatures will increase from 150 ^{o}C to 400 ^{o}C in the material even at low heating rates, as heat loss to surroundings will be low. If we assume that 70 g of shale based drill cuttings is treated in system A (section 4.1), then the absorbed power into a defined cross section of the sample can be estimated by equation 5.2;

$$P_{ab}\text{- heat loss } \left(\frac{KA(T_p-T_s)}{L}\right)=\text{heat gain } \left(\frac{mc_p\Delta T}{t}\right) \qquad \text{Equation 5.2}$$

where, P_{ab} is absorbed power, k is the thermal conductivity, L is the characteristic path of thickness of the sample, A is the heat transfer cross-sectional area, m = mass of sample, C_p = specific heat capacity of drill cuttings, T_p is the temperature of the mineral phase in the cross section of interest, T_s is the temperature of the surrounding solid mineral phase or fluid, and t is time.

Equation 5.2 illustrates what may occur within a defined volume of material with low thermal conductivity will have low heat losses to the surroundings, ensuring the temperature in the material increases. Consider a simple hypothetical case of heat transfer during microwave heating illustrated in Figure 5.7. The thermal conductivity (k) of the quartz reactor is assumed to be 8.4 W/mK, 0.06 W/mK for dry clay and <0.5W/mK for bulk dry drill cuttings ((Farouki, 1986; Yun and Santamarina, 2008). The temperature difference (ΔT_1) across a defined cross section within the matrix will be significantly higher than the temperature difference (ΔT_2) across a cross section near the reactor surface. This is because of the faster rate of heat loss from the surface of the quartz reactor.

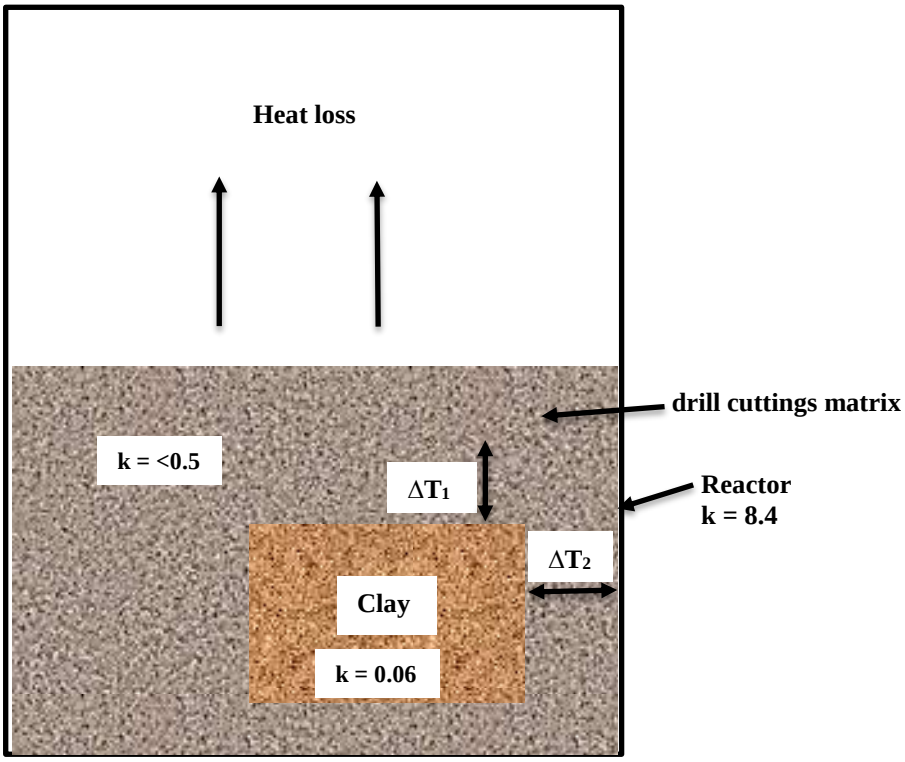


Figure 5.7: Schematic of drill cuttings showing thermal properties.

An increase in temperature to the thermal runaway 'initiation temperature' (400 ^{o}C for the shale-based drill cuttings used in this work) of the continuous microwave system can be prevented by adjusting the residence times in the cavity according to the power density, electric field intensity distribution, and heating rate in the low thermal conductivity materials. Essentially, materials with the lowest thermal conductivities in drill cuttings constitute the rate limiting factor on the efficiency of heat transfer, and ultimately how amenable a cross section of the material will be to thermal runaway.

The second possible reason the material's temperature may increase from 150 ^{o}C to 400 ^{o}C during microwave heating is due to the presence of physically bound water in the sample at 150 ^{o}C – 400 ^{o}C. It is thought that physically bound water will continue absorbing microwaves from 150^{o}C to 400^{o}C before desorption. This supports the suggestion of Robinson et al., (2008) that physically bound water may not be fully desorbed from the drill cuttings matrix till 300 ^{o}C. It is most likely that a combination of low thermal conductivity and microwave absorption in bound water ensures that high temperatures, sufficient to initiate and sustain thermal runaway, are attained during microwave heating of contaminated drill cuttings.

5.2.1.1 Dielectric and heat transfer properties of sandstone based drill cuttings

Empirical observations during experimental runs in the industrial microwave system (system C – section 4.3) show that thermal runaway does not occur when processing sandstone based drill cuttings. Dielectric properties measurements were carried out to explore this. Presented in Figure 5.8 is the dielectric properties of sandstone based drill cuttings used in this work (system A).

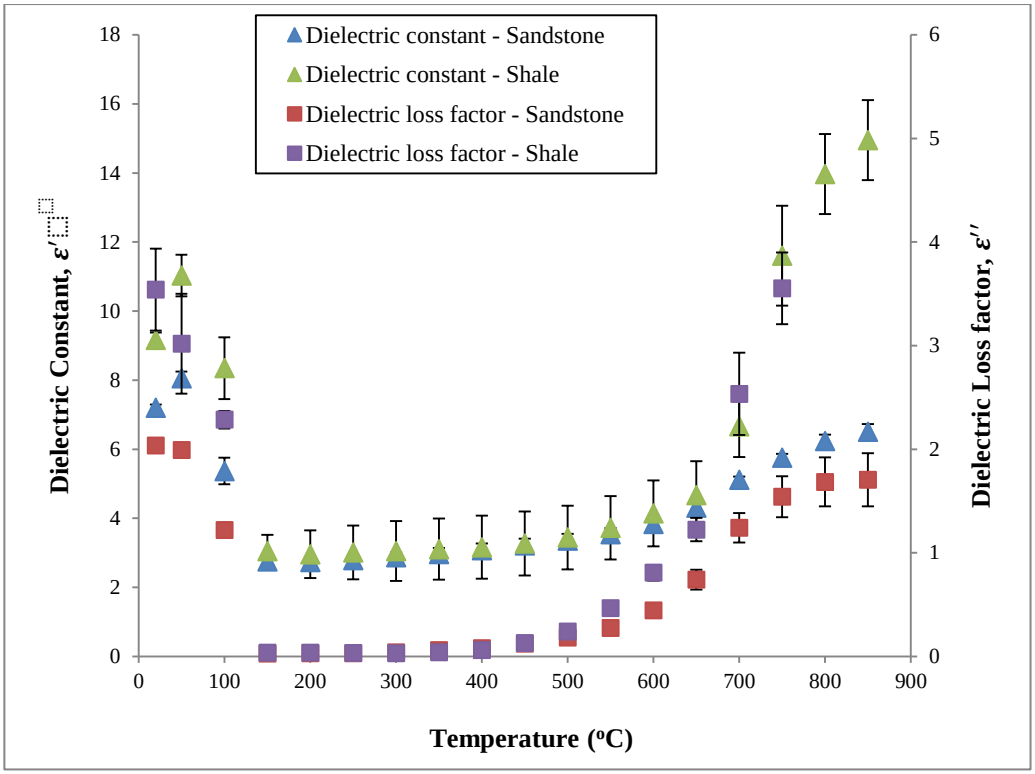


Figure 5.8: Dielectric properties of shale based drill cuttings (13.8 wt% water, 11 wt% oil) and sandstone based drill cuttings (9 wt% water, 8 wt% oil) at 912MHz as a function of temperature. Uncertainty in the dielectric constant data is 0.16-1.45, and 0.001-0.48 for loss factor.

The dielectric constant and loss factor of the sandstone based drill cuttings is lower than the shale based drill cuttings sample from ambient to 150 ºC due to its lower water content. From 150 ºC to 400 ºC, the dielectric properties of both drill cuttings samples are comparable. One can readily see from Figure 5.8 that there is an exponential increase in the dielectric properties of both shale and sandstone based drill cuttings from 400ºC. The exponential increase in dielectric properties after 400 ºC appear to be greater in the shale based drill cuttings, which is thought to be due to mineralogical differences between the two samples. Tables 5-3 and 5-4 shows the typical mineral composition in the sandstone and shale based drill cuttings used in this work.

Table 5-3: Mineral composition in shale based drill cuttings

Mineral	% Composition	Standard Deviation
Anhydrite	37.90	1.47
Calcite	3.50	0.93
Halite	14.60	0.74
Clay	26.50	2.34
Quartz	17.60	0.88
Barite	2.00 -7.00	0.74

Table 5-4: Mineral composition of sandstone based drill cuttings

Mineral	% Composition	Standard Deviation
Anhydrite	14.0	1.47
Calcite	10.40	0.93
Halite	17.80	0.74
Clay	25.00	2.34
Quartz	32.80	0.88
Barite	2.00 – 7.00	0.74

The mineralogy of shale and sandstone drill cuttings differ to some extent. For example, shale based drill cuttings contain a higher clay content and lower quartz content than the sandstone based drill cuttings. According to Figure 5.8, thermal runway will be initiated in both the sandstone and shale based samples if temperatures of 400 ^{o}C and above are reached. However, empirical observations

show that thermal runaway does not occur during microwave processing of sandstone based drill cuttings. This indicates that the thermal runaway initiation temperature (400 ^{o}C in this work) is never attained in the sandstone based matrix during microwave heating. The reason for this is thought to be as a result of the different mineralogical composition in sandstone based cuttings, which is most likely due to the lower concentration of clay and higher quartz concentration in sandstone. Lower clay content means a lower proportion of bound water. It is thought that microwave absorption by bound water causes temperature to increase from 100 ^{o}C to 400 ^{o}C during microwave heating. It is highly likely that sandstone based drill cuttings may not reach the thermal runaway initiation temperature due to the mineralogical differences mentioned above.

The results in Figure 5.6 indicate that the thermal runaway phenomenon is as a result of the dielectric properties of the solid components of the material at high temperatures. Therefore, more emphasis is placed on the solid phase of drill cuttings in the next sections.

5.2.2 Dielectric properties of contaminated drill cuttings between 400 ^{o}C and 850 ^{o}C

Figure 5.6 shows that the dielectric properties of drill cuttings increases exponentially above 400 ^{o}C. The dielectric constant increases from 3.18 at 400 ^{o}C to 12.69 at 850 ^{o}C. This means that the material is 4 times more efficient at storing microwave energy at 850 ^{o}C than at the cold feed stage (20^{o}C in Figure 5.4) into the industrial microwave system. The exponential increase in dielectric properties after 400 ^{o}C causes thermal runaway in the sample, which will then lead to vitrification. A key observation is that the loss factor increased by 10 orders of

magnitude from 350 ^{o}C to 850 ^{o}C (Figure 5.6). The implication, using the shale based drill cuttings in this work as an example, is that the heating rate in the vitrified section can be as high as 200 ^{o}C/s at 800 ^{o}C, 18 times higher than the heating rate at normal operating temperature (100 ^{o}C).

Based on the data from Figure 5.4 and Figure 5.6, the loss factor of the drill cuttings material increases significantly from 400 ^{o}C to 850 ^{o}C. This in turn will cause the temperature of the material to increase during microwave heating. As a result, temperatures in excess of 1000 ^{o}C, where vitrification of the drill cuttings material occur, is reached. Vitrification of the material will most likely occur at 1100 ^{o}C – 1450 ^{o}C (Tedder and Pohland, 1995). Although it is difficult to prove the maximum temperature reached in the vitrified section of drill cuttings during microwave heating, the colour change observed from the brown colour of dried drill cuttings (Figure 5.9) to the dark grey/black colour of vitrified drill cuttings residue (Figure 5.10) may help to assess the magnitude of temperature rise during the vitrification process.



Figure 5.9: Dried shale based drill cuttings (colour – brown).



Figure 5.10: Residue produced from the microwave vitrification of shale based drill cuttings showing a dark grey/black colour distinct from the brown colour before microwave vitrification.

The dark grey/black pigmentation in the vitrified residue is thought to be due to the formation of magnetite (Fe_3O_4) from the thermal reduction of hematite (Fe_2O_3) at high temperatures. Table 5-1 shows that drill cuttings contain iron.

Magnetite is formed from the high temperature reduction of hematite in the presence of catalysts at temperatures up to 1350 ^oC (Chen et al., 2015), and in air at temperatures up to1410 ^oC (Voitkovsky et al., 1995). Based on this, and the fact that high heating rates in the region of 200 $^oC/s$ is possible during vitrification, it is most likely that temperatures during microwave vitrification of drill cuttings increases to 1410 ^oC. This is probably the reason magnetite, and possibly other black minerals (such as iron sulphide) that give the vitreous residue its black pigmentation, are formed.

The reduction of hematite to magnetite is a reversible redox reaction as shown in equation 1.2.

$$1.5\ Fe_2O_3\ (s) \rightleftharpoons Fe_3O_4\ (s) + 0.25\ O_2\ (g) \qquad \text{Equation 5.3}$$

The vitrified residue was placed in a quartz tube and heated in a furnace (in air) to 850 ^{o}C, as part of the procedure of the cavity perturbation technique (section 4.4). Interestingly, the dark grey/black colour of the vitrified sample (Figure 5.10) changed to yellowish brown (Figure 5.11), which is thought to show the oxidation of magnetite in the vitrified material to the more stable hematite.



Figure 5.11: Vitrified drill cuttings showing a yellowish brown colour after oxidation in air to 850^{o}C

The vitrification process is characterised by complex high temperature reactions. If one considers such reactions involving sulphates, for example the high temperature thermal decomposition of anhydrite (equations 5.4 & 5.5), it becomes apparent that these reactions may result in a lower sulphur and oxygen content in vitrified drill cuttings residue. Presented in Table 5-5 is the elemental composition of dry drill shale based drill cuttings and its vitrified residue, and it shows that the sulphur and oxygen content are significantly lower in the vitrified residue.

$$CaSO_4\ (s) \longrightarrow CaO\ (g) + SO_3\ (g) \qquad \text{Equation 5.4}$$

$$CaSO_4\ (s) \longrightarrow CaO\ (g) + SO_2\ (g) + 0.5O_2\ (g) \qquad \text{Equation 5.5}$$

Table 5-5: SEM-EDX analysis showing the elemental composition in drill cuttings and vitrified drill cuttings

Element	**Vitrified shale based drill cuttings**	**Dry (oil-free) shale based drill cuttings**
	Weight (%)	Weight (%)
Carbon	0	0
Oxygen	41.86	37.14
Sodium	2.24	2.76
Magnesium	3.27	2.20
Aluminium	6.44	5.49
Silicon	12.71	17.91
Sulphur	3.70	0.85
Chlorine	2.71	3.71
Calcium	15.05	13.15
Barium	2.16	11.29
Iron	3.41	3.62

Data is the average of 3 runs

5.3 High temperature dielectric properties of the main solid components in drill cuttings

Several complex chemical reactions occur in the solid phase of drill cuttings at high temperatures ≥400 ^{o}C which are important in understanding the dielectric behaviour at those temperatures. Ideally, the high temperature reactions of each mineral content and drilling fluid additive will be studied along with their dielectric properties to gain a full picture of the thermal runaway phenomenon observed at 400^{o}C and above. However, this is beyond the scope of this work. Therefore, this section will focus on the dielectric properties of the major solid minerals (Figure

5.3) which are thought to exert greater influence on the dielectric properties of drill cuttings.

A dynamic thermal analysis, using TGA, was carried out on the solid phase of drill cuttings to assess reactions. This is presented in Figure 5.12 and shows mass loss at high temperatures. Dry shale based drill cuttings (oil and water removed) was tested in the TGA analysis as described in section 4.5.

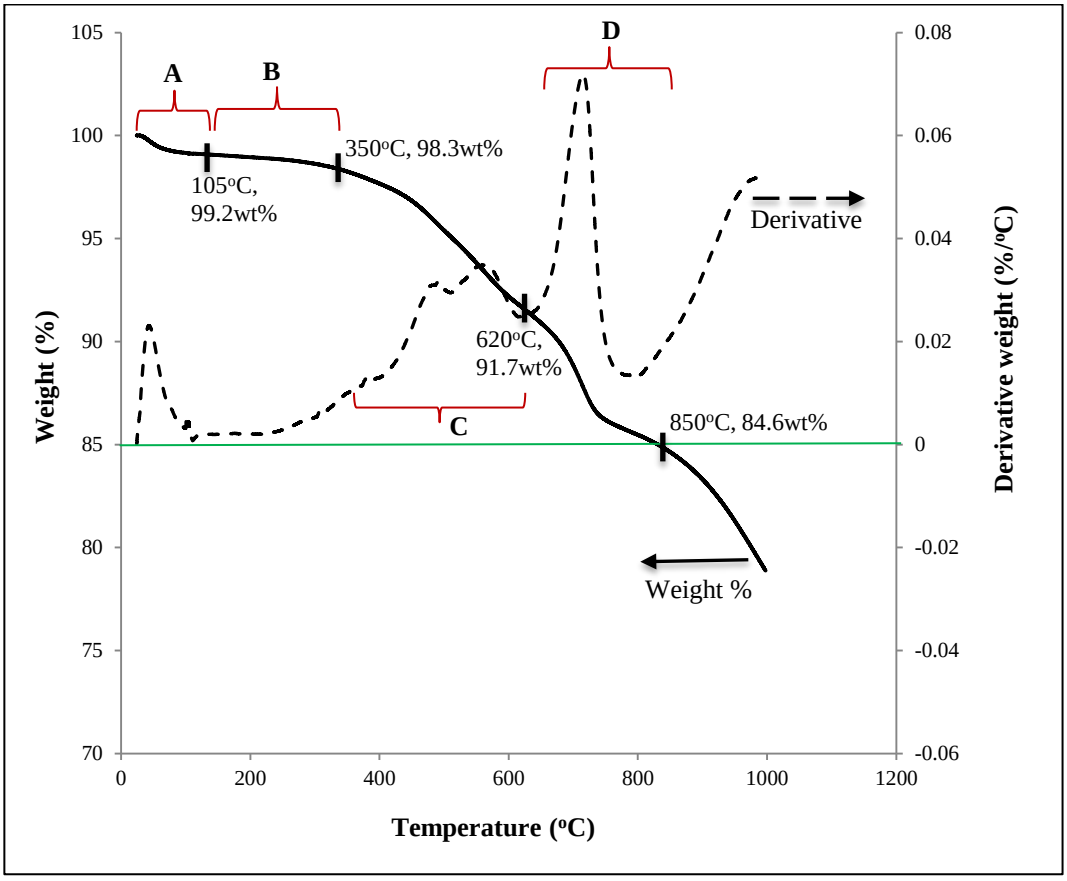


Figure 5.12: Thermogravimetric analysis of shale based drill cuttings; A=loss of moisture; B=loss of hydration and interlayer water; C=loss of chemically bound water from clay minerals (dehydroxylation); D=dehydroxylation and loss of carbon dioxide from calcite. 35mg sample, 5 °C/min heating rate.

The data is Figure 5.12 shows that the material decreases in mass to 99.2wt% between 25 ^{o}C and 105 ^{o}C, corresponding to the dehydration of adsorbed moisture. From 105 ^{o}C to 350 ^{o}C, the mass decreases from 99.2 wt% to 98.3 wt% mainly due to the removal of physically bound interlayer and hydration water. The mass loss between 350 ^{o}C and 850 ^{o}C is 13.7wt% which coincides with the rapid rise in dielectric properties of drill cuttings. There are some minerals present in the drill cuttings (Figure 5.3) such as calcite, kaolinite and montmorillonite which are expected to decrease in mass between 350 ^{o}C and 850 ^{o}C as they decompose and lose their chemically bound water (Balek and Murat, 1996; Grim, 1968; Schmidt et al., 2014). These minerals most likely account for the mass loss seen in Figure 5.12 from 350 ^{o}C – 850 ^{o}C. Other non-clay minerals such as anhydrite and barite will either not decompose or show negligible mass loss between 400 ^{o}C and 850 ^{o}C (Yu and Brouwers, 2012), but their crystalline structure will transform to a more amorphous structure as the temperature increases, potentially improving the dielectric properties of the material.

5.3.1 Calcite

Figure 5.13 shows that calcite is a low loss material, with a loss factor of 0.03 at 400 ^{o}C, decreasing to 0.007 at 800 ^{o}C. This indicates that the dielectric properties of calcite does not affect the thermal runaway observed in drill cuttings from 400 ^{o}C (Figure 5.6). Calcite breaks down to calcium oxide and carbon dioxide at 650 ^{o}C – 720 ^{o}C (Schmidt et al., 2014), as shown in the mass loss of drill cuttings (D in Figure 5.12). Despite the breakdown of calcite at 650 – 720 ^{o}C, the dielectric constant and loss factor remain relatively low (Figure 5.13), indicating that the reactions in calcite at 650 ^{o}C – 720 ^{o}C does not increase the dielectric properties of drill cuttings.

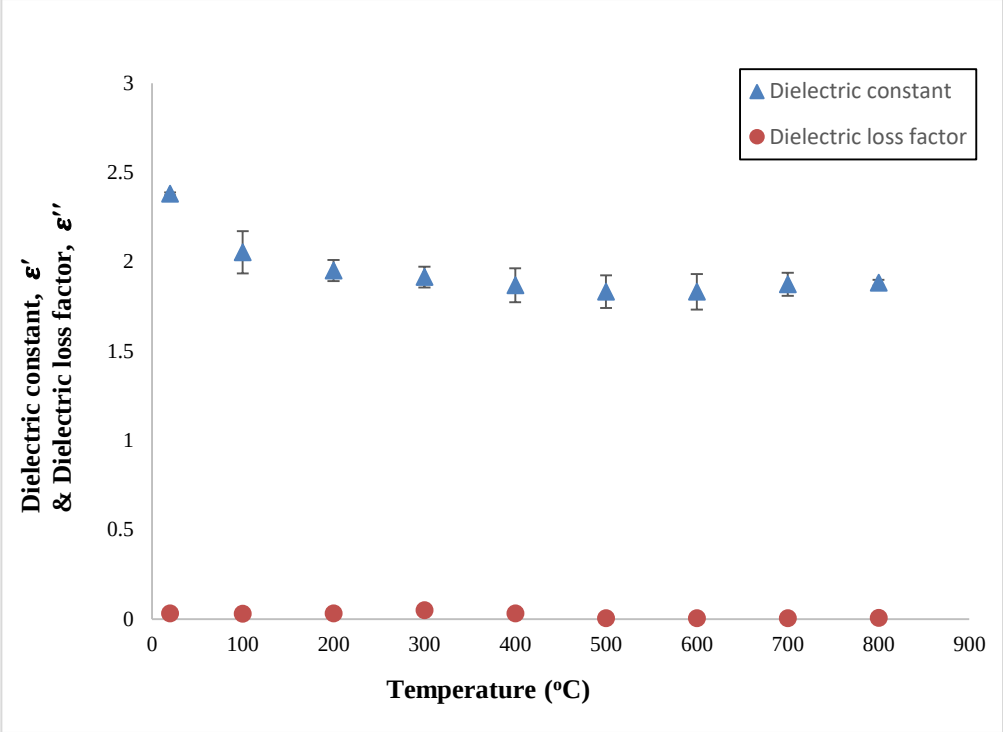


Figure 5.13: Dielectric properties of calcite at 912MHz as a function of temperature. Reagent grade calcite used with 97% purity. Uncertainty in the dielectric constant data is 0.01-0.1, and 0.001-0.003 for loss factor.

5.3.2 Quartz

Quartz is known to be essentially transparent to microwaves at room temperature (Metaxas and Meredith, 2008). Robinson, et al. (2014) noted that quartz is a low loss mineral, and is transparent to microwaves up to 500 °C. Presented in Figure 5.14 is the dielectric properties of quartz from ambient to 600 °C. There appears to be no temperature effect on the dielectric properties, as the dielectric constant and loss factor remained more or less constant. For example, the loss factor was 0.0014 at 400 °C, and 0.0017 at 600 °C. On this basis, it not likely that quartz contributes to the thermal runaway of drill cuttings observed from 400 °C.

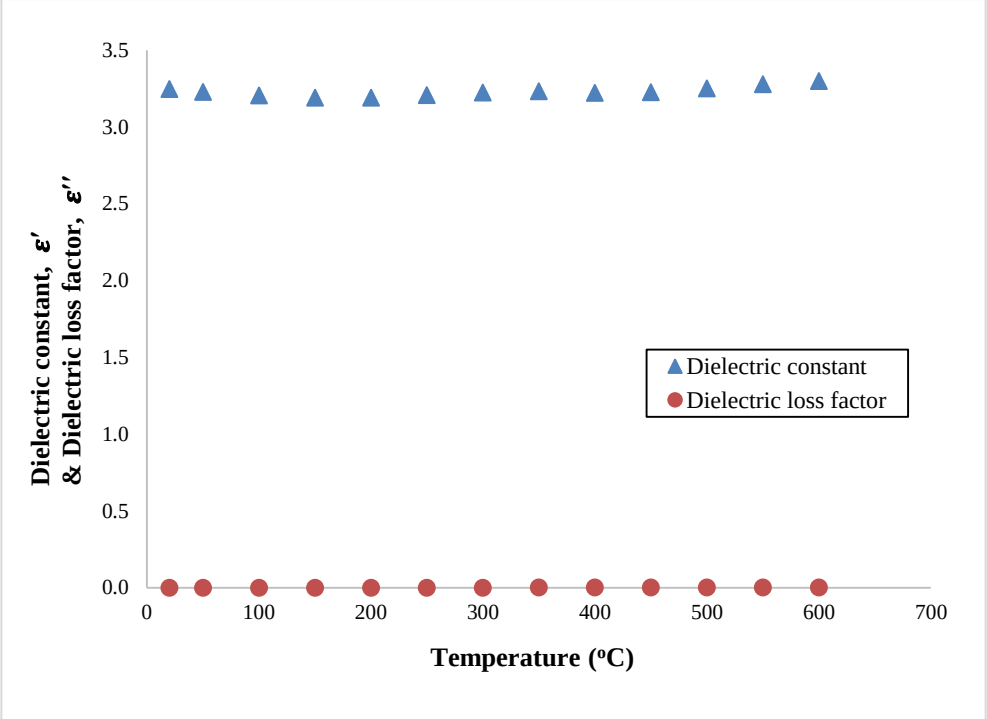


Figure 5.14: Dielectric properties of quartz as a function of temperature at 2.45GHz. Results represent one set of experiments.

5.3.3 Anhydrite and Barite

Presented in Figure 5.15 are the dielectric properties of anhydrite and barite. The dielectric properties of anhydrite is relatively constant at 20–220 °C, which corresponds to the complete dehydration (Strydom et al., 1995; Lindholm et al., 2009). The loss factor is ≤ 0.01 from room temperature to 850 °C, meaning that anhydrite will be transparent to microwaves during microwave heating at 400°C – 850°C.

Barite, another sulphate compound, on the other hand displays a remarkably different dielectric behaviour from anhydrite between 400 °C to 850 °C. The loss factor increases from 0.01 at 400 °C to 1.28 at 850 °C, which indicates that barite contributes to the thermal runaway phenomenon in drill cuttings to a certain extent.

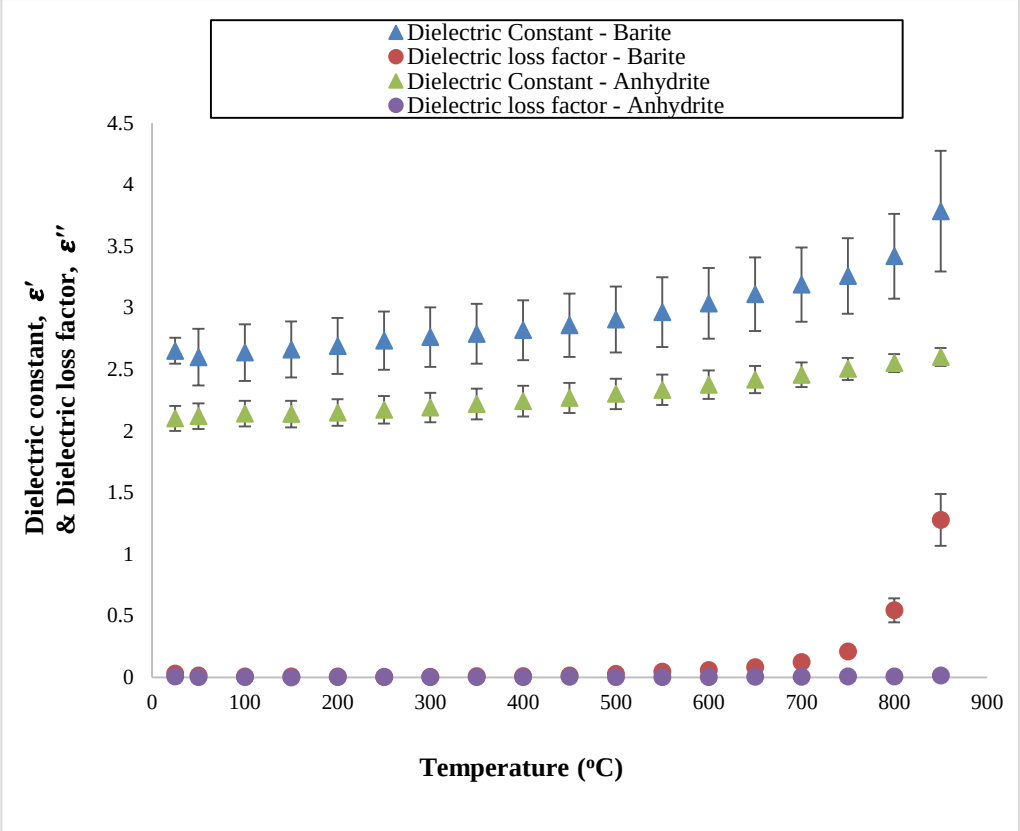


Figure 5.15: Dielectric properties of Anhydrite (99% purity) and Barite (97% purity) at 912MHz as a function of temperature. Uncertainty in the dielectric constant data for barite is 0.11-0.50, and 0.07-0.12 for anhydrite. Uncertainty in the loss factor data for barite is 0.001-0.211, and 0.001-0.004 for anhydrite.

This is likely to be caused by weakening of the bonds between individual barite molecules at high temperatures, which means that the individual molecules are less restricted and are able to respond to an applied electric field. At >750 °C, the exponential increase in loss factor observed for barite suggests that ions are formed as the material breaks down, leading to ionic conduction under microwaves. This result is interesting because barite is an important drilling fluid component common to most drill cuttings produced from drilling operations. For example, barite was found to be approximately 2-7 wt% in the shale based drill cuttings used in this study.

5.3.4 Halite and Clay Minerals

Presented in Figure 5.16 is the dielectric properties of halite. The loss factor of halite is ≤ 0.01 up till 600 ^{o}C, suggesting that the microwave heating in drill cuttings below 600 ^{o}C cannot be attributed to halite. This is most likely because the ionic bonds in the solid crystal structure of halite are relatively rigid at ≤ 600 ^{o}C, and do not respond to an alternating electric field at 912MHz. However, the loss factor rises to 0.02 at 600 ^{o}C, increasing to 2.92 at 750 ^{o}C. This indicates that a greater proportion of ions in the halite structure attain a higher level of mobility at 600 – 750 ^{o}C, leading to microwaves absorption through ionic conduction. As halite melts at approximately 800 ^{o}C, the dielectric properties of halite is expected to increase from 750^{o}C through to the vitrification temperature (1100– 1450 ^{o}C) of the drill cuttings material.

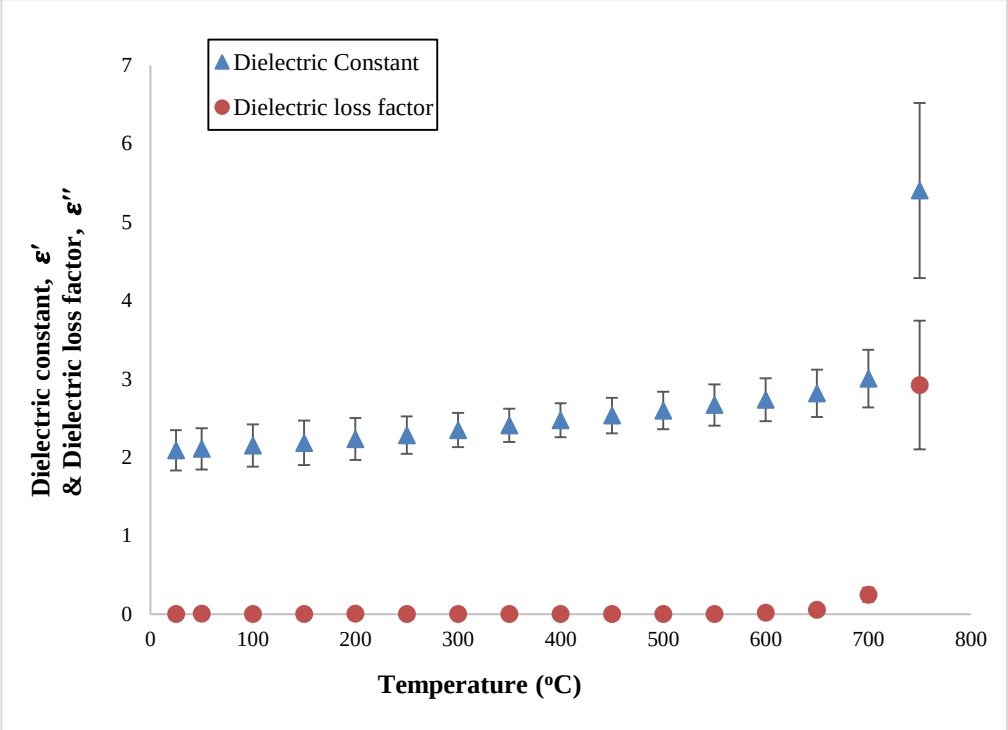


Figure 5.16: Dielectric properties of halite (97% pure) at 912MHz as a function of temperature. Uncertainty in the dielectric constant data is 0.21-1.77, and 0.001-0.819 for the loss factor.

Similarly, ionic conduction is thought to be main reason the dielectric properties of clay minerals increase from 400–850 ^{o}C (Figure 5.17 & 5.18). The increase in dielectric constant and loss factor in clay minerals from 20 ^{o}C to 100 ^{o}C is most likely as a result of interlayer water. Montmorillonite displays better dielectric properties than kaolinite and muscovite at 20–100 ^{o}C mainly due to the ability of its interlayer cations to hydrate to a greater extent, and store a higher proportion of physically bound water. The increase in loss factor of clay minerals from 400– 850 ^{o}C in Figure 5.18 is thought to be mainly due to dehydroxylation (C & D in Figure 5.12), as the chemically bound water (OH^{-} group) in the clay structure become increasingly mobile with increasing temperature.

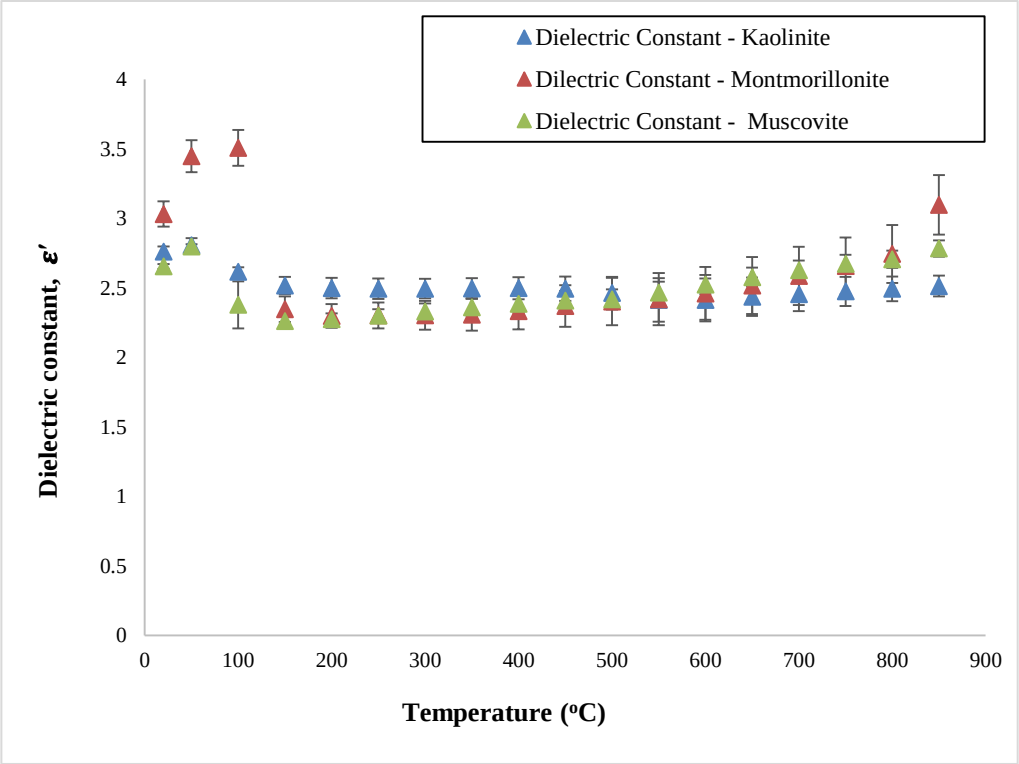


Figure 5.17: Dielectric constant of clays (Kaolinite, montmorillonite and muscovite) at 912MHz as a function of temperature. Data provided by a fellow PhD researcher - Miguel Angel Calvo-Carrascal (personal communication, 2016). Uncertainty in data is 0.03-0.24.

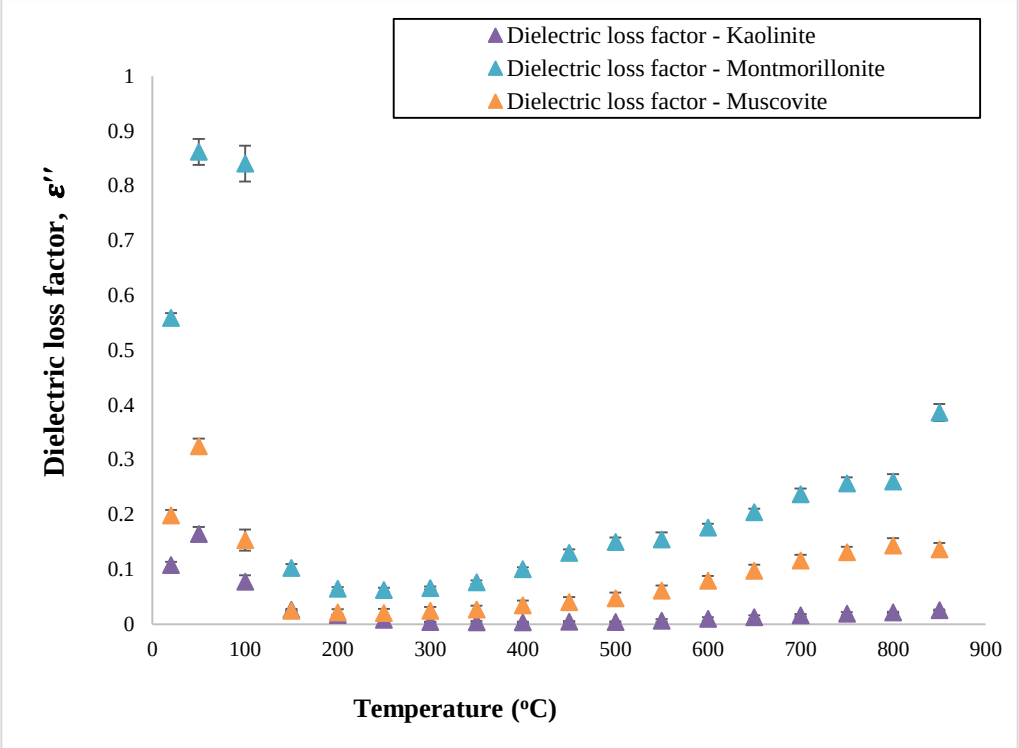


Figure 5.18: Dielectric loss factor of clays (kaolinite, montmorillonite and muscovite) at 912MHz as a function of temperature. Data provided by a fellow PhD researcher – Miguel Angel Calvo-Carrascal (personal communication, 2016). Uncertainty is 0.01-0.04.

The polarisation of the mobile OH^- group under microwave ensures that the dielectric properties of the clay minerals increases from 400 °C and above. In addition, it is possible that interlayer cations also help to improve the ability of the clay minerals to convert microwave power to heat due to increased ionic mobility at higher temperatures. Interlayer cations will probably impact the dielectric properties of the material to a greater extent than the OH^- group at 800 °C and above because a significant proportion of the OH^- group will most likely be lost in the dehydroxylation process (Figure 5.12).

The key microwave absorbing components in the solid phase of drill cuttings have been identified as barite, halite and clay minerals. Figure 5.19 shows a comparison of the rate at which each key microwave absorbing component in the shale based drill cuttings used in this work will interact with microwaves at high temperatures.

It is apparent that the dielectric properties of clay minerals, especially montmorillonite, ensures drill cuttings attain the thermal runaway 'initiation temperature', shown to be approximately 400 ^{o}C for the shale based sample in this work (Figure 5.4). However, at 700 ^{o}C and above, it appears that barite and halite have a greater impact on the dielectric properties of drill cuttings than the clay minerals.

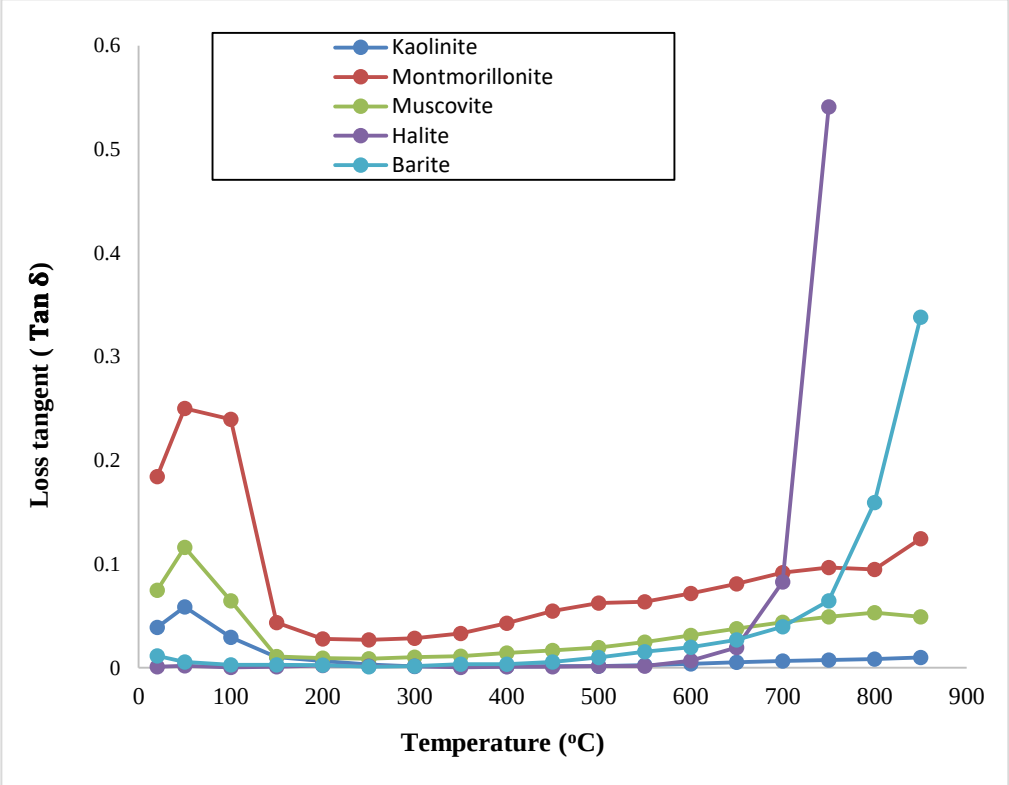


Figure 5.19: Loss tangent of the key solid microwave absorbing components of drill cuttings as a function of temperature.

5.4 Dielectric properties of vitrified drill cuttings

The potential for thermal runaway (vitrification) when drill cuttings stick and accumulate in the cavity during microwave heating has already been shown in this work. However, the dielectric properties of the product of vitrification (dark grey/black residue shown in Figure 5.10) are unknown. An assessment of the high temperature dielectric properties of the vitrified residue is essential in order to understand the potential effect of the accumulation of the residue on the operability of the continuous microwave system. The dielectric properties of the microwave vitrified residues is shown in Figure 5.20. Based on the data, the vitrified residue will absorb microwaves from room temperature to the normal operating temperature (100 ^{o}C) of the microwave system, at a similar rate to dry drill cuttings (Figure 5.9).

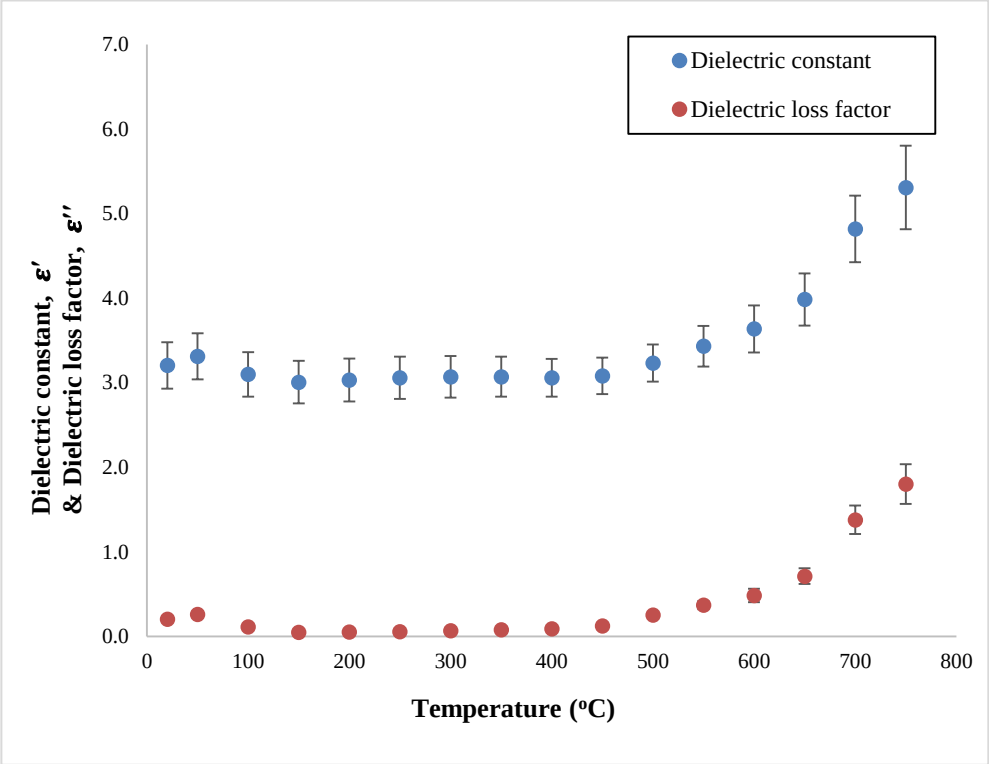


Figure 5.20: The dielectric properties of vitrified drill cuttings as a function of temperature. Uncertainty in dielectric constant data is 0.21-0.49, and 0.01-0.24 in loss factor.

The vitrified material has a low loss factor of 0.05 – 0.09 between 150 ^{o}C and 400 ^{o}C, meaning that although it will still absorb microwaves, it will only heat slowly in this temperature range. Comparing the dielectric loss constant and loss factor of the vitrified residue (Figure 5.20) with that of drill cuttings (Figure 5.4) shows that both materials are extremely inefficient at absorbing microwaves between 150^{o}C and 400^{o}C, taking into account the dielectric properties of drill cuttings under normal operations (20– 100 ^{o}C in Figure 5.4). Therefore, an accumulation of the vitrified residue in the cavity at 20–400 ^{o}C does not pose a greater risk of damaging the cavity than that of dry drill cuttings.

From 400 ^{o}C to 750 ^{o}C the loss factor of the vitrified residue increases significantly by 20 fold (Figure 5.20). However, the dielectric constant only shows a modest increase from 3.06 to 5.31 in the same temperature range. It may appear that drill cuttings will absorb a greater proportion of microwaves, and hence, heat faster at ≥400 ^{o}C than the vitrified residue due to its higher dielectric constant value (Figures 5.4 and 5.20). Nevertheless, a comparison of the loss tangent of the vitrified residue and dry drill cuttings (Figure 5.21) shows that both materials are susceptible to microwaves at similar rates from 400 C to 750 ^{o}C. Therefore, the heating rate, and thus, rate of temperature rise in the vitrified residue will be similar to the rate of temperature rise in drill cuttings as the material vitrifies (thermal runaway). This means that the vitrified residue is just as likely to overheat and damage the cavity as drill cuttings if allowed to accumulate in the cavity at temperatures ≥ 400 ^{o}C. The rotary wheel applicator (section 4.3) is part of a robust material transport system that will ensure that drill cuttings do not accumulate in the cavity over time, thereby preventing thermal runaway.

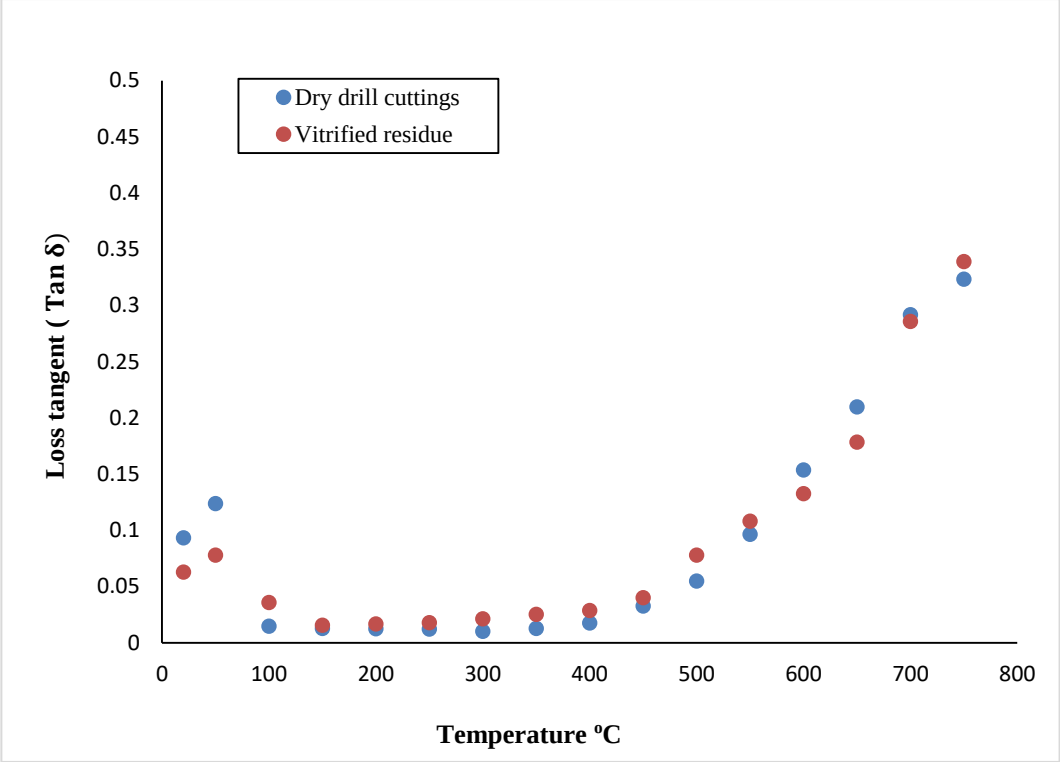


Figure 5.21: Loss tangent of drill cuttings and vitrified residue at 912MHz as a function of temperature

5.5 Conclusion

When drill cuttings accumulate in the applicator during microwave processing, thermal runaway is observed. This work has shown that the thermal runaway phenomenon is as a result of the dielectric properties of the solid components. It was found that the dielectric properties of some key microwave absorbing minerals (clay, halite and barite) increase exponentially at 400 ^{o}C.

It is thought that the temperature increases from the normal operating temperature (100 ^{o}C) to 400 ^{o}C due to the poor heat transfer properties of the mineral components. The oil component was found to be microwave transparent, and does not contribute to the thermal runaway phenomenon.

These findings are important because it is incorporated into the design basis for the industrial system. The system must be operated at <400 ^{o}C to avoid thermal runaway. The electric field intensity, thermal conductivity and residence times are all parameters that need to be considered in order to avoid thermal runaway.

Chapter 6 Effect of shear on energy requirement for the remediation of oil contaminated drill cuttings

6.1 Introduction

The effect of using a twin screw conveyor system as the mechanism of transporting drill cuttings in a microwave process is examined in this chapter. Particular attention is given to the change in physical properties of drill cuttings as a result of the shearing force from the twin screws, and consequently, the effect of the altered properties on the nature of interaction with microwave energy.

This chapter demonstrates that the energy efficiency of a microwave cavity can be significantly reduced by the shearing effect of a twin screw conveyor if such mechanism is used to transport drill cuttings to a microwave cavity. Microwave heating tests were carried out using the experimental apparatus described in (section 4.1) at 1- 5 kW input power. Refer to chapter 4 for details on the experimental methods used to determine oil and water contents, dielectric properties and density.

6.2 Sample Characterisation

The oil contaminated drill cuttings samples used in this study were generated from drilling operations in the North Sea, UK, and sourced from NOV Brandt. Table 6-1 show the water and oil contents and bulk density of the samples as received.

Table 6-1: Properties of drill cuttings. The water and oil contents and density of oil contaminated drill cuttings as received

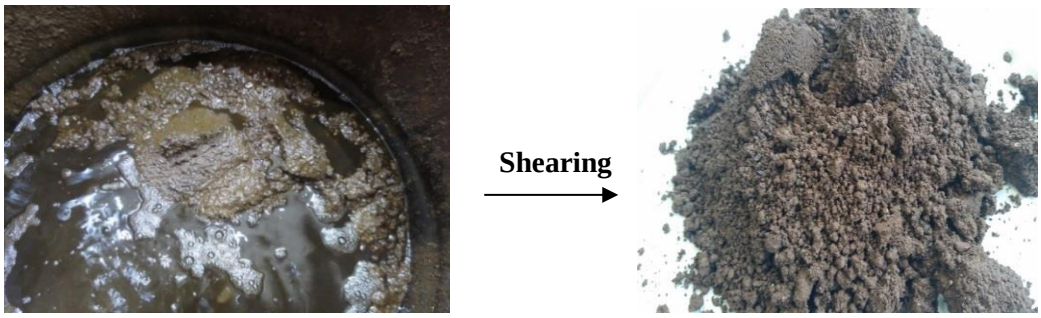
Sample	**Water content (%w/w)**	**Oil content (%w/w)**	**Bulk density (g/cm^3)**
Shale 1	13.80 ± 0.2	9-11 ± 0.5	1.87 ± 0.04
Shale 1A	10 ± 0.2	12 ± 0.5	2.10 ± 0.04
Sandstone	9 ± 0.2	8 ± 0.5	1.55 ± 0.04

The oil content of the samples are significantly greater than the 1 wt% environmental offshore limit. However, previous studies (Shang et al., 2005; Shang et al., 2006) have validated microwave oil remediation to less than 1wt%, therefore, the primary focus of this chapter will be solely on the 'shear effect' of the twin screw transport system and the impact that this has on oil removal.

6.3 Changes to physical properties of drill cuttings from shearing

Empirical evidence from transporting shale based drill cuttings samples through the twin screw feeder showed that the high shear nature of the process caused a change in the consistency of the material. Figure 6.1 shows the typical physical transformation observed when two samples (shale 1 and shale 1A) undergo high levels of shear, and it is interesting to note that the oil and water content does not

change after shearing. Section 3.4 describes where the change in consistency occurs in the current microwave processing concept.



(a) (b)

Figure 6.1: (a) Unsheared (as received) oil contaminated drill cuttings (b) sheared oil contaminated drill cuttings

The change in consistency in the drill cuttings material is not unique, in fact, the high shear influence of a twin screw feeder has been employed to transform the consistency of active pharmaceutical ingredients during granulation techniques (Dhenge et al., 2010; Dhenge et al., 2011) and manufacture of pharmaceutical products. To characterise the change in consistency of the drill cuttings material, bulk densities were measured at different levels of shear. The shale and sandstone samples were sheared, as described in section 4.7, at varying times with the shaft speed set at 210 rpm and 275 rpm. Figure 6.2 shows how the bulk density changed as the materials were sheared over time.

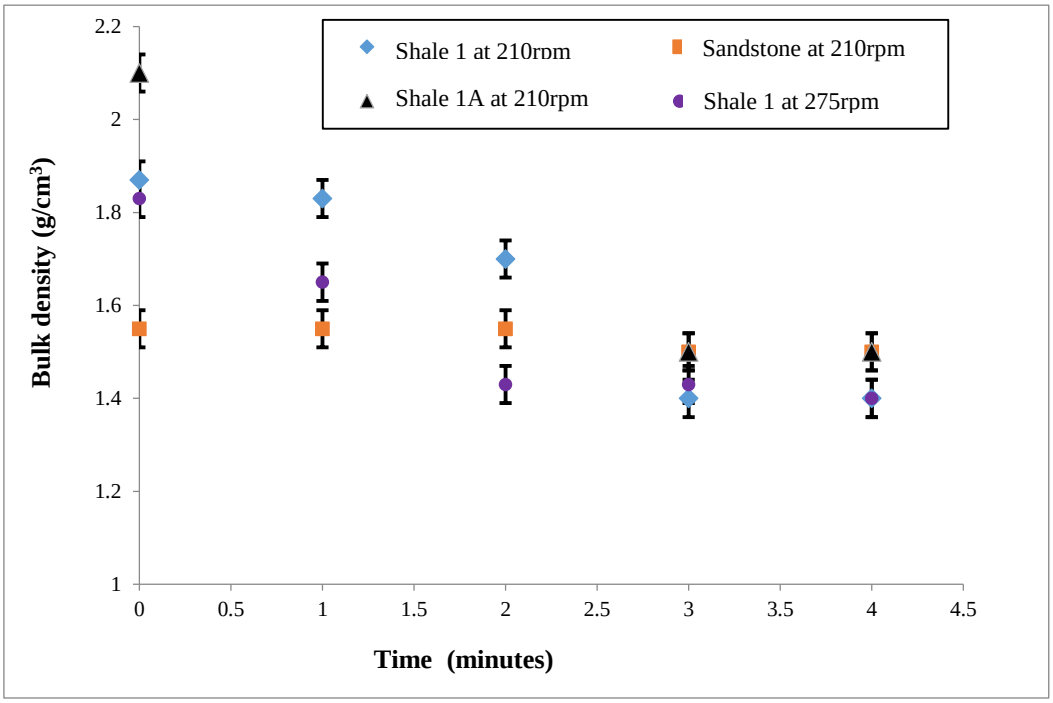


Figure 6.2: Bulk density of drill cuttings at varying times during shearing at 210 rpm and 275 rpm. Uncertainty is 0.04.

Henceforth, when shale is mentioned in this chapter it refers to shale 1 and shale 1A unless otherwise stated. It is immediately obvious that the bulk density of shale reduced with time but that of sandstone remained relatively unchanged. After 3 minutes of shearing at 210 rpm, the bulk density of shale 1 reduced by 25.13%, and the bulk density of shale 1A reduced by 28.57%. The change in bulk density of shale 1 was 0.47 g/cm^3 after 3 minutes and 0.6 g/cm^3 for shale 1A after the same duration of shear, after which no further change in bulk density was observed. The 'terminal' bulk density (1.4 g/cm^3 for shale 1 and 1.5 g/cm^3 for shale 1A) was reached after 3 minutes of shearing.

When the rate of shear was increased to 275 rpm, the rate of change of bulk density was faster than what was observed at 210 rpm for shale 1 (Figure 6.2). At 2 minutes, shale 1 exhibited no further reduction in bulk density which was not attained until

after 3 minutes of shearing at 210 rpm. This indicates that the rate of change of bulk density increases as the rate of shear increases. Previous studies have shown similar change in viscosity as the rate of shear is increased when shearing soil slurries (Carotenuto et al., 2015). This phenomenon is akin to the change in bulk density since viscosity and density are related physical properties. The effect of a higher rate of shear is diminished once the bulk density attains a constant value and no longer reduces.

Although the high shear influence of a twin screw feeder has been known to chemically transform materials (Chang and Halek, 1991), the shearing action of the mixer used in this work is assumed to be capable of only physical transformation in the drill cuttings material. This is because although the temperature of the samples after shearing may be slightly higher after shear, but it is insufficient to cause a change in the bulk oil and water content. The oil and water contents before and after shearing were found to be the same, which supports this argument.

Returning to shear characterisation of the drill cuttings material, the physical transformation observed as the bulk density reduced during the shear of the shale material will now be addressed. It was observed that the wet unsheared material transformed to a material whose characteristics showed a different level of resistance to shear deformation when compared to the unsheared material (Figure 6.1). Chapman (1948) showed that the total resistance to deformation of a soil-liquid mixture may be influenced by the viscosity and density of the fluid occupying the pores. This phenomenon can be used to explain the possible change in resistance to shear as shearing progresses for the shale based sample. At the start of a shearing regime, oil and water present on the surface of the material and the large pores ensures a relatively smooth movement of adjacent solid layers as they

slide over each other. As the shearing of shale progresses, the pores dilate, and the capillary and free water and oil contents move into the pore spaces that were inaccessible before shearing. A follow on from this is that larger pores are created which are increasingly filled with air. This is the main reason for the decrease in bulk density from shearing as the material occupies a larger volume when sheared.

Other workers have also suggested that the bulk density of granular materials may decrease when acted upon by shear (Kabla and Senden, 2009), which is in agreement with the observations in this work. Going by the findings of Chapman (1948), air will present less resistance to deformation when compared with oil and water. Hence, one can infer that sheared shale will be less resistant to shear as bulk density reduces with time.

The change in bulk density may be attributed to the clay content because some clay minerals exhibit similar increase in volume when in contact with water (Grindrod et al., 1999) and organic molecules (Anderson et al., 2010; Deer et al., 1985). The potential contribution of clay minerals to the reduction of bulk density in shale will be discussed later.

Drill cuttings are a natural variable and can vary widely in mineral composition. Hence, it is extremely difficult to predict, if any drill cuttings sample will respond to shear, and the duration that might be required to alter the bulk density in the manner the shale samples in this work did. Complex transformation is expected from drill cuttings when sheared, however, this work postulates various extremes in behaviour when drill cuttings are sheared before microwave heating. By investigating shale based and sandstone based drill cuttings, the extremes are

covered. Shale based drill cuttings show dramatic decrease in bulk density while the sandstone based drill cuttings exhibit constant bulk density.

6.3.1 Why rheology is unsuitable for shear characterisation in this work

Typically, rheology tests are carried out using rheometers to examine a saturated mixture of soil, water and oil, slurry or a colloidal solution of soil particles. However, such tests usually involves a solid volume not more than 45% (Masliyahs, 1992; Chapman, 1948; Carotenuto et al., 2015). At 45% and above, the mixture is not fluid and remains compact after mixing or shearing (Chapman, 1948).

The following is an estimation of the typical solid volumetric composition of the drill cuttings material. The skeletal densities of shale 1 and shale 1A are 2.95 g/cm^3, and 2.89 g/cm^3 for sandstone. If one considers a sample volume of 1 cm^3, and determining the porosity as described in section 4.6, then, the solid volumetric composition is can be estimated and is presented in Table 6-2.

Table 6-2: Composition of the solid phase in the drill cuttings sample in this work

Samples	Solid volume (%)
Shale 1	64.41
Shale 1A	71.19
Sandstone	53.73

Clearly, at 64.41%, 71.19% and 53.73% solid volume, the samples are unsuitable for rheology tests using a typical rheometer. Nevertheless, several rheology tests were performed using a (Rheometrics RDA-lll) rheometer to characterise the

viscoelastic properties, but the apparent viscosity data gathered were determined unreliable as a method of characterisation.

6.3.2 Clay content contribution to bulk density change in drill cuttings

The decrease in bulk density observed in the shale samples is thought to be mainly from the swelling clay mineral components. The major mineral components of drill cuttings were analysed using XRD, and is shown in Figure 6.3 and Figure 6.4. Halite, calcite, anhydrite, barite and quartz are naturally occurring minerals that do not possess any known swelling abilities when in contact with organic liquids or water. In fact, barite on the other hand, is a weighting agent with appreciable compressive strength which may hinder swelling (Saidani et al., 2015).

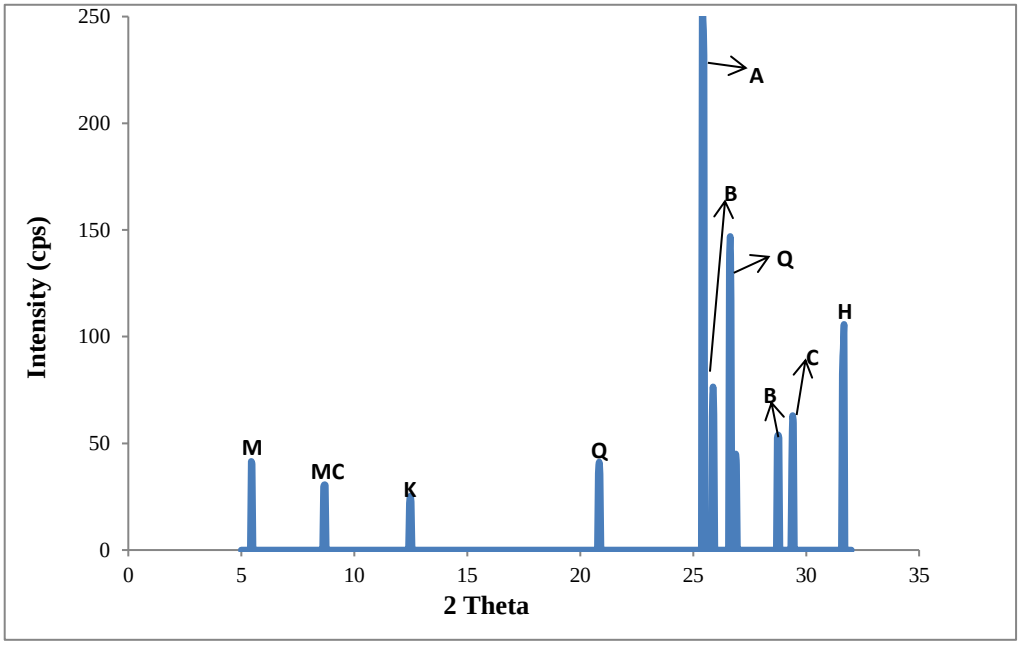


Figure 6.3: XRD showing the major mineral components of shale 1 and shale 2; M-Montmorillonite, MC-muscovite; K-kaolinite; Q-quartz; A-anhydrite; B-barite; C-calcite; H-halite.

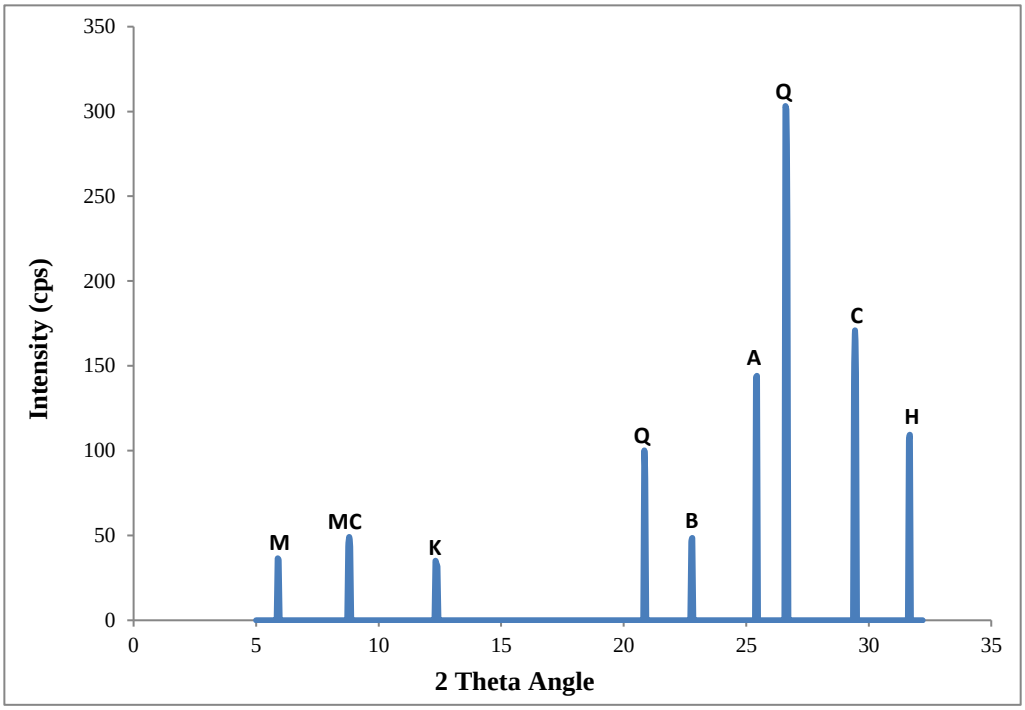


Figure 6.4: XRD showing the major mineral components in sandstone; M-montmorillonite; MC-muscovite; K-kaolinite, Q-quartz; A-anhydrite; B-barite; C-calcite; H-halite.

Muscovite belongs to the mica group and generally do not swell when in contact with water and organic liquids (Deer et al., 1985). It is unlikely that kaolinite, a clay mineral, is responsible for the swelling seen in the shale based samples because it exhibits little or no swelling when in contact with water or organic liquids. This is due to the structure of kaolinite which does not generally permit the exchange of cations because it is electrically neutral. Clay minerals swell when such cations either keep two adjacent sheets apart allowing intercalation of water, or due to the dissociation of the cations which force the clay minerals apart (Foster, 1954; Norrish, 1954). Kaolinite, and if present, some forms of muscovite, may display microscopic swelling. An example of this type of swelling is when dry soil samples absorb a modest amount of moisture from the surrounding atmosphere. This sort of microscopic swelling occurs in most clay minerals and can be discounted as the reason for the macroscopic swelling phenomenon observed in this work. It is

unlikely that any of the aforementioned minerals dictate the swelling phenomenon seen in the shale samples due to the fact that these minerals are also present in the non-swelling sandstone sample.

On the other hand, montmorillonite exhibits swelling properties (Kleijn, 1982; Norrish, 1954; Anderson et al., 2010) capable of the dramatic reduction in bulk density seen in the shale based samples. Swelling in the shale is also enhanced due to the chemistry of the montmorillonite component which allows frequent ionic replacements between the surroundings and the mineral layers. As a result, it has a partially charged structure that attracts ions and water molecules and encourages swelling. In this work, it is thought that shearing induces swelling in the shale based samples from the intercalation of water and oil molecules, together with some cations, between the clay sheets due to the mechanical energy of mixer impellers.

Previous work has shown that montmorillonite possesses a potent swelling ability in a soil-water system with and without agitation of the system (Hensen and Smit, 2002; Miranda-Trevino and Coles, 2003). This supports the empirical evidence that shearing or agitation enhances swelling within the clay component of the drill cuttings samples. Interestingly, the bulk density of the unsheared shale samples was relatively constant during storage. The reason the shale samples did not swell during storage is due to high capillary pressure in the small pores of the clay minerals. An equilibrium is established where water molecules and big organic compounds on the surface and in the large pores of the material cannot overcome the pressure in the small and capillary pores or pry the clay sheets apart. This equilibrium state can only be altered by energy input into system (i.e. from the counter rotating action of the screw feeder).

This work has singled out montmorillonite as a major contributor to the swelling, but it is recognised that other components may account for some swelling to a smaller extent. For example, it is not unusual for other swelling clay minerals such as vermiculite to be found in small quantities in drill cuttings samples. Of note is the presence of clay minerals, and especially montmorillonite, in sandstone (Table 6.3). The reason for this is most likely because bentonite, which contains montmorillonite, is commonly used in drilling muds. Therefore, it is expected that montmorillonite will be a component of most drill cuttings samples.

The most probable reason the bulk density of sandstone drill cuttings used in this work was unchanged during shear is due to the particle size distribution which is presented in Table 6-3. The method used for particle size analysis is detailed in section 4.10.

Table 6-3: Particle size distribution of shale and sandstone based drill cuttings.

	Particle Size	**Volume Fraction %**	**Standard Deviation**
Sandstone	<2 µm	9.68	1.14
	2 – 10 µm	41.19	1.00
	10- 63 µm	48.10	1.57
	>63 µm	1.03	1.51
Shale 1	<2 µm	15.18	1.21
	2 – 10 µm	47.40	1.82
	10 – 63 µm	35.60	1.80
	>63 µm	1.82	1.22

The data shows that the shale sample contains 15.18% of particles less than 2 µm, while the sandstone sample contains 9.68% of these particles. Since clay particles are known to preferably exist as 2 µm or less, the data in Table 6-3 shows clearly that clay minerals are more abundant in the shale material than in the sandstone. Not only does the shale material show a higher concentration of clay minerals, but empirical evidence suggests it must contain a higher proportion of swelling clay minerals (due to bulk density decrease from shear). It should be noted that this is not conclusive evidence on why the shale and sandstone samples in this work responded differently to shear, but it gives an indication of the probable cause.

Presented in Figure 6.5 and Figure 6.6 are the conceptual representations of the oil, water and mineral phases in sheared and unsheared shale based drill cuttings. In Figure 6.5 water is present in the large pores, capillaries and micropores of the clay agglomerates while oil occupies the large pores and cavities. Figures 6.6 illustrate a number of changes to the shale sample after shear, especially in the clay agglomerates.

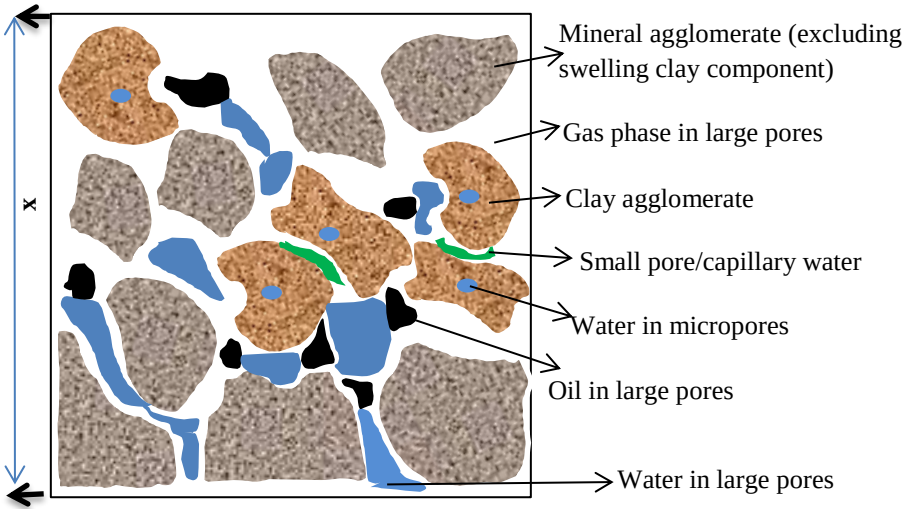


Figure 6.5: Conceptual representation of the water/oil/mineral phases in shale based drill cuttings

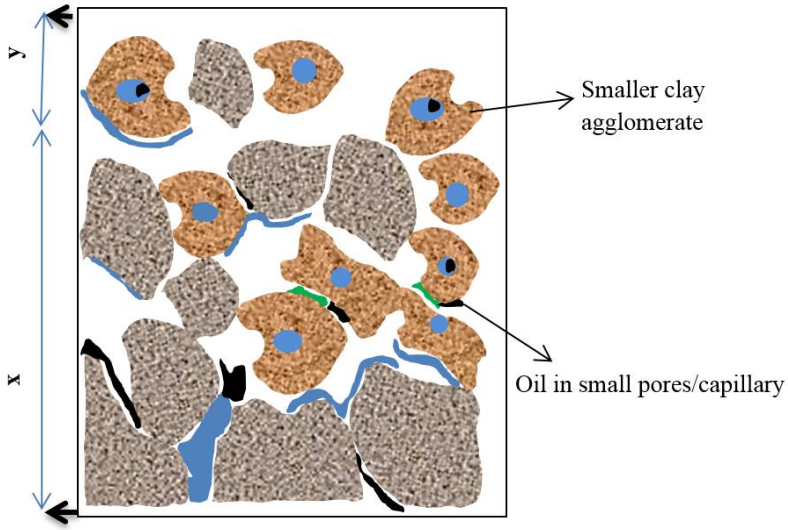


Figure 6.6: Conceptual representation of the water/oil/mineral phases in sheared shale based drill cuttings.

It is thought that as the shale is sheared, water and some oil may be forced into the capillaries and micropores of the clay agglomerates. Naturally, clay and other mineral exist in large agglomerates within the bulk unsheared shale material. During shear, smaller agglomerates are formed from the larger agglomerates which is depicted in Figure 6.6. Smaller clay and other mineral agglomerates are formed from the shear impact. Also shown in Figure 6.6 is significant increase in volume of the shale after shearing. In Figure 6.5, x depicts the height of the unsheared shale sample, and y in Figure 6.6 shows the increase in volume of the same sample with equivalent mass after shearing.

Previous work has shown that resistance to shear stress generally reduces when the solid content decreases and the liquid content increases in a clay-water system (Maciel et al., 2009) up to a point where the mixture displays Newtonian properties when sheared at high liquid content. In our case, the shale material will either not display changes to bulk density if the oil and water content is significantly higher

than we have seen in this work, or take longer to transform. However, this scenario is unlikely in drill cuttings treatment, as it is uncommon for drill cuttings to routinely contain greater than 30wt% liquid content.

6.4 Microwave treatment of sheared and unsheared shale based drill cuttings

Microwave heating tests were carried out using the single mode TM_{010} cavity (section 4.1) with 1-5 kW of microwave power input and 70 g of shale 1. The initial oil and water content is detailed in Table 6-1. Energy inputs were set at 20, 25, 30, 40, and 50 kJ. The specific energy input was calculated from absorbed microwave power and duration of each experiment as described in section 4.1. Henceforth, in this chapter, the level of shear will also be denoted by density. 4-8 microwave heating experiments were carried out. The error bars presented in this chapter are different from the standard deviation shown in Table 6-1. This is due to the heterogeneous nature of the drill cuttings samples and not the precision of the method used for analysis.

Microwave treatment time determines the amount of energy absorbed by each sample. For example, at 1 kW absorbed power, a 23 seconds run is approximately equivalent to 80 kWh/t and a 33 seconds run is equivalent to 120 kWh/t. This is better illustrated in Figure 6.7.

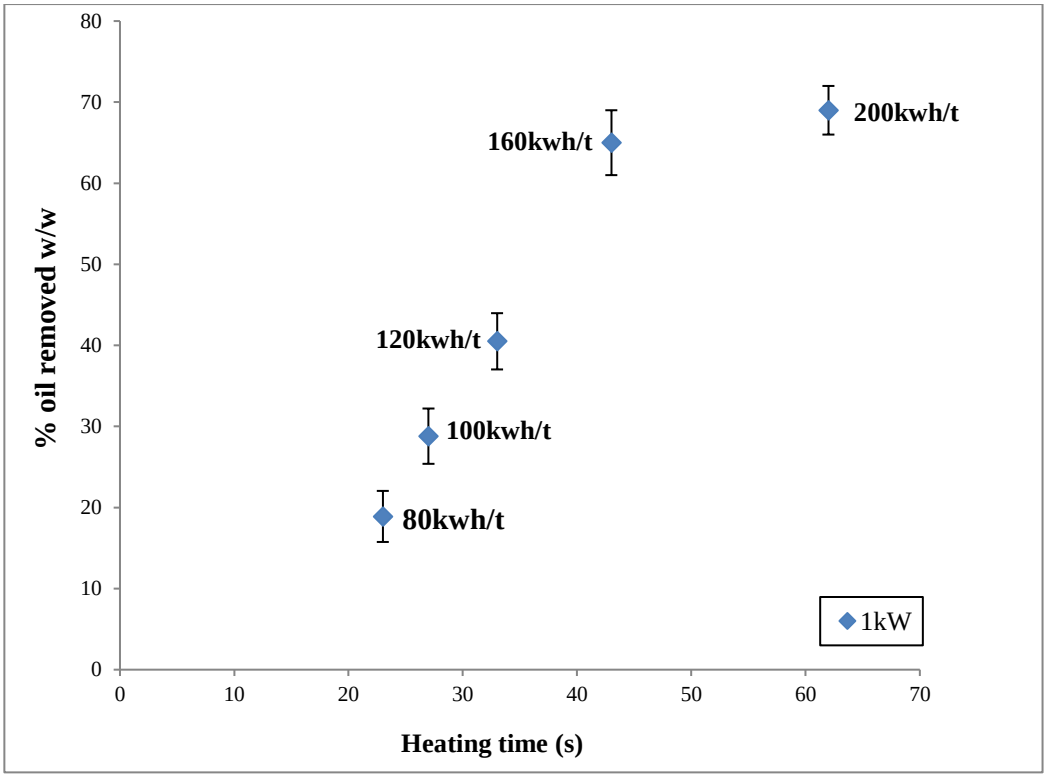


Figure 6.7: Energy input over time during microwave treatment of oil contaminated drill cuttings (shale 1).

6.4.1 Microwave treatment of drill cuttings sheared to 1.4 g/cm^3

Experiments were carried out to determine the 'worst case' scenario in terms of reduction in bulk density through the high shear process. This meant that heating tests were carried out on the lowest bulk density achievable from shearing the shale material. Shale 1 was sheared at 210rpm for 3 minutes from 1.87 g/cm^3 to 1.4 g/cm^3. The data showing the difference in oil removal is presented in Figure 6.8. The data shows that oil removal efficiency is lower at 1.4 g/cm^3 than at 1.87 g/cm^3. For example, to remove 29% oil, 102 kWh/t is required for the unsheared drill cuttings while 123 kwh/t was required for drill cuttings sheared to 1.4g/cm^3. Interestingly, the difference in oil removal exists at all energy inputs between unsheared drill cuttings at 1.87g/cm^3 and the sheared material at 1.4g/cm^3.

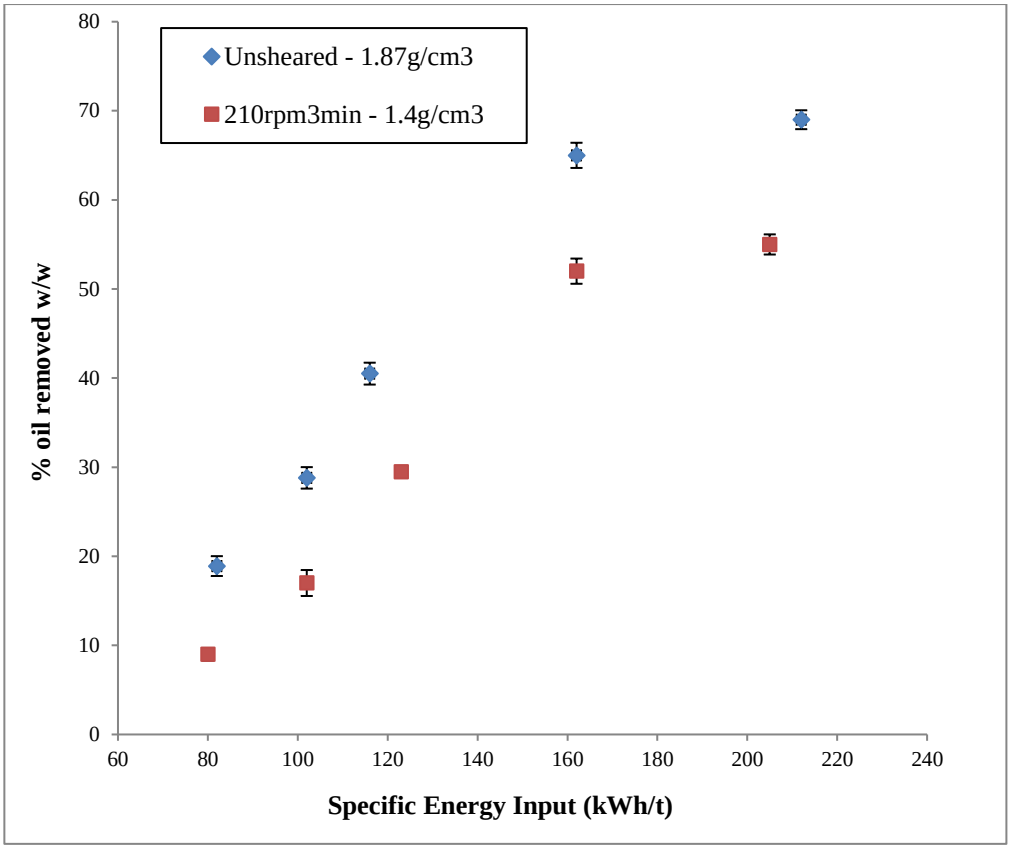


Figure 6.8: Oil removal from unsheared and sheared (210 rpm for 3 minutes) oil contaminated drill cuttings (Shale 1) plotted against specific energy input. Initial oil content – 11 wt%. 1 kW microwave power. Each data point represents 8 experiments. Standard error is 0.64-1.46%.

A possible explanation for this is that as the bulk density of the material reduces, the dielectric constant and dielectric loss factor decreases. Figure 6.9 and Figure 6.10 show the dielectric constant and dielectric loss factor of unsheared (1.87 g/cm^3) drill cuttings and sheared (1.4 g/cm^3) drill cuttings.

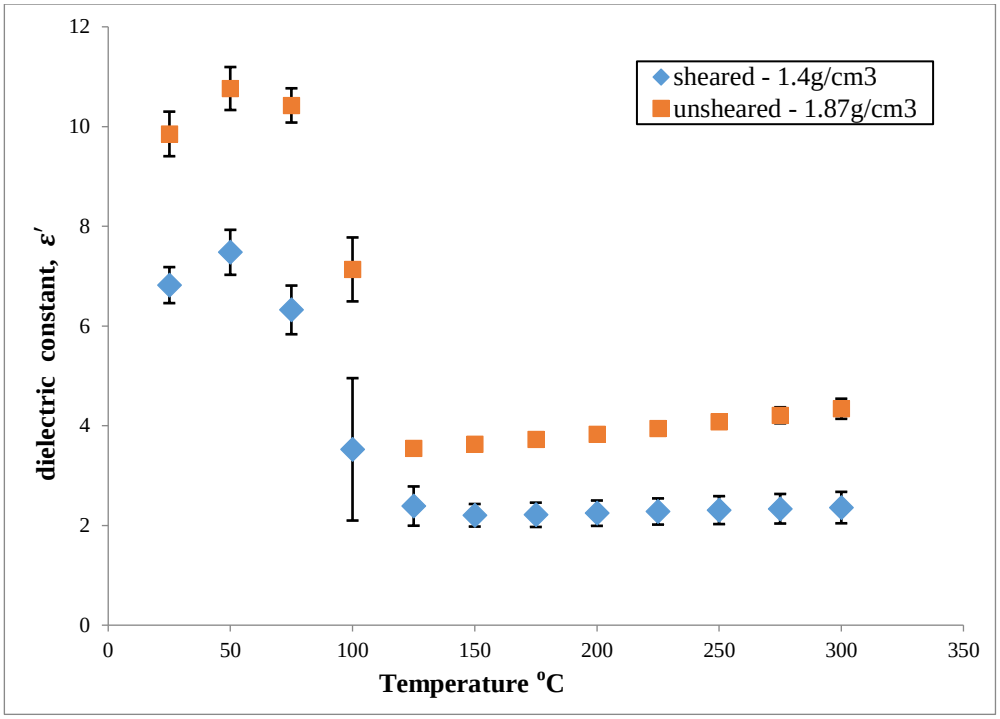


Figure 6.9: Dielectric constant of sheared and unsheared oil contaminated drill cuttings (Shale 1) at 912MHz. Uncertainty as represented by error bars is 0.01-1.35.

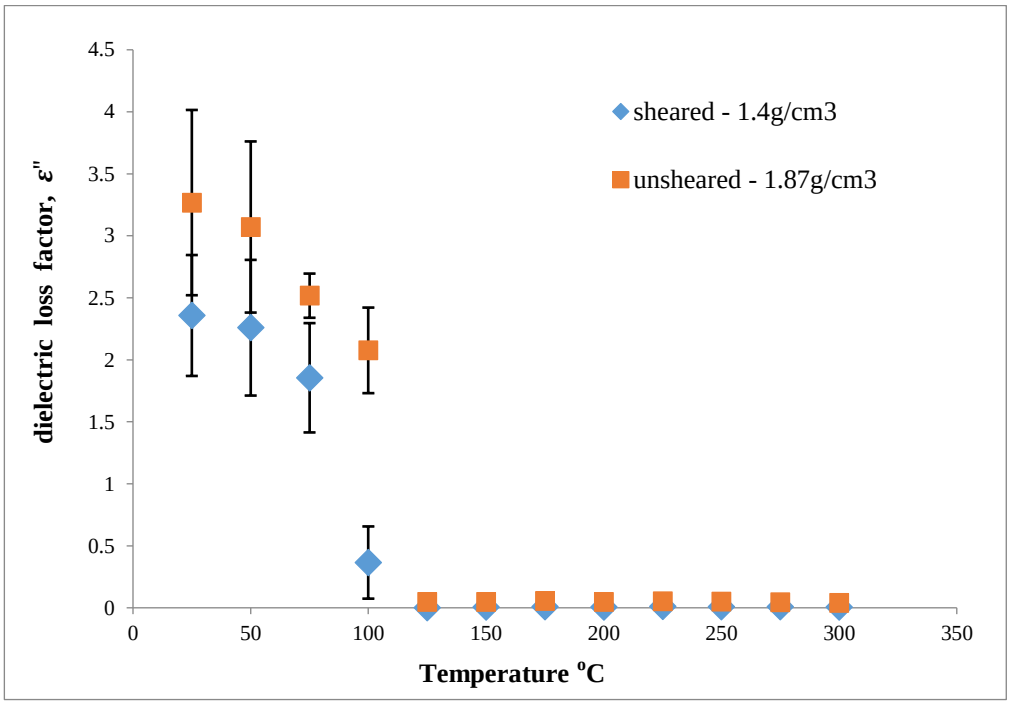


Figure 6.10: Dielectric loss factor of sheared and unsheared oil contaminated drill cuttings (Shale 1) st 912MHz. Uncertainty as represented by error bars is 0.005-0.72.

At 25 ^{o}C, which is closer to the sample temperature at the start of each microwave heating experiment, the dielectric constant and dielectric loss factor at 1.87 g/cm^3 was 9.85 and 3.27, while it was 6.82 and 2.36 at 1.4 g/cm^3.

In both cases, the dielectric loss factor and dielectric constant generally decreases with increasing temperature, which is thought to be as a result of the evaporative loss of the main microwave absorbing phase (water).

Of note is that the dielectric loss factor is 2.08 at 100 ^{o}C for unsheared (1.87 g/cm^3) and 0.37 for sheared (1.4 g/cm^3) at the same temperature. This implies that when shale 1 is 1.87 g/cm^3, it is more likely to heat under microwave at 100 ^{o}C than when sheared to 1.4 g/cm^3. This observation is important because water molecules within the drill cuttings matrix is expected to vaporise at 100 ^{o}C. It appears that more water is vaporised from the sheared material at 100 ^{o}C because water is less physically restrained on the surface and in the larger pores of the material.

The relatively high dielectric loss factor of the unsheared material at 100 ^{o}C suggests that the matrix contains physically restrained water which has not been vaporised at 100 ^{o}C. Physically bound water present in capillaries and the micropores will require more energy, hence higher temperature and pressure, to desorb from the material matrix. It has been suggested that the dielectric constant of bound water in the capillaries of drill cuttings (Robinson et al., 2008), and shown in other granular materials (Metaxas and Meredith, 2008), will increase as the temperature increases. Therefore, one can infer that the reason the unsheared shale display a higher dielectric constant and loss factor is because it maintains a high network of capillary water with a significant proportion possibly unconnected to the surface of the material.

As temperature increases during microwave heating of the unsheared material, first, the power density is concentrated in the less restricted water in the large pores. As the temperature rises further, the capillary water can now absorb microwave energy since the free water is vaporised. This explains why the dielectric loss factor and dielectric constant are higher at 100 ^{o}C.

Another possible explanation why the sheared shale sample may heat less under microwaves is due to a greater surface area and large pores containing air. Air has a dielectric loss factor of zero, and is therefore microwave transparent. Bigger pores filled with air in sheared drill cuttings mass means that the unsheared material will heat better under microwave. In this case, if a material heats better under microwave, it means that the rate of temperature rise within the material is faster.

The power density (P_d) in a material increases with increasing loss factor as shown in section 3.2.4. The rate of temperature rise ($\Delta T/\Delta t$) within a material being heated under microwave is directly related to the power density in the equation below;

$$\frac{\Delta T}{\Delta t} = \frac{P_d}{\rho C_p}$$

where ρ is the density (kg/m^3) and C_p is the specific heat capacity (kJ/kgK). Therefore, the unsheared material attains a higher temperature than the sheared material at the same power and energy input as a result of a higher loss factor.

The dielectric properties of sheared and unsheared drill cuttings provide a plausible explanation for the decrease in oil removal in sheared drill cuttings based on heating rate. Previous work have suggested that oil removal mechanisms such as steam distillation, physical entrainment and direct vaporisation (Shang et al., 2006; Robinson et al., 2008) are based on the rate of temperature rise in the water phase. However, it is thought that there are other complex mechanisms which may also explain the disparity in oil removal. This is fully addressed in chapter 7.

The higher dielectric loss factor and dielectric constant in the unsheared shale material can be attributed to the bound water molecules in the undisturbed small capillary pores. If one considers the disparity in the dielectric loss factor values between the sheared and unsheared material (Figure 6.10) at 100 ^{o}C, the data suggests that bound water in the capillaries will continue to absorb microwaves at temperatures greater than 100 ^{o}C, and hence more energy is needed to completely remove these water molecules. This phenomenon has already been suggested by (Robinson et al., 2008). Under this condition (restricted movement of water in capillaries), bound water does not fully exert its full vapour pressure which is the reason it requires higher temperature, hence higher energy to desorb from the drill cuttings matrix.

Figure 6.11 shows that water removal is more efficient in the sheared material (1.4g/cm^3). For example, 84% of water is removed at 128 kWh/t and 1.4g/cm^3 while 74% was removed at similar energy input at 1.87g/cm^3. In other words, water removal is higher in the sheared material at equivalent energy input. In the sheared material, it is expected that the amount of physically bound water should increase, but the creation of greater surface area may ensure that the energy required to evaporate water from the sheared matrix will be lower.

On the other hand, if energy transfer from the water phase to the oil component (as in steam distillation) is the mechanism of oil removal, then this may explain why oil removal is lower in the sheared material.

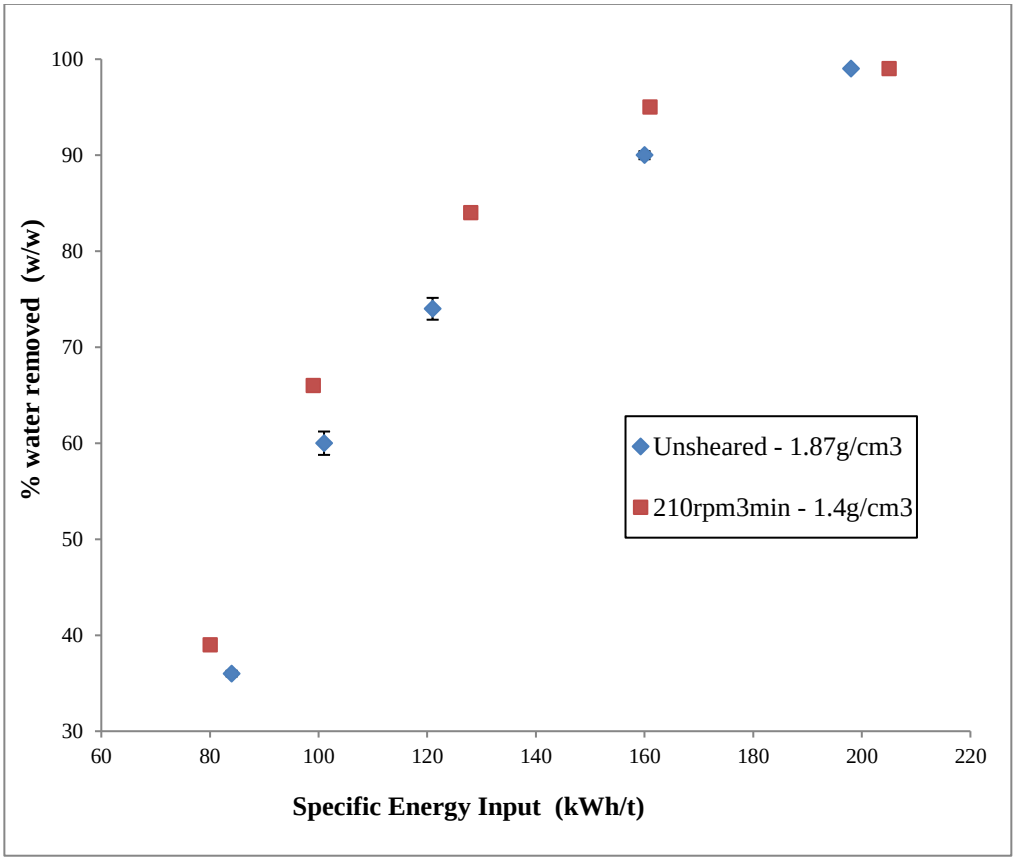


Figure 6.11: Water removal from sheared and unsheared shale based oil contaminated drill cuttings (shale 1). Initial water content – 13.8%. 1 kW microwave power. Each data point represents 8 experiments. Standard error is 0.01-1.14%.

Figures 6.12 and 6.13 show sheared and unsheared drill cuttings samples before and after microwave heating.

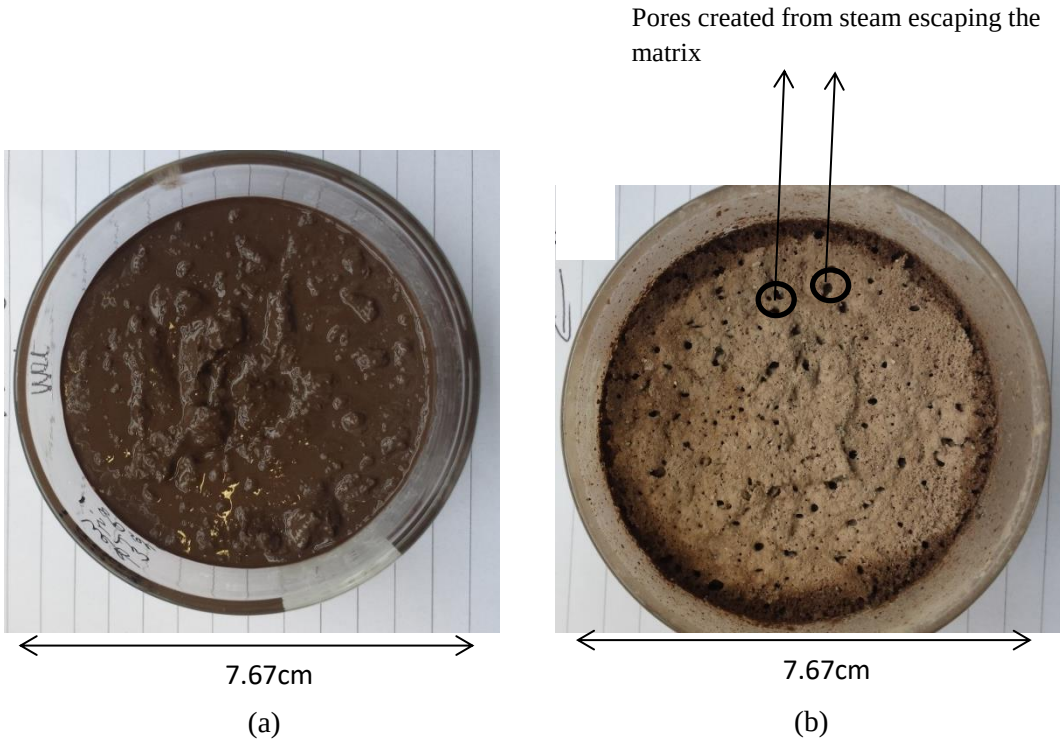


Figure 6.12: Unsheared oil contaminated drill cuttings (Shale 1 at 1.87 g/cm^3) (a) before microwave heating, (b) after microwave heating



Figure 6.13: Sheared oil contaminated drill cuttings (shale 1 at 1.4 g/cm^3) (a) before microwave heating, (b) after microwave heating

Figures 6.12 and 6.13 show that additional pores may be created in the high bulk density unsheared sample after microwave heating, which is thought to be as a result of the capillary water escaping violently as superheated steam at high temperature. This is in agreement with the theory that water molecules in the capillary pores will require higher energy to be removed, and when they do, will escape violently. Essentially, the smaller the pore size, the higher the likelihood of water molecules being physically restrained as they attempt to exit the matrix. This means that the unsheared material exhibits a lower rate of water removal when compared to the sheared counterpart as a result of the capillary water effect.

Agglomerates are clearly visible in the sheared material when compared to the unsheared material which is appears as 'one solid' porous material (Figures 6.12 and 6.13). The consistency of the sheared material suggests that a greater surface area is generated within the sheared material. It is impossible to determine if additional pores were created in the sheared material after microwave heating just by visual inspection because the consistency is essentially the same as before microwave heating. Larger pores created through shear are thought to have more connections to the surface of the material which create sufficient pore volume and escape route for heated pore water. This creates a less restrictive path of escape for water in the sheared material and ensures a more efficient water removal rate.

There can be a significant energy penalty in a microwave process if the bulk density is changed significantly by the chosen material transport mechanism. For example, 24% more energy will be required to remove 18% oil from sheared drill cuttings at 1.4 g/cm^3 when compared to the unsheared material at 1.87 g/cm^3 (Figure 6.8). This energy penalty (24%) represents the worst case scenario for the shale material used in this work.

6.4.2 Microwave Treatment of drill cuttings sheared to 1.7 g/cm^3 and 1.83 g/cm^3

It was noted during microwave experimental runs that the samples all attain approximately 100% water removal at similar energy input (200 kWh/t). At 100% water removal, it is not possible for more energy to be absorbed. Hence the maximum time for microwave heating for each experiment at were determined by the reflected power. As the water content reduces during microwave heating, the dielectric loss factor also decreases; therefore there is an increase in reflected power with time. Beyond 100% water removal, reflected power reached 80%. At this stage, the 20% absorbed power is mostly coupled into the mineral phase. Therefore the experiments were terminated at 80% reflected power at approximately 200 kwh/t.

Presented in Figure 6.14 is the water removal from drill cuttings when sheared from 1.87 g/cm^3 to 1.83 g/cm^3 and 1.7 g/cm^3.

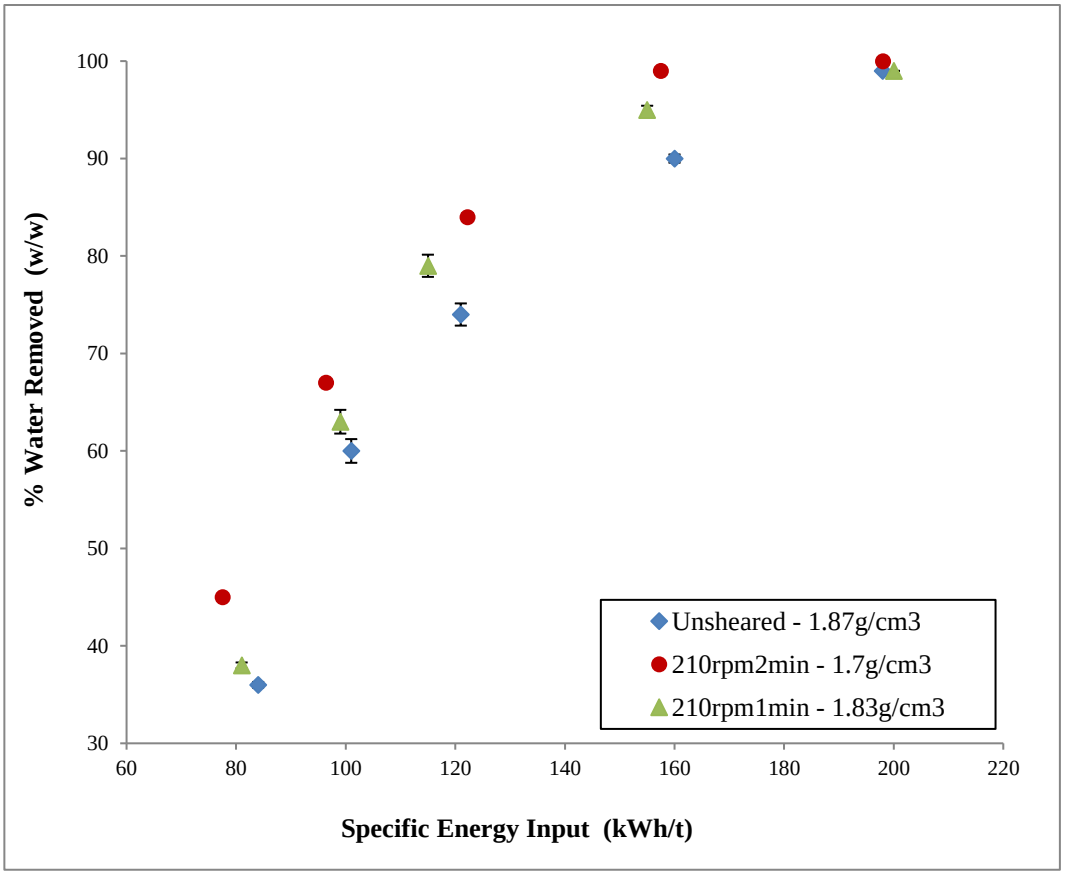


Figure 6.14: Water removal from unsheared and sheared oil contaminated drill cuttings (shale 1) plotted against specific energy input. 1 kW microwave power. Each data point represents 8 experiments. Standard error is 0.01-1.20%.

It is shown that the rate of water removal increases as the bulk density decreases from shearing, and is shown to be consistent with the 1.4 g/cm^3 water removal data. It has already been shown that oil removal is lower at lower bulk density (Figure 6.8), and Figure 6.15 shows the oil removal data for sheared drill cuttings at 1.7 g/cm^3 and 1.83 g/cm^3 appears to be in agreement.

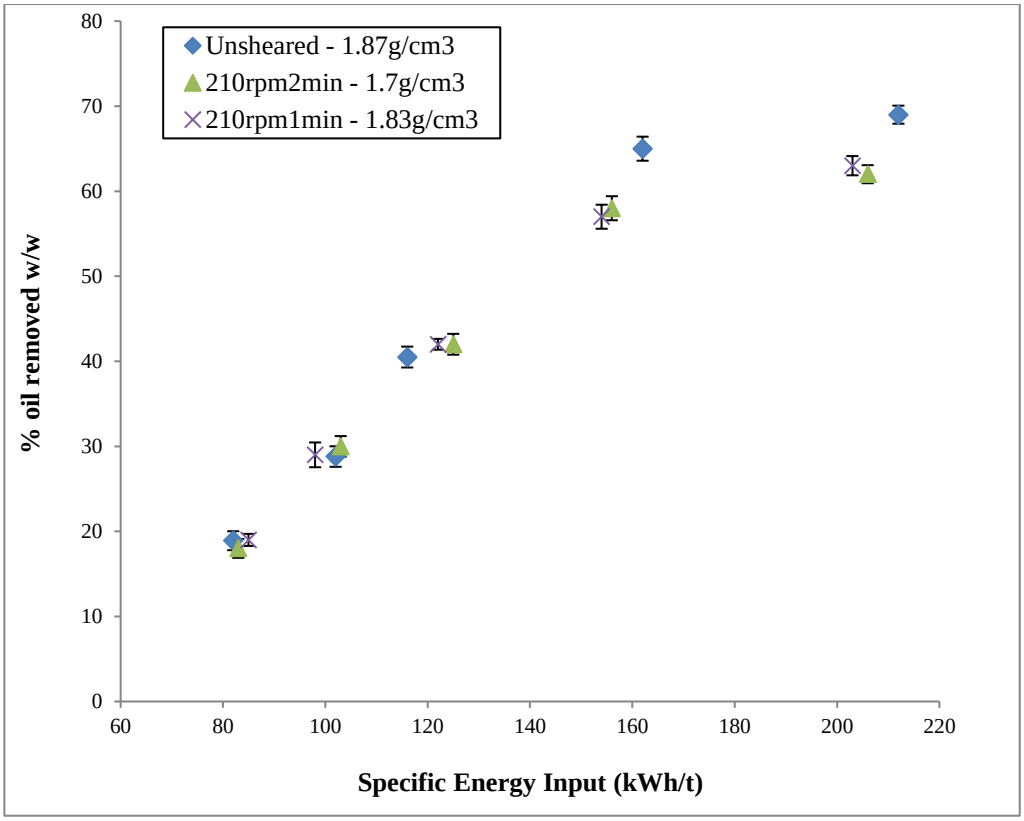


Figure 6.15: Oil removal from unsheared and sheared oil contaminated drill cuttings (shale 1) plotted against specific energy input. 1kW microwave power. Each data point represents 8 experiments. Standard error is 0.64-1.46%.

The initial oil content of the 1.87g/cm^3 and 1.83g/cm^3 samples is 11 wt%, while the initial oil content of the 1.7 g/cm^3 sample is 9 wt%.

It is apparent that the implication of decreasing bulk density is a decrease in oil removal efficiency which is consistent with the data in Figure 6.8. Oil removal efficiency (energy input basis) is similar at 1.7 g/cm^3, 1.83g/cm^3 and 1.87g/cm^3 between 80 kWh/t to 120 kWh/t but differ when energy input is equal to or greater than 160kWh/t.

Consider the oil removal levels at 1.87 g/cm^3 and 1.83 g/cm^3 at different energy inputs. Between 80 kWh/t and 120kWh/t, the level of oil removal is the same. However, small differences in oil removal occur at higher energy input, where it

appears that approximately 7% more oil has been remediated from the unsheared material at 212 kwh/t than at 1.83 g/cm^3 at similar energy input.

When the material was sheared to a bulk density of 1.7 g/cm^3 (Figure 6.15) from 1.87 g/cm^3, the oil removal trend appears similar to that observed for 1.83 g/cm^3, with similar oil remediation at energy inputs below 120 kWh/t, but approximately 7% less oil was removed at greater energy inputs. This is in agreement with the findings at 1.4 g/cm^3 which showed that the microwave heating process is less efficient when bulk density is reduced at equivalent energy input. Although oil removal between 160 kwh/t and 200 kwh/t for 1.83g/cm^3 and 1.7 g/cm^3 appears similar in figure 6.15, the actual amount of oil removed from the 1.7 g/cm^3 sample will be lower since its initial oil content is lower (9 wt%) than the 1.83 g/cm^3 sample (11 wt%).

It should be noted that the dielectric data of shear levels corresponding to 1.83 g/cm^3 and 1.7 g/cm^3 is expected to lie between the unsheared and extreme shear (1.4 g/cm^3). This is backed up by previous work that demonstrated that the dielectric properties of granular materials decreases as bulk density decreases (Robinson et al., 2010; Nelson, 1994; Nelson, 2005).

Away from the mechanisms behind the preferential removal of water from the sheared material, it has been established in this work that oil removal efficiency declines as shear progresses and bulk density reduces in shale based drill cuttings. Since water is the main microwave absorbing phase, it is possible that if energy transfer from the water phase to the oil component, as in previously suggested oil removal mechanisms, determines the efficiency of oil removal, then the unsheared material will ensure longer contact time between water and oil. Hence, the greater

efficiency in oil removal from unsheared drill cuttings as seen in Figure 6.8 and Figure 6.15. This may provide some explanation for the reason why, for example 7% less oil is removed from the sheared shale drill cuttings at 1.7g/cm^3 and 1.83g/cm^3 when compared with the unsheared material at 1.87g/cm^3.

6.4.3 Microwave treatment of sheared and unsheared drill cuttings at 3kW microwave power

This experiment was carried out to determine if the 'shear effect' can be minimised by increasing the power density. Presented in Figure 6.16 is the data showing water removal from unsheared (2.1 g/cm^3) and sheared (1.5 g/cm^3) drill cuttings. The sample size was 70 g with 3 kW input power, and the initial oil and water content before microwave heating is shown in Table 6-1 (Shale1A).

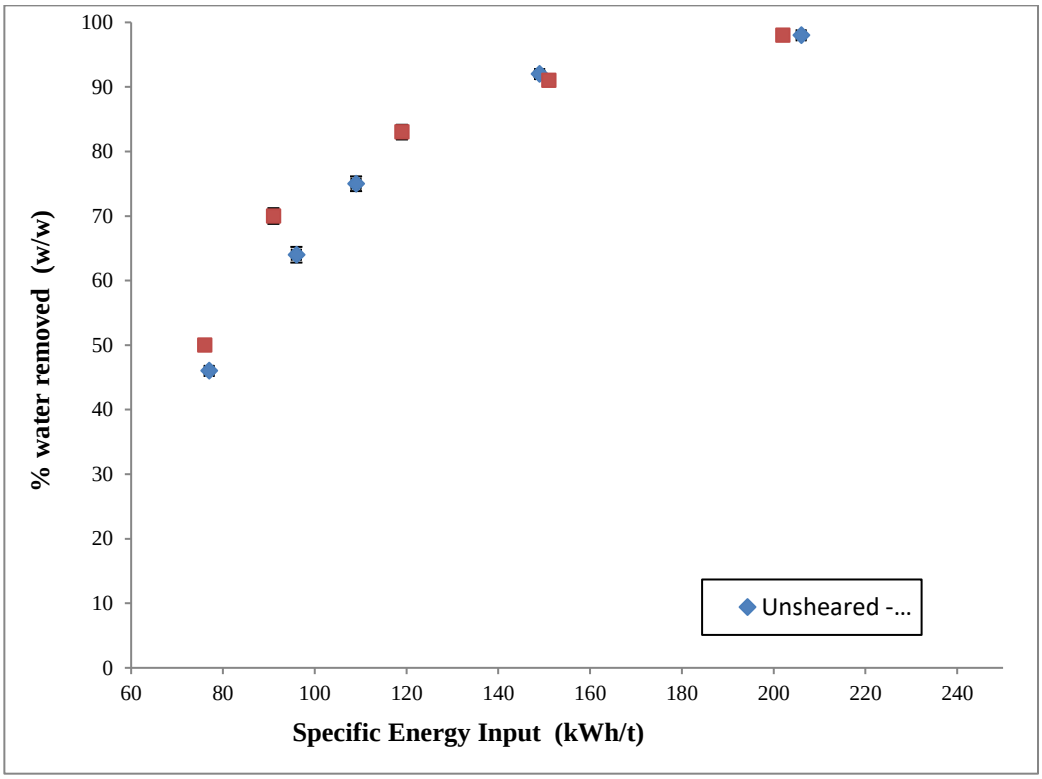


Figure 6.16: Water removal from sheared (210 rpm for 3 min) and unsheared oil contaminated drill cuttings (Shale 1A) plotted against specific energy input. 3kW microwave power. Each data point represents 4-6 experiments. Standard error is 0.01-1.72%.

The water removal levels were found to be slightly higher in sheared drill cuttings than in unsheared drill cuttings below 150 kwh/t energy input. For example, approximately 77 kwh/t was required to remove 50% of water from sheared drill cuttings, while 46% was removed from the unsheared material at the same energy

input. This indicates that the water removal in sheared cuttings at 3 kW is subjected to a similar phenomenon as observed during treatment at 1 kW input microwave power. Interestingly, the 'shear effect' on water removal appears to have been eliminated at energy inputs greater than 150 kWh/t at 3 kW. This was not the case until over 200 kWh/t at 1 kW microwave power input.

Figure 6.17 shows that there are no significant differences in oil removal levels for sheared and unsheared drill cuttings below 200 kWh/t. However, there appears to be a small difference in the amount of oil removed at over 200 kWh/t, where 6% more oil has been remediated from the sheared material.

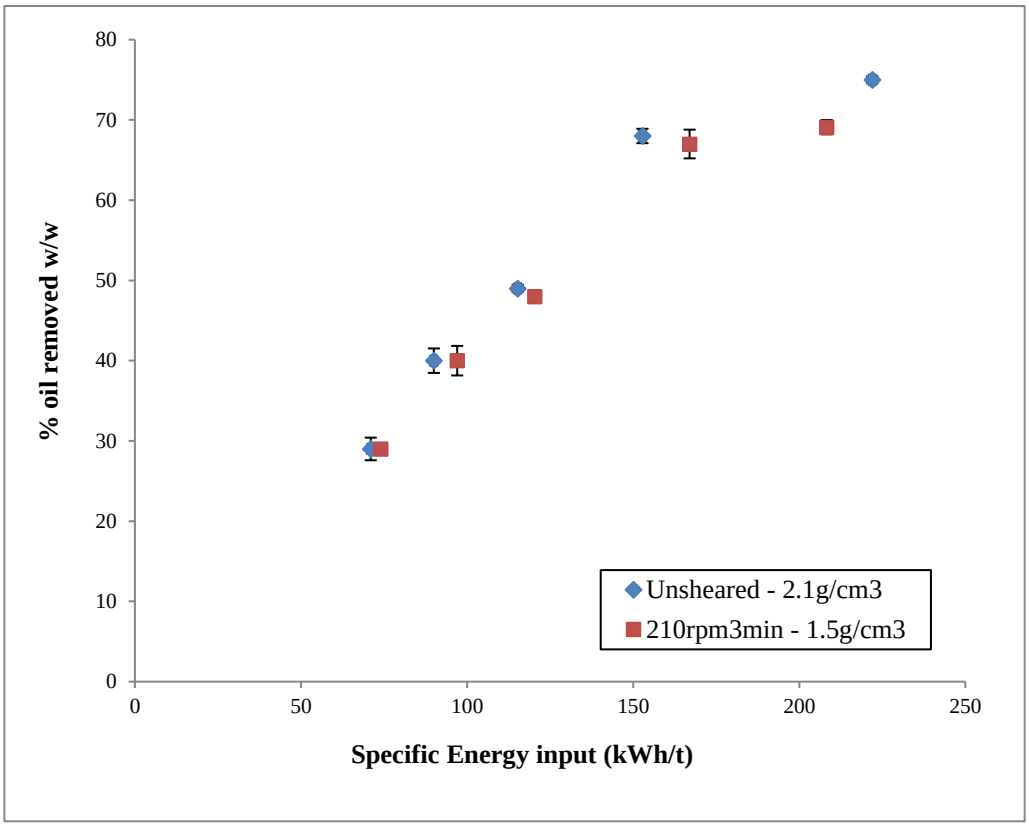


Figure 6.17: Oil removal from sheared (sheared at 210 rpm for 3min) and unsheared oil contaminated drill cuttings (Shale 1A) plotted against specific energy input. 3 kW input microwave power. Each data point represents 4-6 experiments. Standard error is 0.12-1.84%.

A comparison of Figure 6.8 (1 kW data) with Figure 6.17 shows that a higher power density minimises the shear effect on the efficiency of oil removal from drill cuttings. The data in Figure 6.8 (1 kW data) and Figure 6.17 are comparable based on the fact that both set of data show low oil removal levels at the lowest bulk density of the sheared material. In Figure 6.8 (1 kW), the oil removal levels are consistently lower, 10% or more, in sheared drill cuttings than in the unsheared samples at the same energy input. Increasing the power density (Figure 6.17) eliminated the difference in oil removal levels seen at energy input levels below 200kwh/t, but the 'shear effect' persisted at higher energy inputs.

At the same energy input, oil removal levels are higher at 3 kW than at 1 kW. For example, 90 kWh/t is needed to remove 40% oil from the unsheared sample at 3 kW, while 116 kWh/t is required to remove the same quantity of oil from the same material at 1 kW. This is known as the power density effect (Buttress et al. 2016; Robinson et al. 2014), where a higher power density results in improved oil removal.

6.4.4 Microwave treatment of sheared and unsheared drill cuttings at 5 kW input power

Increasing the power input to 3 kW demonstrated that a higher power density can mitigate the reduction in oil removal efficiency caused by shearing although the 'shear effect' was not eliminated. Thus, a new set of experiments were set up to investigate the effect of a further increase in power density on oil removal efficiency with particular focus on energy inputs greater or equal to 200 kWh/t. The sample mass was 70 g with 5 kW power input. The oil and water contents are presented in Table 6-4.

Table 6-4: Oil and water contents of oil contaminated drill cuttings used in microwave heating at 5 kW

Sample (Shale)	**Initial oil content (% w/w)**	**Initial water content (% w/w)**
Unsheared	10	12
Sheared	12	12

Figure 6.18 shows that there are small differences in water removal at energy input below 120 kWh/t between the sheared and unsheared material. 51% water is evaporated at 76 kWh/t from unsheared shale while 56% water was removed at 79 kWh/t from the sheared material. The differences in water removal can be reconciled with the energy input difference. Above 120 kWh/t, water removal is similar for both the sheared and sheared material.

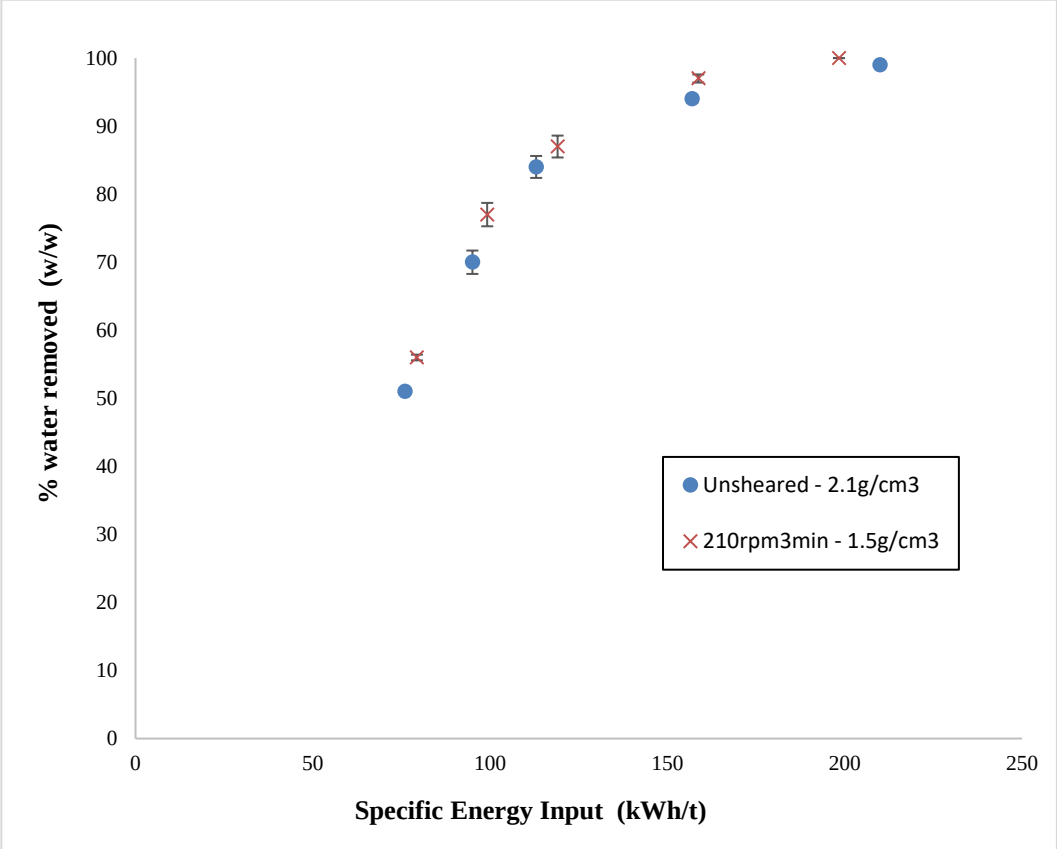


Figure 6.18: Water removal from sheared (210 rpm for 3 min) and unsheared oil contaminated drill cuttings plotted against specific energy input. 5 kW microwave power input. Each data point represents 4 experiments. Standard error is 0.01-1.72%.

The data presented in Figure 6.19 clearly shows that oil removal is the same for sheared and unsheared drill cuttings at 5kW. Furthermore, the disparity in oil removal between sheared and unsheared drill cuttings seen at high energy levels and 1 kW and 3 kW input power no longer exists at 5 kW. This indicates that the 'shear effect' can be eliminated completely if the power density in the sample is sufficient.

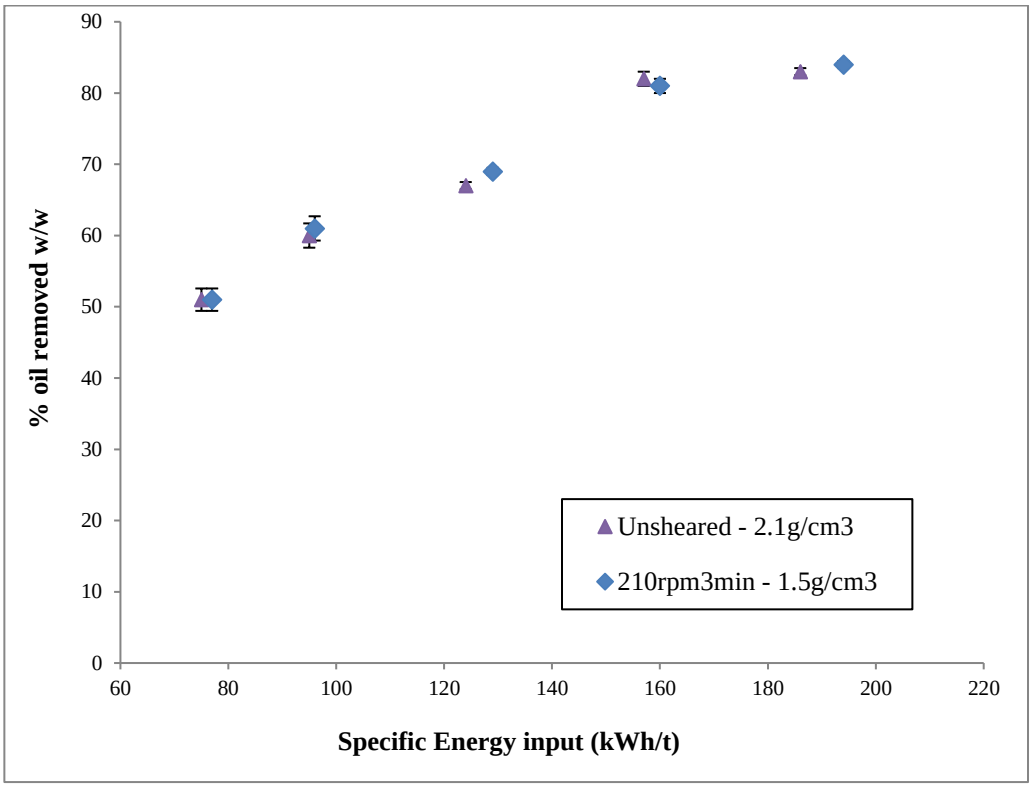


Figure 6.19: Oil removal from sheared (210 rpm for 3min) and unsheared oil contaminated drill cuttings plotted against specific energy input. 5 kW microwave power. Each data point represents 4 experiments. Standard error is 0.5-1.7%.

6.5 Microwave treatment of sheared and unsheared sandstone based drill cuttings

With a constant sample mass of 70 g, microwave heating tests were carried out on sheared and unsheared sandstone at 1 kW. The initial oil and water contents are shown in Table 6-1. Presented in Figure 6.20 is the water removal data from sheared and unsheared sandstone based drill cuttings. There is no apparent difference in the efficiency of water removal between sheared and unsheared sandstone. It is important to mention that although the density remains relatively unchanged, the sandstone material was sheared at 210 rpm for 3 minutes as with the shale samples.

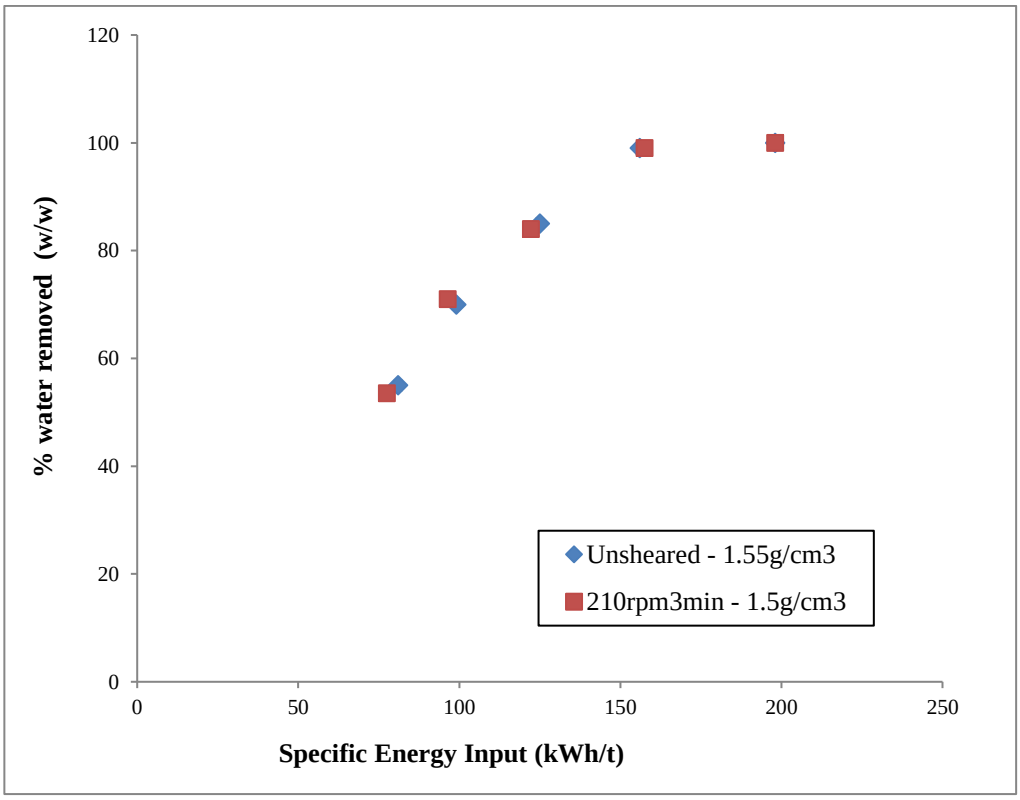


Figure 6.20: Water removal from sheared (210rpm 3min) and unsheared oil contaminated drill cuttings (Sandstone) plotted against specific energy input. 1 kW microwave power. Each data point is an average of two experiments. Standard error is 0.01-1.20%.

The findings presented in Figure 6.20 are interesting because the difference in water removal levels evident between unsheared shale and shale sheared to 1.4 g/cm^3 and 1.5 g/cm^3 was not observed for the sandstone material. This may be attributed to the fact that the bulk density of sandstone is not altered significantly from shearing. Also, it is likely that the surface area has not been changed appreciably from shear, and the proportion of its capillary water has also remained relatively unchanged. The data in Figure 6.20 confirms the hypothesis that if the main determining factor (bulk density) is unchanged from shear, then it is unlikely that there is a significant difference in the mechanism of evaporation or quantity of moisture removed from the drill cuttings matrix.

If one considers Figures 6.21a and 6.21b, there appears to be no difference between the structure of the sheared and unsheared sandstone drill cuttings. This helps to visualise the reason why the bulk density remains relatively constant during shear.

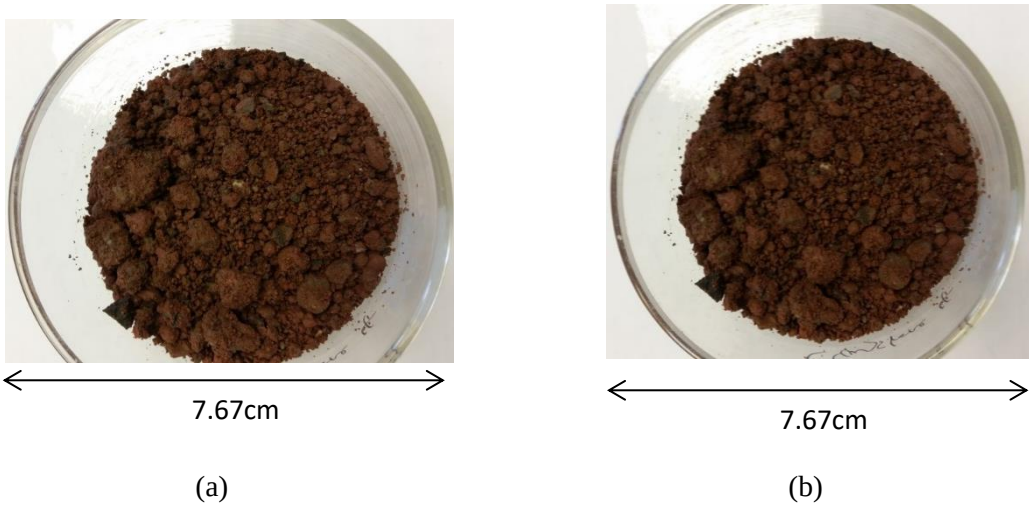


Figure 6.21: Sandstone based oil contaminated drill cuttings (a) Unsheared at 1.55 g/cm^3, (b) Sheared at 210 rpm for 3 minutes to 1.5 g/cm^3

The data presented in Figure 6.22 appears to show that oil removal efficiency from sandstone is not significantly affected by shearing.

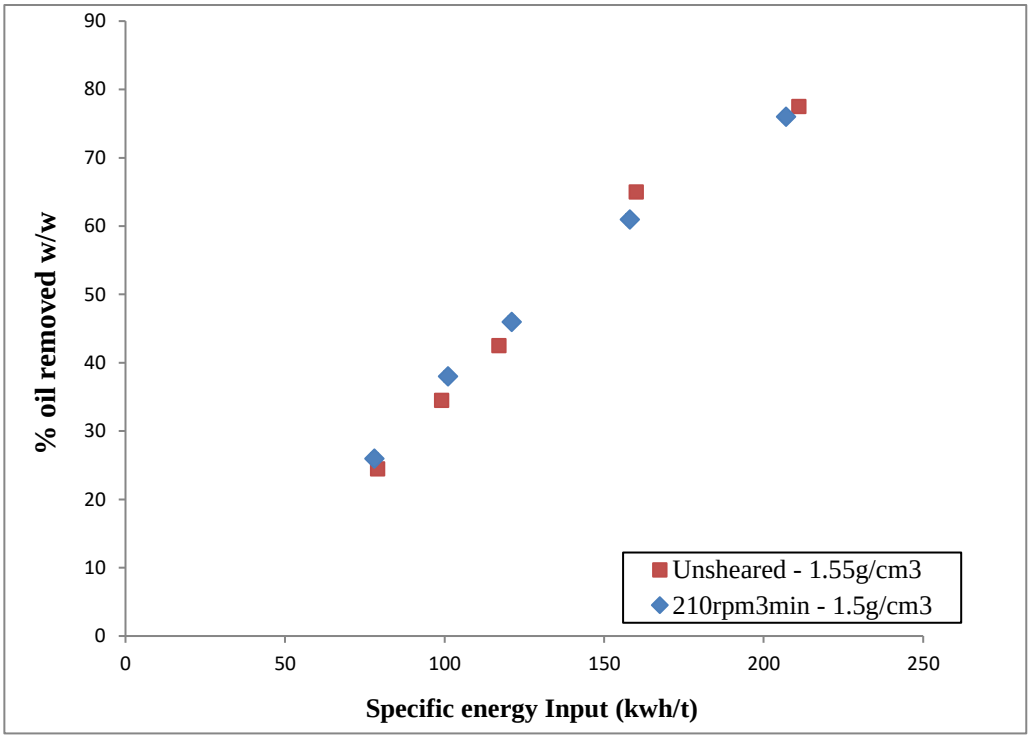


Figure 6.22: Oil removal from sheared (210 rpm for 3 min) and unsheared oil contaminated drill cuttings (Sandstone) plotted against specific energy input. 1 kW microwave power. Each data point is an average of two experiments. Standard error is 0.64-1.46%.

It is interesting to note that the tests are carried out at 1 kW input power, which means that the power density is equivalent to the data presented in Figure 6.8. Clearly, the difference in oil removal efficiency when one compares Figure 6.8 with Figure 6.22 is the magnitude of the change in bulk density in the shale material. The differences (less than 4%) in oil removal seen between 100 kWh/t and 160 kWh/t in Figure 6.22 is thought to be due to variability in the data, with the points expected to close considerably with more experimental data. Crucially, there is no significant difference in oil removal between the sheared and unsheared material at 200 kWh/t and above. This is in contrast to the data in presented in Figures 6.8 and

6.15 where the difference in oil removal between the sheared and unsheared material was at the highest at 200 kWh/t and above.

Therefore, it is a reasonable conclusion that using a twin screw feeder as a transport mechanism for sandstone based drill cuttings will not present a significant loss in oil removal efficiency in the microwave process.

6.6 Conclusion

Material transport, using high-shear twin screw conveyors is shown to have the potential to change bulk density of drill cuttings. The change in bulk density is attributed to the swelling clay component of the shale based drill cuttings material. There was no apparent change in the bulk density of the sandstone based drill cuttings when sheared. This work has shown that the shear levels in all drill cuttings can be characterised by bulk density.

It was shown that the oil removal efficiency of the microwave process decreases with decreasing bulk density for the shale based drill cuttings. This did not apply to the sandstone based material since the bulk density was unchanged during shear.

It was demonstrated that that high power densities can mitigate the effect of shear. In other words, the level of transformation from shear before the microwave applicator is irrelevant if the bulk density is known, and the process operates at a high power density. Therefore, industrial scale microwave systems operating at high power density and high electric field intensity will be needed to mitigate the shear effect of the twin screw conveyor transport process.

Chapter 7 Establishing the dominant mechanism of oil removal during the microwave heating of oil contaminated drill cuttings

7.1 Introduction

Competing mechanisms of oil removal from drill cuttings during microwave heating have been suggested in the past, namely; physical entrainment, direct vaporisation, steam distillation, and steam stripping (Shang et al., 2006; Robinson et al., 2008; Robinson et al., 2009a; Pereira, 2012). However, there is no consensus or conclusive evidence establishing a dominant mechanism(s) of oil removal to date. Knowing the dominant mechanism of removal is crucial because it aids the optimisation of the microwave process and informs the selection and design of appropriate downstream processes and equipment. The current hypothesis is that steam stripping is the dominant mechanism of oil removal, and that the efficiency of oil removal is related to the velocity of steam within the pores of the drill cuttings material. The hydrocarbon mass transfer coefficient is determined empirically and correlated with the steam velocity to validate the steam stripping hypothesis. Furthermore, an empirical mass transfer model is developed relating the mass transfer rate of oil from the drill cuttings material to the velocity of steam through the pores.

The efficiency of oil removal from three microwave processing systems is analysed, taking into consideration the relationship between the rate of oil removal, pore steam velocity, and power density. Empirical measurements from these

systems are compared with theoretical values based on different oil removal mechanisms.

7.2 Oil removal mechanisms from drill cuttings

During microwave processing of drill cuttings, it is known that water is the only absorber of microwave energy within the drill cuttings matrix, whereas other components are essentially microwave transparent (chapter 5). The microwave process operates normally at a bulk temperature approximately 100 ^{o}C, ensuring that energy is dissipated only in the water phase.

7.2.1 Theoretical energy requirement for the oil removal mechanisms

Calculating the theoretical energy required by each oil removal mechanism will give an indication of the energy efficiency of each mechanism, and a basis of comparison with empirical data. The energy requirement for these mechanisms will be examined presently.

The microwave energy required for oil removal in drill cuttings matrix is given by equation 7.1;

$$E = M_w C_{pw} \Delta T_w + M_o C_{po} \Delta T_o + M_r C_{pr} \Delta T_r + M_w L_w + M_o L_o \quad [7.1]$$

Where:

E = Energy required

M = Mass of water

C_p = Specific heat capacity

ΔT = Change in temperature

L = Latent heat of vaporisation

Subscripts = (w – water, o – oil, r – rock)

Some assumptions made in estimating the theoretical energy requirement for each removal mechanism is presented in Table 7-1.

Table 7-1: Parameter assumptions in calculating the theoretical energy requirement of oil removal mechanisms

Parameters	Values

Specific heat capacity	oil[a] = 2 kJ/kgK;
	water[b] = 4.2 kJ/kgK;
	rock[a] = 1.5 kJ/kgK

Latent heat of vaporisation	oil[a] = 800 kJ/kg; water[b] = 2257 kJ/kg
Ambient temperature	20 ^{o}C
Oil content of treated drill cuttings	1 wt%
Water content of treated drill cuttings	0 wt%

a = sourced from (Robinson et al., 2009a) b = sourced from Green and Perry, 1997

The amount of energy required by each oil removal mechanism is affected by the temperature rise of each of the drill cuttings component. Table 7-2 shows the assumed temperature of the components of drill cuttings during microwave treatment. Where no temperature range is given in Table 7-2, the temperature change of the component in equation 7.1 will be zero.

Table 7-2: Temperature of drill cuttings components during microwave heating

	Physical Entrainment (PE)	**Steam Distillation (SD)**	**Steam Stripping (SS)**	**Direct Vaporisation (DV)**
Water	20–100 ^{o}C	20–95 ^{o}C	20–100 ^{o}C	20–100 ^{o}C
Oil	-	20–95 ^{o}C	20– 100 ^{o}C	20– 250 ^{o}C
Rock	-	20–95 ^{o}C	20– 100 ^{o}C	20–250 ^{o}C

For example, the temperature change term for oil and rock is zero in equation 7.1 when estimating the energy requirement for the physical entrainment mechanism. This means that it is assumed that energy is dissipated only in the water phase when physical entrainment is the dominant oil removal mechanism.

Table 7-3 shows the applicable terms from equation 7-1 in calculating the energy requirement for different oil removal mechanisms.

Table 7-3: Applicable terms from equation 7.1 required to estimate the energy requirement for individual oil removal mechanisms. √ - applicable, x – not applicable.

Mechanism	**Term 1**	**Term 2**	**Term 3**	**Term 4**	**Term 5**
PE	√	x	x	√	x
SD	√	√	x	√	√
SS	√	√	x	√	√
DV	√	√	√	√	√

The energy requirement for the steam stripping mechanism is illustrated below using the information in Tables 7.1-7.3.

Equation 7.1 is modified as follows for steam stripping;

$$E_{stripping} = M_w C_{pw} \Delta T_w + M_o C_{po} \Delta T_o + M_w L_w + M_o L_o \quad [7.2]$$

Using 70 g of shale based drill cuttings containing 14 wt% water and 11 wt% oil as a model sample;

Mass of water vaporised (M_w) = $\frac{14}{100} \times 70$ g = 9.8 g

The amount of energy that will be needed to heat 9.8 g water from 20 ^oC to 100 ^oC is as follows;

$$E_w \text{ (kJ)} = \left(\frac{9.8}{1000} \times 4.2 \times 80\right) + \left(\frac{9.8}{1000} \times 2257\right) = 25.41 \text{ kJ}$$

The amount of energy that will be needed to reduce oil from 11 wt% to 1 wt% is as follows;

Mass of oil vaporised (M_o) = ($\frac{10}{100} \times 70$g) = 7 g

$$E_o \text{ (kJ)} = \left(\frac{7}{1000} \times 2 \times 80\right) + \left(\frac{7}{1000} \text{ x } 800\right) = 6.72 \text{ kJ}$$

Energy absorbed by the rock fragments;

$$E_r \text{ (kJ)} = \left(\frac{52.5}{1000} \times 1.5 \times 80\right) = 6.3 \text{ kJ}$$

Total amount of energy ($E_{stripping}$[1,2]) required for steam stripping; $E_o + E_w + E_r$ = 25.41 + 6.72 + 6.3 = 38.43 kJ.

Changing $E_{stripping}$ to specific energy input on mass basis;

$$\text{Specific energy input (kwh/t)} = \left(\frac{38.43\ \text{kJ}}{70\ \text{g}} \times \frac{10^6\ \text{g}}{\text{tonne (t)}} \times \frac{\text{kWh}}{3600\ \text{kJ}}\right) = 152.5\ \text{kWh/t}$$

Therefore, 152.5 kWh/t of microwave energy is required when steam stripping is the dominant oil removal mechanism. Presented in Table 7-4 are the theoretical energy requirements for oil removal from drill cuttings according to the aforementioned removal mechanisms.

Table 7-4: Theoretical microwave energy requirement to reduce oil content to 1 wt% in contaminated drill cuttings (14 wt% water, and 11 wt% oil)

Mechanism of oil removal	Energy required (kWh/t)
Physical Entrainment	101
Steam Distillation	149
Steam Stripping	152.5
Direct Vaporisation	207

The data shown in Table 7-4 is calculated on the basis that only one removal mechanism dominates during treatment of the sample. The data shows that physical entrainment is the most energy efficient, while direct vaporisation is the least energy efficient. A combination of these mechanisms occur during microwave heating, nonetheless, the data is useful in estimating of the relative energy efficiency of each mechanism, and the dominant removal mechanism.

[1] **Calculation is based on the assumption that microwave power supplies sensible heat and latent heat of vaporisation for water.**
[2] **Assumes the mineral phase is transparent to microwave power at 100°C.**

7.2.1 Physical Entrainment

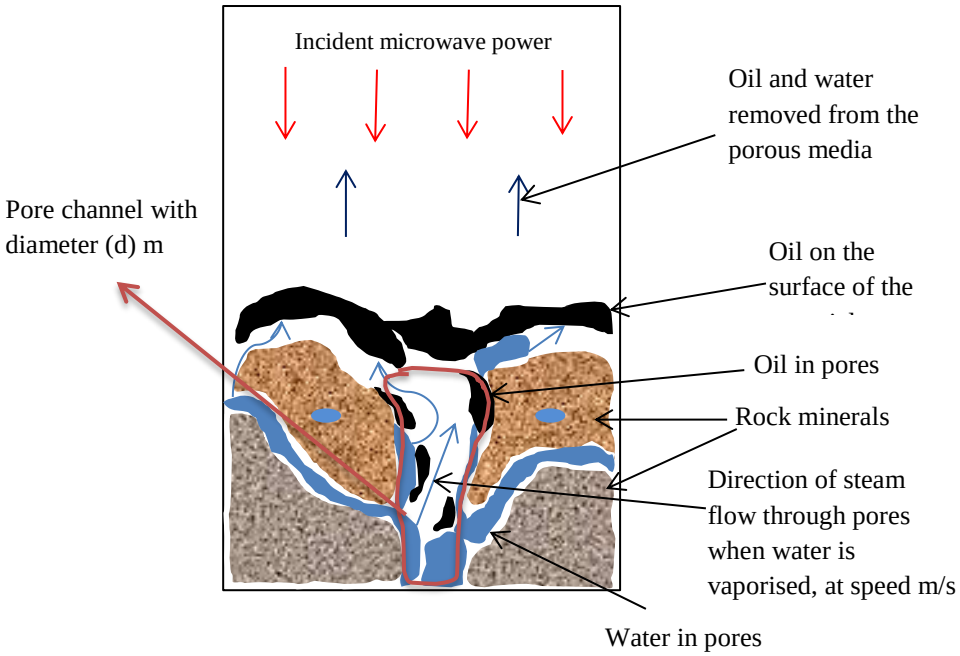
Physical entrainment is the most attractive thermodynamically since it is the most energy efficient mechanism (Table 7-4). Only water within the pores of the drill cuttings is heated and converted to steam, and as steam escapes, oil is physically entrained. Pereira (2012) and Robinson, et al. (2009a) have shown that the minimum energy required to reduce oil to <1 wt% in a continuous microwave processing is 100 – 140 kwh/t. On the other hand, 101 kWh/t (Table 7-4) is the theoretical energy requirement when physical entrainment is the mechanism of oil removal. 101 kWh/t is within range of the expected required energy, as reported by Robinson, et al. (2009), therefore it cannot be ruled out as the main mechanism of removal on an energy basis.

During this mechanism, the oil and rock components are transparent to microwaves and it is assumed that there is negligible heat transfer through conduction or convection from the water phase to the oil. This means that oil should not thermally decompose when removed via physical entrainment. However, gas chromatography analysis of the off gas during microwave heating shows preferential removal of lighter molecules in oil, indicating heat transfer between the vaporised water and desorbed oil (Pereira, 2012). This strongly suggests other competing removal mechanisms with physical entrainment. Moreover, Pereira (2012) reported that the physical entrainment mechanism is not the dominant removal mechanism because it typically accounts for 10-20% of oil removed.

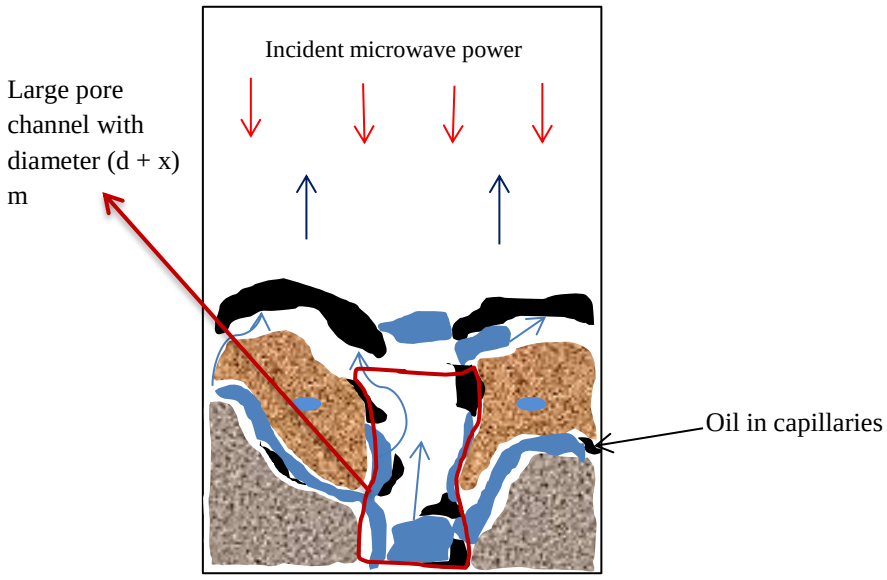
The power density effect is a good premise to compare the oil removal mechanisms. Consider microwave treatment of shale based drill cuttings in system A (Table 6-1, Figure 6.8, Figure 6-19), at approximately 120 kwh/t constant energy input, 40%

oil was removed at 1 kW, while 69% oil was removed at 5 kW. This is the power density effect, which shows a 29% increase in oil removal at the same energy input.

Physical entrainment relies on oil occupying the surface and large pores of the drill cuttings material where it can be fully exploited. Figure 7.1a shows a conceptual representation of a matrix of drill cuttings, oil is mostly located on the surface and in the large pores. Using Figure 7.1a as an example, as input power increases, the general direction of steam flow out of the matrix is largely unchanged. At higher power density, steam is removed from the matrix with higher kinetic energy and hence greater velocity. It is thought that oil removal via physical entrainment increases as power density increases due to increased shear on the material's surface from the escaping steam. However, Pereira (2012) has shown quantitatively that physical entrainment does not dominate in this circumstances, and only accounts for 10-20% oil removal.



(a)



(b)

Figure 7.1: Schematic showing water and oil in the pores of (a) shale based drill cuttings at 1.9 g/cm^3 (b) shale based drill cuttings sheared to 1.5 g/cm^3.

When the matrix structure of the material is significantly altered from different processes such as, highlighted in chapter 6, in material transport. The physical entrainment mechanism may not be fully exploited in these circumstances. Figure 7.1b shows the conceptual representation of the matrix of a drill cuttings sample with a lower bulk density and a higher pore volume than the matrix in Figure 7.1a, both with equivalent oil and water content. The amount of oil located on the surface in Figure 7.1b is lower when compared with Figure 7.1a, also some oil reside in the capillaries in Figure 7.1b. In the case of the matrix in Figure 7.1b, it is thought that vaporised water may not be able to entrain isolated oil droplets in capillaries and smaller pores during a physical entrainment removal mechanism. This suggests a reduction in oil removal efficiency from the matrix in Figure 7.1b when physical entrainment is the dominant removal mechanism. This appears to be the case at low power densities (Figure 6.8, Chapter 6), however, higher power densities eliminate the reduction in oil removal observed in drill cuttings at low bulk densities (Figure 6.19, Chapter 6) and suggests, contrary to a physical entrainment dominated mechanism, a simultaneous heat and mass transfer of the oil phase from the material during treatment.

7.2.2 Direct vaporisation

Direct vaporisation is estimated to be the least energy efficient amongst the potential oil removal mechanisms (Table 7-4). The theoretical energy requirement for direct vaporisation is 207 kWh/t, which is significantly greater than the energy requirement for the other removal mechanisms. Furthermore, the energy requirement is also significantly greater than the energy requirement (100-140 kWh/t) in a continuous microwave process from previous work (Robinson et al.,

2009). This indicates that direct vaporisation cannot be the dominant mechanism of oil removal.

7.2.3 Steam distillation and steam stripping

The energy efficiency of steam distillation (149 kWh/t) and steam stripping (152.5 kWh/t) are similar (Table 7-4), however, oil removal is predominantly by heat transfer from water to the organic phase in steam distillation. In steam distillation, oil and water boil at a temperatures less than 100 ^{o}C because their combined vapour pressure is greater than the surrounding system pressure, if atmospheric. The nature of steam distillation means that the mechanism depends on close contact between oil and water phases in the drill cuttings matrix, suggesting that isolated pockets of oil may not be removed if steam distillation is the main mechanism of removal.

Theoretically, the thermodynamic energy to vaporise a fixed amount of water and oil is constant. When power density is increases, the rate of heat transfer from water to the organic phase may increase, but the thermodynamic energy requirement to heat both phases is unchanged. If steam distillation was considered as the main oil removal mechanism, increasing the power density, at constant energy input, may result in a faster rate of water and oil removal but will not increase the amount of oil removed overall. In other words, the material will attain the bulk operating temperature faster at high power densities but oil removal should be the same with low power densities. It has however been demonstrated that overall oil removal increases with increasing power density (Shang et al., 2006). This strongly suggests the dominance of other mechanisms over steam distillation at high microwave power densities.

At high power densities, high heating rates generate steam at a fast rate, and consequently, drive the bulk movement of steam from the sample depth to the surface and out of the material. The high steam pressure generated in the pores dictates the velocity and bulk flow of gases (steam and oil vapour) from the pores to the material's surface. The higher the power density, the greater the gas pressure generated in the pores, and ultimately, this leads to a faster bulk flow of steam.

The oil removal effect of the bulk flow of steam through the drill cuttings matrix is steam stripping. This hypothesis highlights the similarities and differences between the steam distillation and steam stripping removal mechanisms. Steam distillation is dependent mainly on heat transfer from vaporised water to the oil content. Whereas, steam stripping is as a result of the evaporative effect of steam, which is dependent on steam velocity, and dictates the mass transfer rate of the oil into the steam stripping phase.

The similarities in the theoretical energy requirement for oil removal between steam distillation and steam stripping means that energy requirement alone is insufficient for ruling out either of the mechanisms as the dominant mechanism of oil removal.

In conventional gas stripping, the efficiency of contaminant removal from a fixed bed has been shown to increase at higher gas velocities (Yoon et al., 2002; Van der Ham and Brouwers, 1998). It is thought that similar principles apply where the steam stripping of oil from drill cuttings during microwave heating is dependent on the velocity of the steam through the material. Higher power densities mean higher steam velocities, which can possibly explain the increase in oil removal at higher power densities.

To explore this, the relationship between the velocity of steam in the pores of the drill cuttings material and the mass transfer rate of oil is examined, and used to generate an empirical mass transfer model. In order to build the mass transfer model, the amount of oil and water removed during microwave treatment was determined in the three processing systems described in the sections 4.1 - 4.3.

7.3 Effect of microwave power and heating time on oil and water removal

7.3.1 Microwave treatment of drill cuttings in system A

The oil and water contents and bulk densities of the drill cuttings samples treated in system A (section 4.1) are shown in Table 7-5. The relationship between the oil and water removal and varying energy inputs at 1 kW, 3 kW, and 5 kW microwave powers have been discussed extensively in chapter 6, hence the focus here is the microwave power effect.

Table 7-5: Oil and water content, and bulk density of oil contaminated drill cuttings treated in system A (70 g sample mass)

Sample	Power (kW)	Water content (%w/w)	Oil content (%w/w)	Bulk density (g/cm^3)
Shale 1	1 - 5	8.5 – 14 ±0.2	7.5 – 11.5 ±0.5	1.4 – 2.1 ±0.04
Sandstone	1	9 ±0.2	8 ±0.5	1.55 ±0.04

Figures 7.2 and 7.3 show the effect of microwave power on treatment time, and water and oil removal from shale 1. The results presented is the average of 4 – 8 microwave heating experiments. The error bars are the standard errors of the data set. According to Figure 7.2, at constant sample mass, when microwave power increases, the time required for oil removal decreases. For example, it took 43

seconds to remove 65% oil at 1kW, while treatment at 5kW showed a 5 fold reduction in the time required to achieve 65% oil removal.

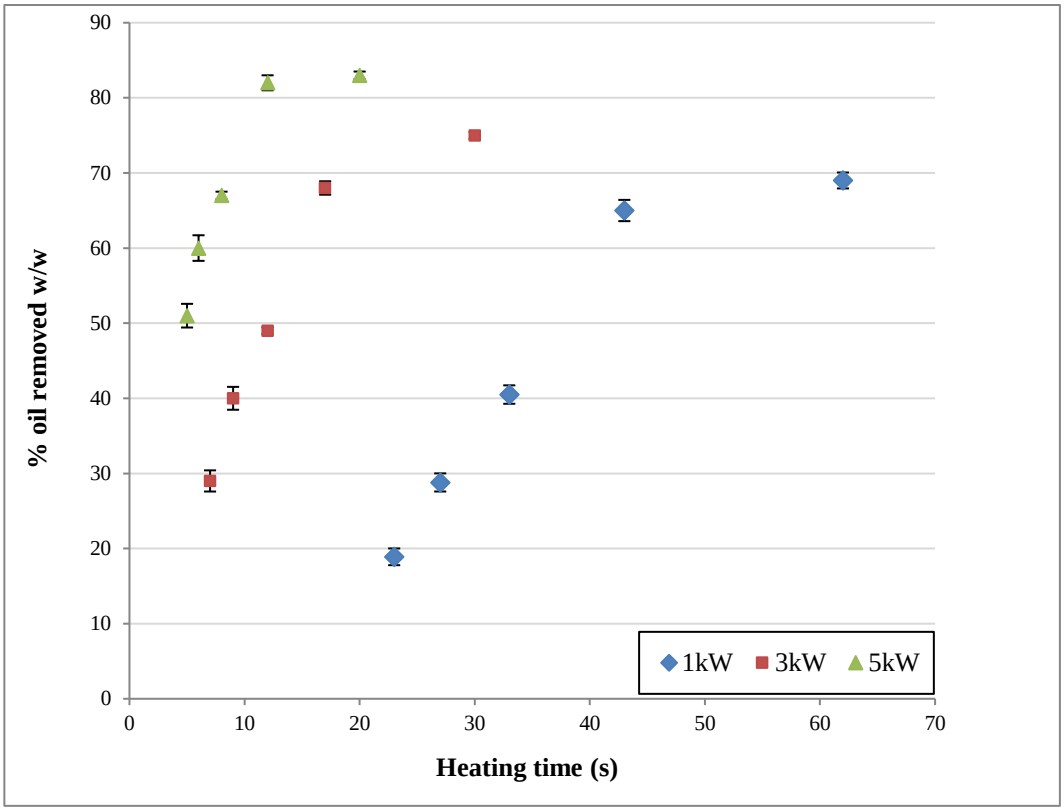


Figure 7.2: Oil removal plotted against heating times for treatment in system A (70 g sample mass). Standard error is 0.12-1.84%.

The water removal from shale 1 at different input powers show a similar trend at high power densities to that of the oil removal (Figure 7.3). Di, et al. (2000) observed similar faster rate of water evaporation with incremental power input from soil. This is the power density effect; a higher power input leads to higher electric field strength within the treated sample and hence grater heating rates and reduced heating times. Results for the sandstone sample show a similar trend of reduced heating times at high powers, but it is not presented in this section as it would only show a duplicate of the microwave power effect in shale 1. The sandstone properties are shown in Table 7-5 because the microwave heating results are used in developing the mass transfer model.

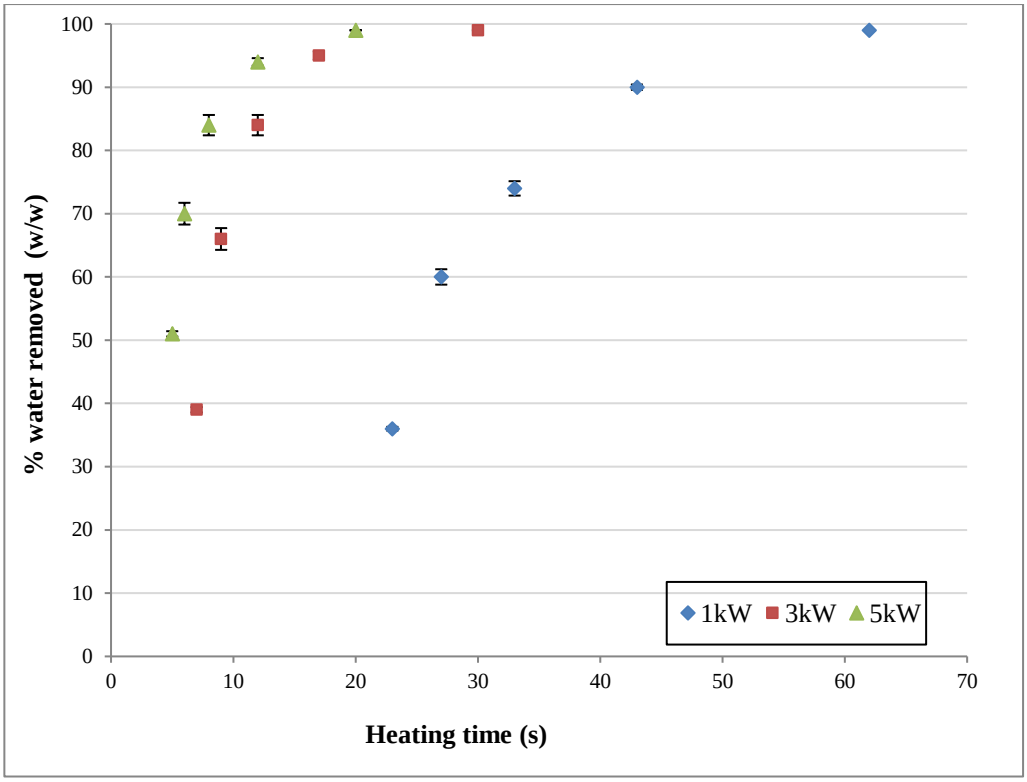


Figure 7.3: Water removal plotted against heating times in system A (70 g sample mass). Standard error is 0.01-1.72%.

7.3.2 Microwave Treatment of drill cuttings in system B

System B was set up to explore the feasibility of a different material handling processing concept for the microwave treatment of oil contaminated drill cuttings, described in section 4.2. Presented in Table 7-6 are the bulk density, oil and water contents of the sample used in system B.

Table 7-6: Oil and water content, and bulk density of oil contaminated drill cuttings in system B (sample mass = 6.5 kg)

Sample	Initial water content (%w/w)	Initial oil content (%w/w)	Bulk density (g/cm^3)
Shale 2	7 .5 ±0.2	9.5 ±0.5	1.95 ±0.04

The cavity in system B consists of two bores which can take 6.5 kg of samples each. For this work, only one bore was filled with 6.5 kg of drill cuttings during microwave heating. As a result, significant reflected power was observed during the experimental runs. Table 7-7 shows the typical incident and reflected power in system B.

Table 7-7: Incident and reflected powers during the microwave heating treatment of drill cuttings in system B

Incident power (kW)	Reflected power (kW)	Absorbed power (kW)
50	10	40
75	11	64
100	27	73
100	9	91

The effect of microwave power on treatment time and oil and water removal in system B is presented in Figures 7.4 and 7.5. The general trend show reduced heating times at higher powers. For example, 83% water removal corresponded to 30 s heating time at 64 kW, and 41 s at 40 kW in Figure 7.4.

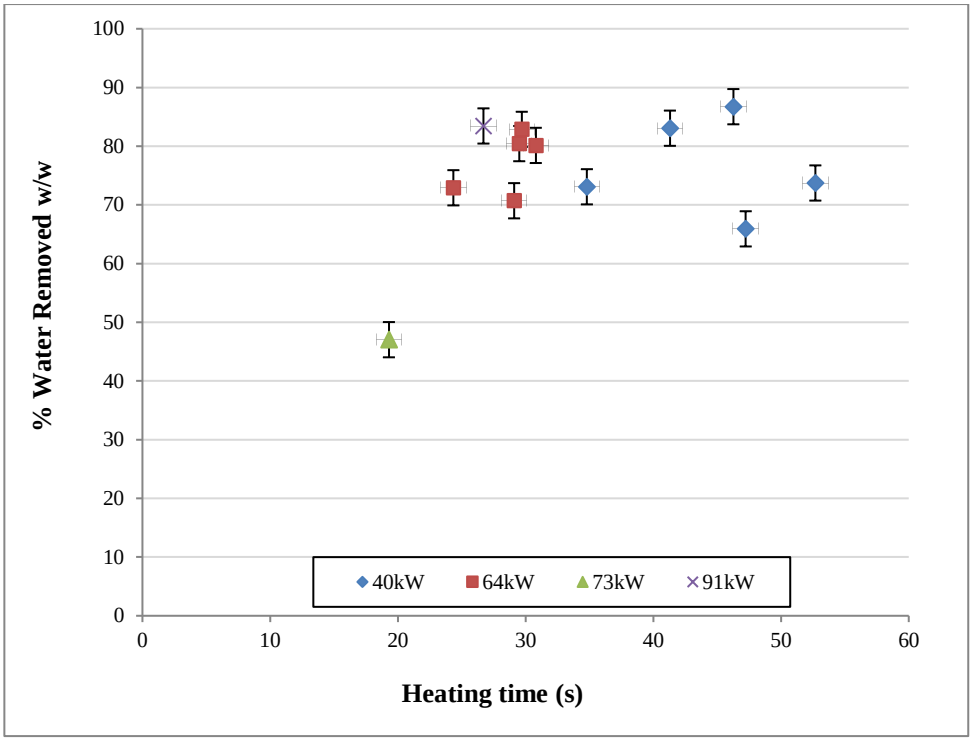


Figure 7.4: Water removal plotted against heating times during microwave treatment of drill cuttings in System B. Standard error is 1.72%.

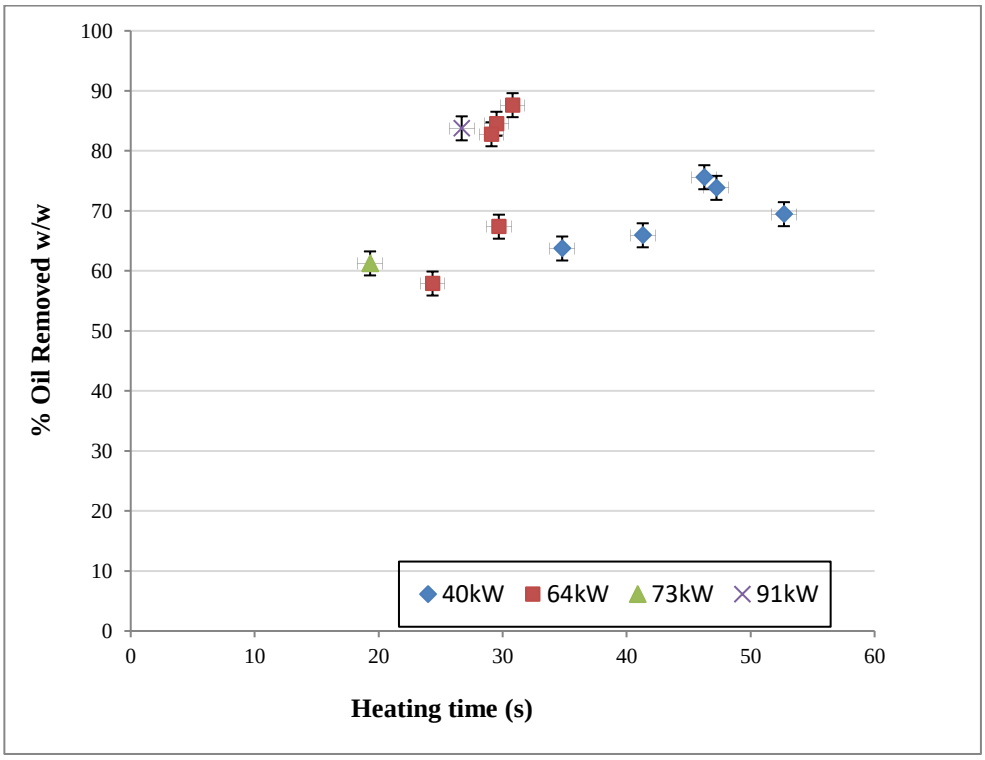


Figure 7.5: Oil removal plotted against heating times during the microwave treatment of drill cuttings in system B. Standard error is 1.84%

In addition, more oil is removed at higher powers and equivalent energy input, confirming the power density effect. This is better illustrated in Figure 7.6 which shows the effect of microwave power on oil removal at constant energy in microwave processing systems A and B. In Figure 7.6, difference between the mass of samples in systems A (70 g) and B (6.5 kg) is rationalised, which allows data from both systems to be combined on the same plot.

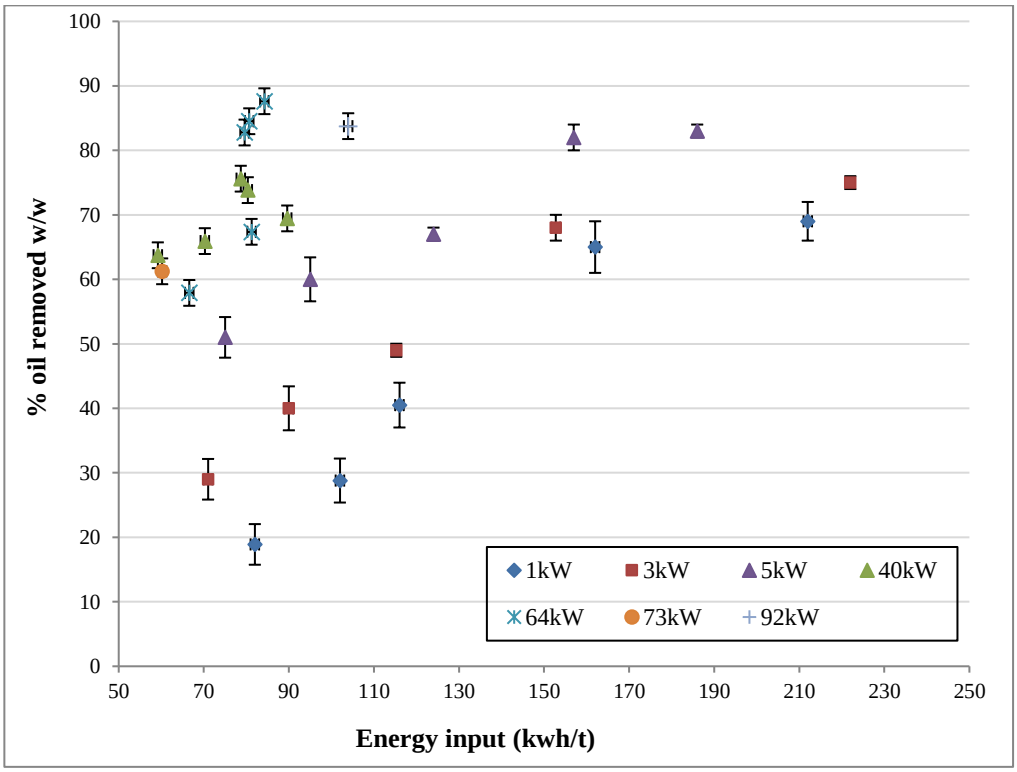


Figure 7.6: Oil removal plotted against energy input, showing that oil removal increases at high power densities and equivalent energy input. Standard error is 0.12-1.84%.

7.3.3 Microwave treatment of drill cuttings in system C

The wheel applicator system (described in section 4.3) is the latest concept in the microwave processing of drill cuttings. Table 7-8 shows the physical properties of the drill cuttings sample treated in this system.

Table 7-8: Oil and water content and bulk density of oil contaminated drill cuttings treated in system C.

Sample	Initial water content (%w/w)	Initial oil content (%w/w)	Bulk density (g/cm^3)
Shale 3	12.7 ±0.2	13.1 ±0.5	1.9 ±0.04

The oil and water removal data from the microwave heating experiments in system C is shown in Table 7-9. The mass flow rate was determined from the wheel speed, and the sample geometry (see details in appendix 1). Table 7-9 shows that at a constant mass flowrate of 0.086 kg/s, an increase in microwave power corresponds to a decrease in oil content, corroborating the power density effect.

Table 7-9: Data from microwave heating tests in system C including the final oil and water content of samples after treatment

Wheel Speed (mm/s)	Bed depth (mm)	Mass flowrate (kg/s)	Input Power (kW)	Average absorbed power (kW)	Final Oil content (%w/w)	Final water content (%w/w)
7	35	0.086	35	26.76	6.2±0.5	2.4±0.2
7	35	0.086	45	31.87	4.6 ±0.5	1.7±0.2
10	28	0.098	35	29.78	6.3±0.5	2.6±0.2
12	25	0.105	35	27.72	7.6±0.5	2.9±0.2
15	22	0.116	35	27.19	6.7±0.5	5.5±0.2

7.4 Steam Velocity: Assessment of steam stripping mechanism

Typically, a microwave evaporating process can be categorised into four stages namely, initial heat-up period, rapid rate of evaporation period, slow evaporation period, and an equilibrium period (Di et al., 2000). Water removal from drill cuttings will undergo similar stages during microwave heating, but is characterised by a 'falling rate' period instead of an equilibrium period in this work. Consider the rate of water evaporation from drill cuttings at 1 kW power input in system A presented in Figure 7.7. The rate of water evaporation was calculated from measuring the water content of the samples before and after microwave heating. Dean and Stark analysis (section 4.12) was used to determine the water content of the samples.

The evaporation rate of water R (g/s) was determined from equation 7.3;

$$R = \frac{M_1 - M_2}{t} \qquad [7.3]$$

where;

M_1 = mass of water in untreated sample (g)

M_2 = mass of water in sample after microwave heating (g)

t = duration of microwave heating (s)

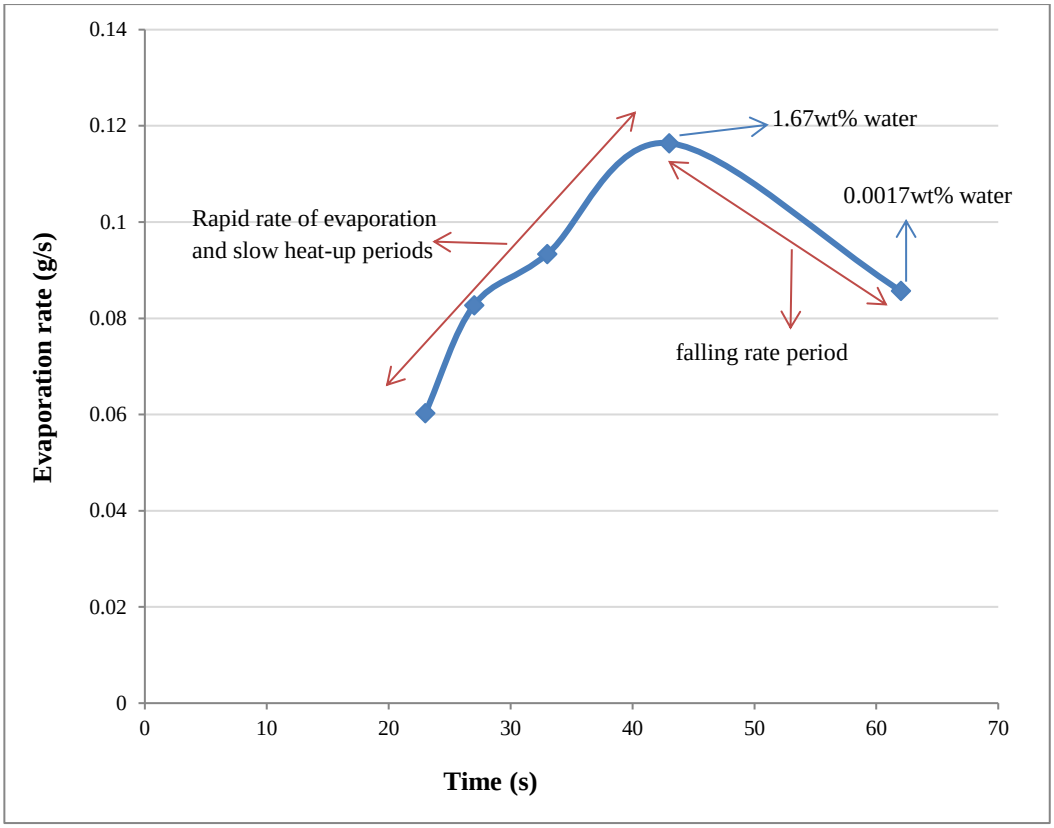


Figure 7.7: Evaporation rate of water from oil contaminated drill cuttings as a function of time (Power = 1 kW, Sample = shale 1, System A)

Figure 7.7 shows that the rapid rate of evaporation and slow evaporation periods occurred before 43 seconds. The falling rate period follows swiftly after, characterised by extremely low water content. At this stage, the material absorbs very low amount of microwave power as the main microwave absorbing phase is depleted. Low moisture leads to a steady temperature in the material in equilibrium with microwave power. The time required to reach the falling rate period is different for varying drill cuttings samples, as it depends on power density and heating rate, and can only be accurately determined empirically.

Analysis of the various periods of evaporation rate is essential in determining steam velocity. The water removal data from the falling rate period is excluded from

steam velocity calculations in this work because most of the water has been evaporated at this stage.

The water contents of the drill cuttings samples after treatment in systems B and C (Figure 7.4 and Table 7-9) indicate that the evaporation rate period in these systems have not reached the falling rate period. For illustration purposes, Figure 7.7 shows that the water content at the start of the falling rate period is 1.67wt% which was reduced to less than 0.1wt% at the end of the experiments. Whereas, from Table 7-9 the water content at the end of each experiment in system C is greater than 1.67wt%.

The steam velocity is estimated from equation 7.4;

$$u_g = \frac{Q}{A} \qquad [7.4]$$

where;

u_g = steam velocity through the pores of the material (m/s)

Q = steam volumetric flow rate (m^3/s)

A = cross sectional area of the material through which steam flows (m^2)

The steam volumetric flowrate is defined as;

$$Q = \left(\frac{M_1 - M_2}{\rho}\right) \div t \qquad [7.5]$$

where;

M_1 = mass of water in the untreated sample (kg)

M_2 = mass of water in treated sample (kg)

ρ = density of steam (kgm^{-3})

t = treatment time (s)

The steam velocity calculations for the microwave processing systems are detailed in appendix 2.

7.4.1 Effect of microwave power and porosity on steam velocity

Power density and porosity have been identified as the main factors affecting the velocity of steam through the pores of drill cuttings.

The relationship between power density and rate of temperature rise of water (heating rate) during microwave heating is given by equation 7.6;

$$\frac{\Delta T}{\Delta t} = \frac{P_d}{\rho C_p} \qquad [7.6]$$

where $(\Delta T/\Delta t)$ is the heating rate, and P_d is the power density. The full derivation of equation 7.6 is detailed in appendix 4. Equation 7.6 shows that as microwave power density increases, the heating rate in water increases, which means that steam is generated at a faster rate. This is illustrated in Figure 7.8, which shows that steam velocity through the material's pores increases as microwave power increases.

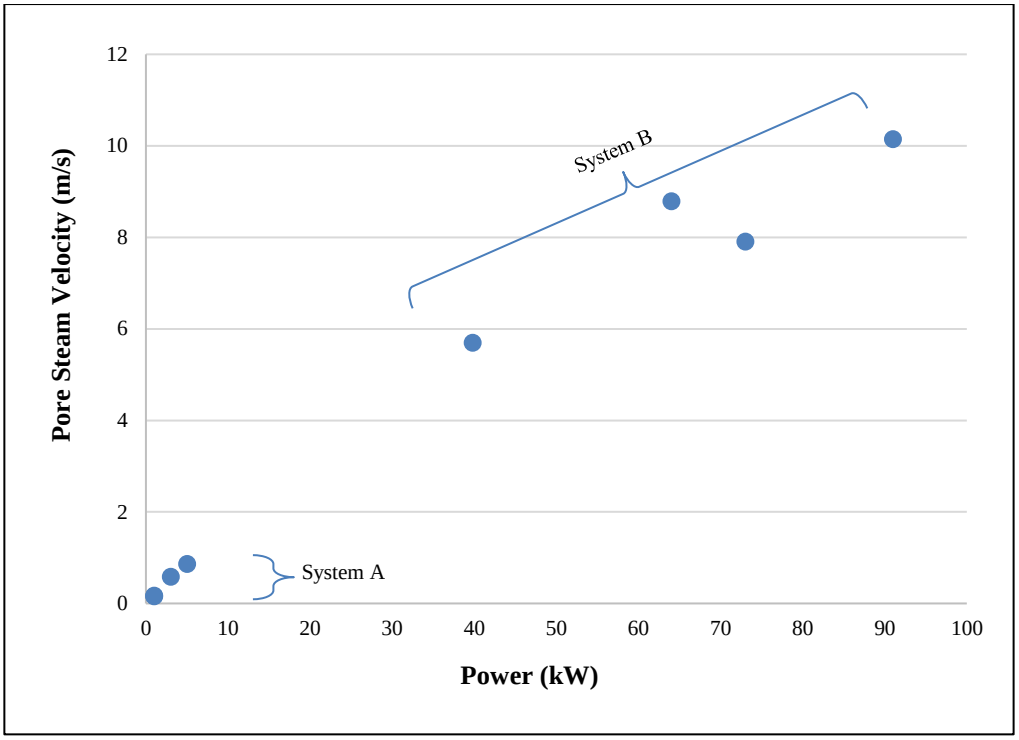


Figure 7.8: The relationship between pore steam velocity and microwave power during microwave treatment of drill cuttings at 80 kWh/t in systems A and B.

The size of the pores affect the interstitial steam velocity. When a material mainly consists of small pores and capillaries, the average cross sectional area of the pores will be smaller than materials characterised by larger pores. From equation 7.4, smaller pore cross sectional area corresponds to high steam velocity, which indicates lower steam velocity through that larger pores with greater areas.

Porosity was estimated from the bulk density and skeletal density of the material (section 4.6). Drill cuttings naturally consists of varying pore sizes, however, in this work macropores and micropores are incorporated, and the average pore size (porosity) is used in estimating the flow area. Therefore, materials with the greatest porosity will have the largest cross sectional (flow) areas and lowest bulk densities, and vice versa for materials with high bulk density. The relationship between cross sectional (flow) areas and steam velocity is shown in equations 7.4 and 7.5. Method for determining steam velocity at varying porosities is detailed in appendix 2.

Table 7-10 shows the effect of porosity on steam velocity during microwave heating, and as anticipated, lower steam velocity is observed in materials with higher porosity.

Table 7-10: The relationship between microwave power, porosity and steam velocity during microwave heating of oil contaminated drill cuttings (shale 1, system A, 80 kWh/t energy input)

Porosity	**Microwave power (kW)**	**Steam velocity (m/s)**
0.37	1	0.168
0.49	1	0.124
0.29	5	0.863
0.47	5	0.697

Recall that Figure 7.1a represents a drill cuttings matrix with a higher bulk density than the matrix in Figure 7.1b, which means that the porosity of the matrix in Figure 7.1a is smaller. If both matrices contain the same oil and water content, and are treated under microwave at equivalent power input, the steam velocity through matrix in Figure 7.1a will be higher due to the fact that the porosity is smaller.

It was shown in chapter 6 that oil removal decreases at greater porosities and low microwave power densities (Figure 6.8, Chapter 6), suggesting that lowering the porosity will increase oil removal. This is thought to be partly due to lower pore steam velocities at greater porosities, and indicates that steam stripping is a major determinant factor in oil removal.

7.4.2 Mass transfer coefficient

The mass transfer coefficient is linked to the velocity of the stripping medium in the generalised correlation using dimensionless groups as follows;

$$Sh = bRe^{c}Sc^{0.33} \qquad [7.9]$$ (Comiti et al., 2000)

where Sh is the Sherwood number, Re is the modified Reynolds number, Sc is the Schmidt number, b and c are constants determined empirically. Equation 7.9 is used because it is relevant for the determination of mass transfer coefficient of fluids in a fixed bed of porous media.

$$Sh = \frac{k_g d_p}{D_a} \qquad [7.10]$$

$$Re = \frac{\rho u_g d}{\mu(1-\varepsilon)} \qquad [7.11]$$

where;

k_g = gas phase mass transfer coefficient (m/s)

d_p = characteristic length of diffusion or bulk transport, defined as the mean particle size (m)

D_a = diffusion coefficient of oil in the stripping medium (m^2/s)

ρ = density of the stripping medium (kg/m^3)

u_g = steam velocity (m/s)

d = diameter of 'bulk flow' pore channel (m)

μ = viscosity of the stripping medium (kg/ms)

ε = porosity

D_a in equation 7.10 can be calculated from;

$$D_a = 3.185 \times 10^{-10} \times \frac{T^{1.75}}{P_{total}} \qquad [7.12]$$ (Van der Ham and Brouwers, 1998)

T is the bulk sample temperature in Kelvin, P_{total} is the system pressure in bar.

Equations 7.10 and 7.11 show that mass transfer coefficient is directly proportional to the Sherwood number, and steam velocity is directly proportional to the Reynolds number. Therefore mass transfer coefficient (k_g) and pore steam velocity (u_g) may be related as follows;

$$k_g = bu_g^c Sc^{0.33} \qquad [7.13]$$

Schmidt number (Sc) is defined as;

$$Sc = \frac{\mu}{D_a \rho} \qquad [7.14]$$

Schmidt number is more suited to a diffusion dominated process as it shows the ratio of momentum to mass diffusivity (Wilkins et al., 1995). The parameters, especially viscosity (μ) of gases in the Schmidt number in equation 7.14 generally remain unchanged at constant temperature, therefore, the parameters in equation 7.14 are assumed constant.

The Schmidt number is generally less than or equal to 1 in gases and in the region of 10^3 in liquids (Suga and Kubo, 2010). See Table 7-11 for relevant parameters and constants in calculating the Schmidt number. Schmidt number was determined to have a value of 2 in this work.

Therefore, Equation 7.13 can be re-written as;

$$k_g = 1.26bu_g^c \qquad [7.15]$$

As the oil content of drill cuttings is a multicomponent organic material with a boiling point range 40– 250 ^{o}C, as a result, decene was used to model its behaviour during microwave treatment. This is to simplify the calculation of physical constant and parameters such as diffusion coefficient.

The physical constants and parameters used in the calculation of the modified Reynolds number and Schmidt number is shown in Table 7-11.

Table 7-11: Parameters and physical constants used in calculating Schmidt number and Reynolds number

Constants and parameters	**Value**
Viscosity, μ	1.22 x 10^{-5} kg/ms
Diffusion coefficient, D_a	1.018 x 10^{-5} m^2/s
Density, ρ	0.59 kg/m^3
Diameter of pore channel, d	estimated from A in equation 7.4

Diffusion coefficient is calculated using equation 7.12 (1atm and 378K). The density and viscosity data were sourced from (Rogers and Mayhew, 1995)

7.4.3 Estimating the mass transfer coefficient empirically

The mass transfer coefficient can be estimated from empirical methods as follows;

$J = k_g(p_i - p_b)$ [7.16] (Sherwood et al., 1975; Tamir and Merchuk, 1978)

where;

J = net molar flux of oil into the steam stripping medium (mol/m^2s)

k_g = gas phase mass transfer coefficient (m/s)

p_b = partial pressure of oil in the bulk gas phase, converted to concentration in mol/m^3 (appendix 3)

p_i = vapour pressure of oil at the interface with the stripping gas, converted to concentration in mol/m^3 (appendix 3)

The partial pressure of oil in the bulk gas is assumed to be negligible and given a value of zero.

The vapour pressure was calculated from equation 7.17;

$$\ln p_i = C1 + \frac{C2}{T} + C3\ln T + C4T^{C5} \quad [7.17] \quad \text{(Green and Perry, 1997)}$$

where p_i is in Pascals, and T is temperature in kelvins. C1, C2, C3, C4 and C5 are constants.

Equation 7.16 is rearranged as;

$$k_g = \frac{J}{p_i - p_b} \quad [7.18]$$

The denominator in equation 2.5 is constant because of the isothermal operation of the microwave processing system is assumed, and it represents the driving force for the steam stripping process. pi was determined to be 0.1298 atm or 0.004185

mol/dm^3. See appendix 3 for details on the molar flux (J) and vapour pressure (p_i) calculation.

In previous studies (Wilkins et al., 1995; Yoon et al., 2002; Van der Ham and Brouwers, 1998), the relationship between the mass transfer coefficient and gas velocity in a fixed bed of granular materials was presented in a modified version of equation 7.9 as follows;

$$Sh_o = bPe^c \qquad [7.19]$$

where Sh_o is the modified Sherwood number and Pe is the Peclet number. The constants b and c are the same as in equation 7.9. Peclet number is used because it is more appropriate than Schmidt number in representing mass transfer in gas stripping systems.

The modified Sherwood number is defined as;

$$Sh_o = \frac{k_g a d_p}{D_a} \qquad [7.20]$$

$k_g a$ is the lumped mass transfer coefficient, and a is the specific interfacial area. Given the challenges in estimating the specific interfacial area, the overall (k_g) mass transfer coefficient is used in this work, with the assumption that the specific interfacial area does not change significantly with treatment time.

The Peclet number is defined as;

$$Pe = f(Re,Sc) = \frac{u_g d_p}{D_a} \qquad [7.21]$$

It should be noted that Peclet number is also directly proportional to the steam velocity, meaning that the power of the Peclet number (c in equation 7.19) will be equal to the power of the velocity. The Peclet number was calculated for the range of microwave heating experiments in processing systems A – C to give an

indication of the mass transfer characteristics in the samples in these systems. Peclet number was calculated using the parameters and constants in Table 7-11. The mean particle size (d_p) value used is 10µm, the steam velocity was calculated from equation 7.4. The Peclet number results are presented in Table 7-12.

7.4.4 Mass transfer model

The effect of pore steam velocity on mass transfer coefficient is presented in Figures 7.9, 7.10 and 7.11. The data is presented by transforming equation 7.15 to ln-ln plot of mass transfer coefficient against steam velocity, which should yield a straight line with gradient c if steam stripping dominates oil removal. The results reflect the high pore steam velocities observed in this work. The gradient of the plots is equal to constant c in equations 7.15 and 7.19, and is equal to the powers of velocity, Reynolds number and Peclet number.

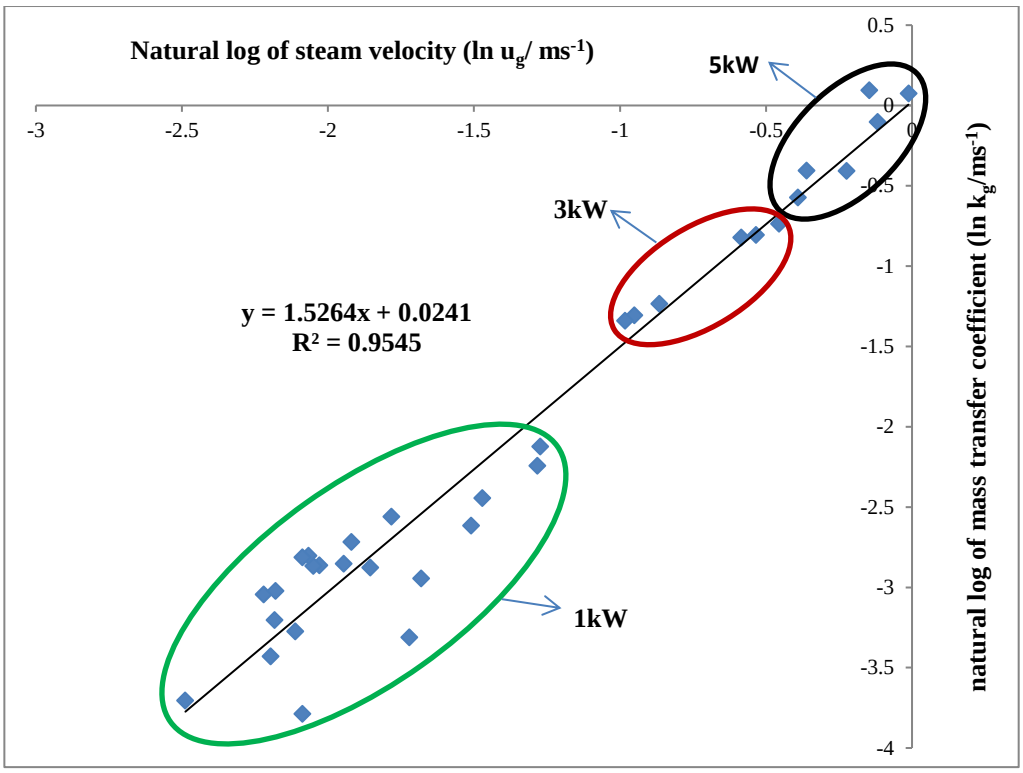


Figure 7.9: The effect of steam velocity on mass transfer coefficient during microwave heating of oil contaminated drill cuttings (System A).

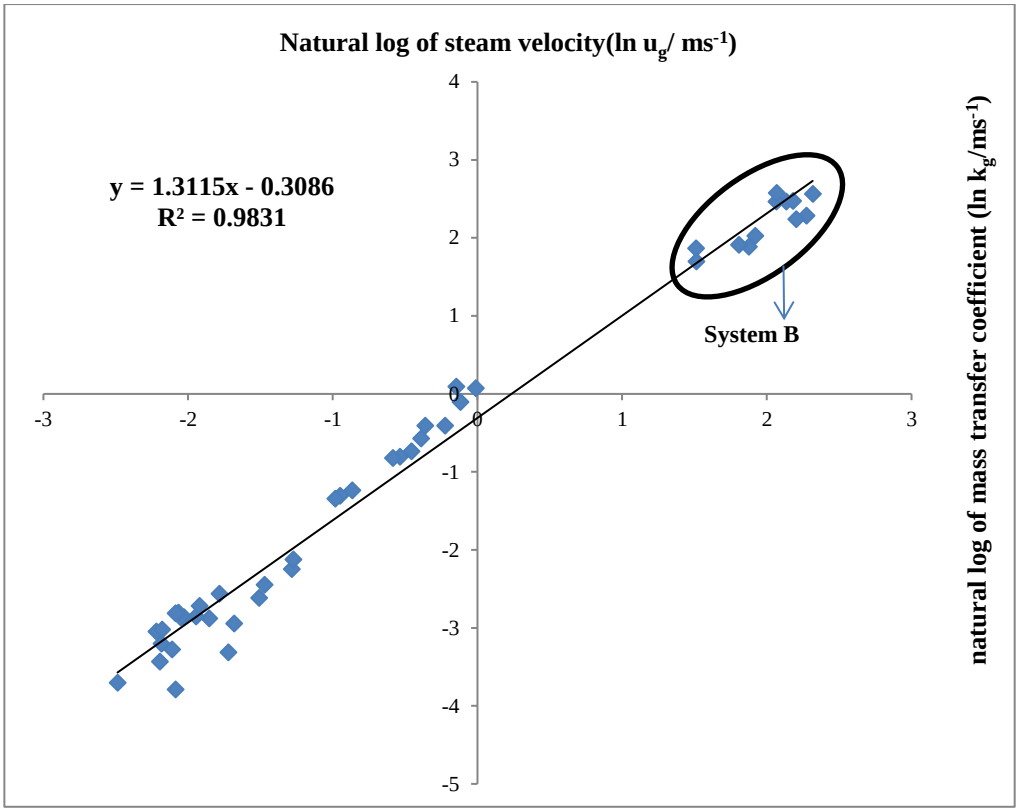


Figure 7.10: The effect of steam velocity on mass transfer coefficient during microwave treatment of oil contaminated drill cuttings (System A and B).

It is clear from the data that increasing steam velocity results in higher mass transfer rate of oil from the drill cuttings material. A crucial point to note from Figure 7.9 and Figure 7.10 is the high positive correlation between mass transfer coefficient and steam velocity. The mass transfer coefficient of oil into the steam stripping medium increases as the steam velocity increases. This strongly suggests that the rate of oil removal from drill cuttings is highly dependent on the mass transfer rate of vaporised water from the material.

The steam velocity and mass transfer coefficient data from the three microwave processing systems is presented in Figure 7.11.

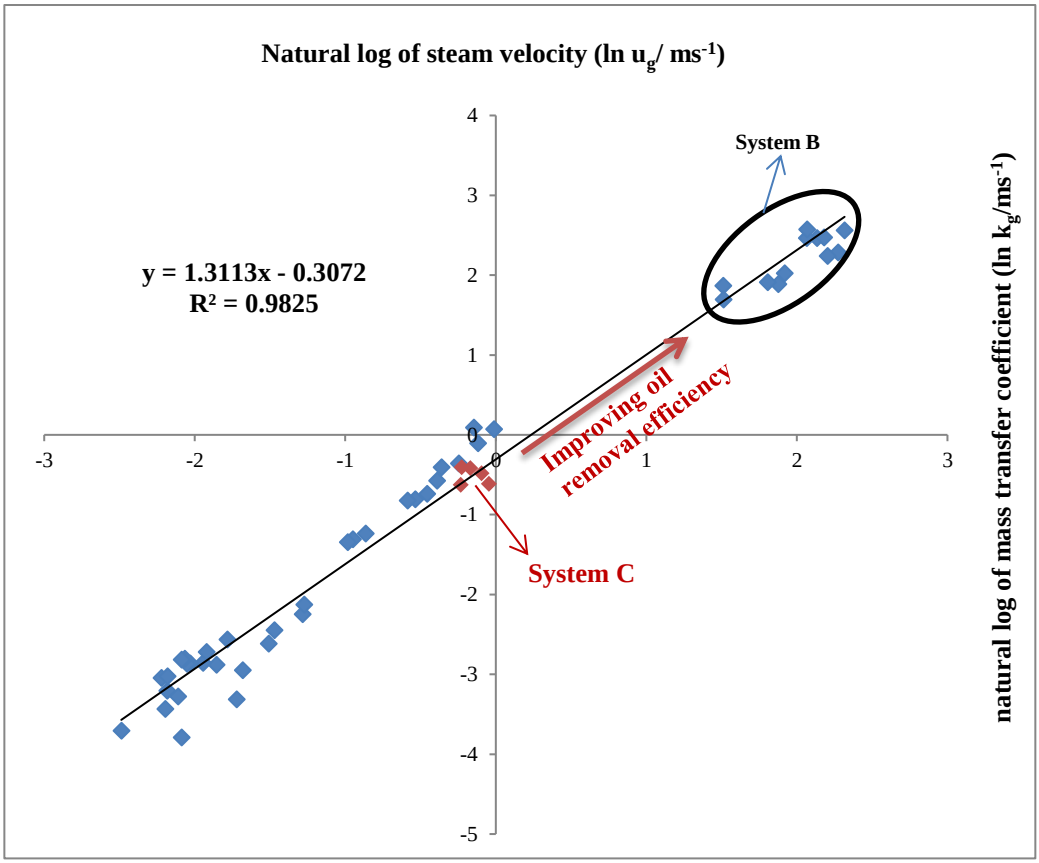


Figure 7.11: The effect of steam velocity on mass transfer coefficient during the microwave treatment of oil contaminated drill cuttings (System A, B and C).

The range of data from system C is limited to establish an individual trend, nonetheless, the efficiency of oil removal of the system can be improved by increasing the mass transfer coefficient into the steam stripping phase. This may be realised by increasing the power input or redesigning the cavity to ensure greater electric field intensity, hence higher heating rates and greater steam velocities within the samples.

It is noteworthy that many separate variables (different sample oil and water content, sample geometries, batch and continuous microwave heating systems, and

different microwave operating frequencies) are brought together by the trend in Figure 7.11. All these variables lie on one curve, indicating that they can be explained by steam velocity.

This is important because for the first time it is demonstrated empirically that the rate of water removal as steam from the drill cuttings material (steam stripping) is the most effective variable for oil removal. Steam distillation cannot be the dominant oil removal mechanism in this case since it is not dependent on steam velocity. Therefore, the dominant mechanism of oil removal is steam stripping.

Since physical entrainment accounts for 10-20% oil removal (Pereira, 2012), it is postulated that steam stripping accounts for up to 80% oil removal from drill cuttings during microwave heating.

It has already been discussed in this chapter that increase in oil removal at high microwave power cannot be explained adequately by physical entrainment and steam distillation removal mechanisms. However, it is known that steam velocity increases when microwave power increases (Figure 7.8), which then improves oil mass transfer rate out of the sample. It is clear that this phenomenon is steam stripping, and provides a more robust explanation of the power density effect on oil removal than has been previously suggested.

The steam velocity and mass transfer coefficient data from microwave heating tests in processing systems A, B and C were used to generate mass transfer models which are presented in equation 7.22. The constant c (equation 7.15) is the gradient of mass transfer coefficient vs steam velocity, and b was estimated from simple linear regression.

For the combination of systems A, B and C, the mass transfer coefficient and velocity relationship is as follows;

$k_g = 0.923u_g^{1.31}$ (SEE = 0.26, P < 0.005, R^2 = 0.9825) [7.22]

Constants b and c are unchanged when inserted into the Sherwood number correlations. Equation 7.9 can be written as;

$Sh_0 = 0.923Re^{1.31}$ (Systems A, B and C)

and equation 7.19 written as;

$Sh_0 = 0.923Pe^{1.31}$ (Systems A, B and C)

7.4.4 Comparison of mass transfer model with previous work in conventional gas stripping

Presented in Table 7-12 are mass transfer models developed in this work, and those developed from conventional stripping of similar media in literature.

Table 7-12: Comparison of mass transfer models from microwave and conventional gas stripping of fixed beds

	Mass transfer model	**Gas velocity (m/s)**	**Peclet number (d_p)**
Wilkins, et al. (1995)	$Sh_0 \alpha 10^{-2.79}Pe^{0.62}$	0.0025 – 0.015	$0.05 < P_e < 2$
Yoon, et al. (2002)	$Sh_0 \alpha 10^{-2.77}Pe^{0.68}$	0.005 – 0.015	
Van der Ham & Brouwers (1998)	$Sh_0 \alpha 10^{-3.03}Pe^{0.88}$	0.0453 – 0.186	$5 < P_e < 60$
This work (Systems A,B and C)	$Sh_0 \alpha 0.923Pe^{1.31}$	0.117 - 9.7206	$0.13 \leq P_e \leq 62$

The empirical mass transfer models developed in this work reflects the high pore gas velocities observed during microwave heating of drill cuttings. Models developed from air/steam stripping in granular fixed beds of conventional systems are characterised by lower pore steam velocities. The data in Table 7-12 shows that the power of the Peclet number (Pe) generally increases as gas velocity increases, and it is higher in this work than in conventional gas stripping. Comparison of this work with the correlation of Wilkins, et al. (1995) shows that the power of Pe increases from 0.62 to 1.31. Yoon, et al. (2002) also proposed the power of Pe as 0.68. Interestingly, both set of workers recorded a pore gas velocity of 0.0025 –

0.015 m/s, which is significantly less than 0.117 – 9.7206 m/s observed in this work.

During the steam stripping of a fixed bed of contaminated soil, Van der Ham and Brouwers (1998) reported the power of Pe as 0.88, an increase from the findings of Wilkins, et al. (1995) and Yoon, et al. (2002), but lower than the Pe power in this work. Inspection of the pore gas velocities in Table 7-12 shows that the gas velocities in the work of Van der Ham and Brouwers (1998) also fall between the velocities of Wilkins, et al. (1995) and Yoon, et al. (2002) and the high pore steam velocities in this work. The high Reynolds number of the steam flow (Table 7-13), which is indicative of turbulent flow regimes, reflects the high pore gas velocities in this work. This supports the hypothesis of an advection dominated mass transfer of oil during microwave heating.

Table 7-13: Peclet and Reynolds number, and mean particle size from mass transfer correlations in literature and this work

	Peclet number	Modified Reynolds number (Re')	Particle size (d_{50}) µm
Wilkins et al. (1995)	$0.05 < P_e < 2$	-	240 - 1200
Yoon et al. (2002)	-	-	-
Van der Ham & Brouwers (1998)	$5 < P_e < 60$	-	264 - 625
This work (Systems A,B and C)	$0.13 \leq P_e \leq 62$	1171 - 41318	2-10

The lower velocity and Pe powers coupled with smaller pore gas velocities (Table 7-12) in conventional stripping processes is a reflection of the mass transfer limitations in conventional gas stripping. Such limitations are due to the following;

- As stripping gas is introduced from an external source into a fixed bed, therefore there is resistance to gas flow provided by bed particles and smaller pores.
- Gas will only move through the most permeable sections of the bed without flowing through the less permeable regions. This is channeling or bypassing, which may cause regions of a fixed bed of contaminated soil to remain untreated, and is particularly enhanced by high residual moisture levels.

Channeling restricts the stripping gas access to contaminants entrapped in the less permeable regions of a fixed bed, which decreases the efficiency of the conventional gas stripping process. In contrast, microwave heating utilises water present in the pores of a fixed bed as the stripping gas by rapid conversion of in situ water to steam. As a result, channeling is minimised and the mass transfer rate increases significantly during microwave heating. This means that microwave heating can benefit fixed bed systems by greatly improving the mass transfer rate. In the case of a fixed bed of contaminated drill cuttings or contaminated soil, it means that the material can be stripped in its natural form, rather than relying on the introduction of high pressure gas from an external source as in conventional gas stripping.

An important point to note is that high velocity and P_e powers are thought to be achievable under microwave heating because channeling is minimised, and in situ water is used as the stripping gas phase.

7.5 Conclusion

Competing mechanisms of oil removal from contaminated drill cuttings such as direct vaporisation, steam distillation, steam stripping and physical entrainment were analysed. It was demonstrated that the dominant mechanism of oil removal during microwave heating is steam stripping.

Empirical mass transfer models were developed from the microwave heating experiments in three different processing systems. The mass transfer rate of oil from the material and the pore steam velocity were used to develop the models. It was shown that steam velocity explains all the experimental data and rationalises all the variables (microwave frequencies and power densities, batch and continuous systems, sample geometries, and different oil and water contents).

It was shown that power density and porosity affects steam velocity, with high velocities observed at lower porosities and higher power densities. Finally, microwave heating induces steam velocities greater than gas or steam velocities in conventional gas stripping, and is thought to minimise channeling often associated with conventional gas stripping within fixed beds. As a result, there is greater mass transfer of oil during microwave heating as indicated by the high power of Peclet number and velocity in the mass transfer models.

Chapter 8 Conclusions and Future Work

Microwave treatment is able to reduce the oil content to the required environmental disposal limit of <1wt%. Nonetheless, there are issues from a process engineering stand-point that pose significant challenges to the establishment of a robust microwave treatment system. This work has identified the major processing issues as; 1) thermal runaway, and 2) effect of material transport on the energy efficiency of the microwave system. Moreover, this work for the first time, establishes that the main mechanism of oil removal from contaminated drill cuttings during microwave heating is evaporative mass transfer via steam stripping.

8.1 Thermal runaway

Under normal microwave processing conditions (approximately 100 ^{o}C), water is the main microwave absorber within the drill cuttings matrix. However, longer residence times in the cavity may result in thermal runaway (vitrification) and hence the mechanical damage of the cavity. The longer the material remains in the cavity, the greater the possibility of thermal runaway. It was found that during continuous or semi-continuous microwave processing of clay or shale based contaminated drill cuttings, the material sometimes sticks to the cavity wall, increasing the residence time beyond the optimum or specified residence time, and as a result the material overheats and damages the cavity.

The drill cuttings material was found to display low microwave absorption qualities from 100^{o}C – 400 ^{o}C, meaning that the material is essentially transparent to microwave energy in this temperature range. Nonetheless, localised temperatures

in the bulk material may increase from 100 ^{o}C to 400 ^{o}C during processing, as a result of the poor heat transfer properties of the bulk material.

Thermal runaway occurred when localised temperatures reached 400 ^{o}C in the contaminated drill cuttings matrix, inducing vitrification of the mineral phase. It is shown that the dielectric constant and loss factor of the drill cuttings material increased exponentially between 400 ^{o}C and 850 ^{o}C, which is thought to have caused the temperature to rise from 400 ^{o}C to over 1400 ^{o}C inducing vitrification.

It is shown that the oil contaminant is a low loss material, and essentially transparent to microwave energy. It was found that oil does not contribute to the increase in dielectric constant and loss factor of the material at temperatures >400 ^{o}C, meaning that the exponential temperature rise cannot be attributed to the oil component.

The increase in dielectric constant and loss factor at temperatures >400 ^{o}C was found to be as a result of the dielectric properties of the clay, halite and barite components of the solid mineral phase. This work shows that the dielectric constant and loss factor of the clay components increase exponentially at 400 ^{o}C. At ≥700 ^{o}C, the barite and halite components of the mineral phase absorb more microwaves than the clay components. This showed that although thermal runaway was not initiated in barite and halite at 400 ^{o}C, these components ensured the vitrification temperature of ≥1400^{o}C is reached. The vitrification phenomenon, which has been shown to cause burn and mechanical damage to the boron nitride cavity, is attributed to the dielectric behaviour of the clay, barite and halite components of the drill cuttings material at high temperatures.

Essential to achieving an ‘optimum residence time’ in the cavity in a continuous or semi-continuous microwave treatment system is selecting an appropriate method of transporting the drill cuttings material through the cavity. The chosen material transport strategy should ensure that a dead zone is not created within the cavity where the material adheres to the wall of the cavity and accumulate over time. This will reduce the risk of thermal runaway.

8.2 Effect of material transport on the energy efficiency of the microwave process

Material transport within the microwave system, using high shear twin screw conveyors, is shown to have the potential to change the bulk density and porosity of the drill cuttings material. It is shown that the oil removal efficiency decreases as a result.

Clay or shale based drill cuttings have been shown empirically to swell, and hence decrease in bulk density when sheared. In contrast, sandstone based drill cuttings do not display any significant changes in bulk density when sheared. The bulk density of shale based cuttings can be reduced by approximately 29% with high levels of shear. This is shown to translate to a reduction in energy efficiency of up to 25% in the applicator during treatment when compared to the unsheared shale based material at low power densities. In other words, more oil is removed from the matrix of unsheared shale based cuttings than from the sheared material at equivalent microwave power and energy inputs.

The bulk density of the sandstone based material was unchanged after shearing, consequently, oil removal was found to be the same from sheared and unsheared sandstone based drill cuttings.

Shearing was shown to increase the porosity of the shale based cuttings, meaning that if drill cuttings material responds to shear by lowering its bulk density, the overall void volume and surface area are consequently increased.

At high power densities, it was found that using a material transport strategy that alters the bulk density and porosity of the drill cuttings material does not reduce the energy efficiency of the microwave treatment system. Industrial scale microwave systems that utilise a high electric field intensity will therefore mitigate the shearing effect of the material handling system.

8.3 Mechanism of oil removal

The energy requirement for the physical entrainment mechanism of oil removal is the lowest amongst all the mechanisms considered in this work. However, physical entrainment accounts for 10-20% oil removal. Direct vaporisation was ruled out as the main mechanism of oil removal as the energy required to reduce oil levels to less than 1 wt% through direct vaporisation is 50% than that observed empirically.

Higher oil removal was observed at high power densities as a result of the pore steam velocity within the drill cuttings. This phenomenon is as a result of the bulk movement of steam in the material, with the oil removed by steam stripping. Steam stripping was established as the dominant mechanism of oil removal, and is thought to account for up to 80% oil removal. It was found that the steam stripping mechanism provided a more robust explanation for greater oil removals observed at high power densities than the other oil removal mechanisms evaluated. This is particularly relevant to the industrial system because the industrial microwave treatment systems operate at high power densities.

Mass transfer models were developed showing the relationship between steam velocity and mass transfer rate of oil from drill cuttings during microwave heating. It was found that the pore steam velocities in this work were significantly greater than observed in the conventional gas stripping of similar media. This translated to a high positive correlation between the steam velocity (u_g) and the mass transfer coefficient (k_g) of the oil, shown as $k_g = 0.923u_g^{1.31}$ and $Sh_o = 0.923Pe^{1.31}$, in this work. The empirical models developed in this work show that velocity has a greater effect on the mass transfer rate in microwave stripping than in conventional stripping of fixed beds. The velocity correlation is achieved despite there being separate variables within the data set.

The power of the Peclet number was found to be 1.31, which is higher than the power of the Peclet number (generally <1) in conventional stripping of fixed beds. This means that the stripping efficiency of fixed beds in microwave systems is more efficient than in conventional systems. Furthermore, the high power of Peclet number in this work shows that channeling can be reduced significantly in microwave heating.

8.4 Future Work

The industrial microwave system is currently being optimised for field trials. The efficiency of oil removal in the microwave cavity can be optimised in a number of ways including;

1) Developing a predictive model based on the mass transfer correlations developed in this work. This model will relate process efficiency to the electric field intensity and power density in the cavity, which can be used in future design and optimisation of the cavity. The steam velocity can be determined as described in chapter 7, and then translated to power density requirements for the system. The power density can be used as an essential input into the design of system geometry, and can be utilised in numerical simulation for predicting the corresponding electric field intensity requirement.
2) Predicting the temperature that thermal runaway will be initiated during processing according to the mineralogy of the reservoir being drilled. This will give the microwave system flexibility to operate in several oil fields. A library can be created which will contain the thermal analysis, heat transfer properties and dielectric properties of each of the solid phase components in drill cuttings. A model can be developed from this library using dielectric mixing rules, where the composition of the solid phase can be used to predict the dielectric properties of drill cuttings at high temperatures. This can subsequently be used to determine the maximum residence time within a given microwave processing system.
3) Characterisation of the screw conveyors by determining the torque required to change the bulk density of contaminated drill cuttings by a specific factor,

taking into consideration the initial bulk density, water and oil content, and mineralogy. If the change in bulk density can be predicted before the material reaches the applicator, the power density in the applicator can be adjusted accordingly.

Chapter 9 References

Abramovitch, R. A. et al., 1999. Insitu decomposition of PCBs in soil using microwave energy. *Chemosphere*, 38(10), pp.2227–2236.

Acierno, D., Barba, A.A., and D'Amore, M., 2003. Microwaves in Soil Remediation from VOCs.1: Heat and mass transfer aspects. *Environmental and Energy Engineering*, 49(7), pp.1909–1921.

Agrawal, D.K., 1998. Microwave processing of ceramics. *Current Opinion in Solid State and Materials Science*, 3(5), pp.480–485.

All About Circuits, 2016. Waveguides, Chapter 14 - Transmission Lines. Available at: http://www.allaboutcircuits.com/textbook/alternating-current/chpt-14/waveguides/ [Accessed August 30, 2016].

Anderson, R.L et al., 2010. Clay swelling — A challenge in the oilfield. *Earth-Science Reviews*, 98, pp.201–216.

Arthur, E., and Lord, J., 1998. Steam stripping organics from "fluidized" soils (versus confined soils). *Journal of Environmental Engineering*, 124(4), pp.390–394.

ASTM D-95, 2010. Standard Test Method for Water in Petroleum Products and Bituminous Materials by Distillation.

Atwater, J.E., and Wheeler, R.R., 2003. Complex permittivities and dielectric relaxation of granular activated carbons at microwave frequencies between 0.2 and 26 GHz. *Carbon*, 41(9), pp.1801–1807.

Balek, V., and Murat, M., 1996. The emanation thermal analysis of kaolinite clay minerals. *Thermochimica Acta*, 282–283(SPEC. ISS.), pp.385–397.

Ball, A. S., Stewart, R.J., and Schliephake, K., 2012. A review of the current options for the treatment and safe disposal of drill cuttings. *Waste Management & Research*, 30(5), pp.457–473.

Bernier, R. et al., 2003. Environmental aspects of the use and disposal of non aqueous drilling fluids with offshore oil and gas operations, *International association of oil and gas.*

Binner, E. et al., 2014. A Review of Microwave Coal Processing. *Journal of Microwave Power and Electromagnetic Energy*, 48(1), pp.35–60.

Bottcher, C., and Bordewijk, K., 1978. *Theory of Electric Polarization* Vol II. Amsterdam: Elsevier Science.

BP, 2016. Energy Outlook. Available at: https://www.bp.com/content/dam/bp/pdf/energy-economics/energy-outlook-2016/bp-energy-outlook-2016.pdf [Accessed August 24, 2016].

BP, 2015. Statistical Review of World Energy. Available at: https://www.bp.com/content/dam/bp/pdf/energy-economics/statistical-

review-2015/bp-statistical-review-of-world-energy-2015-full-report.pdf [Accessed June 20, 2016].

Bradshaw, S., Delport, S., and Van Wyk, E., 1997. Qualitative measurement of heating uniformity in a multimode microwave cavity. *Journal of Microwave Power and Electromagnetic Energy*, 32(2), pp.88–95.

Breuer, E., 2004. Drill Cuttings accumulations in the Northern and Central North sea: a review of environmental interactions and chemical fate. *Marine Pollution Bulletin*, 48, pp.12–25.

Buettner, B.H.M., and Daily, W.D., 1995. Cleaning contaminated soil using electrical heating and air stripping. *Journal of Environmental Engineering*, 121(8), pp.580–589.

Buttress, A.J. et al., 2016. Development and evaluation of a continuous microwave processing system for hydrocarbon removal from solids. *Chemical Engineering Journal*, 283, pp.215–222.

Carotenuto, C. et al., 2015. Rheology of natural slurries involved in a rapid mudflow with different soil organic carbon content. *Colloids and Surfaces A: Physicochemical and Engineering Aspects*, 466, pp.57–65.

Chandrasekaran, S., Ramanathan, S., and Basak, T., 2012. Microwave Material Processing - A Review. *Fluid Mechanics and Transport Phenomena*, 58.

Chang, K.L.B., and Halek, G.W., 1991. Analysis of Shear and Thermal History During Co-Rotating Twin-Screw Extrusion. *Journal of Food Science*, 56(2), pp.518–531.

Chapman, B.G., 1948. the Thixotropy and Dilatancy a Marine Soil. *Queen Mary College, London*, pp.123–140.

Chen, F. et al., 2015. Kinetics of the Reduction of Hematite Concentrate Particles by Carbon Monoxide Relevant to a Novel Flash Ironmaking Process. *Metallurgical and Materials Transactions B: Process Metallurgy and Materials Processing Science*, 46(4), pp.1716–1728.

Chen, S.X., 2008. Thermal conductivity of sands. *Heat and Mass Transfer*, 44(10), pp.1241–1246.

Childs, J.D. et al., 2005. Surfactant-Enhanced Treatment of Oil-Based Drill Cuttings. *Journal of Energy Resources Technology*, 127(2), p.153.

Comiti, J., Mauret, E., and Renaud, M., 2000. Mass transfer in fixed beds : proposition of a generalized correlation based on an energetic criterion., *Chemical Engineering Science*, 55, pp.5545–5554.

Council Directive (1999), Landfill of Waste, 99/31/EC.

Cullity, B., 1956. *Elements of X-Ray Diffraction*. Massachusetts - Addison-Wesley Publishing Company.

Daan, R., and Mulder, M., 1996. On the short-term and long-term impact of

drilling activities in the Dutch sector of the North Sea. *ICES Journal of Marine Science*, 53, pp.1036–1044.

Daniel, V. V., 1967. *Dielectric Relaxation*, First.Edition, London: Academic Press Inc. (London) LTD.

Davies, J. et al., 1984. Environmental Effects of the use of oil-based drilling muds in the North Sea. *Marine Pollution Bulletin*, 15(10), pp.363–370.

Dawei, L.I. et al., 2009. Microwave thermal remediation of crude oil contaminated soil enhanced by carbon fiber. *Journal of Environmental Sciences*, 21(9), pp.1290–1295..

Deer, W. A., Howie, R. A and Zussman, J., 1985. *An Introduction to the Rock Forming Minerals.* 10th ed. London: Longman.

Derrick, M.J., 2001. Effective Environmental Compliance in the Gulf of Mexico. *World Energy Magazine*.

Dhenge, R.M. et al., 2011. Twin screw wet granulation: Effect of powder feed rate. *Advanced Powder Technology*, 22(2), pp.162–166.

Dhenge, R.M. et al., 2010. Twin screw wet granulation: Granule properties. *Chemical Engineering Journal*, 164(2–3), pp.322–329.

Di, B.P., Chang, D.P., and Dwyer, H.A., 2000. Heat and Mass Transfer During Microwave Steam Treatment of Contaminated Soils. *Journal of Environmental Engineering*, 126(12), pp.1108–1115.

Dobson, M. et al., 1985. Microwave Dielectric Behavior of Wet Soil-Part II: Dielectric Mixing Models. *IEEE Transactions on Geoscience and Remote Sensing*, GE-23(1), pp.35–46.

DoITPoMS, 2016. Polarisation Mechanisms. Available at: https://www.doitpoms.ac.uk/tlplib/dielectrics/polarisation_mechanisms.php [Accessed July 12, 2016].

Dong, Y., McCartney, J.S., and Lu, N., 2015. Critical Review of Thermal Conductivity Models for Unsaturated Soils. *Geotechnical and Geological Engineering*, 33(2), pp.207–221.

Dubey, M.K. et al., 2016. Comparative study of radio-frequency and microwave heating for phytosanitary treatment of wood. *European Journal of Wood and Wood Products*, 74(4), pp.491–500.

Eldridge, R., 1996. Oil contaminant removal from drill cuttings by supercritical extraction. *Industrial & engineering chemistry research*, 5885(95), pp.1901–1905.

Erle, U. et al., 2000. Dielectric Properties of Emulsions and Suspensions: Mixture Equations and Measurement Comparisons. *Journal of Microwave Power and Electromagnetic Energy*, 35(3), pp.185–190.

Falciglia, P.P., Urso, G., and Vagliasindi, F.G.A., 2013. Microwave heating

remediation of soils contaminated with diesel fuel. *Journal of Soils and Sediments*, 13(8), pp.1396–1407.

Farouki, O.T., 1986. Thermal Properties of Soils. *Series on Rock and Soil Mechanics*, 11, p.136.

Ferro, V., and Mirabile, S., 2009. Comparing particle size distribution analysis by sedimentation and laser diffraction method. *Journal of Agricultural Engineering*, 2, pp.35–43.

Folorunso, O. et al., 2012. Continuous energy efficient exfoliation of vermiculite through microwave heating. *International Journal of Mineral Processing*, 114–117, pp.69–79.

Foster, M.D., 1954. The Relation Between Composition and Swelling in Clays. *Clays and Clay Minerals*, 3, pp.205–220.

Gabriel, C. et al., 1998. Dielectric parameters relevant to microwave heating. *Chemical Society Review*, 27.

Gerrard, S. et al., 1999. Drill cuttings piles in the North Sea: management options during platform decommissioning. *Centre for Environmental Risk Research Report No 31*, (31), p.224.

Gierke, J.S., and Mckenzie, B., 1992. Vapor Transport in Unsaturated Soil Columns: Implications for Vapor Extraction. *Water Resources Research*, 28(2), pp.323–335.

Gilmour, A., 2007. The Cutting Edge in Drilling-Waste Management. *Oilfield Review*, pp.54–67.

Gray, J. et al., 1990. Detection of initial effects of pollution on marine benthos: an example from the Ekofisk and Eldfisk oilfields, North Sea . *Marine Ecology Progress Series*, 66, pp.285–299.

Green, D.W., and Perry, R.H., 1997. *Perry's Chemical Engineer Handbook.* 8th ed. New York: McGraw-Hill.

Grim, R.E., 1968. *Clay mineralogy - International series in the earth and planetary sciences* 1st ed. New York: McGraw-Hill.

Grindrod, P., Peletier, M., and Takase, H., 1999. Mechanical interaction between swelling compacted clay and fractured rock, and the leaching of clay colloids. *Engineering Geology*, 54(1–2), pp.159–165.

Growcock, F.B., and Patel, A.D., 2011. The revolution in Non-Aqueous Drilling Fluids. *American Association of Drilling Engineers*. Available at: http://www.slb.com/~/media/files/miswaco/technical_papers/non_aqueous_drilling_fluids.pdf [Accessed April 22, 2016].

Hall, D., Ben-Omran, M.M., and Stevenson, P.J., 1999. Field and temperature dependence of dielectric properties in BaTiO3-based piezoceramics. *Journal of Physics: Condensed Matter*,10, pp.461–476.

Hallikainen, M.T. et al., 1985. Microwave Dielectric Behavior of Wet Soil-Part I: Empirical Models and Experimental Observations. *Geoscience and Remote Sensing, IEEE Transactions on*, GE-23(1), pp.25–34.

Hasted, J., 1973. *Aqueous Dielectrics.* First Edition. London: Chapman and Hall Ltd.

Hensen, E.J.M., and Smit, B., 2002. Why clays swell. *Journal of Physical Chemistry B*, 106(49), pp.12664–12667.

Hoekstra, P., and Doyle, W.T., 1971. Dielectric relaxation of surface adsorbed water. *Journal of Colloid And Interface Science*, 36(4), pp.513–521.

Health and Safety Executive (HSE), 2000. *Drilling Fluids Composition and the use within the UK Offshore Drilling Industry*. Avaialable at: http://www.hse.gov.uk/research/otopdf/1999/oto99089.pdf [Accessed April 23, 2016].

IOGP, 2009. Drilling fluids and health risk management. *International Association of Oil and Gas producers*. Available at: http://www.ogp.org.uk/pubs/396.pdf [Accessed May 23, 2016].

IOGP, 2016. Drilling waste management technology review. *International Association of Oil and Gas Producers*. Available at: http://www.iogp.org/pubs/557.pdf [Accessed September 1, 2016].

Jones, D. A. et al., 2002. Microwave heating applications in environmental engineering—a review. *Resources, Conservation and Recycling*, 34(2), pp.75–90.

Jorissen, F.J. et al., 2009. Impact of oil-based drill mud disposal on benthic foraminiferal assemblages on the continental margin off Angola. *Deep-Sea Research Part II: Topical Studies in Oceanography*, 56(23), pp.2270–2291.

Kabla, A.J., and Senden, T.J., 2009. Dilatancy in slow granular flows. *Physical Review Letters*, 102(22), pp.2–5.

Kawala, Z., and Atamanczuk, T., 1998. Microwave-Enhanced Thermal Decontamination of Soil. *Environmental Science & Technology*, 32(17), pp.2602–2607.

Kearl, P.M., Korte, N.E., and Beale, J.S., 1991. Vapor Extraction Experiments with Laboratory Soil Columns : Implications for Field Programs. *Waste Management*,11, pp.231–239.

Kim, J. et al., 2012. Review of microwave assisted manufacturing technologies. *International Journal of Precision Engineering and Manufacturing*, 13(12), pp.2263–2272.

Kingman, S., Vorster, W., and Rowson, N., 2000. The effect of microwave radiation on the processing of plabora copper ore. *The Journal of The South African Institute of Mining and Metallurgy*.pp.197-204.

Kleijn, W.B., 1982. A Model of Clay Swelling and Tactoid Formation. *Clays and*

Clay Minerals, 30(5), pp.383–390.

Lam, S.S., and Chase, H.A., 2012. A review on waste to energy processes using microwave pyrolysis. *Energies*, 5(10), pp.4209–4232.

Larhed, M., and Hallberg, A., 2001. Microwave-assisted high-speed chemistry: A new technique in drug discovery. *Drug Discovery Today*, 6(8), pp.406–416.

Lester, E. et al., 2006. The potential for rapid coke making using microwave energy. *Fuel*, 85, pp.2057–2063.

Lidström, P. et al., 2001. Microwave assisted organic synthesis—a review. *Tetrahedron*, 57(45), pp.9225–9283.

Lindholm, J., Brink, A., and Hupa, M., 2009. Cone calorimeter – a tool for measuring heat release rate. *Finnish-Swedish Flame Days 2009*, (May 2012), p.4B.

Maciel, G.D.F., Santos, H.K.D., and Ferreira, F.D.O., 2009. Rheological analysis of water clay compositions in order to investigate mudflows developing in canals. *Journal of the Brazilian Society of Mechanical Sciences and Engineering*, 31(1).

Mahmood, A., Mohammed, A., and Arash, S., 2012. Comparative study of using oil-based mud versus water-based mud in HPHT fields. *Advances in Petroleum Exploration and Development*, 4, pp.18–27.

Martin, J.H., and Raymond, L.C., 1985. Determination of the oil content of soils. *Hazardous and Industrial solid waste: Fourth symposium*.

Masliyahs, J., Rajinder, P., and Yuhua, Y., 1992. Rheology of clay-in-oil suspensions wuth added water droplets. *Chemical Engineering Science*, Vol. 47, No. 5, pp. 967-970.

Mehdizadeh, M., 2015. *Microwave applicators and probes for material heating, sensing, and plasma generation* Second., Oxford: Elsevier.

Melton, H.et al., 2000. Offshore Discharge of Drilling Fluids and Cuttings - A Scientific Perspective on Public Policy. *Brazilian Petroleum Institute*.

Meredith, R., 1998. *Engineers' Handbook of Industrial Microwave Heating*. First edition. London: The Institution of Electrical Engineers.

Metaxas, A.C., and Meredith, R.J., 2008. *Industrial Microwave Heating.* Third edition. London: The Institution of Engineering and Technology.

Mikhail, Sh.R., and Guindy, N.M., 2007. Rates of low-temperature dehydration of montmorillonite and illite. *Journal of Applied Chemistry and Biotechnology*, 21(4), pp.113–116.

Miranda-Trevino, J.C., and Coles, C.A., 2003. Kaolinite properties, structure and influence of metal retention on pH. *Applied Clay Science*, 23(1–4), pp.133–139.

Missen, R.W., Mims, C.A. and Saville, B.A., 1999. *Introduction to Chemical reaction Engineering and Kinetics*, New York: John Wiley & Sons.

Mutyala, S. et al., 2010. Microwave applications to oil sands and petroleum: A review. *Fuel Processing Technology*, 91(2), pp.127–135.

Neff, J.M., 2005. *Composition, Environment Fates, and Biological Effect of Water Based Drilling Muds and Cuttings Discharged to the Marine Environment: A Synthesis and Annotated Bibliography*. Avaialable at: http://www.hse.gov.uk/research/otopdf/1999/oto99089.pdf [Accessed November 23, 2015].

Nelson, S.O., 2005. Density-permittivity relationships for powdered and granular materials. *IEEE Transactions on Instrumentation and Measurement*, 54(5), pp.2033–2040.

Nelson, S.O., 2010. Fundamentals of dielectric properties measurements and agricultural applications. *The Journal of microwave power and electromagnetic energy*, 44(2), pp.98–113.

Nelson, S.O., 1994. Measurement of microwave dielectric properties of particulate materials. *Journal of Food Engineering*, 21, pp.365–384.

Nelson, S.O., and Trabelsi, S., 2012. Factors influencing the dielectric properties of agricultural and food products. *The Journal of Microwave Power and Electromagnetic Energy*, 46(2), pp.93–107.

Norrish, K., 1954. The swelling of montmorillonite. *Disc. Faraday Soc.*, 18, pp.120–134.

Oil & Gas UK, 2016. Activity Survey. Available at: http://oilandgasuk.co.uk/wp-content/uploads/2016/02/Oil-Gas-UK-Activity-Survey-2016.pdf [Accessed August 2, 2016].

Oil & Gas UK, 2015. Environment Report. Available at: http://oilandgasuk.co.uk/wp-content/uploads/2015/11/Environment-Report-2015-FINAL-for-PDF-reduced.pdf [Accessed August 25, 2016].

Oil and Gas Authority, 2016. Oil and gas: field data. Available at: https://www.gov.uk/guidance/oil-and-gas-uk-field-data#uk-oil-and-gas-reserves-and-resources [Accessed September 15, 2016].

Okpokwasili, G., and Nnubia, C., 1995. Effects of oil spill dispersants and drilling fluids on subsurface specificity of marine bacteria. *Waste Management*, 15(7), pp.515–520.

Van Oort, E., 2003. On the physical and chemical stability of shales. *Journal of Petroleum Science and Engineering*, 38(3–4), pp.213–235.

OSPAR 2000, Oslo and Paris Commision (OSPAR 2000/3).

Pereira, I.S.M., 2012. *Microwave Processing of Oil Contaminated Drill Cuttings*, PhD Thesis, University of Nottingham.

Reeb, J., and Milota, M., 1999. Moisture Content by the oven-dry method for industrial testing, Oregon State University. Available at: http://ir.library.oregonstate.edu/xmlui/bitstream/handle/1957/5190/Moisture_Content_ocr.pdf [Accessed September 3rd, 2014].

Reimer, L., 1998. *Scanning Electron Microscopy: Physics of image formation and microanalysis* Second Edition. New York: Springer-Verlag.

Risman, P.O., 1991. Terminology and Notation of Microwave Power and Electromagnetic Energy. *Journal of Microwave Power and Electromagnetic Energy*, 26(4), pp.243–250.

Robinson, D., 2004. Calculation of the Dielectric Properties of Temperate and Tropical Soil Minerals from Ion Polarizabilities Using Clausius-Mosotti Equation. *Soil Science Society of America Journal*, 68, pp.1780–1785.

Robinson, D.A., Cooper, J.D., and Gardner, C.M.K., 2002. Modelling the relative permittivity of soils using soil hygroscopic water content. *Journal of Hydrology*, 255(1–4), pp.39–49.

Robinson, J. et al., 2014. Microwave processing of Oil Sands and contribution of clay minerals. *Fuel*, 135, pp.153–161.

Robinson, J. et al., 2015. Microwave Pyrolysis of Biomass: Control of Process Parameters for High Pyrolysis Oil Yields and Enhanced Oil Quality. *Energy & Fuels*, 29(3), pp.1701–1709.

Robinson, J., Kingman, S., and Onobrakpeya, O., 2008. Microwave-assisted stripping of oil contaminated drill cuttings. *Journal of Environmental Management*, 88(2), pp.211–218.

Robinson, J.P. et al., 2012. Microwave remediation of hydrocarbon-contaminated soils - Scale-up using batch reactors. *Separation and Purification Technology*, 96, pp.12–19.

Robinson, J.P. et al., 2009a. Remediation of oil-contaminated drill cuttings using continuous microwave heating. *Chemical Engineering Journal*, 152(2–3), pp.458–463.

Robinson, J.P. et al., 2010. Scale-up and design of a continuous microwave treatment system for the processing of oil-contaminated drill cuttings. *Chemical Engineering Research and Design*, 88(2), pp.146–154.

Robinson, J.P. et al., 2009b. Separation of polyaromatic hydrocarbons from contaminated soils using microwave heating. *Separation and Purification Technology*,69(3), pp.249–254.

Robinson, J.P. et al., 2008. Thermal desorption and pyrolysis of oil contaminated drill cuttings by microwave heating. *Journal of Analytical and Applied Pyrolysis*, 81(1), pp.27–32.

Rogers, G.F., and Mayhew, Y., 1995. *Thermodynamic and Transport Properties of Fluids*, Oxford: Blackwell Publishers Ltd.

Rojas-Avelizapa, N.G. et al., 2007. A field trial for an ex-situ bioremediation of a drilling mud-polluted site. *Chemosphere*, 66(9), pp.1595–1600.

Saarenketo, T., 1998. Electrical properties of water in clay and silty soils. *Journal of Applied Geophysics*, 40(1–3), pp.73–88.

Sacilik, K., Tarimci, C. and Colak, A., 2007. Moisture content and bulk density dependence of dielectric properties of safflower seed in the radio frequency range. *Journal of Food Engineering*, 78, pp.1111–1116.

Sadiq, R. et al., 2003. Marine Water Quality Assessment Of Synthetic-Based Drilling Waste Discharges. *International Journal of Environmental Studies*, 60(4), pp.313–323.

Saidani, K., Ajam, L., and Ben Ouezdou, M., 2015. Barite powder as sand substitution in concrete: Effect on some mechanical properties. *Construction and Building Materials*, 95(October), pp.287–295.

Saim, N. et al., 1997. Extraction of polycyclic aromatic hydrocarbons from contaminated soil using soxhlet extraction, pressurised and atmospheric microwave-assisted extraction, supercritical fluid extraction and accelerated solvent extraction. *Journal of Chromatography A*, 791(1–2), pp.361–366.

Schindler, D., 2010. Tar sands need solid science. *Nature*, 468(7323), pp.499–501.

Schmidt, M.P. et al., 2014. Structural changes upon dehydration of amorphous calcium carbonate. *Crystal Growth & Design*, 14, pp.938–951.

Shang, H. et al., 2012. Influence of materials dielectric properties on the petroleum oil removal from waste under microwave irradiation. *The Canadian Journal of Chemical Engineering*, 90. pp.1465-1471.

Shang, H. et al., 2006. Microwave treatment of oil-contaminated North Sea drill cuttings in a high power multimode cavity. *Separation and Purification Technology*, 49(1), pp.84–90.

Shang, H. et al., 2005. Treatment of oil-contaminated drill cuttings by microwave heating in a high-power single-mode cavity. *Industrial and Engineering Chemistry Research*, 44(17), pp.6837–6844.

Sheen, J., 2005. Study of microwave dielectric properties measurements by various resonance techniques. *Measurement*, 37, pp.123–130.

Sheng, J. et al., 2013. Temperature dependence of the dielectric constant of acrylic dielectric elastomer. *Applied Physics A*, 110, pp.511–515.

Sherwood, T., Pigford, R., and Wilke, C., 1975. *Mass Transfer*. 2nd edition. New York: McGraw-Hill.

Sporring, S. et al., 2005. Comprehensive comparison of classic Soxhlet extraction with Soxtec extraction, ultrasonic extraction, supercritical fluid extraction, microwave assisted extraction and accelerated solvent extraction for the determination of polychlorinated biphenyls in soil. *Journal of*

Chromatography A, 1090, pp.1–9.

Strydom, C.A. et al., 1995. The thermal dehydration of synthetic gypsum. *Thermochimica Acta*, 269–270(C), pp.631–638.

Stuerga, D., 2006. *Microwave-Material interactions and dielectric properties, Key ingredients for mastery of chemical microwave process. Microwaves in Organic Synthesis.* Available at: http://citeseerx.ist.psu.edu/viewdoc/download?doi=10.1.1.455.3957&rep=rep1&type=pdf [Accessed June 24, 2015].

Stucki, J.W., Bish, D.L., and Mumpton, F.A., 1963. *Thermal Analysis in Clay Science (Volume 3)*. Published by The Clay Mineral Society.

Suga, K., and Kubo, M., 2010. Modelling turbulent high Schmidt number mass transfer across undeformable gas-liquid interfaces. *International Journal of Heat and Mass Transfer*, 53(15–16), pp.2989–2995.

Tamir, A., and Merchuk, J.C., 1978. Efffect of diffusivity on gas-side mass transfer coefficient. *Chemical Engineering Science*, 33, pp.1371–1374.

Tedder, W.D., and Pohland, F.G., 1995. Emerging Technologies in Hazardous Waste Management V. *American Chemical Society*.

Thostenson, E.T., and Chou, T.-W., 1999. Microwave processing: fundamentals and applications. *Composites Part A*, 30(9), pp.1055–1071.

Turner, K., 2001. Bioremediation of drill cuttings from oil based mud, PhD Thesis, University of Nottingham.

Van der Ham, A.G., and Brouwers, H.J.H., 1998. Modelling and experimental investigation of transient, nonequilibrium mass transfer during steam stripping of a nonaqueous phase liquid in unsaturated porous media. *Water Resources Research*, 34(1), pp.47–54.

Voitkovsky, Y., Kreynin, S., and Kharakhan, M., 1995. On kinetics of high-temperature air reduction of hematite. *Physics of the solid earth*, pp.349–351.

Vollmer, M., 2004. Physics of the microwave oven. *Food Physics (Physics Education)*, 39.

Vongpradubchai, S., and Rattanadecho, P., 2009. The microwave processing of wood using a continuous microwave belt drier. *Chemical Engineering and Processing: Process Intensification*, 48(5), pp.997–1003.

Wilkins, M.D., Abriola, L.M., and Pennell, K.D., 1995. An experimental investigation of rate-limited nonaqueous phase liquid volatilization in unsaturated porous media:Steady state mass transfer. *Water Resources Research*, 31(9), pp.2159–2172.

Wraith, J.M., and Or, D., 1999. Temperature effects on soil bulk dielectric permittivity measured by time domain reflectometry: Experimental evidence and hypothesis development. *Water Resources Research*, 35(2), pp.361–369.

Xie, W. et al., 2001. Thermal characterization of organically modified montmorillonite. *Thermochimica Acta*, 367–368, pp.339–350.

Yeung, P.Y., Johnson, R.L., and Acharya, S.N., 1994. An improved procedure for determining oil content in wet soils. *Alberta Environmental Centre*.

Yoon, H. et al., 2002. Effect of water content on transient nonequilibrium NAPL – gas mass transfer during soil vapor extraction. *Journal of Contaminant Hydrology*, 54, pp.1–18.

Yu, Q., and Brouwers, H.J., 2012. Thermal properties and microstructure of gypsum board and its dehydration products: A theoretical and experimental investigation. *Fire and Materials*, 36, pp.575–589.

Yun, T.S., and Santamarina, J.C., 2008. Fundamental study of thermal conduction in dry soils. *Granular Matter*, 10(3), pp.197–207.

Zhong, H. et al., 2011. Shale inhibitive properties of polyether diamine in water-based drilling fluid. *Journal of Petroleum Science and Engineering*, 78(2), pp.510–515.

Appendices

Appendix 1

Method for calculating flowrate in the rotary wheel system (System C)

The heating tests were carried out in a Brandt's facility that processes oil contaminated drill cuttings. The mass flowrate of drill cuttings through the cavity of the rotary wheel system was estimated using the following method.

Data from the wheel applicator tests is shown in table 1A

Table 1A: Data from rotary wheel applicator system testing (Initial oil content – 13.7 wt%, Initial water content – 12.7 wt%)

Wheel Speed (mm/s)	Incident Power (kW)	Bed Depth (mm)	Absorbed power (kW)	Wheel Discharge	
				Oil (w/w)	Water (w/w)
7	35	35	26.76	6.2	2.4
10	35	28	29.78	6.3	2.6
12	35	25	27.72	7.6	2.9
15	35	22	27.19	6.7	5.5
7	45	35	31.87	4.6	1.7

Cavity length = 250mm

Cavity breadth = 185mm

The sample bed depth depends on varying factors such as the oil and water content of drill cuttings and the speed of the screw conveyor that transports the

material to the cavity. The sample bed depth is monitored continuously by a level indicator.

The flow rate is estimated from the volume of sample in the cavity in an instant. In other words, assuming that the cavity is a fixed bed process, and determining the duration for the system to process the fixed bed volume at a given wheel speed.

In the case of a bed depth of 35mm and wheel speed of 7mm/s (table 1A), the sample volume is estimated as follows;

Volume = cavity length × cavity breadth × bed depth [1.1]

Volume = 250mm × 185mm × 35mm = 1618750 mm^3=$1.619\left(10^{-3}\right)$ m^3

It is assumed that the material extends to the breadth and length of the cavity without gaps in the volume calculation.

Residence time for 1.619 (10^{-3}) m^3 at 7 mm/s sample is given as;

$$\frac{\text{Cavity length (m)}}{\text{wheel speed (m/s)}} = 35.7\text{s}$$

Bulk density of the drill cuttings sample treated is 1900kgm^{-3}

Mass of drill cuttings treated in 35.7s is given as;

density × volume = $1900 \times 1.619\left(10^{-3}\right) = 3.076$ kg

Mass flowrate is determined from;

$$\frac{\text{mass (kg)}}{\text{time (s)}} = \frac{3.076}{35.7} = 0.086 \text{ kg/s}$$

Appendix 2

Determination of pore steam velocities

Apart from power density, steam velocity depends on the average pore size (porosity) and the average cross sectional area in the pores.

The steam velocity is estimated from;

$$u_g = \frac{Q}{A} \qquad [2.1]$$

u_g = steam velocity through the pores of the material (m/s)

Q = steam volumetric flow rate (m^3/s)

A = cross sectional area of the material through which steam flows (m^2)

A is defined as; $A = A^* \times \text{porosity}$ [2.2]

A* is the cross sectional area of the drill cuttings material (which may be equal to the evaporating surface cross sectional area of the reactor or cavity), with diameter d_m, as shown in figure 2A, and $d_m > d_p$.

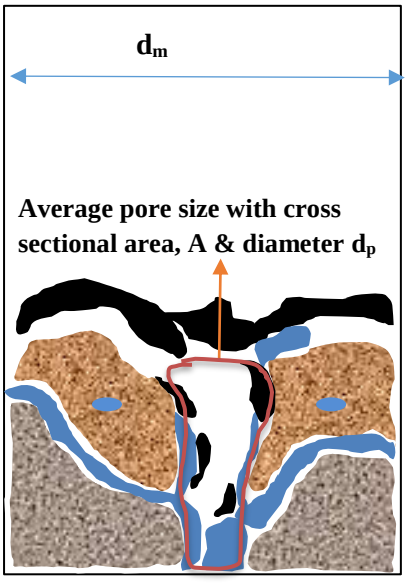


Figure 2A: Schematic of oil contaminated drill cuttings showing the average pore diameter and the diameter of the material's surface

The volumetric flowrate Q can be estimated from equation 2.3;

$$Q = \left(\frac{M_1 - M_2}{\rho}\right) \div t \qquad [2.3]$$

where;

M_1 = mass of water in the untreated sample (kg)

M_2 = mass of water in treated sample (kg)

ρ = density of steam (kgm^{-3})

t = treatment time (s)

Consider 70 g of drill cuttings (14wt% initial water content) treated for approximately 33s at 1kW. The mass of water left in the material after microwave heating is 2.548g (74% water removed). The steam density is given as 0.59 kgm^{-3}.

Using equation 2.3, Q is calculated as $3.7247(10^{-4})$ m^3/s

Porosity is calculated from the bulk density and the skeletal density of the material. Consider shale based drill cuttings with a bulk density of $2.1g/cm^3$, and skeletal density of $2.95g/cm^3$.

Porosity of the material can be estimated as follows;

$$1 - \frac{\text{bulk density}}{\text{skeletal density}} = 1 - \frac{2.1}{2.95} = 0.288$$

Low bulk density results in high porosity and vice versa

If A* is given as $0.004621m^2$, then, according to equation 2.2, A is calculated as $0.00133m^2$

Therefore, steam velocity can be estimated using equation 2.1 as follows;

$$u_g = \frac{3.7247 \times 10^{-4}}{0.00133} = 0.28 \text{ m/s}$$

At a higher porosity value, A will increase according to equation 2.2, which means that the steam velocity decreases according to equation 2.1.

Table 2A shows the parameters in the microwave systems needed to determine steam velocity. The volumetric flow rate can be estimated from the water removal data in chapter 7.

Table 2A: The bulk density, porosity and calculated flow areas of oil contaminated drill cuttings

Sample	Power (kW)	Bulk density (kg/m^3)	Porosity	Cross sectional flow area, A x 10^{-4} (m^2)
Shale 1 (System A)	1	2.1	0.288	1.331 x 10^{-4}
	1	1.83	0.380	1.751 x 10^{-4}
	1	1.7	0.424	1.958 x 10^{-4}
	1	1.5	0.492	2.271 x 10^{-4}
	3 - 5	2.1	0.288	1.331 x 10^{-4}
	3 - 5	1.55	0.475	2.193 x 10^{-4}
Shale 2 (System B)	40 - 92	1.95	0.324	2.546 x 10^{-3}
Shale 3 (System C)	35 - 45	1.9	0.360	1.898 x 10^{-2}

Appendix 3

Method for determining the molar flux of oil and mass transfer coefficient

The molar flux of oil into the stripping gas phase is given as;

$J = k_g(P_i - P_b)$ [3.1]

where;

J = net molar flux of oil into the steam stripping medium (kmol/m^2s)

k_g = gas phase mass transfer coefficient (m/s)

P_b = partial pressure of oil in the bulk gas phase (atm), converted to kmol/dm^3

P_i = vapour pressure of oil at the interface with the stripping gas (atm), converted to kmol/dm^3

P_b is assumed to zero

J can be estimated from;

$$J = \frac{G}{A} \quad [3.2]$$

G is the molar flowrate, and A is the cross sectional flow area (see appendix 2)

G can is given as;

$$G = \frac{G_f - G_i}{t \times M_a}$$

where;

G_f = initial oil content (kg)

G_f = oil content after treatment (kg)

t = treatment time (s)

M_a = molar mass of oil (kg/kmol)

Mass transfer coefficient is calculated from equation 3.1 by first determining the vapour pressure of oil.

Pi can be calculated from;

$$\ln P_i = C1 + \frac{C2}{T} + C3\ln T + C4T^{C5} \qquad [3.3]$$

where P_i is in Pascals, and T is temperature in kelvins. C1, C2, C3, C4 and C5 are constants. Decene is used to model oil, and table 3A shows the value of the constants used in estimating the vapour pressure.

Table 3A: Constants for estimating the vapour pressure of decene

Constants	Value
C1	68.401
C2	-7776.9
C3	-6.4637
C4	6.3750×10^{-18}
C5	6

The vapour pressure of decene at 378K (approximately bulk processing temperature) was estimated as 0.1298atm.

Equation 3.3 can be rearranged to;

$$k_g = \frac{J}{P_i - P_b} \qquad [3.4]$$

Which gives mass transfer coefficient (k_g) in kmol/m^2satm

Pi is converted from pressure (atm) to concentration (kmol/m^3) as follows;

At standard temperature and pressure (273K and 1atm), 1 mol of gas in the material's pores occupy 22.4 dm^3.

Therefore the concentration is estimated as follows;

$$\frac{0.1298\text{atm}}{1\text{atm}} \times \frac{273\text{K}}{378\text{K}} \times \frac{1\text{mol}}{22.4\text{dm}^3} = 0.004185 \text{ mol/dm}^3$$

Using the concentration units, mass transfer coefficient (k_g) can be calculated in m/s

Appendix 4

Derivation of the equation showing the relationship between power density and heating rate

The power density (kW/m^3) is given by;

$$P_d = 2\pi f \varepsilon_o \varepsilon'' |E|^2 \qquad [4.1]$$

where;

P_d = power density

f = microwave frequency

ε_o = permittivity of free space

ε'' = dielectric loss factor

E = electric field intensity

Energy required to raise the temperature of a material can be determined from;

$$MC_p\Delta T \qquad [4.2]$$

M is the mass of material, C_p is the specific heat capacity, and T is the temperature.

Equation 4.2 can be re-written to account for heating rate as;

$$MC_p \frac{\Delta T}{\Delta t} = \frac{\text{Energy (KJ)}}{\text{Time (s)}} = \text{power (kW)} \qquad [4.3]$$

t is the microwave treatment time

Equation 4.1 is re-arranged to give power (kW);

$$\text{Power (kW)} = 2\pi f \varepsilon_o \varepsilon'' |E|^2 \times \text{ volume } (m^3) \qquad [4.4]$$

Power in equation 4.3 is equal to power equation 4.4, therefore heating rate is given as;

$$\frac{\Delta T}{\Delta t} = \frac{2\pi f \varepsilon_o \varepsilon'' |E|^2 \times \text{volume } (m^3)}{MC_p} \qquad [4.5]$$

Since M = mass of substance (kg), then equation 4.5 can be re-written as;

$$\frac{\Delta T}{\Delta t} = \frac{2\pi f \varepsilon_o \varepsilon'' |E|^2}{\rho C_p} \qquad [4.6]$$

Equation 3.6 can also be written as;

$$\frac{\Delta T}{\Delta t} = \frac{P_d}{\rho C_p} \qquad [4.7]$$

Appendix 5

Electric Field Distribution in System A

The figures below show the electric field distribution in the applicator of system A during microwave treatment. The finite element was used to solve for the average electric field, given the power input. COMSOL Multiphysics software was used to perform the modelling. Figures 5A – C show the average electric field distribution (v/m) at different temperatures during treatment, which were used in estimating heating rates in the samples (Chapter 5).

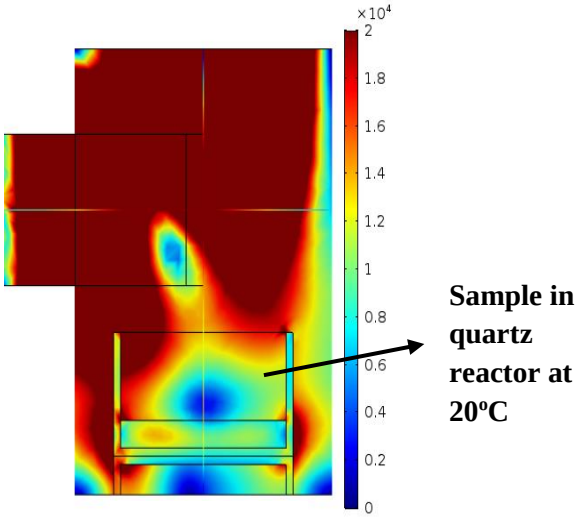


Figure 5A

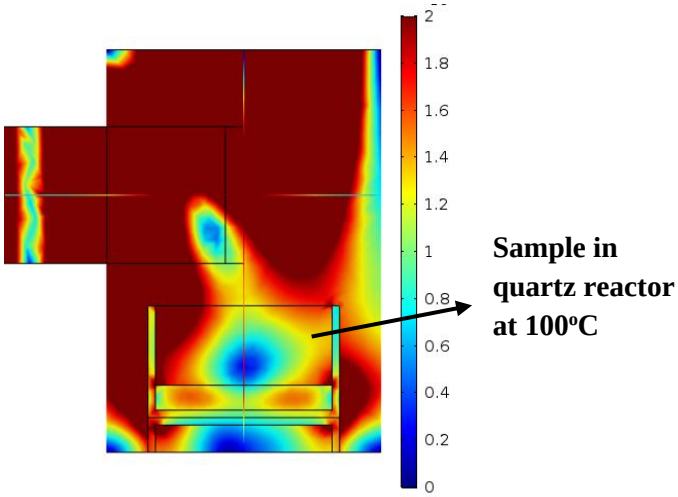


Figure 5B

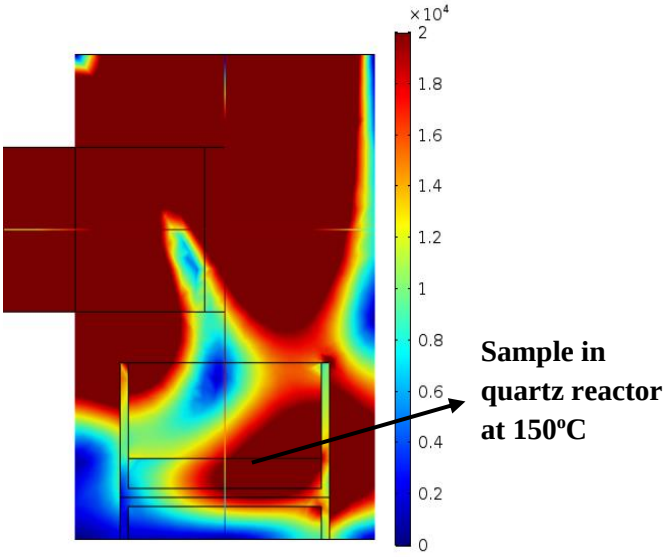

×10^4
2
1.8
1.6
1.4
1.2
1
0.8
0.6
0.4
0.2
0
Sample in
quartz reactor
at 150ºC

Figure 5C